Non-Invasive Shock Wave Stimulated Periosteum for Bone Tissue Engineering

by

Cathal John Kearney

Submitted to the Harvard/MIT Division of Health Sciences and Technology
in partial fulfillment of the requirements for the degree of

Doctor of Philosophy

at the

MASSACHUSETTS INSTITUTE OF TECHNOLOGY

February 2011

Author .....
Harvard/MIT Division of Health Sciences and Technology
January 28, 2011

Certified by .....
Myron Spector, Ph.D.
Professor of Orthopaedic Surgery (Biomaterials), Harvard Medical School
Senior Lecturer, Department of Mechanical Engineering, MIT
Thesis Supervisor

Accepted by .....
Ram Sasisekharan, Ph.D.
Director, Harvard-MIT Division of Health Sciences and Technology
Edward Hood Taplin Professor of Health Sciences & Technology and Biological Engineering

Non-Invasive Shock Wave Stimulated Periosteum for Bone Tissue Engineering

by

Cathal John Kearney

Submitted to the Harvard/MIT Division of Health Sciences and Technology
on January 28, 2011, in partial fulfillment of the
requirements for the degree of
Doctor of Philosophy

Abstract

The cambium cells of the periosteum, which are known osteoprogenitor cells, have limited suitability for clinical applications of bone tissue engineering due to their low cell number (2-5 cells thick). Extracorporeal shock waves (ESWs) have been reported to cause thickening of the cambium layer and subsequent periosteal osteogenesis. This work proposes that ESW-therapy can be used as a non-invasive, inexpensive, and rapid method for stimulating cambium cell proliferation, and investigates the use of these cells for orthotopic bone growth.

The response of periosteal cells to ESWs was evaluated using two different energy densities applied to either the intact femur or tibia of the rat. Just four days after application of ESWs, there was a significant 3- to 6-fold increase in cambium cell number and thickness. The most effective treatment of those tested was high dose ESW applied to the tibia. Immunohistochemical staining of the proliferated cells demonstrated osteoblasts and bone formation (osteocalcin stain); it also demonstrated extensive vonWillebrand factor expression, which reveals the vascular contribution to the proliferating cambium layer.

In a rabbit model, ESW-thickened cambium layer cells were overlaid in situ on a porous calcium phosphate scaffold. At two weeks post-surgery, there was a significant increase in all outcome variables for the ESW-treated group when compared with controls: a 4-fold increase in osteoprogenitor tissue in the scaffold upper half, a 10-fold increase in osteoprogenitor tissue above the scaffold, and a 2-fold increase in callus size. The results successfully demonstrated the efficacy of ESW-stimulated periosteum for bone tissue engineering.

Thesis Supervisor: Myron Spector, Ph.D.
Title: Professor of Orthopaedic Surgery (Biomaterials), Harvard Medical School
Senior Lecturer, Department of Mechanical Engineering, MIT

Acknowledgments

At the outset of the PhD, I told myself that this is a huge personal undertaking – that *I* have to make lots of sacrifices and that *I* have lots of hard work ahead. Now that I'm finally at the end stage of the thesis, I realize that although I was ultimately responsible, there were a lot of people other people that made sacrifices to help along the way.

First and foremost, I would like to thank Dr. Myron Spector for giving me the opportunity to work on this project. He was truly committed not just to the project, but also to my education. He was an excellent advisor on all matters academic, professional, and personal and this work would simply not have been possible without him. Perhaps the greatest compliment I can think of is that when I (hopefully!) lead my own research group someday, I aspire to treat my own students with the same dedication and thoughtfullness that Dr. Spector treated me with.

The second key mentor I had was Dr. Hu-Ping Hsu, the orthopaedic surgeon in the Spector lab who worked closely with me to complete all the surgeries. He certainly went beyond his call of duty, working tirelessly to ensure completion of my studies while advising and mentoring me along the way. He also became a great friend during the course of the project – I value our personal relationship as much as our professional one.

The Thesis Committee members, Dr. Martha Gray, Dr. Simona Socrate, and Dr. Myron Nevins all played key roles in guiding me through my research. From the outset, they encouraged me to achieve the best research results possible and helped me find the tools and the questions to achieve this aim. I am eternally grateful for their advice, support, and encouragement.

I had the pleasure of working with some wonderful collaborators that enabled the research to be completed. Dr. Robert Padera at the Brigham and Women's Hospital was an excellent resource for all questions pathology and hisotology related. Dr. Robin Cleveland and his student Jonathan Kracht at Boston University were great at fielding many of my shock wave related questions, as well as providing equipment

for, and aiding in, several of the measurement experiments. Dr. Thibault Prevost and Kristen Bernick from the Socrate Lab were also a huge help in completing the measurement experiments and providing the necessary equipment. Scott Malstrom and the Koch Institute (MIT) provided training, access, assistance for the microCT work, which was a huge benefit to the rapid analysis of the rabbit study results. Dafang Zhang (HMS) was the main driving force behind the lubricin study and it was a pleasure to work with him and Thomas Cheriyan (VA Boston) on the study. I also had two undergraduate students, Sunny Lee and Hui Xia, help with various aspects of the project. I hope they got as much from my mentoring as I got from their input!

To all the faculty that helped me during my time here at MIT, be it through classes or other forms of mentoring, I really appreciate all the input I had – thanks for making MIT a challenging and rewarding experience. Thanks especially to my Masters thesis advisors Dr. Mary Boyce and Dr. Christine Ortiz for guiding me through my first two years at MIT. And to Prof. Yannas (and Dr. Spector) for the great opportunity to work as a Teaching Assistant in their classes and learn the art of teaching from two of the best I've met.

For funding support, I would like to acknowledge the Fulbright Association, the HST Martinos Felloship program, and the VA Boston Healthcare System. For materials and supplies, I would like to acknowledge SANUWAVE Health Inc. for providing us with two shock wave devices and continuous supplies and information; and EMS for supplying us with the dolorclast and continuous supplies and information. I would also like to thank Geistlich Pharma for supplying the anorganic bovine bone material.

I would like to say a huge thank you to all the administrative staff I worked with at MIT and the VA, especially in HST and MechE at MIT and the VA animal facility staff. Everybody went beyond the call of duty!

To all members of the Spector Lab past and present for being wonderful colleagues and friends, and for helping out in numerous ways during the study. And to all my peers at MIT and Harvard whom I had the pleasure to work and socialize with these past few years.

Of course, it wasn't all work! A huge shout out to my various Irish friends, roomates, and ski-trip buddies (esp. Conor, Rory, Carlos, Barbara, Frank, Christina, Alex). And to the HST crew that made late night studying fun (and late night not-studying more fun) (esp. Danilo, Tina, Ben, Tasha, Nick, Uri, Liz).

Thanks to Sharon's family & friends (esp. Linda, Wayne, Christina and Matt) for taking me all over New England and beyond, and for being not only a great support and help but also great friends. It was all a blast and I look forward to many more happy occasions together! Thanks too to Brigid for working with Sharon on editing the thesis!

A special thanks goes to my family, particularly my parents, who have patiently helped me through 24.5 yrs of education I've been blessed to have their support, encouragement, and love through it all. It really is a privilege to have been given the time and space to pursue my academic endeavors and it all started way back when, with their encouragement from day 1. I'm eternally grateful. Thanks also to my brothers: Seaghan, Lorcan, and Paraic for the help, encouragement, and inspiration along the way, and for all the fun times! Finally, for my grandparents who always valued education, I hope I made – and continue to make – you proud.

Finally, to Sharon, who I was so lucky to meet right as I started HST. She has stuck with me through the ups and downs, and has always been there for me in good times and bad. She has been a constant supporter and has helped out in every way she could (including editing the thesis!). I love you so much and I know there'll be more ups and downs in the future, but this process has shown we can work through them all together. Thanks for all the laughs and good times – I'm looking forward to many many more!

Contents

List of Figures

List of Tables

Chapter 1

Introduction

Bone is one of the more regenerative of the musculoskeletal tissues, which is due to its vascular network and constant turnover throughout life (Trueta, 1963). However, following large losses of bone (e.g., osteolysis, severe fractures, bone tumor resection, and mandibular resorption), there is an insufficient framework for spontaneous tissue repair (Bruder and Fox, 1999; Burg et al., 2000; Hutmacher, 2000; Laurencin et al., 1999; Muschler et al., 2004). There are several options for bone loss therapies, which can be subdivided into (A) autograft, (B) allograft, and (C) tissue engineering strategies. Despite many advances in the field of tissue engineering, the current clinical gold standard is the autograft, which is both osteoinductive and osteogenic. However, autografts are known to cause donor site morbidity, typically undergo resorption when transplanted, and are subjected to limitations of available graft tissue (Bruder and Fox, 1999; Hutmacher, 2000). Secondary issues that may be resolved by alternative strategies include the necessity for multiple surgical procedures and the technical challenge associated with graft harvesting of the bone (e.g. a dental surgeon harvesting autograft bone from the iliac crest requires specific additional training).

For numerous clinical applications, tissue engineering strategies have been proposed as a method of generating and integrating new tissue with existing host tissue that shares essential functions (Atala et al., 2008; Langer and Vacanti, 1993). Tissue engineering strategies use a combination of some or all of the components of the tissue engineering triad: (1) a scaffold material; (2) a cell source; and (3) growth

factors/regulators (Atala et al., 2008; Langer and Vacanti, 1993). Traditionally, *tissue engineering* was the terminology used to describe the formation of tissue in vitro using isolated cells that were seeded on a scaffold and grown under ideal conditions with the optimum regulators. The neo-tissue would then be implanted into the body; *regenerative medicine* was used to refer to tissue regeneration strategies that focused on adapting the host system response by scaffolds and/or growth factors to form new and functional tissue, instead of scar tissue, following insult. However, these fields overlap extensively, and in contemporary literature tissue engineering includes regenerative medicine strategies, as well as strategies that combine sheets of cells or tissue grafts with scaffolds and/or regulators.

Although there have been several promising bone tissue engineering strategies, there is a constant search for suitable cell sources when the local environment has an insufficient supply. Currently, the alternatives are exogenous cell sources (which are limited by regulatory approval and many are still in the R&D phase) or the harvesting of cells for culture over a period of weeks to months, which is the expensive option (for a review, see Bruder and Fox (1999)). Supplemental cell sources are particularly important for defects requiring bone augmentation, where there is a need for bone deposition/growth out from the cortical bone surface (e.g., alveolar ridge augmentation and osteolytic bone loss near joint prostheses). A tissue engineering strategy that successfully exploits an intraoperatively available cell source and rivals or outperforms the autograft would offer a valuable clinical alternative to the autograft procedure for many applications in orthopaedics and oral-maxillofacial surgery (Dattani, 2007; Hutmacher, 2000).

The periosteum consists of a thin layer of progenitor cells (cambium cells) that line the cortical bone, with a fibrous sheet above them; it is ideally suited to bone augmentation due to its physiologic location and its known osteogenic properties. The main issue that precludes periosteum from being used for these strategies is the low cambium cell number; however, we know from their primary role in fracture healing that these cells are highly proliferative. This thesis explores a novel therapeutic strategy: an extracorporeal shock wave device is used to stimulate rapid periosteal

cell proliferation. The periosteal sheet is then overlaid on a porous calcium phosphate scaffold, which provides contour, to form bone orthotopically.

1.1 Bone loss

Bone loss occurs following either a reduction in mechanical loading on the bone or a change in the bone environment. This is described by Wolff's theory:

$$\Delta Bone\ Structure = f(\Delta Mechanical\ Stimulus, Physiologic\ Mechanisms) \quad (1.1)$$

In pathological changes, an alteration in the bone microenvironment can occur due to systemic changes by endocrine signaling (e.g., osteoporotic changes), or due to local paracrine signaling (e.g. macrophage released factors), which favor bone resorption over bone deposition during remodeling. Additionally, there can be an acute loss of bone resulting from trauma (e.g., severe fractures) or surgery (e.g. bone tumor resection). In this work, we focus on applications of local bone loss, where there is a defined local boundary that needs orthotopic bone tissue generation (i.e., bone growth will be above the surface of the native cortical bone). Two specific clinical scenarios are described below.

1.1.1 Alveolar ridge augmentation

Following tooth loss or extraction, the mechanical load of the the tooth on the underlying alveolar ridge of the mandible or maxilla is removed. In accordance with Wolff's theory, there is a change in mechanical loading and the alveolar ridge undergoes bone resorption (see fig. 1-1). In order for there to be sufficient bone volume to harbor and support subsequent dental implants, it is first necessary to fill the defect in the alveolar ridge.

Clinically, there are three strategies in use for filling the defect. The first strategy uses autografts alone. However, this is no longer recommended as the grafts have been reported to resorb by up to 50% (Vermeeren et al., 1996). The second strategy,

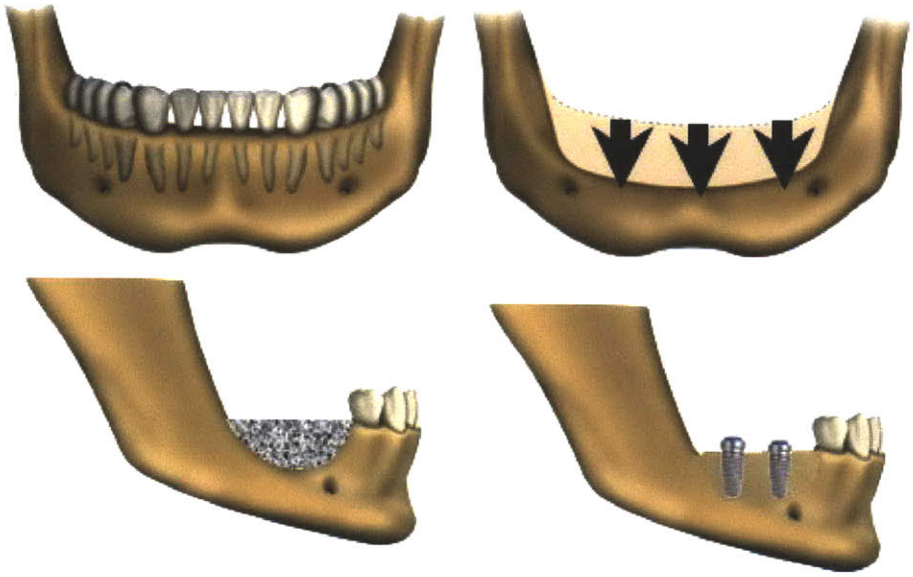

Figure 1-1 – Following the loss of teeth, the mechanical loading on the mandibular ridge is removed and the bone resorbs. To enable dental implants to be placed, the alveolar ridge has to be augmented vertically. This is accomplished by using either bone grafting or a biomaterial to regrow the bone.

distraction osteogenesis, is based on the orthopaedic method of creating a separation in bone, which responds by generating new bone to fill the gap (Chiapasco et al., 2004). The separation can be periodically increased to continue the bone augmentation process. This procedure, although very effective, is costly, technically difficult, and very timely (Chiapasco et al., 2004). In the third strategy, guided bone regeneration (GBR), the volume of bone to be regenerated is outlined with a membrane (e.g., titanium reinforced expanded-polytetrafluoroethylene (e-PTFE) membrane) (Chiapasco et al., 2004; Simion et al., 2001). This membrane is used to contain a blood clot, autogenous bone chips, allograft, or regenerative templates (Chiapasco et al., 2004; Simion et al., 2001, 1998, 2006, 2009; Tinti and Parma-Benfenati, 1998). These strategies have shown varying degrees of success, with the autologous bone chips being one of the most effective fillers (Simion et al., 2001). There is ongoing investigations into this, with different scaffolds and regulators being studied that may help overcome the drawbacks of autologous grafting (e.g., morbidity of the donor site, technical difficulty). The other issue with this approach lies in membrane exposure due to soft tissue dehiscence (up to 27%), which has to be carefully managed to avoid infection

(Chiapasco et al., 2004). Two studies, using off-the-shelf scaffolds, have espoused the value of periosteal cells to bone generation in these defects: the groups where there was no membrane blocking periosteal cell infiltration into the scaffold outperformed the groups in which there was a membrane in place (e.g. Simion et al. (2009, 2006)).

1.1.2 Osteolysis

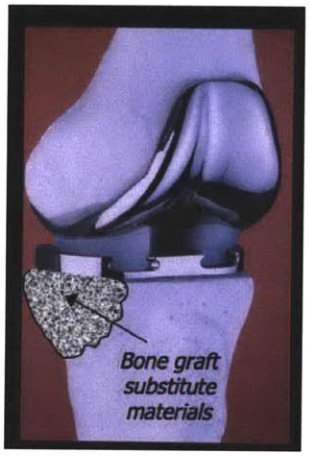

Figure 1-2 – Osteolytic regions result from the macrophage response to wear particles released from (total knee) replacement prostheses. The macrophages release factors that stimulate osteoclasts to resorb bone. Autografts or biomaterials may be required to fill defect and generate new bone.

Osteolysis, the active resorption of bone, occurs due to an inflammatory response to wear particles released from prosthetic devices. The wear particles induce an inflammatory cascade that leads to bone loss periprosthetically and also in the neighboring bone. Osteolysis was identified by the NIH as the most significant long-term adverse effect with total hip replacement implants due to implant loosening, bone loss impeding revision surgeries, and fracture (NIHCDP, 1995). In extreme cases, it has been necessary to implant an entire allograft of long bone, which carries the risk of disease transfer, when autografting/revision surgery was not possible. For this reason, osteolytic lesions have become one of the most targeted applications of bone tissue engineering strategies, with marrow derived MSCs and periosteal derived MSCs previously proposed as cell sources for these strategies (see fig.1-2) (Dattani,

2007; Hutmacher and Sittinger, 2003).

Osteolytic and resorbed mandible regions could benefit from a clinical technique for renegerating bone orthotopically on the surface of cortical bone; this is the primary focus of the thesis.

1.2 Bone tissue engineering

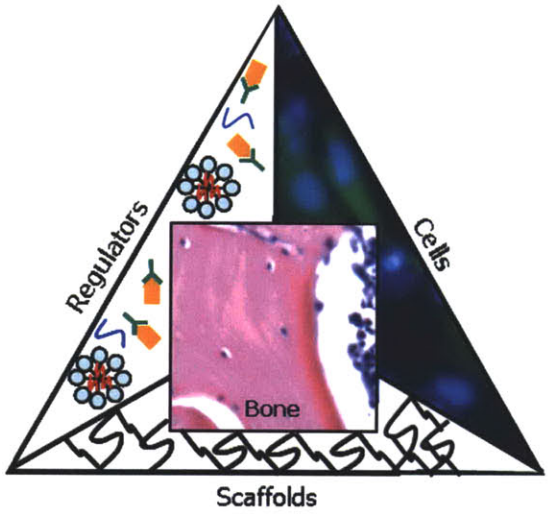

Figure 1-3 – The tissue engineering triad: one to three components of the tissue engineering triad (cells, scaffolds, regulators) are combined to generate bone tissue.

Bone tissue engineering strategies use a combination of some or all of the components of the tissue engineering triad: (1) a scaffold material; (2) a cell source; and (3) growth factors to generate bone (see fig.1-3) (Atala et al., 2008; Langer and Vacanti, 1993).There have been many excellent reviews that highlight the role of scaffolds (Burg et al., 2000; Hutmacher, 2000) and growth factors (Boden, 1999; Chen et al., 2004; Lieberman et al., 2002; Wozney, 2002) in bone tissue engineering strategies, and these fields continue to evolve. In bone tissue engineering, the scaffold material is typically required to have sufficient mechanical stiffness, strength, and toughness to remain structurally intact during osteogenesis. For this reason the scaffolds used have consisted of bioceramics (e.g., hydroxyapatite, deproteinized bone

allograft and xenografts) and biopolymers (e.g., poly(lactide-co-glycolide), poly-L-lactide, demineralized bone matrix); or composites (e.g., poly(lactide-co-glycolide) and hydroxyapatite) (Burg et al., 2000; Hutmacher, 2000).

Bone morphogenetic proteins (e.g., BMP-2, BMP-7), as well as platelet derived growth factor (PDGF), are known to be potent bone forming stimuli (Boden, 1999; Chen et al., 2004; Lieberman et al., 2002; Wozney, 2002). Techniques are being continuously developed to effectively deliver these agents by combining them with scaffold materials or to employ gene therapy techniques to stimulate their production (Boden, 1999; Chen et al., 2004; Wozney, 2002). In this work, the primary concern is not to evaluate the effectiveness of scaffolds or growth factors for bone tissue engineering, instead the aim is to demonstrate a novel way of accessing a cell source for bone tissue engineering.

For the defects in which there is a large volume of bone that has been lost, such as those described in sections 1.1.1 and 1.1.2, there is typically a need to include a supplemental cell source as part of a tissue engineering solution. Potential cell sources are reviewed by Bruder and Fox (1999). Example cell sources are: bone marrow derived mesenchymal stem cells (MSCs), periosteal cells, perichondrial cells or synovial cells. Marrow derived MSCs are a plausible option but are multipotent and need to be directed along a specific lineage (Herzog et al., 2003). The other three sources are not a viable, intraoperatively available, supplemental cell source because of their low cell quantity. However, as is evident from the physiology of fracture healing, periosteum can undergo dramatic proliferation. Hence, it is believed that with appropriate tools the periosteal cambium cells can be stimulated to proliferate and subsequently be used as a cell source for bone regeneration (Hutmacher and Sittinger, 2003). A thickened periosteum has the dual advantage of increasing the yield of cells for the filling of larger defects, while decreasing the technical difficulty in harvesting the tissue. That the cambium cells have an overlying fibrous layer gives the periosteum the additional advantage that these cells have their own suturable 'delivery vehicle.'

1.3 Periosteum

The periosteum is comprised of two layers of tissue: the inner cambium layer made up of progenitor cells, capillaries, nerves, and osteoblasts; and the outer fibrous layer comprised of fibroblasts, fibrous tissue, and vessels (Malizos and Papatheodorou, 2005). It is a well vascularized tissue and its vessels nourish the outer one-third of the diaphysis (Malizos and Papatheodorou, 2005).

Documentation of the osteogenic potential of periosteum in the context of its contribution to fracture healing and use as an autograft for bone reconstruction dates back to the mid 1700s (King and Melbourne, 1976; Hutmacher and Sittinger, 2003; Bassett, 1962). During fracture healing, the periosteal cells play a central role in returning the bone to its normal architecture (Aro et al., 1990). Proximal to the fracture site, proliferating periosteal cells form hyaline cartilage and distal to the defect, the periosteal cells differentiate to osteoblasts and begin to lay down woven bone. Fibroblasts in the granulation tissue in the central portion of the defect, which is filled with a hematoma immediately following fracture, differentiate into chondroblasts and lay down hyaline cartilage. Periosteal cells also migrate into this region and form cartilage and bone. The cartilage undergoes endochondral ossification and eventually this immature bone tissue undergoes remodeling, maturing to osteonal bone.

The multipotent character of periosteal cambium cells has been demonstrated by numerous studies demonstrating their chondrogenic potential (O'Driscoll and Fitzsimmons, 2001; Emans et al., 2005), and more recent work also showing the adipogenic capability of these cells (Choi et al., 2008). However, for applications dependent on its progenitor cells, periosteum is limited by its low cell number (2-5 cells), which also makes its harvest technically difficult (O'Driscoll, 2001).

1.3.1 Periosteum for tissue generation

Periosteal cambium cells, which are key contributors to fracture healing, form both bone and cartilage. Hence, periosteum has primarily been investigated for formation of these two tissue types.

Periosteum for bone tissue generation

The earliest report of periosteal osteogenesis dates back to 1742, when Duhamel (1742) placed silver wires under the periosteum of long bones. After several weeks of implantation, these wires were embedded in bone matrix. In the mid 1800s, Ollier (1860) demonstrated that transplanted periosteum could also induce new bone formation. In a 1925 paper, Blaisdell (1925) described periosteum as consisting of two fundamental layers, and described the inner layer as containing osteblast-like cells. Several papers, including papers from Fell (1932), Lavender (1938), and Press (1924), further established the osteogenic potential of periosteum and the reduction of this potential in aged individuals. Fell (1932) was the first to report on the culturing of periosteum and to demonstrate its ability to form mineralized extracellular matrix under appropriate culture conditions. Cohen and Lacroix (1955) transplanted periosteal grafts orthotopically and ectopically (intraoccularly and to the kidney subcapsule) and found bone formation at all sites, with the orthotopic transplant the

Figure 1-4 ***(facing page)*** – Examples of several bone tissue engineering strategies that utilize periosteum. (A) Example of subperiosteal scaffold implantation for periosteal bone growth (adapted from Stevens et al. (2005)). Alginate gel (white arrow, top panel of (A)) was implanted in a subperiosteal pocket in a rabbit model to create an in vivo bioreactor. The periosteal cambium cells proliferated and formed bone through intramembranous bone formation primarily, but also through endochondral ossification (Ps = periosteum; CT = cortical bone; scale bar 100 μ m). (B) Example of a harvest-culture-implant approach used in a canine model (adapted from Mizuno et al. (2006)). After 30-40 days in culture, the periosteal explants are wrapped around a furcation defect in canine mandibular premolars. Bone was successfully regenerated using the cultured periosteal explants. (C) Example of cultured periosteal cells seeded on a scaffold for bone tissue engineering (Isogai et al., 2000). Bovine periosteal cells are harvested and seeded on a scaffold, which is implanted subcutaneously in mice. By week 3 there is cartilage formation (white arrows) and by week 12 it has undergone ossification and bone formation (asterisk). (D) Example of a scaffold implanted above the periosteal cambium layer (Thomson et al., 1999). In this ovine model, a molded tissue chamber is filled with scaffold material; the periosteal cells migrate into the scaffold and regenerate bone. In the right panel (H & E), a chamber (10mm cross-section) that had morsellized bone graft as the scaffold material is filled with new bone at 2 months. (E) Example of periosteal graft used alone for bone tissue engineering (King and Melbourne, 1976). Periosteal strips are elevated from the tibial bone and sutured to form a tube of tissue; at 6 months radiographs show osteogenesis has occurred within the periosteal pedicle graft.

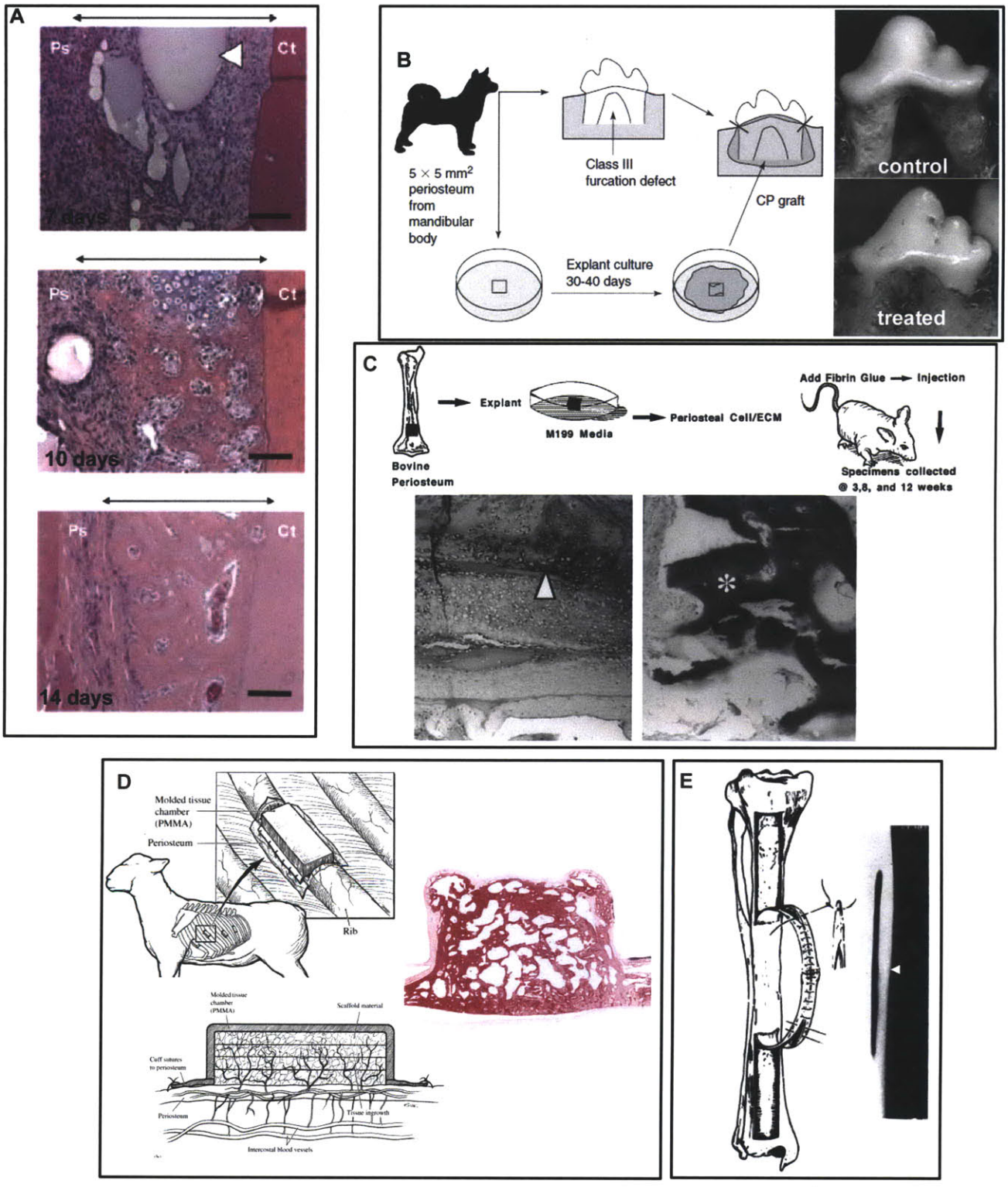
A
Ps
Ct
7 days
Ps
Ct
10 days
Ps
Ct
14 days
B
5 × 5 mm2 periosteum from mandibular body
Class III furcation defect
CP graft
Explant culture 30-40 days
control
treated
C
Bovine Periosteum
Explant
M199 Media
Periosteal Cell/ECM
Add Fibrin Glue
Injection
Specimens collected @ 3,8, and 12 weeks
D
Molded tissue chamber (PMMA)
Periosteum
Rib
Molded tissue chamber (PMMA)
Scaffold material
Cuff sutures to periosteum
Periosteum
Tissue ingrowth
Intercostal blood vessels
E

most osteogenic.

Bone tissue engineering strategies that use periosteum as the primary cell source have evolved around these principal studies over the past two decades (fig. 1-4). Several authors have used the tissue as a raised flap, with and without scaffolds, to generate bone in situ (e.g., King and Melbourne (1976); Melcher and Accursi (1971); Stevens et al. (2005)). Other authors have placed scaffold above the periosteal cambium layer to create blocks of bone tissue (e.g. Thomson et al. (1999)). Free grafts have also been used – with and without scaffolds – for bone formation in various models (e.g., Poussa and Ritsilä (1979); Poussa (1980); Ranta et al. (1981); Takato et al. (1986)). Finally, both free periosteal grafts (Mizuno et al., 2006), and isolated periosteal cambium cells (Isogai et al., 2000; Jaquiéry et al., 2005; Ueno et al., 2007) combined with scaffolds, have been grown in culture and implanted to demonstrate bone formation in vivo.

The focus of this thesis is the generation of bone orthotopically using ESW-stimulated periosteum in combination with a subperiosteally implanted porous calcium phosphate scaffold.

Periosteum for cartilage tissue generation

Clinically, one of the most frequent uses for periosteum is as a free tissue flap that is used to contain cultured autologous chondrocytes within a chondral defect. In this procedure, pioneered by the group of Brittberg et al. (1994), autologus chondrocytes are cultured for a period of weeks and implanted back into the patient's chondral defect. The defect is then sealed with a periosteal flap, which further supplies a chondrocytic cell source (periosteal cambium cells) to the defect.

Rubak et al. (1982) pioneered the technique of periosteal arthroplasty, whereby the periosteum alone is used to fill both chondral and osteochondral defects. In this strategy the periosteum is harvested from the proximal tibia, and transplanted to the chondral defect site. Here, it is sutured to surrounding cartilage, with the cambium layer face up. Favorable results both experimentally and clinically have been reported (O'Driscoll and Fitzsimmons, 2001). O'Driscoll's group have made

many developments on this strategy by combining it with continuous passive motion, introducing growth factors, and adding a culturing step to stimulate cambium cell proliferation and chondrogenesis (O'Driscoll et al., 1994; O'Driscoll, 2001; O'Driscoll and Fitzsimmons, 2001; Reinholz et al., 2009, 2008; Saris et al., 1999). There have been fewer attempts to combine cultured periosteal cells with scaffolds for cartilage repair than there have been for bone repair; however, the use of scaffolds and periosteal grafts for healing osteochondral defects has been proposed (e.g., Mardones et al. (2005)).

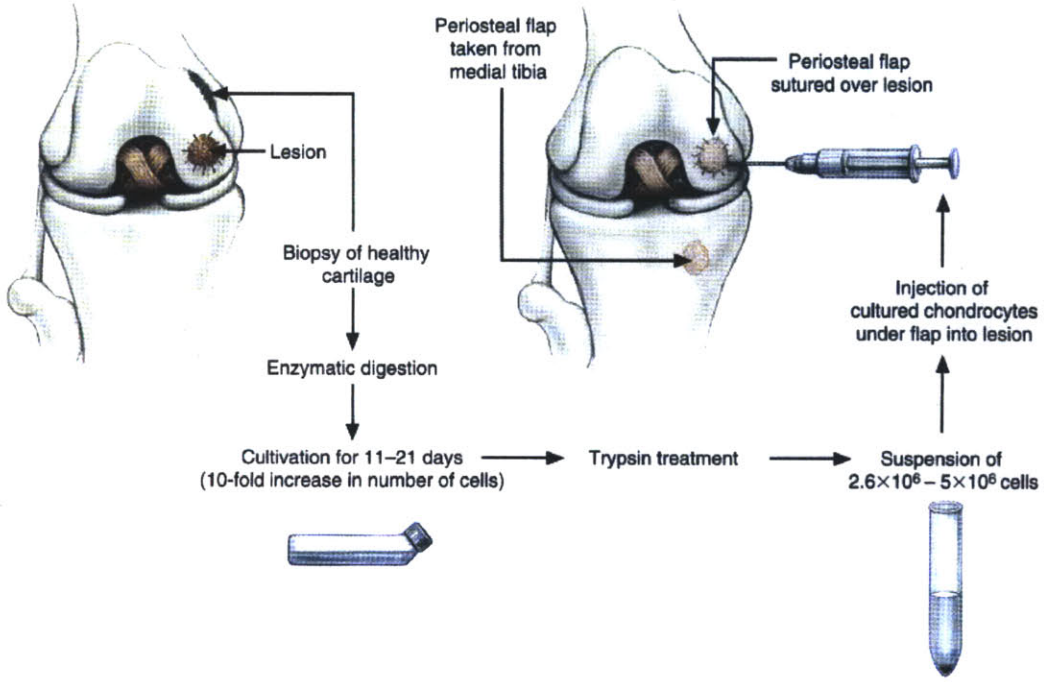

Figure 1-5 – Autologous chondrocyte transplant technique: Cells are harvested from a healthy cartilage site in the patient, and grown in culture. The cell suspension is then implanted into the cartilage defect site, and a free periosteal flap is used to seal the defect and provide additional cells (from Brittberg et al. (1994)).

This section is included to demonstrate the successful use of periosteum in a tissue engineering strategy; however, the role of periosteum in cartilage tissue engineering is not investigated in this work.

1.3.2 Thickening of periosteal cambium layer

Previous investigators have reported techniques aimed at thickening the cambium layer of periosteal cells for use in tissue engineering strategies. O'Driscoll's group injected TGF-β1 subperiosteally to stimulate periosteal proliferation and to initiate chondrogenic differentiation of the cambium cells (Reinholz et al., 2009). Simon et al. (2003) investigated the use of surgical techniques to stimulate periosteal cell proliferation in a caprine model. The authors performed surgical release of the periosteum which resulted in cambium cell proliferation and subsequent bone formation within the proliferated layer. Mizuno et al. harvested periosteum in a canine model, cultured it for 30-40 days, and used it to regenerate bone in a canine periodontal defect (Mizuno et al., 2006). In periosteal explants stimulated with cyclic hydrostatic pressure in an in vitro bioreactor a significant increase in cambium layer thickness was found when compared with cultured, non-mechanically stimulated controls (Saris et al., 1999). Isolated cambium layer cells can also be caused to proliferate by culturing (e.g. Mizuno et al. (2006); Isogai et al. (2000); Jaquiéry et al. (2005); Ueno et al. (2007)).

While all of the above strategies can successfully result in proliferation of cambium cells, they require procedures which can be costly and time-consuming.

1.4 Extracorporeal shock waves

Our supposition is to employ extracorporeal shock waves (ESWs) as a non-invasive and rapid way of safely and reliably stimulating the proliferation of the periosteal osteoprogenitor cells for use in orthotopic bone generation strategies after only a few days. A shock wave is a high positive pressure acoustic pulse wave, followed by a lower pressure tensile wave (Chung and Wiley, 2002; Gerdesmeyer and Lowell, 2007). Importantly for this study, ESWs have been reported to stimulate periosteal osteogenesis following thickening of the periosteal cambium layer (Takahashi et al., 2004; Tischer et al., 2008). For medical applications, the peak ESW pressures lie in the range of 5-120MPa; the rise time is on the order of 10-100ns; and the pulse width

is on the order of $1\mu s$ (Chung and Wiley, 2002; Gerdesmeyer and Lowell, 2007). ESWs have shown efficacy for several musculoskeletal disorders including calcific tendonitis of the rotator cuff, plantar fasciitis, and non-unions (Birnbaum et al., 2002; Haupt, 1997; Takayama and Saito, 2004). In the US, several devices are FDA approved for treatment of calcific tendonitis and plantar fasciitis.

1.4.1 Extracorporeal shock waves: Historical perspective

Shock wave technology has been known to the medical community since the 1980s, when lithotripters were first used to break up kidney stones. However, the first recorded effect of shock waves on human tissue was during World War II, when depth charge explosions resulted in a condition now called blast lung (Gerdesmeyer and Lowell, 2007; Strash and Perez, 2002). The lung tissue of submariners was found to have ruptured following these depth charge explosions without any externally visible signs of damage (Gerdesmeyer and Lowell, 2007; Strash and Perez, 2002). The first experiments performed on biological tissue followed in the 1960s and were commissioned by Germany's Ministry for Defence. These experiments scientifically determined the detrimental effects of shock waves on lung tissue and also recorded the minimal side effects on connective tissue, fat, and muscle (Gerdesmeyer and Lowell, 2007; Strash and Perez, 2002). After proving with in vitro models in the 1970's that shock waves could be used to disintegrate kidney stones, the first patient was treated with lithotripsy in 1980 (Gerdesmeyer and Lowell, 2007; Strash and Perez, 2002). To this day lithotripsy remains the gold standard clinically for disintegration of kidney stones.

Based on its success in lithotripsy, it was hypothesized that shock waves could be used to break up the calcific deposits found in the rotator cuff of patients with calcific tendonitis (Ogden et al., 2004; Strash and Perez, 2002). Post treatment, the results indicate that there is an improvement in pain scores; however, the calcific deposit remains in place in many instances (Ogden et al., 2004; Strash and Perez, 2002). Subsequent animal models illustrated a repair/remodeling process was taking place, which led to the conclusion that shock waves can be used as a noninvasive

energy source to initiate repair of damaged tissue. Since this discovery, shock waves have been proposed as a therapeutic aid for repair in a variety of soft tissues and indications (e.g., Chung and Wiley (2002); Gerdesmeyer and Lowell (2007); Haupt (1997); Ogden et al. (2001); Shrivastava and Kailash (2005); Takayama and Saito (2004)).

1.4.2 Extracorporeal shock waves: Technology

Shock waves are pressure waves of less than 1μs duration in which a high amplitude compression peak is immediately followed by a lower magnitude tensile (cavitation) wave (see fig. 1-6). There have been numerous reviews of ESWs used for lithotripsy (Chow and Streem, 2000; Tombolini et al., 2000; Shrivastava and Kailash, 2005) and more recently for a wide array of other medical applications (Chung and Wiley, 2002; Shrivastava and Kailash, 2005; Takayama and Saito, 2004), specifically in orthopaedics (Chung and Wiley, 2002; Takayama and Saito, 2004). ESWs have been employed clinically for the treatment of chronic plantar fasciitis (Ogden et al., 2004; Speed et al., 2003; Theodore et al., 2004; Wang et al., 2006) and for other ligament and tendon problems (including rotator cuff problems) (Cosentino et al., 2004; Rompe et al., 2001). Despite the fact that the mechanisms of action of ESWs are not yet fully understood, this form of therapy continues to prove itself to be safe and effective for the treatment of many disorders.

Electrohydraulic generation

The earliest shock wave lithotripsy devices, and the technology still commonly used today, are based on electrohydraulic shock wave generation. The basics of their operation are outlined in 1-7. During electrohydraulic shock wave generation, a high energy electric discharge is ignited between two electrodes in a conductive water bath (Gerdesmeyer and Lowell, 2007; Weiss, 2006). A capacitor, with approximately 20kV of charge is connected to two metal electrodes (through a fast high-voltage switch). This creates a thin current path (leader) between the two electrodes which are ap-

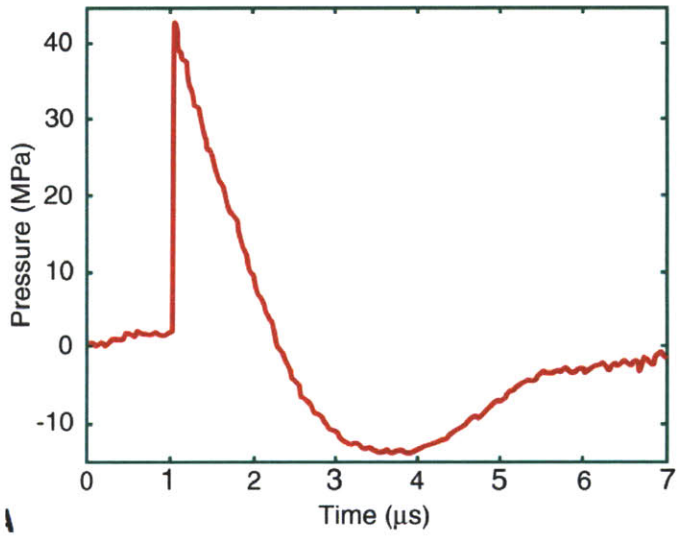

Figure 1-6 – Sample of single ESW pulse emitted from a Dornier (Dornier MedTech America, Inc, Kennesaw, GA) electrohydraulic ESW apparatus. The pressure rises abruptly to a pressure on the order of $1x10^1$MPa at the shock front, has a pulse width on the order of 1μs, and is followed by a lower amplitude tensile wave (adapted from Cleveland and McAteer (2006)).

proximately 1mm apart. Several different leaders are formed and when one of these reaches the opposite electrode, there is a rapid build up of current between the two electrodes that rapidly heats up the space between the electrodes, forming a plasma bubble. This bubble expands at supersonic velocity, compressing the surrounding liquid to a pressure on the order of 100MPa. This wave travels as a spherical wave losing energy rapidly, to the point that non-linearities are no longer present after several millimeters. Since most treatments are deep inside tissue, an elliptical reflector is used to redirect the wave so that it recombines with the forward traveling component at the secondary focus – the treatment zone.

Although the electrohydraulic form of ESW generation is the most commonly used form of shock wave generation, there are some drawbacks with the technique. First, the formation of underwater shock waves with spark gaps is a stochastic process and thus there is a certain degree of spatial variation. Second, the electrodes wear down and need to be replaced by new ones when the gap between them becomes too large and the spark is no longer formed. The final disadvantage relates to the loud popping

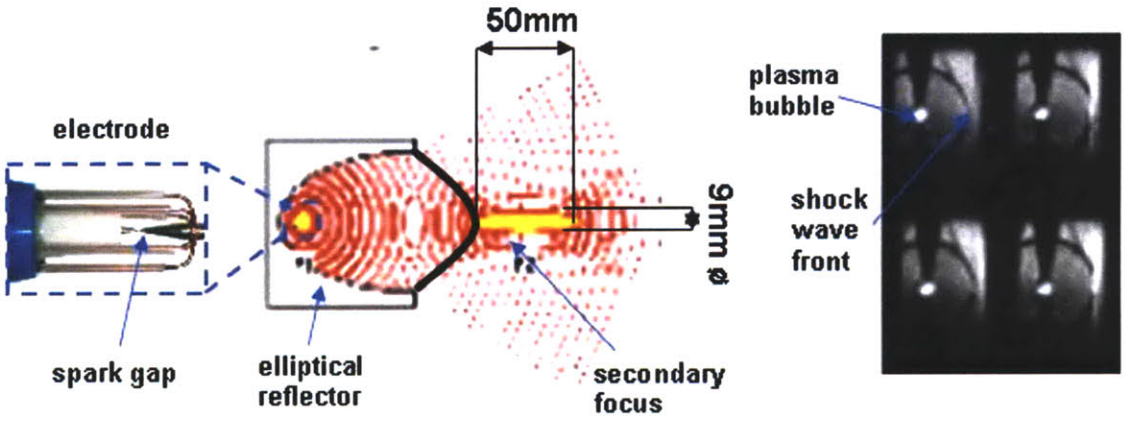

Figure 1-7 – Electrohydraulic shock wave generation: A high voltage ($\sim$1x10^{1}kV) is applied across two electrodes, which causes a spark discharge and a plasma bubble that compresses the surrounding medium. The wave is focused by means of an elliptical reflector and the energy concentrated in the focal treatment zone (adapted from Weiss (2006)).

sound that is experienced upon collapse of the plasma bubble, which can be a source of discomfort to patients and/or clinicians during treatment.

Electromagnetic generation

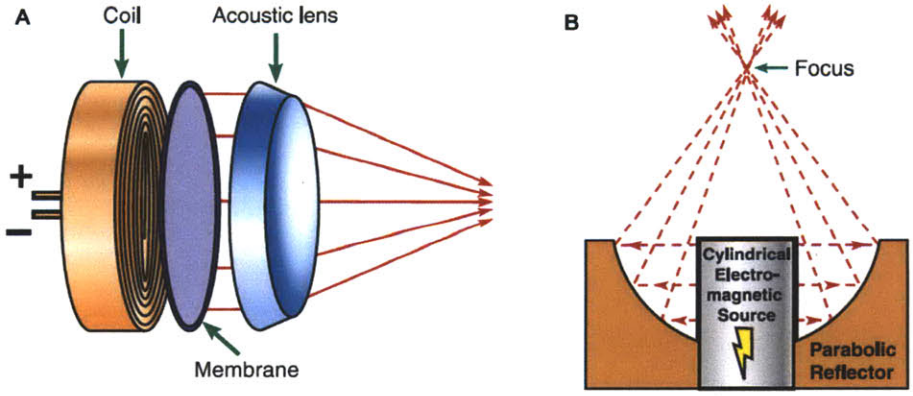

Figure 1-8 – Electromagnetic shock wave generation: Similar to loudspeakers, an electric coil surrounds a magnetic core, and electomagnetic induction is used to propel the structure forward. The energy is focused by means of (A) an acoustic lens or (B) by a parabolic reflector (adapted from Cleveland and McAteer (2006)).

This technique is analogous to the generation of acoustic waves in loudspeakers, which relies on the principal of electromagnetic induction (Gerdesmeyer and Lowell,

2007; Weiss, 2006). Two configurations are used to generate these waves. In the first configuration, a flat coil is used to create a planar wave, which can then be focused through an acoustic lens. In the second setup, a cylindrical coil creates a divergent wave, which is then focused using a rotation paraboloid. The advantage of the cylindrical wave is that it can be more easily focused deep in the body. However, it is limited by lens material, and generally the shock wave energy passes through the skin in a very narrow region, which causes more pain at the application site.

Piezoelectric generation

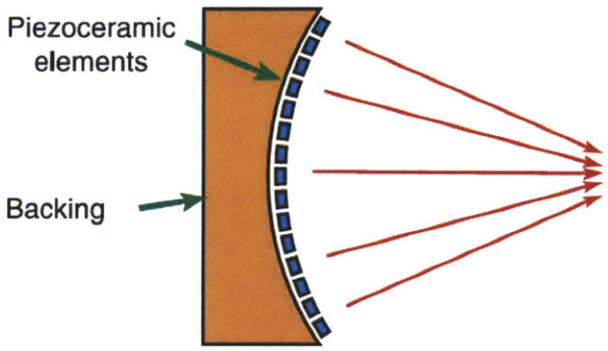

Figure 1-9 – Piezoelectric shock wave generation: A voltage pulse is applied to an array of peizoelectric crystals simultaneously and these move in synch to propel the surrounding media forward creating a shock wave at the focal zone (adapted from Cleveland and McAteer (2006)).

Piezoelectric transducers have been used in the field of ultrasound for a long time. Piezoelectric materials undergo strain in response to applied voltage (~1-10kV for shock wave applications). For shock wave generation, a large array of these transducers are arranged spherically and simultaneously excited (Gerdesmeyer and Lowell, 2007; Weiss, 2006). This co-ordinated pulse results in a convergent spherical wave that reaches treatment levels at the center of the sphere. These systems are more easily controlled and are more repeatable than the electrohydraulic systems, however, their treatment area is relatively small. This can be partially overcome by placing a second layer of piezoelectrics in the system.

Pneumatic generation

In pneumatic generation, the principle employed is analagous to the jack-hammer of split-Hopkinson bar (Gerdesmeyer and Lowell, 2007; Weiss, 2006). These devices employ an air pressure pulse to propel a projectile forward. This projectile strikes a solid surface, which in the case of shock wave treatment is attached to the skin. These waves are planar and generally unfocused, making them suitable for more shallow treatments. They are quite repeatable and may reduce the requirements for anaesthesia and analgesics.

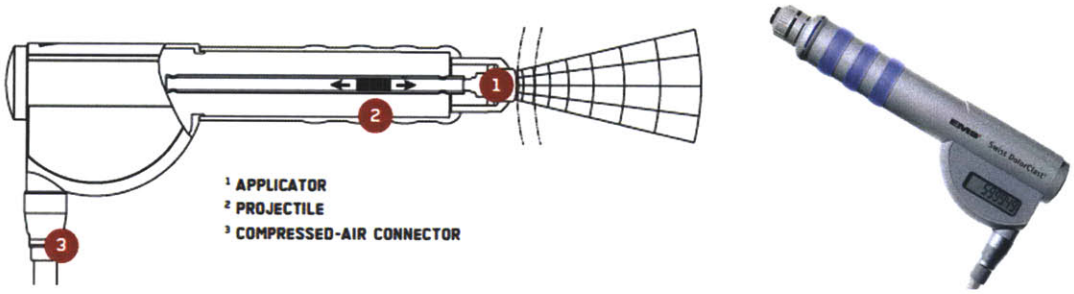

Figure 1-10 – Pneumatic shock wave generation: an air pressure burst is used to propel a projectile forward. This strikes the treatment head resulting in a pressure pulse (adapted from http://www.ems-company.com).

1.4.3 Response of bone tissue to extracorporeal shock waves

Given its healing success in several tissues, a fracture model in rats was used to interrogate the osteogenic potential of shock waves in the late 1980s (Haupt, 1997). These early studies illustrated that fracture healing was enhanced by the shock waves based on radiological, histological, and biochemical assays (Haupt, 1997).

Since these early studies, ESWs have been shown to be effective – within certain dose settings – in stimulating osteogenesis (Delius et al., 1995; McClure et al., 2004; Ogden et al., 2001; Takahashi et al., 2004; Tischer et al., 2008). Studies have demonstrated osteogenesis following ESW treatment in normal long bones in rat (Takahashi et al., 2004), rabbit (Delius et al., 1995; Tischer et al., 2008), and equine (McClure et al., 2004) models. In the rat model, where only the periosteum was assessed, by

day 4 the periosteum had dramatically proliferated, and it had matured by day 14 to new bone (Takahashi et al., 2004). The rabbit studies both reported periosteal and endosteal bone formation, but, endosteal bone formation was only found to be statistically significant in one of the studies (Tischer et al., 2008; Delius et al., 1995).

The early reports of ESWs applied to fracture healing yielded mixed results; success rates reported for shock wave inducing complete union ranged from 35% to 91% (Haupt, 1997). However, with appropriate patient selection and treatments, ESW therapy has been shown to be successful for the treatment of non-unions and delayed unions in both human and animal models (Birnbaum et al., 2002; Cacchio et al., 2009; Johannes et al., 1994; Ogden et al., 2001; Rompe et al., 2001; Schaden et al., 2001; Wang et al., 2001). ESWs have also proven efficacious in segmental defect rat models (Chen et al., 2003, 2004), and pseudoarthrosis in humans (Haupt, 1997). The use of ESWs to stimulate repair and pain relief in patients with osteonecrosis of the femoral head was also explored clinically and had successful results (Ludwig et al., 2001; Wang et al., 2008, 2005). Recently, unfocused ESWs have been proposed as a treatment for osteopenia and osteoporosis based on encouraging findings in a rat model (Jagt et al., 2009).

1.4.4 Extracorporeal shock waves: Mechanism

To date, the emphasis of ESW application has been on their clinical application, whereas their mechanism of action on bone cells has remained poorly understood. It has been reported that (in vivo) ESWs can induce microdamage and initiate a regenerative response, but the molecular and cellular mechanisms of this effect are still unknown (Gerdesmeyer and Lowell, 2007; Ogden et al., 2001; Takayama and Saito, 2004). Early studies on ESW-stimulated osteogenesis believed that (micro-)fractures were the key stimulus for osteogenesis (e.g., Ikeda et al. (1999); Sukul et al. (1993)); however, more recent reports have disproved this (Delius et al., 1995; McClure et al., 2004; Tischer et al., 2008). Some studies have suggested that subperiosteal separation may contribute to perisoteal bone apposition (Delius et al., 1995; Takahashi et al., 2004; Tischer et al., 2008), but solid evidences confirming this hypothesis are still

lacking. McClure et al. (2004) disputed this claim, comparing the response of surgically elevated periosteum with ESW-stimulated periosteum in an equine model. The ESW-stimulated regions had increased osteogenesis when compared with periosteal elevation alone. Finally, increased regional blood flow and/or the release of angiogenic factors (McClure et al., 2004; Ogden et al., 2001; Jagt et al., 2009); recruitment and differentiation of MSCs, possibly resulting from marrow hypoxia (Chen et al., 2004; Delius et al., 1995; McClure et al., 2004; Ogden et al., 2001; Jagt et al., 2009; Wang et al., 2002); and upregulation of osteogenic factors (e.g. BMP-2, VEGF (Wang et al., 2001; Tamma et al., 2009; McClure et al., 2004; Hofmann et al., 2008; Wang et al., 2002)) have all been proposed as possible ESW mechanisms of action in bone.

1.5 Thesis goals

This thesis deals with a new therapeutic approach for regenerating bone orthotopically. The emphasis is on growing bone on the cortical bone surface, which would have applications in bone regeneration in oral and maxillofacial surgery (e.g., alveolar ridge resorption), as well as in orthopaedics (e.g., osteolysis). The central hypothesis is that extracorporeal shock wave (ESW)-stimulated periosteum enhances bone formation in porous biomaterials implanted under the periosteum. The overall goal of this work is to demonstrate the efficacy of an ESW-thickened periosteum as an overlay on a porous calcium phosphate scaffold for the orthotopic growth of bone.

Chapter 2

Application of extracorporeal shock waves to periosteal cell proliferation: a rat model

2.1 Introduction

The periosteum is comprised of two layers of tissue: the inner cambium layer made up of progenitor cells and the outer fibrous layer comprising fibroblasts. Documentation of the osteogenic potential of periosteum in the context of its contribution to fracture healing and use as an autograft for bone reconstruction dates back to the mid 1700s (Bassett, 1962; Hutmacher and Sittinger, 2003; King and Melbourne, 1976). The multipotent character of periosteal cambium cells is illustrated by numerous studies demonstrating their chondrogenic potential (Emans et al., 2005; O'Driscoll and Fitzsimmons, 2001) and more recent work also showing the adipogenic capability of these cells (Choi et al., 2008). However, for applications dependent on its progenitor cells, periosteum is limited by its low cell number (2-5 cells), which also makes its harvest technically difficult (O'Driscoll, 2001).

Given the wide range of potential clinical applications using periosteum as a cell source for tissue regeneration, several previous attempts have been made to increase

the cambium cell number in vivo. One approach, evaluated in rats (Joyce et al., 1990) and rabbits (Reinholz et al., 2008, 2009), was to inject TGF-β1 subperiosteally to stimulate periosteal cell proliferation. A second goal of this work was to stimulate chondrogenic differentiation of the periosteal cells. In the rat study, daily injections of TGF-β1 and 2 (200ng) were found to stimulate cartilage and bone (intramembranous and endochondral) formation within the cambium layer. TGF-β2 was more proliferative and tissue area peaked at 60mm^2 (day 15). This was comprised of endochondral bone, intramembranous bone, and cartilage.

A second approach, using a caprine model, investigated the use of surgical release of the periosteum to stimulate periosteal cell proliferation and osteogenesis (Simon et al., 2003). In this model, the cambium cell layer thickness peaked at day 8 at a maximum of 170μm, and increased from 2-3 cells thick to up to 10-20 cells thick. This tissue underwent osteogenesis by day 16. Mizuno et al. (2006) harvested periosteum in a canine model, cultured it for 30-40 days, and used it to regenerate bone in a canine periodontal defect. At 4 weeks the cultured graft was 100μm, and approximately 10-12 cells thick. At week 6 the graft had thickened to 200μm; however, the authors report that the graft had low cell density and was primarily extracellular matrix. The grafts successfully demonstrated bone generation in a canine alveolar bifurcation defect. Since the injection of growth factors, additional surgery, and the harvesting and culturing of tissues have several drawbacks (one or more of the following: cost, time, requirement for additional surgery, localization of growth factor), a non-invasive method – such as shock waves as proposed herein – would overcome some of these drawbacks and would likely be more cost effective (the current cost of the ESW treatment is on the order of $200 per session).

In medical applications, shock waves are characterized by a high positive pressure acoustic pulse wave (peak pressure 5-120MPa; rise time <100ns; pulse width $\sim$1μs), followed by a lower pressure tensile wave (Gerdesmeyer and Lowell, 2007; Weiss, 2006). Extracorporeal shock wave (ESW) technology has been used clinically since the 1980s, when lithotripters were first used to break up kidney stones (Gerdesmeyer and Lowell, 2007; Strash and Perez, 2002). More recently, ESW therapy has also

shown efficacy for several musculoskeletal disorders, including calcific tendonitis of the rotator cuff, plantar fasciitis, and psuedoarthrosis (Haupt, 1997; Takayama and Saito, 2004). ESWs have been reported to cause periosteal osteogenesis following thickening of the periosteal cambium layer in rats (Takahashi et al., 2004) and rabbits (Tischer et al., 2008). In the rabbit study, the periosteal cambium layer proliferated rapidly and osteogenesis was initiated by day 10. In the rat study, the cambium layer was a cell-rich layer $\sim 400\mu$m thick at day 4, which underwent osteogenesis by day 14.

In this study, we investigated and quantified the proliferative effect of shock waves on rat periosteum. The objectives were to determine the effects of energy flux density (0.15 vs. 0.40 mJ/mm^2) and anatomic location (femur versus tibia) on the periosteal cell number, cambium layer thickness, and inflammatory response. A further objective was to determine if a lower energy flux density than previously described as the minimum (0.5mJ/mm^2; Tischer et al. (2008) in rabbits) could be used to stimulate osteogenesis. All doses used were consistent with treatments currently employed for musculoskeletal disorders clinically (Birnbaum et al., 2002; Gerdesmeyer and Lowell, 2007). The primary goals of this chapter were (1) to demonstrate periosteal cell proliferation following ESW-stimulation; (2) to compare two different anatomic locations; (3) to compare high vs. low (0.40 vs. 0.15mJ/mm^2) energy flux density; and (4) to investigate bone formation intraperiosteally. A secondary goal was to evaluate the inflammatory response and hemorrhage in the samples.

2.2 Materials and methods

2.2.1 Experimental design

The proliferative effect of ESWs on rat periosteum was evaluated at 4 days and 7 days post ESW-treatment. These time points were chosen based on previous reports of a proliferated cell layer at day 4 and osteogenesis initiation by day 7 (Takahashi et al., 2004; Tischer et al., 2008). The ultimate plan to elevate or harvest ESW-stimulated periosteum for bone (and cartilage) reconstruction is predicated on transplanting the

periosteum with its proliferative progenitor cell population prior to the formation of bone (i.e., at day 4).

The study groups were designed to have a minimum of 6 animals per group for analysis. The power calculation was based on determining as significant a difference between treated and control limbs of 30% for select outcome variables (e.g., number of periosteal cells, cambium layer thickness), assuming a standard deviation of 15% and $\alpha = \beta = 0.05$. Problems associated with specimen retrieval and processing resulted in loss of some samples, resulting in an n <6 for a small number of groups.

			Treatment[2]; "Dose"			
Exp.[1]	**Location**	**n**	**Energy Density [mJ/mm^2]**	**Number of Shocks/ session**	**Number of sessions**	**Sacrifice, Days[3]**
1	Femur	8	0.15	1000	3 at 1wk intervals	7
2	Femur	6	0.40	3000	1	4
3	Tibia	6	0.40	3000	1	4
4	Tibia	6	0.15	3000	1	4

Table 2.1 – Rat ESW-study experimental groups: Group 1 was a pilot study that underwent a different treatment regime than the other groups. Group 2 vs. Group 3 was used to compare the effect of high dose ESW on periosteum from two different anatomic locations (femur vs. tibia). Group 3 vs. Group 4 was used to compare the effects of high (0.40mJ/mm^2) vs. low (0.15mJ/mm^2) energy flux density at the same anatomic location (tibia).

Twenty-six rats were used in this study, divided into four experimental groups (see table 2.1). Two electrohydraulic shock wave sources were used: the EvoTron (SANUWAVE Health, Inc., Alpharetta, GA) and the OssaTron (SANUWAVE), both of which have an ellipsoid focal zone approximately 1cm in diameter and 5cm long. In the pilot experiment (Group 1), it was anticipated that ESWs may affect the peripheral nerve of the animals. Lewis rats (female; 12wo; 185-195g) were used for this group as they do not self-mutilate following damage to the peripheral nerve. Based on

[1]Lewis rats were used as pilot animals in Group 1. The other Groups (2-4) used Sprague-Dawley rats.

[2]The energy flux density of 0.15mJ/mm^2 was applied by the EvoTron apparatus and the treatment of 0.40mJ/mm^2 was applied by the OssaTron apparatus.

[3]Time after final treatment session.

treatment doses currently employed for musculoskeletal disorders (Birnbaum et al., 2002), three therapy sessions of 1000 shocks ($4s^{-1}$) were used on this experimental group at 1wk intervals. The 'low-dose' EvoTron source ($0.15mJ/mm^2$) was used to deliver the shock waves at a frequency of $4s^{-1}$. Histologically, the results of Group 1 did not indicate any adverse effects on the peripheral nerve; thus, Sprague-Dawley (S-D) male rats (400-450g) were used for the remaining experimental groups (Groups 2-4) due to their larger size and previous demonstration of periosteal osteogenesis (Takahashi et al., 2004).

In Group 2, the left femur of 6 S-D males was treated with the OssaTron in one session of 3000 shocks ($0.40mJ/mm^2$; $4s^{-1}$; high dose) based on previous data (Takahashi et al., 2004), and sacrificed at day 4. In Group 3, the objective was to evaluate the effects of ESWs on periosteum at a different anatomical position (tibia vs. femur) using the same dose as Group 2 (high dose). The final group, Group 4, examined the effects of ESWs at a lower energy density (3000 @ $0.15mJ/mm^2$) to Group 3, but at the same anatomical location (tibia). The mechanism of ESW-stimulated periosteal cell proliferation is discussed in Chapter 3 and not addressed herein.

2.2.2 Animal model and experimental procedures

All procedures were approved by the VA Boston Healthcare System Institutional Animal Care and Use Committee. Rats were anaesthetized using 2% isoflurane and placed in the prone position in preparation for the shock wave treatment. The pressure in the OssaTron head was adjusted so that the treatment (secondary) focus was centered at the applicator tip, which was coupled with ultrasound gel to the shaved hindlimb. For Groups 1 and 2, the shock wave device was oriented such that the shock wave source was positioned on the lateral side of the femur, angled slightly posteriorly, with the center of the focal zone 2cm distal to the hip joint. For Groups 3 and 4, the device was positioned on the lateral side of the tibia, angled slightly posteriorly, at 1.5cm distal to the center of the knee joint. All doses used are consistent with treatments currently employed for musculoskeletal disorders clinically (Gerdesmeyer

and Lowell, 2007; Takayama and Saito, 2004).

2.2.3 Histological processing and immunohistochemistry

Animals were euthanized by CO_2 inhalation. The femur – or tibia – along with surrounding soft tissue, was resected, fixed in 10% buffered formalin, and decalcified using 10% formic acid. The section of the femur underlying the shock focus was obtained (Groups 1 and 2) using a diamond saw (Buehler Isomet, Lake Bluff, IL), and the cross-sections paraffin embedded. For the tibia samples (Groups 3 and 4), 3 sections were taken: 2 sections were taken at ± 1.5mm from the center of the shock focus; and the third section was taken 4.5 mm proximal to the center of the shock focus. The samples were then embedded in paraffin and the blocks sectioned on a microtome. Seven-μm-thick microtomed sections were deparaffinized and stained with hematoxylin and eosin (H&E) for the identification of cells and with Masson's trichrome for collagen identification.

2.2.4 Histomorphometric analysis

Using H&E stained slides, cell counts were performed on the cambium layer of Groups 2, 3 and 4. Cell counts were taken in an area 50μm wide (along the circumference of the periosteum) and through the entire thickness of the cambium layer (i.e from the cortical bone surface to the periosteal fibrous tissue layer). For the femur, cell counts were made at 8 locations around the circumference of the bone, each spaced at 45°. For the tibia, cell counts were made at 9 locations around the circumference of the bone, each spaced at 40° (see fig.2-2). At each location, a digitized image of the periosteum was taken and ImageJ software (NIH; http://rsbweb.nih.gov/ij/) was used to perform cell counting and layer thickness measurements. All counts were made by the author. Figure 2-2 illustrates the circumferential changes in cell count and cambium layer thickness. On each radial axis – which crosses the bone in the inset micrographs at the location corresponding to where the measurement was taken – the 95% confidence interval of the measurement lies within the bands (blue

= shock; red = control) on that axis. Cell densities were evaluated in cells/μm^2 by dividing the cell count by the area evaluated (50μm x cambium layer thickness). Areas where periosteum was damaged due to processing were omitted from the analysis. If there was bone already formed at a site, the most proximal 50μm band of periosteal cells was measured. For Groups 3 and 4, two-factor analysis of variance (ANOVA) (circumferential position and distance along the tibia) was used to verify that the ESW treated samples at $\pm$ 1.5 mm from the center of the shock focus did not have a statistically different variation in any of the outcome variables, and thus were averaged at each point for analysis.

To compare the side effects of the ESW doses used on various tissues at the two different anatomic locations, the slides were semi-quantitatively analyzed for hemorrhage, inflammation, and bone formation. A grading system was defined as described in table 2.2.

For the femur samples, inflammation and hemorrhage scores were recorded for the anterior half and posterior half; for bone formation analysis, the samples are scored in four quadrants: antero-lateral, antero-medial, postero-lateral, postero-medial. In the tibia, the anterior is defined as 0°, with the angle increasing towards the lateral side, and the shock wave positioned at approximately 120°. Three regions were defined as follows: Region I between 0°and 120°; Region II between 120°and 240°; and Region III between 240°and 0°.

2.2.5 Statistical analysis

All data are reported as mean $\pm$ standard error of the mean (SEM). Paired Student t-tests were used to compare ESW groups with control groups. Two-factor ANOVA with $\alpha = 0.05$ was used to evaluate the effects of ESW and circumferential position on cell count, cambium layer thickness, and cell density. For Groups 3 and 4, two-factor ANOVA was used on the ESW data only to evaluate the effects of circumferential position and distrance from the center of the shock focus on cell count, cambium layer thickness, and fibrous layer thickness. For all tests, p-values of <0.05 were considered significant.

Inflammation Score:	
0	No inflammation
1	1 or more small (barely visible through 10x objective) inflammatory cell infiltrates
2	1 or more medium (visible through 10x objective) inflammatory cell infiltrates
3	1 or more large (immediately visible in 10x objective) inflammatory cell infiltrates
4	Tissue necrosis and/or granulation tissue formation
5	Abscess
Hemorrhage Score:	
0	No hemorrhage
1	1 or more small (barely visible through 10x objective) hematomas
2	1-3 or more medium (visible through 10x objective) hematomas
3	>3 or more medium (immediately visible in 10x objective) hematomas
4	1 or more large (immediately visible in 10x objective) hematomas
Bone Formation Score:	
0	0% bone formation within proliferated periosteum
1	0-10% bone formation within proliferated periosteum
2	11-50% bone formation within proliferated periosteum
3	51-75% bone formation within proliferated periosteum
4	76-100% bone formation within proliferated periosteum

Table 2.2 – Details of scoring scheme used in reporting soft tissue inflammation, hemorrhage, and areal percentage of cambium layer filled with new bone.

2.3 Results

2.3.1 Group 1: Pilot study

H&E stained slides from the center of the shock focus demonstrated histological changes consistent with periosteal osteogenesis and/or persiosteal cell proliferation on the postero-medial side of the bone. In 6 of the 8 treated samples, there was evidence of periosteally deposited bone, which was seen as bone on the postero-medial corner that had formed radially outwards from a basophilic cement line (*viz.* prior bone surface). Since bone surface labeling was not used during the study, this result could

Figure 2-1 ***(facing page)*** – Micrographs of periosteum in the (A, C, E, and G) non-treated control and (B, D, F, and H) ESW-treated limbs of rats in (A, B) Group 1, (C, D) Group 2, (E, F) Group 3, and (G,H) Group 4. Hematoxylin and eosin stain. Black outlines and arrows show the cambium layer periosteal cells. In all ESW treated groups, there is significant thickening of, and proliferation of cells within, the periosteal cambium layer.

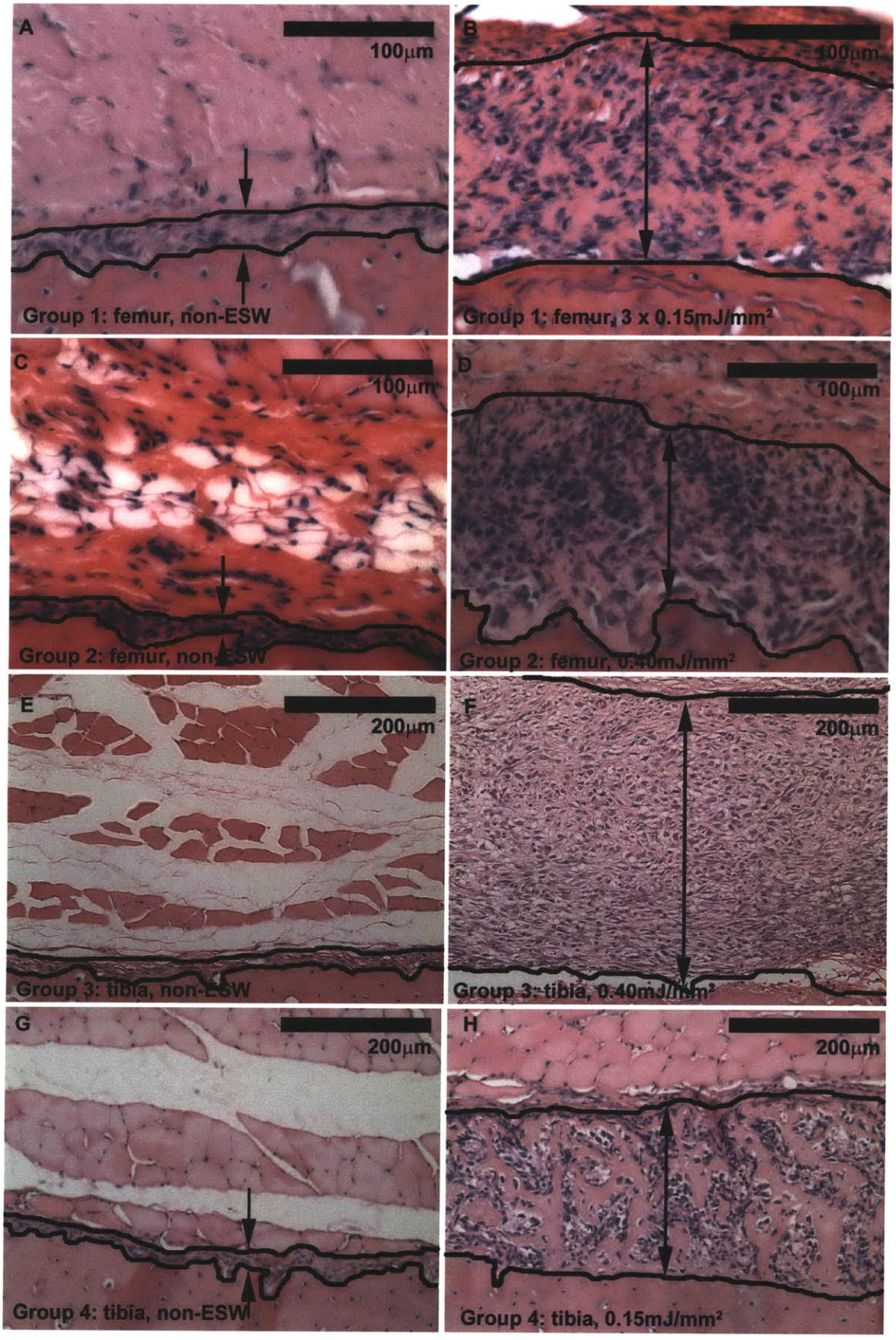
A
100μm
Group 1: femur, non-ESW
B
100μm
Group 1: femur, 3 x 0.15mJ/mm²
C
100μm
Group 2: femur, non-ESW
D
100μm
Group 2: femur, 0.40mJ/mm²
E
200μm
Group 3: tibia, non-ESW
F
200μm
Group 3: tibia, 0.40mJ/mm²
G
200μm
Group 4: tibia, non-ESW
H
200μm
Group 4: tibia, 0.15mJ/mm²

not be confirmed and no statistical analysis was completed. However, this feature was not seen on controls. In the remaining 2 of 8 rats in the pilot study, a markedly thickened periosteum, primarily postero-medially (see fig. 2-1), was observed. The thickened periosteum resulted from proliferation of the cambium layer cells. There were no overt effects under light microscopy of this shock wave dose on peripheral nerves or other tissues within the shock wave focal zone.

Based on our inflammation and hemorrhage scoring system described in table 2.2, all 8 samples scored 0 in the inflammation category and 7 of 8 samples scored 0 in the hemorrhage category. The eighth sample (which had residually thickened periosteum) was scored at 2 for hematoma on the posterior half.

2.3.2 Group 2: Femur, 0.40mJ/mm^2

The ESW-treated limbs displayed a significant (3-fold) increase in the number of cambium cells compared to controls (see table 2.3, fig. 2-1 C and D; and fig. 2-2A). Mitotic figures were evident within the proliferated cambium layer cells of all ESW-treated samples. Within the group of five animals, three of the treated limbs showed a dramatic thickening of the periosteal cambium layer (mean cell count = 64 $\pm$ 3; n = 24); two of the treated limbs had a less dramatic thickening (cell count = 23 $\pm$ 1; n = 16). The increased cell numbers resulted in a significant (approximately 3-fold) thickening of the cambium layer and the cell number density was similar for the ESW-treated and control groups (t-test, p = 0.39). The fibrous layer was found to be significantly thicker for the ESW-treated group (41 $\pm$ 3.8 μm vs. 30 $\pm$ 3.8 μm; n = 30 positions; t-test, p = 0.024). Two-factor ANOVA showed a significant effect of shock on cell count (p <.0001; power = 1.0) and on cambium layer thickness (p <.0001; power = 1), but no significant effect of position, or interaction effect, was found on cell count, cambium layer thickness, or fibrous layer thickness.

Osteogenesis was initiated in just four days in the treated limbs, with small areas of periosteal immature woven bone (ranging from 30μm x 30μm to 140μm x 80μm; see table 2.4) found in the three samples with more pronounced thickening of the periosteum (see fig. 2-3a). No bone formation was seen in the non-treated control

Group	ESW	cell count[1] (mean ± SEM)	n	paired t-test p-value
Group 2: Femur - 0.40mJ/mm^2	Y	47 ± 4	39	<.0001
	N	15 ± 1		
Group 3: Tibia - 0.40mJ/mm^2	Y	89 ± 5	52	<.0001
	N	15 ± 1		
Group 4: Tibia - 0.15mJ/mm^2	Y	43 ± 3	53	<.0001
	N	15 ±1		

Group	ESW	cambium layer thickness (μm; mean ± SEM)	n	paired t-test p-value
Group 2: Femur - 0.40mJ/mm^2	Y	84 ± 9	39	<.0001
	N	26 ± 3		
Group 3: Tibia - 0.40mJ/mm^2	Y	252 ± 14	52	<.0001
	N	29 ± 4		
Group 4: Tibia - 0.15mJ/mm^2	Y	90 ± 8	53	<.0001
	N	20 ± 3		

Group	ESW	Cell Density (10^3 cells/mm^2; mean ± SEM) mean ± SEM)	n	paired t-test p-value
Group 2: Femur - 0.40mJ/mm^2	Y	14 ± 1	39	0.387
	N	16 ± 1		
Group 3: Tibia - 0.40mJ/mm^2	Y	8 ± 0.4	52	<.0001
	N	16 ± 0.9		
Group 4: Tibia - 0.15mJ/mm^2	Y	13 ± 0.7	53	<.0001
	N	19 ± 0.9		

Table 2.3 – Cell counts, cambium layer thickness, and cell density for the center sections from Groups 2, 3, 4. All groups demonstrated significant increases in periosteal cell proliferation and cambium layer thickness following ESW treatment. The tibial groups also demonstrated a significant decrease in cell density following ESW treatment, which is attributed to the increased extracellular matrix formed by the cells as they initiate osteogenesis.

[1] Cell counts were taken in an area 50μm wide and through the entire thickness of the cambium layer (tibia - 9 locations, 40°spacing; femur - 8 locations, 45°spacing).

Rat #:	**Grp. 2 #1**	**Grp. 2 #2**	**Grp. 2 #3**	**Grp. 2 #4**	**Grp. 2 #5**
Inflammation :					
Anterior	0	0	3,4	3,4,5	2
Posterior	3,4	3,4	3,4	3,4	0
Hemorrhage :					
Anterior	0	0	2	0	1
Posterior	1	0	2	3	0
Bone Formation :					
Antero-lateral	0	0	1	1	2
Antero-medial	0	0	1	2	2
Postero-lateral	0	0	1	2	1
Postero-medial	0	0	1	2	1

Table 2.4 – Analysis of inflammation, hemorrhage, and bone formation for ESW treated animals in Group 2 (femur, 0.40mJ/mm^2). Samples typically demonstrated some inflammation in the surrounding soft tissue, and the majority of the samples demonstrated bone formation (refer to 2.2 for scoring scheme).

limbs. Four of the five samples showed some degree of inflammation (graded 3 or 4), consisting of an infiltrate of neutrophils, monocytes, and macrophages that was typically found dispersed around myocytes. Some blood vessels could be identified as having a disrupted epithelium through which the inflammatory cells were escaping; however, many vessels within the shock focus appeared normal and unperturbed by the ESWs.

There were also typically regions of tissue undergoing necrosis, with/without granulation tissue formation, where heavy inflammatory infiltrates were found. One sample had evidence of an abscess within the region of the shock focus. Variable degrees of hemorrhage were identified among the shock samples with four out of five samples graded 1 or more, and two out of five samples graded 2 or 3. The control limbs showed no inflammation or hemorrhage. The shocked sample of one of the six rats was lost during histological processing.

2.3.3 Group 3: Tibia, 0.40mJ/mm^2

The results for this experimental group are reported as: the center group (the averaged values at each position of the ± 1.5mm datasets) and the periphery group (the values from the group 4.5mm proximal to the center of the shock focus).

Shocked samples from the center of the focal zone had a significant (6-fold) increase in the number of cambium layer cells over controls (table 2.3, fig. 2-1 E and F; and fig. 2-2B). Mitotic cells were evident within the cambium layers of all ESW-treated samples. Sections from the periphery had a significant (approximately 5-fold) increase in the number of cambium layer cells over controls (87 ± 7 cells vs. 19 ± 1; n = 52 positions; t-test, p<0.0001). For both groups, the cambium cell proliferation resulted in a thickened cambium layer (center group: 8-fold increase, see table 2.3 & fig. 2-2C; t-test, p<.0001and fig. 2-2C. Periphery group: 270 ± 23 μm vs. 43 ± 4 μm; n = 52 positions; t-test, p<.0001). The cell density was found to be significantly less (by a factor of 1.6-2) for the shock wave groups for both the center data and the periphery data when compared with controls (center group: 8 ± 0.4 x10^3 cells/mm^2 vs. 16 ± 0.9 x10^3 cells/mm^2; n = 52 positions; t-test, p<.0001; periphery group: 7 ± 0.3 x10^3 cells/mm^2 vs. 11 ± 0.7 x10^3 cells/mm^2; n = 52 positions; t-test, p<.0001). The fibrous layer was found to be significantly thicker in the ESW samples (by a factor of 2.5) when compared to controls (center group: 35 ± 1.9 μm vs. 14 ± 1.5 μm; n = 52 positions; t-test, p<.0001. Periphery group: 50 ± 4.6 μm vs. 25 ± 2.7 μm; n = 52 positions; t-test, p<.0001). Two-factor ANOVA (circumferential position and location from the center of the shock wave zone) applied to only the ESW-treated samples revealed a significant effect of circumferential position on cell

Figure 2-2 ***(facing page)*** – Graph of confidence intervals (95%) for periosteal cell counts (A, B, D) and cambium layer thickness (C, E) at positions around the circumference of the bone for the ESW (blue, outer band) and control (red, inner band) groups for: (A) Group 2 (n=5); (B and C) Group 3 center group (n=6); and (D and E) Group 4 center group. The positions at which the radial axes intersect the outer cortex of the inset histological micrographs correspond to the locations where the cell counts were taken (in an area 50μm wide and through the entire thickness of the cambium layer). The shock wave source was aligned with the 120°axis in all groups.

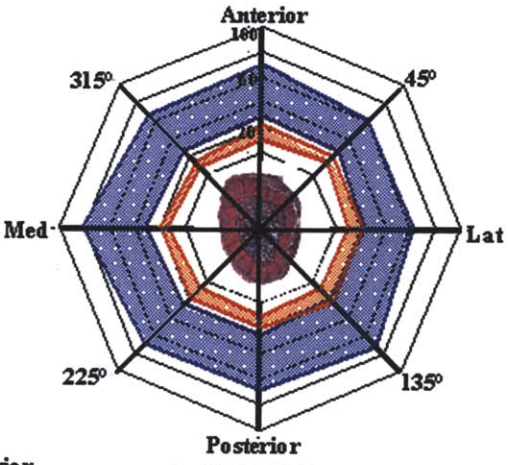

A: GROUP 2

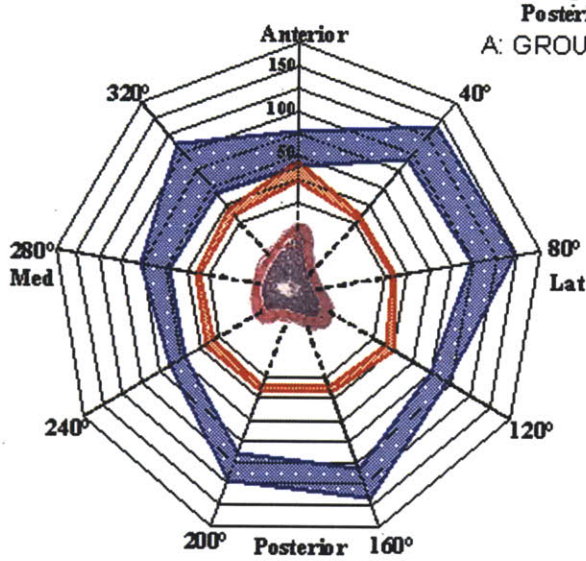

B: GROUP 3

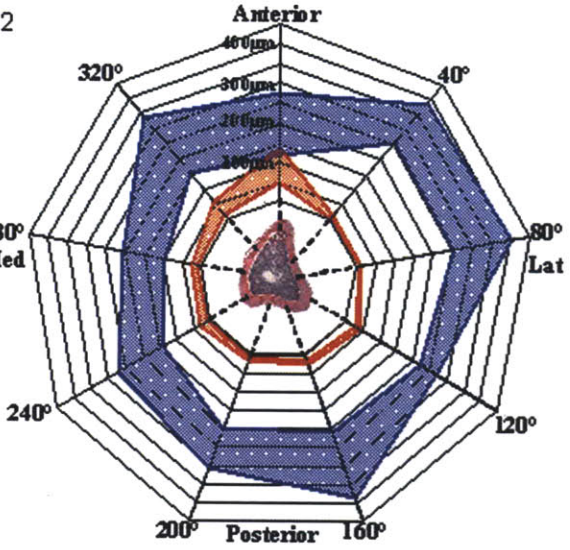

C: GROUP 3

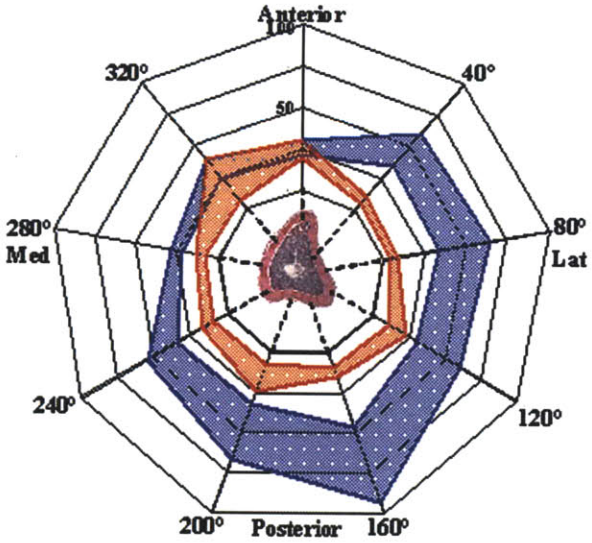

D: GROUP 4

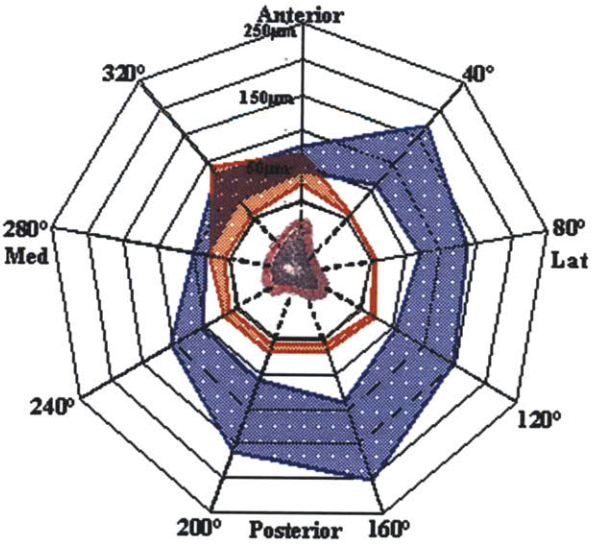

E: GROUP 4

Rat #:	Grp. 3 #1	Grp. 3 #2	Grp. 3 #3	Grp. 3 #4	Grp. 3 #5	Grp. 3 #6
Inflammation :						
Region I	2	3,4	0	3,4	2	1
Region II	2	3,4	3,4	3,4	3,4	2
Region III	1	3,4	3,4	3,4	1	1
Haemorrhage :						
Region I	0	2	0	3	2	2
Region II	4	1	2	4	2	1
Region III	1	1	0	2	1	1
Bone Formation :						
Region I	1	1	2	1	2	1
Region II	0	0	1	0	2	2
Region III	2	1	1	0	2	2

Table 2.5 – Analysis of inflammation, hemorrhage, and bone formation for ESW treated animals in Group 3 (tibia, 0.40mJ/mm^2). The majority of samples demonstrated some inflammation or hemorrhage in the surrounding soft tissue and intraperiosteal bone formation (refer to 2.2 for scoring scheme).

count ($p<0.0001$, power = 1.0) and cambium layer thickness ($p<0.0001$, power = 0.99); and a significant effect of sample height on cell density ($p=0.038$; power = 0.54) and fibrous layer thickness ($p = 0.002$; power = 0.917). All other combinations were not significant, including interaction effects.

There was evidence of osteogenesis within the proliferated periosteum of the treated limbs. The sizes of the immature woven bone areas were similar to those described for treated limbs in Group 2 above. However, small interconnections were seen between the woven bone condensations in this group (see fig. 2-3B). Each of the six rats displayed a grade of at least 1 for the bone formation in the ESW-treated periosteum. No bone formation was seen in the non-treated control limbs (see table 2.5).

There was a variable degree of inflammation for the ESW-treated samples. The makeup and description of the inflammatory response was comparable to that described in Group 2, with at least 1 region in each rat graded 2 for inflammation. There was a variable degree of hemorrhage observed on the slides with each rat displaying a region graded at a minimum of 2.

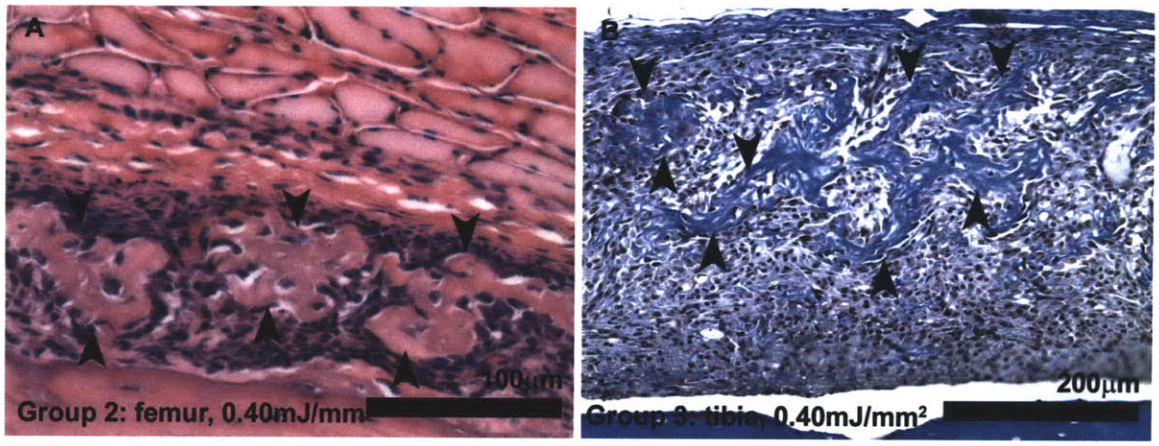

Figure 2-3 – Example of bone formation within proliferated cambium layer of periosteal cells 4 days post-ESW treatment (A) of a femur from Group 2 (H & E), and (B) of a tibia from Group 3 (Masson's trichrome). The Masson's trichrome highlights the dense collagen framework within the woven bone. Arrowheads mark bone edge.

2.3.4 Group 4: Femur, 0.15mJ/mm^2

As in Group 3, the samples from ± 1.5mm from the center of the shock focus were found to have no significant differences using two-way ANOVA and are averaged here and reported as the center group; samples 4.5mm from the center of the shock focus are referred to as the periphery group.

Shocked samples from the center group had a significant (3-fold) increase in the number of cambium layer cells over controls (see table 2.3, fig. 2-1 G and H; and fig. 2-2D). The shocked samples from the periphery group also had a significant (~4-fold) increase in the number of cambium layer cells over controls (62 femur, 0.40mJ/mm^2 6 cells vs. 15 femur, 0.40mJ/mm^2 1; n = 27 positions; t-test, p<0.0001). Mitotic figures were evident within the cambium layers of all ESW treated samples.

For both groups the cambium cell proliferation resulted in a thickened periosteal cambium layer (center group: 4.5-fold increase, see table 2.3 and fig. 2-2E and fig. 2-2C; t-test, p<.0001. Periphery group: 158 ± 14 μm vs. 26 ± 3 μm; n = 27 positions; t-test, p<.0001). The cell density was found to be significantly less dense (by a factor of 1.5-1.7) for the shock wave groups for both the center data and the periphery data (center group: 13 ± 0.7 x10^3 cells/mm^2 vs. 19 ± 0.9 x10^3 cells/mm^2; n = 53 positions; t-test, p<.0001; periphery group: 9 ± 0.6 x10^3 cells/mm^2 vs. 15 ± 0.9

Rat #:	Grp. 4 #1	Grp. 4 #2	Grp. 4 #3	Grp. 4 #4	Grp. 4 #5	Grp. 4 #6
Inflammation :						
Region I	0	0	0	1	0	0
Region II	0	1	0	2	2	2,4
Region III	0	0	0	2	1	1
Haemorrhage :						
Region I	0	0	0	4	0	1
Region II	0	0	0	1	1	1
Region III	0	0	0	0	0	1
Bone Formation :						
Region I	3	2	2	1	2	2
Region II	2	2	2	1	2	2
Region III	0	2	1	2	2	1

Table 2.6 – Analysis of inflammation, hemorrhage, and bone formation for ESW treated animals in Group 4 (tibia, 0.15mJ/mm^2). This group still demonstrated inflammation and hemorrhage; however, it was scored lower than the femur and tibia high dose samples (Groups 2, 3; refer to 2.2 for scoring scheme).

x10^3 cells/mm^2; n = 27 positions; t-test, p<.0001). The fibrous layer was not found to be significantly thicker in the ESW samples when compared to controls (center group: 23 $\pm$ 3 μm vs. 17 $\pm$ 3 μm; n = 52 positions; t-test, p = .005; periphery group: 27 $\pm$ 4 μm vs. 18 $\pm$ 3 μm; n = 27 positions; t-test, p = .018). Two-factor ANOVA (circumferential position and location along the tibia) applied to only the ESW samples revealed a significant effect of circumferential position on cell count (p<.0001, power = 0.99), cambium layer thickness (p = .0089, power = 0.925), and fibrous layer thickness (p<0.0001, power = 1.0); and a significant effect of sample height on cell count (p = .0002, power = 0.984), cambium layer thickness (p<0.0001, power =1.0), and cell density (p = .0001; power = 0.99). All other combinations were not significant, including interaction effects.

There was evidence of early osteogenesis within the proliferated periosteum of the treated limbs. The sizes of the immature woven bone areas ranged from approx. 10μm x 20μm to 80μm x 220μm, with interconnectivity between regions as described previously. The bone formation was graded 2 for at least one region in each of the 6 rats, with the majority of the bone formation found in Regions I and II.

There was a variable degree of inflammation for the ESW-treated samples, with three rats displaying only 1 region (of a total of 9 regions) with any inflammation. The other three rats had at least one region graded as a 2. Of note is that fewer regions of the Group 4 rats displayed no inflammation (10 of 18), compared to the Group 3 results (1 of 18). There was a variable degree of hemorrhage observed on the slides, with three animals displaying no hemorrhage: two with a maximum grade of 1, and only one animal with a region that was graded 4 – only one of six rats had greater than trace hemorrhage in the Group 4 rats, which was a statistically significant decrease from the Group 3 rats (one of six vs. six of six; Fisher's exact test, $p = 0.015$; comparing tables 2.5 vs. 2.6). Hemorrhage, which is an essential aspect of inflammation, was reduced by reducing the ESW dose.

2.4 Discussion

The objectives of this study were to determine the effects of energy flux density (0.15 vs. 0.40 mJ/mm^2) and anatomic location (femur vs. tibia) on the periosteal cambium layer cell number. For all groups evaluated, cambium layer cell counts, and cambium layer thickness, were significantly increased following ESW treatment when compared to controls. The higher dose of ESWs resulted in a thicker periosteum compared to the lower dose (Group 3 vs. Group 4; t-test, $p<.0001$), which is consistent with previous findings (Tischer et al., 2008). However, the results presented here demonstrate a lower threshold for periosteal proliferation ($0.15mJ/mm^2$) when compared with a previous study that reported a minimum energy density of $0.5mJ/mm^2$ was required for periosteal osteogenesis (Tischer et al., 2008). The data presented here show that a lower energy density, which reduces inflammation, can be used to stimulate the cambium cells. Tibial periosteum displayed a greater degree of cellular proliferation in response to ESWs compared to the femur (Group 3 vs. Group 2; t-test, $p<.0001$; tibia vs. femur). The larger amount of soft tissue surrounding the femur may cause more attenuation of the shock wave than occurs for the tibia.

In the pilot study group (Group 1), eight Lewis rats were followed for 7 days after

the last of three ESW sessions, which were performed at one-week intervals. Two of the animals in this group had residually thickened periosteum and the other six animals demonstrated histological changes indicative of periosteal osteogenesis. The differences between the 4- and 7-day sacrifice groups are consistent with previous reports that describe cambium cell proliferation and subsequent osteogenesis, which is initiated by day four (Takahashi et al., 2004; Tischer et al., 2008). In the remaining groups –which were treated in a single session and analyzed at day 4 – the two processes overlap with mitotic cambium cells found concurrently in samples that demonstrated osteogenesis. Although cell mitosis (i.e. proliferation) and osteogenesis are seen at day four in all samples, the tibia sample treated with the lower dose had more than 10% bone in 13 of 18 regions, compared with 7 of 18 for the tibia high dose and 5 of 20 for the femur high dose. Thus, although regions of proliferating cells (cells undergoing mitosis) are seen within a sample at day four, if a smaller control volume is taken, the cells proliferate and then undergo osteogenesis. This osteogenic stimulus is advantageous for bone formation applications, and may exclude the need for regulators that are often necessary for use with mulitpotent MSCs and other cell sources. For the tibial groups – but not the femur group – cell density was found to be reduced when compared to controls. This is attributed to the increased extracellular matrix production contributing to osteogenesis.

Previous reports of ESW-periosteal osteogenesis sectioned the bones in a longitudinal manner, and found increased osteogenesis on the side closest to the shock wave source (Takahashi et al., 2004; Tischer et al., 2008). In this study, bones were evaluated in axial cross-section to investigate circumferential differences in periosteal thickness, which was anticipated due to wave attenuation as it passes through the bone. Group 2 did not demonstrate any significant effect of circumferential position on the cell response, however, Groups 3 and 4 demonstrated a significant effect of position, with increased proliferation and thickening occurring in the regions (I and II) closest to the shock source.

For the tibial samples, the effect of position along the length of the bone was examined by taking 3 sections: two at $\pm$ 1.5mm from the center of the shock focus

and the third at 4.5mm proximal to the center of the shock focus. Based on previous results, we anticipated a tapering effect on the proliferation at positions away from the shock focus. For the higher energy dose (Group 3), no significant effect of height was found, since 4.5mm is just inside the boundary of the shock focus. For the lower energy dose (Group 4), a significant effect of height was found; however, for the samples at 4.5mm proximal to the center of the shock focus had higher values of cambium cell proliferation and thickness. This is indicative of a tapering effect and the reversal in the order may come from the stochastic nature of electrohydraulic ESW generation or to an experimental misalignment of the ESW device. It is noted that there were only 3 ESW samples analyzed for this group (the others were lost to processing), which may skew the results.

In our rat model, we saw varying degrees of inflammation in the surrounding tissue, some of which resulted in necrotic muscle cells and granulation tissue at day four. The degree of inflammation was also dose dependent. For use of ESWs as a periosteal stimulant, it is possible that there is an optimum dosing that strikes a balance between proliferation and inflammation. As stated earlier, the treatments used are within the current ranges employed in the clinic; thus, inflammation may not manifest itself in a clinical setting.

With the exception of a small number of samples – which had an inflammatory cell infiltrate – the fibrous layer was structurally unchanged in the ESW groups when compared with controls. The fibrous layer was found to be slightly increased in the ESW samples of each group, although this was only statistically significant for Group 3. This provides a suturable layer for surgical use, which may be advantageous over mesenchymal stem cells or other cell sources, as the fibrous sheet can act as a delivery vehicle and can support the cells.

This study demonstrated the use of ESW as a non-invasive and rapid way of stimulating the periosteal cambium cells to proliferate. The advantage of the proliferated and thickened periosteal layer is two-fold. First, the proliferated cells provide more cells for surgical or tissue engineering strategies. Second, the thickened layer reduces the technical difficulty in harvesting the periosteal cells for use, which increases the

probability of successful cambium layer – and not just fibrous layer – tissue harvest. Our model proposes a relatively inexpensive, non-invasive, and safe way to stimulate periosteal cell proliferation.

2.5 Summary

This study explored the effects of ESWs on periosteal cambium cell proliferation. The effects of energy flux density on periosteal cell proliferation was studied by comparing a high dose (3000 shocks 0.40mJ/mm^2 energy flux density) to a low dose treatment (3000 shocks 0.15mJ/mm^2 energy flux density) in the rat tibia. Consistent with previous investigations, the higher dose of ESWs resulted in a thicker periosteum compared to the lower dose. However, the results presented here demonstrate a lower threshold for periosteal proliferation (0.15mJ/mm^2) when compared with a previous study that reported a minimum energy density of 0.5mJ/mm^2 was required for periosteal osteogenesis (Tischer et al., 2008). The data presented here demonstrate a lower energy density (down to 0.15mJ/mm^2), which reduces inflammation, can be used to stimulate the cambium cells. The effect of anatomical location was also investigated by applying the high dose to the tibia and femur. Tibial periosteum displayed a greater degree of cellular proliferation in response to ESWs; this was attributed to the increased attenuation of the wave in the larger muscle mass surrounding the femur. In all groups, there was evidence of osteogenesis, seen as small bone islands, within the proliferated periosteal layer. This suggests that ESW stimulates periosteal cells in the rat to undergo osteogenic differentiation.

Chapter 3

Proliferated cells of the periosteum following extracorporeal shock wave therapy: an immunohistochemical study in rats

3.1 Introduction

Chapter 2 described our findings in rat periosteum at day 4 after application of 3000 shock waves at two different energy flux densities (high = 0.40mJ/mm^2; and low = 0.15mJ/mm^2). The results demonstrated robust periosteal cell proliferation, and immature bone formation by day 4. This is consistent with other authors who have reported periosteal osteogenesis following thickening of the periosteal cambium layer in rats (Takahashi et al., 2004) and rabbits (Tischer et al., 2008).

The Takahashi et al. (2004) study was performed in a rat model with a similar energy flux density (0.5mJ/mm^2) to our high dose model. In contrast to our study, however, ESW was applied using an electromagnetic apparatus and the waves applied to the ventral femur. Samples analyzed at day 21 post-ESW demonstrated increased bone mineral content (BMC; 8.46%) and bone mineral density (BMD; 5.8%) for the

ESW-treated samples when compared with controls. In situ hybridization was performed on samples from days 4, 7, and 14 for collagens I (principal collagen found in bone matrix), II (principal collagen found in hyaline cartilage), and X (principal collagen found in hypertrophic and mineralizing cartilage); and for osteoblastic activity (osteocalcin and osteopontin). Immediately following shock wave treatment, the authors reported periosteal separation and subperiosteal hemorrhage adjacent to the exposure site. By day four, there was proliferation of the cambium layer cells and immature bone formation within the periosteum, with markers of osteoblast cell activity (positive for osteopontin, osteocalcin, and collagen X). There were also clusters of round cells (on the side where the ESW-treatment was applied) that had strong expression for collagen II, weak expression of collagen I, and no collagen X, which is indicative of immature chondrocytes. By day seven, there was progression of bone formation and maturation of the chondrocytes, which only expressed collagen II (i.e. they will not differentiate into hypertrophic chondrocytes). By day 14, there was remodeling of the periosteal bone, which was now non-trabeculated, compact bone. Based on these observations, the authors concluded the principal mode of bone formation in the rat following ESW treatment is intramembranous (and not endochondral) bone formation. The authors suggest direct activation of osteoblasts, periosteal separation, or undetectable microfractures, could be the mechanism stimulating periosteal cell proliferation; however, they note that no fractures were observed in any of the samples in the study.

In the Tischer et al. (2008) study, 30 rabbits were given doses of 1500 shocks at an energy flux density ranging from 0 - 1.2mJ/mm^2 and sacrificed at day 10 for analysis. Analysis was performed using epiflouescent illumination (to examine oxytetracycline injections at days 5, 9), contact microradiography, and Giemsa-Eosin staining. Periosteal osteogenesis was found at energy flux densities of 0.5mJ/mm^2 and higher, and the volume increased with increasing dose. Cortical and trabecular fractures and periosteal detachment were observed, but the authors state that periosteal proliferation occurred with minimal production of microfractures and suggest that other molecular mechanisms play a role in releasing growth factors that stimulate bone formation.

Other studies that did not focus on periosteal osteogenesis, but instead investigated the effects of ESW on both physiological and pathological (e.g. acutely fractured) bone, report the release of several growth factors (e.g. TGF-β1, VEGF, and BMP) and secretion of neurotransmitter Substance-P, all of which are known to contribute to osteogenesis and/or neovascularization (Chen et al., 2003, 2004; Maier et al., 2003; Wang et al., 2002, 2003, 2008). These growth factors may be released following the previously mentioned microfractures and periosteal separation, or could result from bone marrow hypoxia, increased regional bloodflow, or a hereto unspecificed "direct cytostimulation" (McClure et al., 2004). In summary, there is still no universal agreement or conclusive evidence on the exact mechanism of periosteal osteogenesis following ESW-treatment.

Unsurprisingly, the field is at a similar position in terms of understanding the mechanism of shock wave repair for other tissues in the musculoskeletal system. Similar effects are proposed: cavitation induced microdamage, which stimulates repair; growth factor release/upregulation; neovascularization; direct cellular effects including membrane damage; and nitric oxide release, which causes vasodilation and increases regional blood flow (Chung and Wiley, 2002; Gerdesmeyer and Lowell, 2007; Takayama and Saito, 2004).

In the previous chapter, we quantified the proliferative effect of shock waves on rat periosteum. In this chapter, the cell population comprising the proliferated periosteal cambium layer is explored. This contributes to our understanding of the effects of ESWs and may help elucidate the mechanism responsible. The phenotype of the various cells was explored using four immunohistochemical markers. Osteocalcin (OCalc) is expressed by osteoblasts and is also found within the bone matrix (Ducy et al., 2000). This stain is used to jointly identify osteoblast cells and to confirm the supposed finding of woven bone reported in Chapter 2. To identify cartilage formation in the periosteal cambium layer, collagen type II (CollII) was stained for. α-Smooth muscle actin (SMA) staining was performed as it is expressed in several connective tissue cells including fibroblasts, chondrocytes, and osteoblasts (Kinner et al., 2002). SMA is expressed during fracture healing by osteoblasts and other cells in the pro-

liferated cambium layer (Kinner et al., 2002) and by migrating endothelial cells (i.e. forming new vessels) (Madri and Marx, 1992). VonWillebrand factor is expressed by endothelial cells and is commonly used as a vessel marker (Wagner, 1990). During angiogenic sprouting, cells at the growing end of the vessel are mitosing and migrating and express a combined endothelial/smooth muscle cell phenotype (i.e. they're positive for SMA and vWF); cells in the pre-existing vessel express an endothelial phenotype (i.e. vWF positive, SMA negative) (Madri and Marx, 1992). That prior work has associated endothelial cells and pericytes with osteogenesis, prompted the evaluation of these cell types in the ESW-proliferated periosteum (Brighton et al., 1992; Diaz-Flores et al., 1992).

3.2 Materials and methods

3.2.1 Experimental design

The rats used in this study were those used in experiment Group 3 (high dose, tibia) as described in Chapter 2. Sections from ± 1.5mm were stained with antibodies for vWF for endothelial cells; SMA for pericytes, migrating/mitosing endothelial cells, and smooth muscle cells; CollII for chondrocytes; and OCalc for osteoblastic cells. The slides were then analyzed semi-quantitatively.

3.2.2 Animal model and experimental procedures

All procedures were approved by the VA Boston Healthcare System Institutional Animal Care and Use Committee. As described in Chapter 2, rats were anaesthetized using 2% isoflurane and placed in the prone position in preparation for the shock wave treatment. The left hindlimb was shaved and ultrasound gel was applied to acoustically couple the skin and shock source. The shock wave device was positioned on the lateral side of the tibia, angled slightly posteriorly, at 1.5 cm distal to the center of the knee joint. The OssaTron was used to deliver 3000 shocks ($0.40 mJ/mm^2$; $4 s^{-1}$; 'high dose') in one treatment session.

3.2.3 Histological processing and immunohistochemistry

Animals were euthanized by CO_2 inhalation at day 4 after ESW treatment. The tibiae and surrounding soft tissue were processed as previously described. Microtomed sections from 1.5mm proximal and 1.5mm distal to the center of the shock focus (and contralateral non-treated controls) were stained with antibodies to the following proteins using immunohistochemistry: SMA, vWF, CollII, and OCalc. Immunohistochemical staining was performed using the LSAB-2 System (Dako, Carpinteria, CA) with a Dako Autostainer. With the exception of the primary antibody and corresponding negative controls, the immunohistochemical processing was identical for each as follows: The deparaffinized and rehydrated sections were digested in 0.1% protease XIV for 40mins, followed by quenching of endogenous peroxidase with 3% hydrogen peroxide (10min). Nonspecific binding was blocked by using protein block serum-free (Dako, Carpinteria, CA: Protein Block Serum-Free X0909) and the slides were then incubated with primary antibody for 15mins (SMA: clone 1A4, monoclonal anti-SMA isotype IgG2A, Sigma A5228, Sigma-Aldrich Corp., St. Louis, MO; CollII: monoclonal anti-Collagen type II isotype IgG2a, obtained from the Developmental Studies Hybridoma Bank, Iowa City, Iowa); or 30mins (vWF: polyclonal anti-vWF antibody, DAKO A0082); or 60mins (OCalc: monoclonal antibody [OC4-30] to osteocalcin isotype IgG2a, abcam ab13418, Abcam Inc., Cambridge, MA) at room temperature. For negative controls, the procedure was identical except that the primary antibodies were replaced with IgG2a mouse negative control for SMA, CollII and OCalc; and negative rabbit control IgG fraction for vWF control (all negative controls were acquired from Dako, Carpinteria, CA) diluted to the same protein concentrations. Sections were then incubated with a biotinylated secondary antibody (15min) followed by streptavidin conjugated horseradish peroxidase (15min; LSAB-2 kit, K0609, Dako, Carpinteria, CA). Labeling was achieved using an aminoethyl carbazole (AEC) chromogen kit (Dako K3461, Dako, Carpinteria, CA). Counterstaining was performed with Mayers hematoxylin.

3.2.4 Histomorphometric analysis

Immunohistochemically stained slides were semi-quantitatively assessed. Three regions were defined as follows: Region I between 0°and 120°; Region II between 120°and 240°; and Region III between 240°and 0°(see Chapter 2, fig. 2-2). The percent of cells staining were evaluated as: 0 - no cells staining; 1 - trace (0-10%); 2 - 11-50%; 3 - 51-75%; and 4 - 76-100%.

3.2.5 Statistical analysis

A contingency table (Fishers exact test) was used to analyze the immunohistochemical data by counting the total number of samples with a 0 or 1 grade (trace staining) and the samples with a 2, 3, or 4 grade (>10% cell expression), and comparing ESW and control groups within each region. For all tests, p-values of <0.05 were considered significant.

3.3 Results

All ESW treated samples demonstrated cambium cell proliferation: the center group of the focal zone had a significant (6-fold) increase in the number of cambium layer cells, and an 8-fold increase in cambium layer thickness, over controls. Immature bone islands were observed at 4 days post-ESW, ranging in size from 30μm x 30μm to 140μm x 80μm, with small interconnections between them (see figure 2-3). Masson's trichrome stain was used to demonstrate the dense collagen framework within the immature trabeculae.

Immunohistochemical staining for osteocalcin

Bone tissue in both the ESW-treated and control tibiae stained positive for OCalc, which served as positive internal controls; all negative immunohistochemical control sections showed no chromogen labeling. Normal bone was found to have OCalc staining within the extracellular matrix (ECM) and within the cytoplasm, or lining the

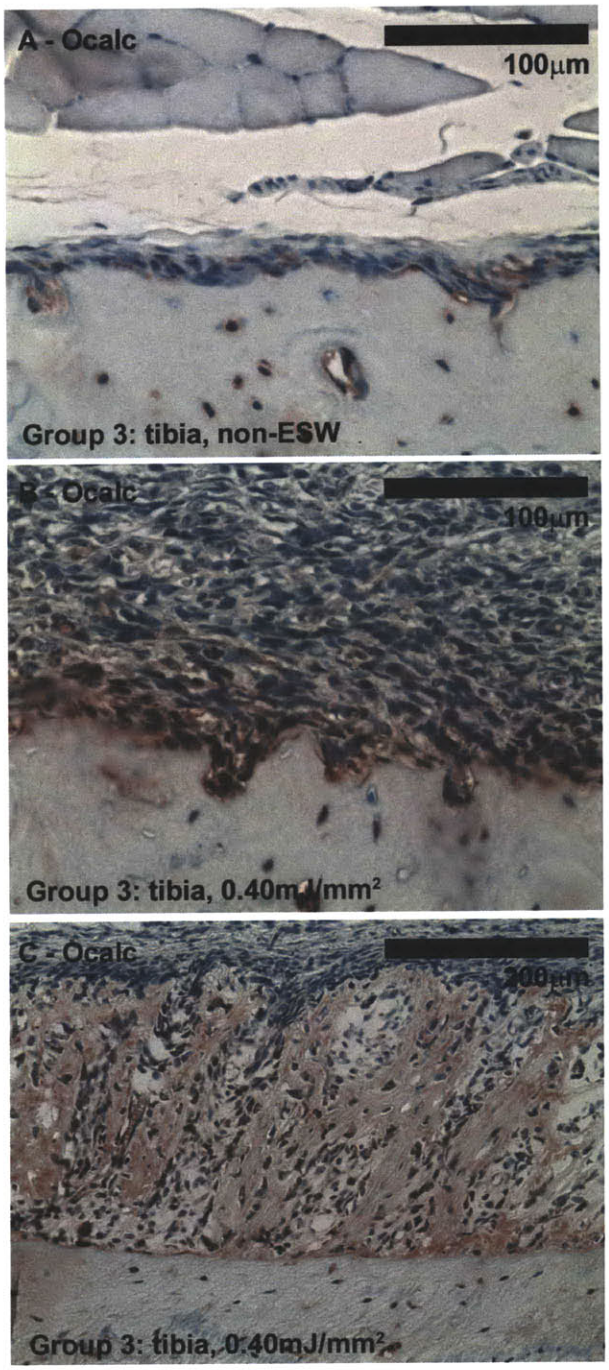

Figure 3-1 – Examples of osteocalcin expression (red chromogen) in (A) normal rat tibia, and expression following ESW (B,C) in Group 3 rats. (A) Osteocalcin staining is found lining the cortical bone surface and in the very inner layer of periosteal cells. (B) Following application of ESWs, cells lining the bone continued to express osteocalcin, although the thickness of this cell layer was increased. (C) Most intraperiosteal trabeculae formed following ESW-stimulation were found to have diffuse or punctate osteocalcin staining.

lacunae, of osteocytes (see fig. 3-1A). In the control (non-ESW) tissue OCalc was found expressed in the normal periosteum to varying degrees but only for cells sitting on the cortical bone surface (see fig. 3-1A; table 3.1). For areas with very thin periosteum, understandably, this results in a high percentage of cells expressing OCalc. For cells that were expressing OCalc, the stain was diffuse within the cytoplasm, or appeared to be diffusing from the cell and lining the cortical bone surface.

For cells in the proliferated periosteum expressing OCalc, it was most commonly found in cells lining the cortical and immature bone. On the cortical bone surface, there was a layer of cells lining the cortical bone surface (5-10 cells thick) that were expressing OCalc. The majority of the immature trabeculae contained OCalc staining, which was typically diffuse within the matrix or in more intense spots of staining (fig.3-1C). This OCalc appeared to be coming from cells trapped within the immature matrix (osteoblasts/osteocytes) or from osteoblasts lining, or in close proximity to the trabeculae, which had OCalc staining in their cytoplasm and in the ECM surrounding them. There was also positive OCalc staining surrounding the fibulae of ESW-treated samples. This staining followed a similar trend as the tibial periosteum, with the immature woven bone and neighboring cells staining positive as well as cells close to the cortical bone surface.

For the thin non-ESW periosteum, most cells on the cortical bone surface stained positive for OCalc (fig. 3-1A). Ten percent or more cells were found to express OCalc in 12 of 18 regions in controls (6 animals, 3 regions per animal; see table 3.1). Eleven of 18 regions in the ESW samples had >10% of cells expressing OCalc within the cambium layer. No statistical difference was found for these samples in any of the regions ($0.28 < p < 0.72$).

Immunohistochemical staining for von Willebrands factor

Endothelial cells and megakaryoctyes showed vWF staining, which served as positive internal controls. There is no evidence in the literature of any non-vascular cells expressing vWF in the periosteum, and thus all positive cells are presumed to be endothelial cells. In non-shocked periosteum, vWF was expressed in vessels or in

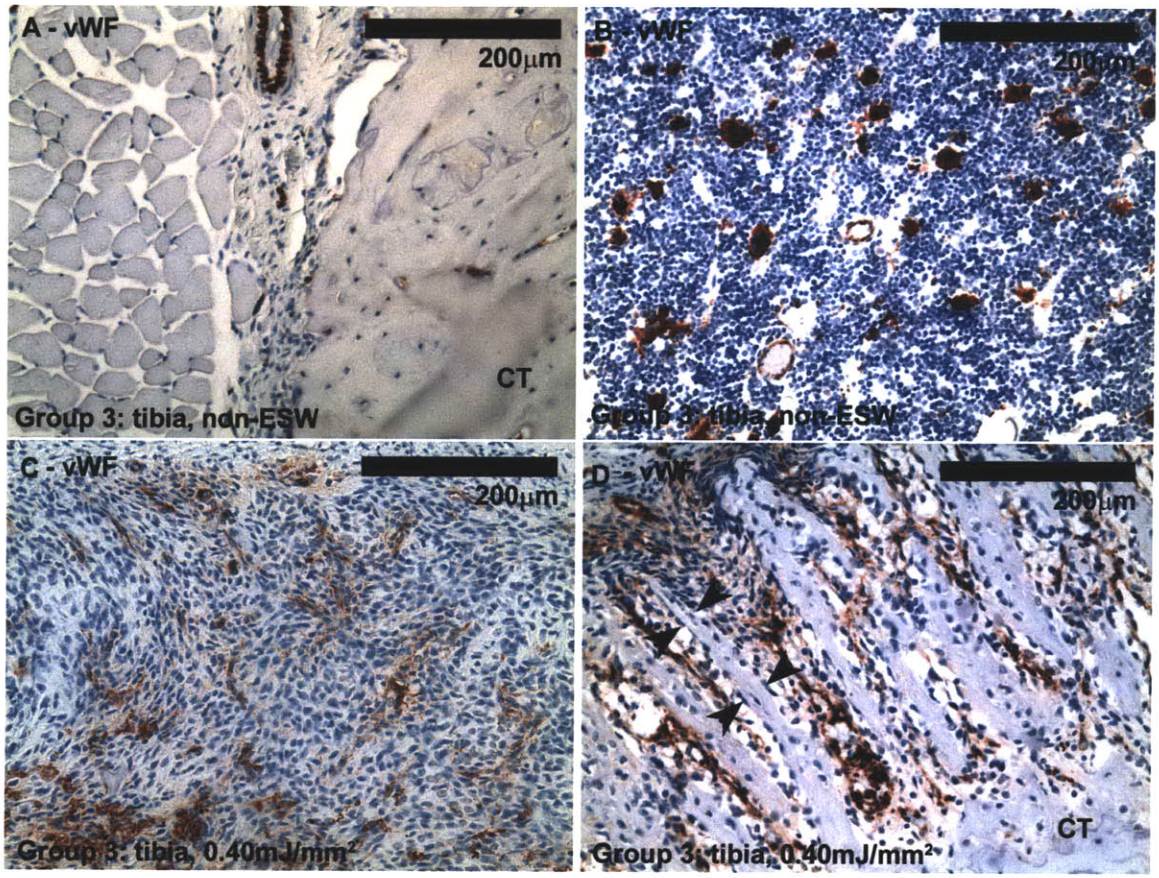

Figure 3-2 – vWF expression (red chromogen) in (A, B) non-ESW treated samples and (C, D) ESW-stimulated samples. (A) Control periosteal tissue shows positive expression in endothelial cells exclusively; and in (B) the marrow endothelial cells and megakaryocytes stain positive. (C, D) vWF expression in cambium layer cells in a section for ESW treated samples in Group 3. In (C) vWF staining is seen throughout the cambium layer cells; in (D) vWF positive cells line spicules of newly forming bone that extend outwards from the cortical bone surface (one of which is marked with black arrowheads, the rest are parallel). CT = cortical bone.

small clumps around individual cells (capillaries).

For cells in the proliferated periosteum expressing vWF, it was often found as a tight ring around the nucleus; for cells with increased expression, a more intense stain was seen as punctate staining in the cytoplasm (fig. 3-2 A, B). When vWF was expressed in endothelial cells, it was an intense signal that filled the majority of the cytoplasm. For the proliferated periosteum, extracellular vWF staining was also found within the matrix (ECM), where it appeared as a faint stain on strands of ECM or as small clumps that (on occasion) were associated with hemorrhage. In the ESW samples, vWF-positive cells were typically dispersed throughout the cambium layer. In some areas, vWF-positive cells lined the newly forming bone trabeculae (Fig. 3-2B). In the soft tissue of the ESW-treated samples, vWF was occasionally expressed by cells in the inflammatory infiltrates.

For the ESW-treated samples, 12 of 18 periosteum regions (see table 3.1) had >10% of cells expressing vWF, compared with 3 of 18 for the control group (see 3-2A, B). Region I was the only region that demonstrated a statistically significant difference by Fishers Exact test ($p = 0.03$; Region II, $p = 0.28$; Region III $= 0.12$).

Immunohistochemical staining for α-smooth muscle actin

Perivascular cells in the SMA-stained slides demonstrated intense SMA staining, which served as positive internal controls; all negative immunohistochemical control sections demonstrated no chromogen labeling. For non-treated samples, non-endothelial vascular cells expressed SMA. When non-vascular cells were SMA positive, they were typically the cells sitting on the the cortical bone surface. In ESW treated samples, cells with positive SMA stain showed chromogen labeling that was intracellular, perinuclear, and typically found on one side of the nucleus (although there was no obvious universal directionality). For cells with high SMA expression, staining was more diffuse within the cell. The location of the SMA-expressing cells varied among the samples, but was typically found in clusters of neighboring cells in different areas within the thickened cambium layer. In some (but not all) cases these groups of cells were those surrounding, lining, or within the regions of immature bone

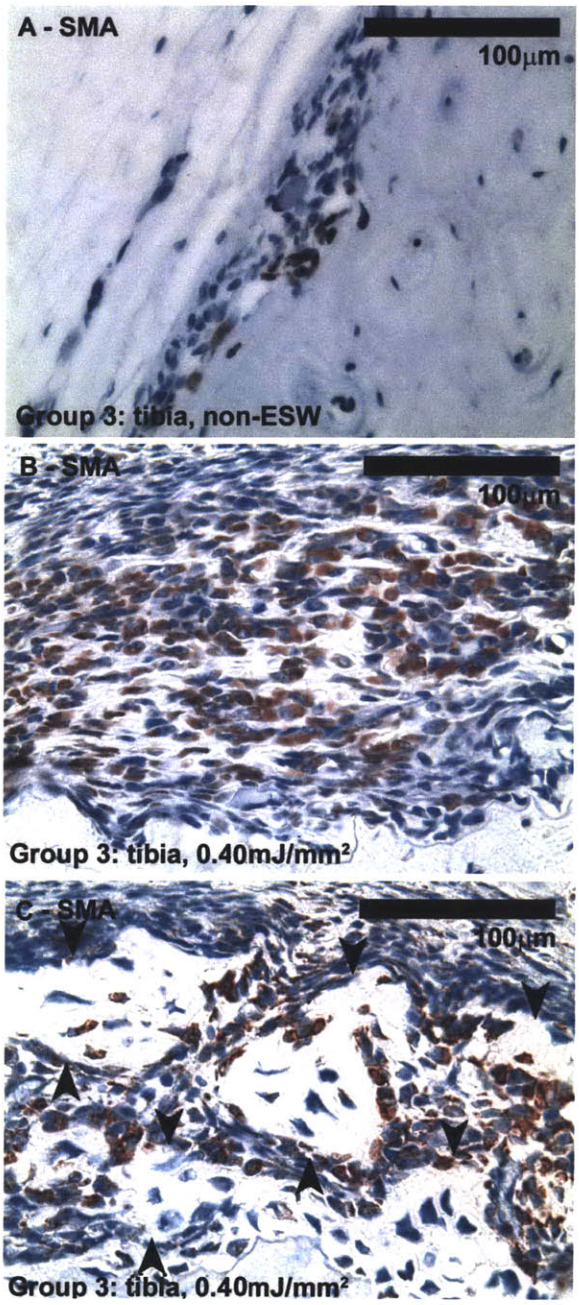

Figure 3-3 – SMA expression (red chromogen) in (A) control and (B, C) ESW-proliferated periosteal cells. The control samples demonstrate chromogen staining around some vessels and in some of the cells sitting on the cortical bone surface. For proliferated periosteum, SMA positive cells were found (B) in proliferated layer without extensive new bone formation, and (C) in cambium layer within and around newly forming bone (arrows).

	Rat #1		Rat #2		Rat 3		Rat #4		Rat #5		Rat #6		
	ESW	CTL	ESW	CTL	ESW	CTL	ESW	CTL	ESW	CTL	ESW	CTL	p
% vWF													
Region I	1	0	2	1	1	1	2	1	2	1	2	1	**0.03**
Region II	1	1	3	1	1	1	3	1	2	2	2	2	**0.28**
Region III	1	0	2	1	1	1	2	1	2	1	2	2	**0.12**
% SMA													
Region I	2	1	2	1	3	0	2	0	1	NA	1	1	**0.045**
Region II	2	1	2	1	3	0	NA	0	1	NA[4]	0	1	**0.08**
Region III	1	1	1	1	1	0	0	0	1	2	1	0	**0.5**
% OCalc													
Region I	1	1	2	2	2	1	2	2	2	2	2	3	**0.5**
Region II	1	1	1	2	1	1	2	2	1	2	2	2	**0.28**
Region III	1	1	3	2	2	1	1	3	2	3	2	3	**0.72**

Table 3.1 – Results of semi-quantitative analysis of vWF, SMA, and OCalc immunohistochemical staining. The percentage of cells staining was evaluated as: 0 = no cells staining; 1 = trace (0-10%); 2 = 11-50%; 3 = 51-75%; and 4 = 76-100%. The p-value is for Fishers exact test, which was calculated by counting the total number of samples with trace staining (0 or 1 grade) and the samples with >10% cell expression (i.e., 2, 3, 4 grade) and comparing ESW and control groups within each region. Region I was significant for both SMA and vWF staining following ESW. Region I = 0 - 120°; Region I = 120 - 240°; and Region3 = 240 - 360° (refer to figure 2 -2). The shock wave entered from approximately 120°. ESW = extracorporeal shock wave; CTL = control; NA = not available.

formation (Fig. 3-3C). Occasional cells within the inflammatory infiltrates of the soft tissue of ESW-treated samples expressed SMA.

For the ESW-treated samples, 7 of 18 regions had more than 10% of cells staining positive for SMA, compared with 1 of 18 for controls (Fig. 3-3; table 3.1). Region I was the only region that demonstrated a statistically significant difference (p = 0.045; Region II, p = 0.08; Region III = 0.5).

Immunohistochemical staining for collagen type II

Articular cartilage from the knee joint of rats was used as a positive control for CollII staining. Neither the proliferated periosteum nor the control periosteum demonstrated any CollII expression.

3.4 Discussion

The objective of this chapter was to begin to identify the various cell types within the periosteal cambium layer - specifically the cell types that are found within the layer

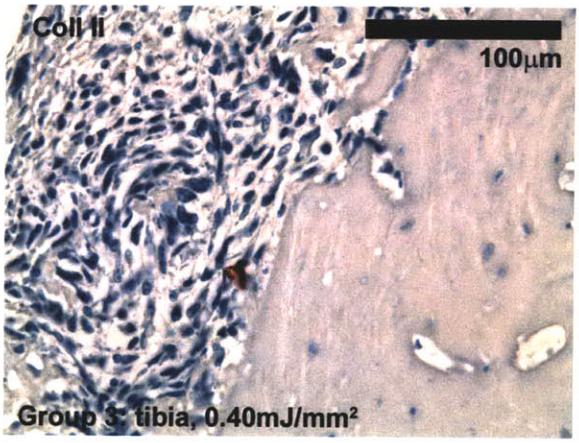

Figure 3-4 – ESW stimulated proliferated periosteum stained immunohistochemically for collagen II: Only one positive cell (red chromogen) was found in the ESW treated samples. The non-ESW control samples also demonstrated no collagen II stain. Articular cartilage from the knee of rat joints stained positive for collagen II.

following ESW stimulation. The periosteal cambium layer cells have been described as MSCs with varying degrees of "stemness" - ranging from being an osteoprogenitor cell population (Bassett, 1962; Hutmacher and Sittinger, 2003; King and Melbourne, 1976) to, more recently, a chondrogenic (Emans et al., 2005; O'Driscoll and Fitzsimmons, 2001) and adipogenic cell population (Choi et al., 2008). Additionally, the periosteum cambium layer, as with most tissues, consists of a subset of vascular and neural cells. Following damage to the periosteum (e.g. fracture), its ability to form cartilage and bone is well known (Hutmacher and Sittinger, 2003; Simon et al., 2003). Following ESWs, osteogenesis – and to a lesser degree chondrogenesis – were found to occur in both rats and rabbits (Takahashi et al., 2004; Tischer et al., 2008).

Our immunohistochemical studies on control/normal periosteum were consistent with previous work. There was a small subset of cells that were SMA positive (e.g. connective tissue cells or perivascular cells); a subset of vWF positive cells, some of which formed distinct vascular lumens; and a subset of ocalc positive cells that lined the bone (i.e. osteoblastic cell phenotype). There was no evidence of CollII cells within the control periosteum tissue.

The ECM and cells in and around the new intraperiosteal trabeculae in treated samples stained positive for OCalc, indicating ESWs stimulate periosteal cells to

differentiate down an osteogenic pathway. There was no evidence of collagen II expression – nor of cells with chondrocytic morphology – in either the normal or ESW treated periosteum, which suggests that the cambium cells in this study underwent intramembranous ossification and not endochondral ossification. This osteogenic stimulus is advantageous for bone formation applications; however, for use of these cells for cartilage regeneration, it may be necessary to harvest the tissue at an earlier timepoint or to treat the periosteum with chondrogenic factors. A previous study of ESW stimulated periosteum in rats also reported intramembranous – and not endochondral – ossification was the primary form of ossification (Takahashi et al., 2004). In contrast to our study, they did find some cells with a chondrocytic phenotype; however these cells never expressed collagen X, and thus did not typify hypertrophic chondrocytes. Further, the chondrocytes were not found in samples at day 14. Since both of these studies were performed in rats, and in the hindlimbs, it is possible there would be more cartilage formation in response to ESW in a different species or bone.

For the majority of the ESW treated slides, SMA expressing cells were found in clusters, typically co-localized with the newly forming intraperiosteal trabeculae. This was not always the case, however, and it is likely that SMA is expressed during different active stages of the process of periosteal proliferation and osteogenesis, as seen in fracture healing studies of SMA (Kinner et al., 2002). VonWillebrand factor was found to be extensively expressed by cells in the proliferated periosteum following ESW. vWF positive cells lined many newly forming bone trabeculae in a pattern indicative of blood vessels. The presence of vWF and SMA within endothelial cells during various phases of angiogenesis has previously been described (Madri and Marx, 1992). At the leading edge, endothelial cells are found to express both SMA and vWF concurrently; once there is lumen formation, the cells express vWF but not SMA (Madri and Marx, 1992). In the proliferated periosteum of these samples, there are some regions with higher vWF expression than SMA expression, which suggests that there has been rapid vascularization of these regions in just four days. Collectively, these data indicate the ESW-stimulated cambium layer contains SMA and vWF positive cells, which may reflect proliferating vascular cells. Future studies

are needed to determine the role of these cells in ESW-promoted osteogenesis.

Early studies believed microfractures and/or elevation of the periosteum were possible mechanisms of ESW stimulated osteogenesis. More recent studies do not suggest these were the primary stimuli for periosteal osteogenesis (McClure et al., 2004; Takahashi et al., 2004; Tischer et al., 2008). In the Takahashi et al. (2004) study, no fractures were found in rats, and the McClure et al. (2004) study did not find any fractures in horses. The Tischer et al. (2008) study did observe microfractures in rabbits; however, the authors did *not* believe that they were the primary stimulus. The McClure et al. (2004) study – which used an equine model for ESW-periosteal osteogenesis – also performed periosteal elevation (surgically) in the same animals that were treated with ESW. They found the osteogenic stimulus from ESW was greater than that achieved with the periosteal elevation alone, and concluded that a hereto undescribed mechanism that acted at the cellular level was responsible for the proliferation. In this study, there were no microfractures found in any of the samples on light microscopy, and although there was subperiosteal hemmorhage (i.e. a possible indicator of prior periosteal elevation) in a small subset of samples, this did not coincide with areas that had the most dramatic proliferation. The studies that reported periosteal elevation reported it as an immediate response to ESW (i.e. no longer present at day 4), which we did not examine. However, combining our data with previously published reports, it does not seem likely that microfractures or periosteal elevation are exclusively responsible for the cambium cell proliferation.

Of note from previous studies (both in bone and in other musculoskeletal models) is the localized increase in vascularization following ESW (Gerdesmeyer and Lowell, 2007; Shrivastava and Kailash, 2005; Takayama and Saito, 2004). In our ESW-treated periosteal samples, 12 of 18 regions (6 rats, 3 regions per rat) had >10% vWF postive cells, compared to 3 of 18 for controls; however, only Region I was found to be statistically significant. As a marker of vascularization, these cells demonstrate the strong vascular contribution to periosteal osteogenesis. Previous studies have espoused the contribution of endothelial cells and pericytes (which line the newly forming vessels), to osteogenesis – suggesting they differentiate to an osteoblast phenotype (Brighton

et al., 1992; Diaz-Flores et al., 1992). The idea of endothelial cells being a multipotent stem cell that could differentiate into osteoblasts, chondrocytes, and adipocytes, was also recently reported (Medici et al., 2010). Although this data cannot conclusively prove the hypothesis that the increased endothelial cell population differentiated into an osteoblastic cell following ESW, the large percentage of vWF positive cells within the proliferated cambium cell population suggests neovascularization following ESWs may play a central role in periosteal osteogenesis. The mechanism of stimulation of neovascularization following ESWs is still not understood.

3.5 Summary

Chapter 2 demonstrated the robust proliferation of periosteal cambium cells following ESW-treatment. In this study, the cell population was interrogated using immunohistochemical staining. The results demonstrated a population of osteoblastic cells, endothelial cells, and smooth muscle actin positive cells, which may be activated osteoblasts, migrating endothelial cells, or other types of connective tissue cells. The OCalc stain, which was found within the immature bone trabeculae, confirmed this was an osseous matrix as predicted from the H&E and Masson's trichrome results (Chapter 2). No collagen II postive cells – or cells that had a chondrocytic morphology – were found within the proliferated cambium layer, and it was concluded that ESWs applied to rat periosteum are not a stimulant of chondrogenesis. Further, consistent with previous reports, intramembranous – and not endochondral– ossification appears to be responsible for the immature osteogenesis that is observed within the proliferated periosteum. The data did not show any microfractures at day 4 and does not support the hypothesis that this is the mechanism responsible for ESW-stimulated osteogenesis. Most strikingly, the data shows a strong contribution of endothelial cells to the cell population. These cells have previously been described as osteoprogenitor (chondroprogenitor, and adipoprogenitor) cells, and it is possible that the stimulation of neovascularization associated with ESWs plays a central role in osteogenesis. Further studies are needed to substantiate this claim.

Chapter 4

The application of extracorporeal shock wave thickened periosteum to bone tissue engineering: in situ and free graft models in the rabbit

4.1 Introduction

Bone is one of the more regenerative of the musculoskeletal tissues due to its vascular network and its constant turnover throughout life (Trueta, 1963). However, following large losses of bone (e.g., mandibular resorption, osteolysis, severe fractures, and bone tumor resection) there is an insufficient framework for tissue repair (Bruder and Fox, 1999; Burg et al., 2000; Hutmacher, 2000; Laurencin et al., 1999; Muschler et al., 2004). The current clinical gold standard is to treat these defects with autografts; however, autografts are known to to undergo resorption at the treatment site, cause morbidity at the harvest site, and the volume that can be treated is limited in size by the harvest volume (Bruder and Fox, 1999; Burg et al., 2000; Laurencin et al., 1999; Vermeeren et al., 1996). Furthermore, autografting requires an additional surgical procedure and this may be technically challenging in certain situations (e.g., dental

surgeon requiring non-oral bone source) (Burg et al., 2000; Laurencin et al., 1999).

Unsurprisingly, there have been numerous approaches to treating these defects with various tissue engineering approaches that combine one or more components of the tissue engineering triad: cells, scaffolds, and growth factors (Bruder and Fox, 1999; Burg et al., 2000; Hutmacher, 2000; Langer and Vacanti, 1993; Laurencin et al., 1999; Muschler et al., 2004). In vitro tissue generation prior to implantation is advantageous as the culture environment, shape, and load bearing, can be carefully controlled (Bruder and Fox, 1999; Hutmacher, 2000; Langer and Vacanti, 1993; Laurencin et al., 1999; Muschler et al., 2004). These strategies are expensive; moreover, there are technical challenges upon implantation (especially for larger defects): mantaining cell viability, revascularizing the tissue, and integrating the tissue biologically and mechanically (Hutmacher, 2000; Muschler et al., 2004). In vivo engineering of bone using strategies that combine porous ceramic, or demineralized bone, scaffolds with marrow derived stem cells and/or bone morphogenetic proteins has been more successful (Bruder and Fox, 1999; Burg et al., 2000; Hutmacher, 2000; Laurencin et al., 1999; Muschler et al., 2004). However, these strategies can be complex and costly, and they require careful management.

The periosteum is comprised of two layers of tissue: the inner cambium layer, which consists of progenitor cells, and the outer fibrous layer comprising fibroblasts. Periosteal cambium cells are promising for bone tissue engineering applications because of their ability to proliferate, their osteogenic potential, and their accesibility (Arnsdorf et al., 2009; Choi et al., 2008; Cohen and Lacroix, 1955; Hutmacher and Sittinger, 2003). The thinness of periosteum can be advantageous as it can be quickly revascularized. However, for applications dependent on its progenitor cells, periosteum is typically limited by its low cell number (2-5 cells), which also makes its harvest technically difficult (O'Driscoll, 2001). To overcome this drawback, various strategies have been developed to increase the cambium cell number by surgical trauma, culture, or growth factor injection (Arnsdorf et al., 2009; Hutmacher and Sittinger, 2003; Mizuno et al., 2006; Reinholz et al., 2009; Simon et al., 2003; Stevens et al., 2005). The overall goal of this chapter is to demonstrate the efficacy of an ESW-thickened

periosteum as an overlay on a porous calcium phosphate scaffold for the orthotopic growth of bone.

The work performed in rats described in Chapter 2 demonstrated robust periosteal cambium cell proliferation just 4 days after application of extracorporeal shock waves (ESW) at 0.40mJ/mm^2 energy flux density to the tibia. The immunohistochemical descriptions of this tissue in Chapter 3 demonstrated that the tissue was differentiated down an osteogenic pathway. This prompted the investigation of the use of the ESW treated periosteal tissue as a cell source for bone tissue engineering. In this study, we examined the suitability of ESW-stimulated periosteal cells combined with a porous calcium phosphate scaffold for orthotopic bone growth in rabbits both in situ and as a free flap. A rabbit model was chosen over the rat model due to their larger size, which facilitated implantation of larger scaffolds. The overview of our therapeutic approach is represented schematically in figure 4-1.

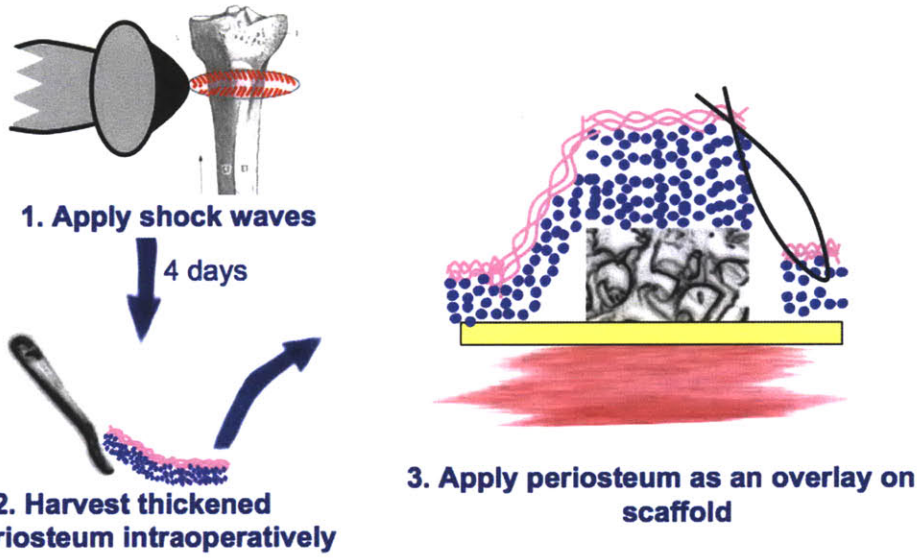

Figure 4-1 – Schematic overview of proposed therapeutic approach: ESW therapy will be applied at day 0 to stimulate periosteal cell proliferation. At day 4 post-ESW, the cells are elevated (or harvested as a free graft) and overlaid on a porous calcium phosphate scaffold.

The chapter is divided into three studies. The first study (S1) used 6 animals and ESW-stimulated (3000 shocks at 0.40mJ/mm^2 energy flux density applied to the medial tibia) was elevated in situ and an anorganic bovine bone scaffold implanted

subperiosteally at 4 days post-ESW. The results of this study demonstrated an improper alignment calibration for the ESW device, which was corrected for the second study.

In the second study (S2), there were 4 groups. The first two groups were used to compare ESW-treated periosteum (3000 shocks at 0.40mJ/mm^2 energy flux density applied to the medial tibia) with non-ESW treated (control) periosteum. The second two groups in this study compared the osteogenic response of ESW-treated and control periosteum following subperiosteal implantation of a bovine bone scaffold at day 4. The animals were sacrificed for analysis at 2wks post scaffold implantation.

In the third study (S3), there were 3 groups, all of which used periosteal free grafts. In the first group of S3, control (non-ESW) periosteum was transplanted as a free autograft onto the upper surface of an anorganic bovine bone scaffold, which was implanted in the medial proximal tibia and was flush with the outer cortical bone surface. The periosteal graft was sutured to surrounding periosteum. The second group of S3 was identical, with the exception that ESW-stimulated periosteum was used as the free autograft (at 4 days post-ESW-treatment). In the final group of S3, ESW-stimulated free autografts were transplanted to the ipsilateral femur and tied down to an anorganic bovine bone scaffold. This scaffold was placed in the medial condyle of the femur and extended above the height of the cortical bone surface. The periosteum was tied to the block and not in contact with the surrounding periosteal tissue, which had been surgically retracted from the implant site.

Animals were sacrificed 4 days post-ESW treatment, or 2wks post scaffold implantation, and evaluated qualitatively using microCT. Histology was performed on decalcified sections from all groups; histomorphometric analysis was performed on the S2 groups to quantify the tissue response.

4.2 Materials and methods

4.2.1 Experimental design

32 Adult New Zealand White Rabbits (4-4.5kg) were used in total, divided into 3 studies. The studies and their groups are described in table 4.1.

For all groups that had ESW treatment, the treatment used was the most proliferative treatment found in the rat studies reported in Chapter 2: 3000 shocks at an energy flux density of 0.40mJ/mm^2 applied to the medial proximal tibia[1]. For all groups that had a scaffold implant, a calcium phosphate scaffold was used. The scaffold material was provided by Geistlich (Geistlich Pharma, Switzerland) and consists of anorganic bovine bone. The scaffold was chosen based on its previous successful demonstration of periosteal bone formation following subperiosteal implantation (Simion et al., 2006).

Study 1 (S1) consisted of one group (S1.A), which was used to develop the ESW treatment and surgery techniques for periosteal elevation. The ESW-stimulated periosteum was elevated off the bone at 4 days post-ESW, and a pocket created wherein an anorganic bovine bone scaffold (Geistlich, Switzerland) was placed (5.5mm ⌀x 1.65mm deep) and the periosteum sutured back to surrounding periosteal tissue. A variation in the results of this group was observed and attributed to improper (z-direction) alignment of the shock wave focal zone. This was corrected in Study 2.

Study 2 (S2) consisted of 4 experimental groups. Groups S2.A and S2.B were used to compare the control periosteum (S2.A) and ESW-stimulated periosteum (S2.B) at day 4 post-ESW, and to confirm the proliferative effect of the selected treatment dose (3000 shocks at an energy flux density of 0.40mJ/mm^2). S2.C and S2.D were used to compare the response of control (S2.C) and ESW-stimulated periosteum (S2.D) to subperiosteal scaffold implantation. The scaffold/surgery was identical to that described for S1.A, with the exception that the z-positioning (penetration depth) of the ESW focal zone was corrected for.

[1]In chapter 2 the treatment was applied to the lateral side of the tibia, with the periosteum closest to the shock wave source proliferating the most. Since the medial side is most commonly used for periosteal graft harvest ESW-treatment was applied to the medial side in for these studies.

	Description	ESW	n
Study 1 (S1): Pilot shock wave stimulated periosteum + subperiosteal scaffold study			
Grp. S1.A	**Pilot shock wave (ESW) + subperiosteal scaffold group:** At day 4 post-ESW, a scaffold was implanted under ESW-stimulated periosteum. Animals are sacrificed at 2 wks post-op.	3000 shocks 0.40mJ/mm^2	6
Study 2 (S2): Histomorphometrically analyzed ESW vs. control periosteum groups with and without subperiosteal scaffold.			
Grp. S2.A	**Non-ESW (control) group:** untreated contralateral limbs from Group S2.B animals	None	6
Grp. S2.B	**ESW-periosteum group:** Animals are sacrificed 4 days post shock	3000 shocks 0.40mJ/mm^2	6
Grp. S2.C	**Control periosteum + subperiosteal scaffold group:** scaffold was implanted under control periosteum (medial proximal tibia). Animals are sacrificed at 2 wks post-op.	None	6
Grp. S2.D	**ESW-periosteum + subperiosteal scaffold group:** At day 4 post-ESW, scaffold was implanted under ESW-stimulated periosteum. Animals are sacrificed at 2 wks post-op.	3000 shocks 0.40mJ/mm^2	6
Study 3 (S3): Free periosteal graft studies			
Grp. S3.A	**Free control periosteal autograft transplanted onto scaffold in contralateral tibia:** Free (non-ESW) periosteal graft was transplanted to scaffold implanted in contralateral proximal tibia, which was aligned with outer cortical bone surface. Periosteum was sutured to surrounding periosteum at implant site. Animals are sacrificed at 2wks post-op.	None	2
Grp. S3.B	**Free ESW-stimulated periosteal autograft transplanted onto scaffold in contralateral tibia:** 4 days post-ESW, free periosteal graft was transplanted to scaffold implanted in contralateral proximal tibia, which was aligned with outer cortical bone surface. Periosteum was sutured to surrounding periosteum at implant site. Animals are sacrificed at 2wks post-op.	3000 shocks 0.40mJ/mm^2	4
Grp. S3.C	**Free ESW-stimulated periosteal autograft transplanted onto scaffold in ipsilateral femur:** 4 days post-ESW, free ESW-stimulated periosteal autograft was transplanted to scaffold implanted in distal femur that extends above cortical bone surface. Periosteum ws tied onto graft and not sutured to surrounding periosteum, which has been surgically retracted from implant site. Animals are sacrificed at 2wks post-op.	3000 shocks 0.40mJ/mm^2	2

Table 4.1 – Experimental groups for the Chapter 4 animal studies. S1 was used to evaluate the ESW-treatment conditions and positioning, and surgical technique. S2 groups, which evaluated the periosteal response in situ, were analyzed hisotmorphometrically to quantify the tissue responses. S2.A vs. S2.B were used to compare ESW-stimulated periosteum with control periosteum; S2.C vs. S2.D were used to compare the response of ESW-stimulated and control periosteum to subperiosteal scaffold implantation. S3 consisted of 3 groups, which evaluated the response of free periosteal autografts. S3.A vs. S3.B compared the response of control and ESW-stimulated free periosteal autografts transplanted to scaffolds in the contralateral tibia and sutured to surrounding periosteum. S3.C evaluated the response of a free ESW-stimulated periosteal autograft transplanted to the ipsilateral femur, but onto a scaffold that extended past the cortical bone surface, and not sutured to surrounding periosteum.

S2 groups were all analyzed histomorphometrically using H&E stained slides of decalcifed sections and were designed to have 6 animals per group. The power calculation was based on determining as significant a difference between treated and control limbs of 30% for select outcome variables (e.g., callus total area, percent scaffold filling), assuming a standard deviation of 15% and $\alpha = \beta = 0.05$.

Study 3 (S3) consisted of 3 groups. Groups S3.A and S3.B were used to compared control (S3.A) and ESW-stimulated (S3.B) free periosteal autografts transplanted to the contralateral tibia. In S3.A (n = 2), control periosteum was harvested from the medial tibia as a free graft and transplanted to the contralateral medial proximal tibia. The implant site was prepared by drilling a defect 5mm ⌀ in the right medial tibia. The defect was filled with the anorganic bovine bone scaffold (4.9mm ⌀), which was push-fit into the defect and aligned with the cortical bone outer surface medially and touched the lateral cortical bone inside the marrow cavity for stabilization. The periosteal transplant (8mm ⌀, from the contralateral tibia) was overlaid on the scaffold and sutured to the surrounding periosteum, which was retracted very slightly from the defect. S3.B (n = 4), underwent the same surgery and treatment with the exception that ESW-stimulated periosteum was used for the free graft at 4 days post-ESW treatment (3000 shocks 0.40mJ/mm^2).

In S3.C (n = 2), ESW-stimulated periosteum was transplanted to the ipsilateral femur at 4 days post-ESW (3000 shocks 0.40mJ/mm^2). For this group, the defect was placed in the distal femur (5.8mm ⌀ x 3.0mm deep) and the scaffold (5.8mm ⌀ x 4.5mm deep) was placed so that it was raised 1.5mm above the bone surface. The periosteum was tied down on top of the scaffold but not attached to the surrounding periosteum, which was trimmed away from the implant site region.

4.2.2 Animal model, shock wave application, and surgery

All procedures were approved by the VA Boston Healthcare System Institutional Animal Care and Use Committee.

Shock wave application

Shock waves were applied as previously described in the rat study. Briefly, the ESW treatment was applied using the OssaTron (SANUWAVE Health, Inc., Alpharetta, GA) operating at 28kV (energy flux density of 0.40mJ/mm^2). The rabbit was anaesthetized using Ketamine (10mg/kg) and ace promazine (0.5mg/kg) for induction and given isoflurane (1-2%; endotracheal intubation) and O_2 throughout the procedure. The pressure in the treatment head was adjusted to ensure the secondary focus was centered at the applicator tip, which was coupled to the shaved medial proximal tibia using ultrasound gel. Note that for Group S1.A, this adjusment was not calibrated for before each treatment, but this was corrected for in S2. The device was oriented perpendicular to the rabbit femur and positioned along the centerline of the medial aspect of the tibia (approximately 10mm from the patellar tendon midline) at 17.5mm distal to the center of the knee joint (approximately 7.5mm up from the base of the tibial tuberosity). 3000 shocks were delivered (4s$^-$1) in one treatment session. Ketofen was given for 24hrs post-ESW (subcutaneously 2mg/kg).

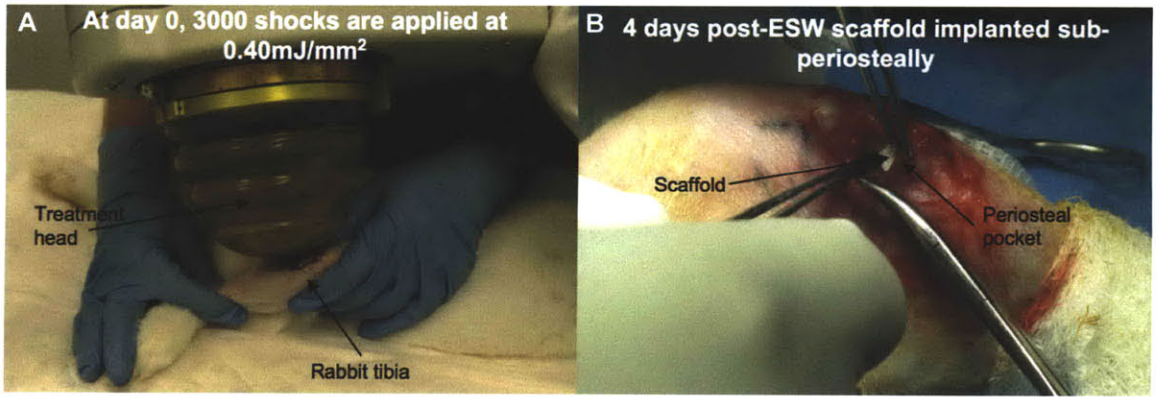

Figure 4-2 – Photographs of rabbits undergoing treatment in Study 2: (A) ESW treatment being applied to rabbit medial tibia. (B) 4 days post-ESW treatment, a periosteal pocket was created and a porous calcium phosphate scaffold was implanted subperiosteally.

Scaffold preparation

The calcium phosphate scaffolds used in this study consist of anorganic bovine bone with pore sizes distributed from 200 - 800μm. The scaffolds were provided by Geistlich (Geistlich Pharma, Switzerland) as blocks measuring 1cm x 1cm x 2cm. To prepare them for implantation, the scaffolds were sliced to the correct depth using a diamond saw (Buehler Isomet, Lake Bluff, IL) with water as a lubricant, operating at 325rpm.

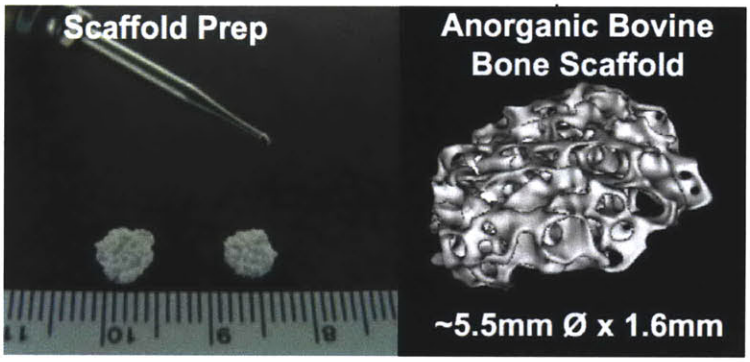

Figure 4-3 – Calcium phosphate anorganic bovine bone scaffolds prepared for the Study 2 surgeries (Groups S2.C,D). (A) Scaffold and burr following preparation. (B) MicroCT image of the scaffold demonstrating its porous architecture (200 - 800μm diameter pores) in 3-D.

The scaffolds for the S2 groups were trimmed to 5.5mm diameter using a burr operating at slow speed. Water was used as a lubricant. For the S3 groups, the cylinders were cored out using disposable skin biopsy punches (Integra Miltex Inc., York, PA) as a trephine in a drill press. The drill was operated at slow speed and water was used as a lubricant.

All scaffolds were sterilized with Sterrad sterilization (Brigham & Women's Hostpital, Boston, MA), which uses low-temperature, hydrogen peroxide gas plasma technology to sterilize medical equipment.

Surgery

Study 2: Groups S2.C and S2.D

The rabbits were anaesthetized as described for ESW application above and all surgical procedures were carried out under sterile conditions. A 1.5cm skin incision – on the medial side of the ipsilateral limb that the ESW dose was applied to – was made, and the tibia medial condyle (periosteal harvest site) was exposed (only a thin layer of fascia underlies the skin). Using a scalpel, the periosteum was scored in an arc above the implant site (i.e. on the side of the implant most proximal to the knee joint). A periosteal elevator was used to elevate the periosteum and create a pocket for the implant. The periosteal elevator was used to scrape the cortical surface after elevation of the periosteum in an attempt to remove all cells down to the cortical bone surface. The implant site was lubricated with saline, and the scaffold was placed into the periosteal pocket. The elevated periosteum was then approximated to the local periosteum using 4 x 6-0 sutures. The soft tissues and skin were replaced and sutured closed. Ketofen (2mg/kg) and cefazolin (20mg/kg) were given subcutaneously for 48 hrs post-op and animals were sacrificed at the end of 2wks.

Study 3: Groups S3.A, S3.B, and S3.C

The rabbits were anaesthetized as described for ESW application above and all surgical procedures were carried out under sterile conditions. A 1.5cm skin incision – on the medial side of the ipsilateral limb that the ESW dose was applied to – was made, and the tibia medial condyle (periosteal harvest site) was exposed (only a thin layer of fascia underlies the skin). The circumference of the periosteal graft was scored using an 8mm biopsy punch and the graft was elevated off the bone using a periosteal elevator. The periosteum was flattened (the periosteum contracts immediately following release from the bone), placed on a sterilized tongue depressor, and stored in saline while the implant site was prepared.

With the exception of the scaffold and defect size differences (described in the *Experimental design* section above), the surgical technique for groups S3.A, B (tibia

implant), and S3.C (femur implant) were identical as follows. A 1.5cm incision was made at the implant site, and the skin and musculature retracted laterally to expose the implant site. The local periosteum was removed where the defect was to be drilled (note that for the tibial implants (S3.A,B) the local periosteum was maintained as best as possible around the defect site; for the femoral implant (S3.C), the local periosteum was removed in a region equal to the scaffold diameter + 3mm). A surgical drill, with a stop for the appropriate depth, was used to create the defect. The defect was reamed out in the femoral samples (S3.C) to flatten the bottom surface. For the tibial implants (S3A,B), the periosteal graft was overlaid on the scaffold and sutured to the local periosteum using 6-0 sutures. In the femoral implants (S3.C), the periosteum was tied down onto the implant using suture and push fit into the defect. The muscle, fascia and skin was replaced and sutured closed. Ketofen (2mg/kg) and cefazolin (20mg/kg) were given subcutaneously for 48 hrs post-op. Animals were sacrificed at 2wks post-op.

Analysis

Following sacrifice, the implants and surrounding bone were excised and imaged using micro-computed tomography (microCT) (GE Healthcare eXplore Locus; 27μm 88min Short Scan; GE Healthcare, Piscataway, NJ). Subsequently, the samples were formalin fixed and decalcified using 10% formic acid prior to paraffin embedding. Using a microtome, 10 to 12 x 8μm axial cross-sections were removed at 1mm increments along the bone. These slides were then stained with H&E and inspected under light microscopy.

Histomorphometric analysis of S2 samples

Groups S2.A vs. S2.B: ESW-periosteum vs. control periosteum (no scaffold implanted)

Groups S2.A and S2.B were used to compare the shock wave stimulated periosteum at day 4. Two serial sections, 1mm apart, were analyzed. In each section,

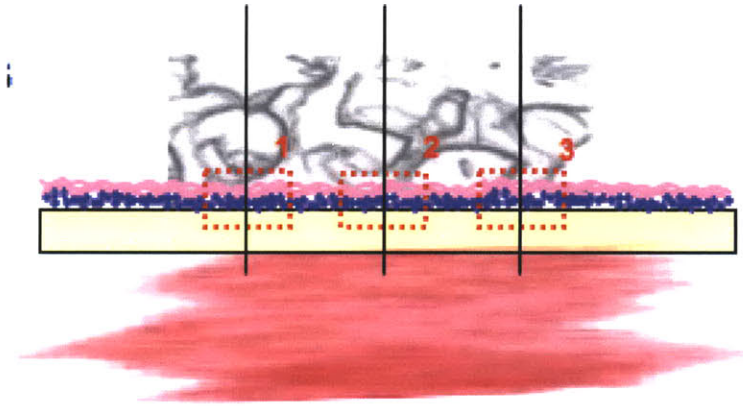

Figure 4-4 – S2.A, B: Schematic illustration of the three locations where 50μm bands were imaged and cell counts/cambium layer thickness measurements were made.

three locations were marked on the medial tibia for analysis; they were positioned to coincide with the area where the scaffold center would be and at ± 1.5mm from this point (see figure 4-4). The side regions coincide with the average scaffold diameter measured on H&E (4.6mm) minus half the scaffold thickness (0.8mm). Cell counts were taken in an area 50μm wide (along the circumference of the periosteum) and through the entire thickness of the cambium layer (i.e from the cortical bone surface to the periosteal fibrous tissue layer). At each location, a digitized image of the periosteum was taken and ImageJ software (NIH; http://rsbweb.nih.gov/ij/) was used to perform cell counting and to take cambium layer thickness measurements.

Groups S2.C vs. S2.D: control perisoteum + subperiosteal scaffold vs. ESW-periosteum + subperiosteal scaffold

To eliminate edge effects, the two centermost of the four (1mm apart) serial sections that showed scaffold cross-sections were analyzed, and the values obtained from these two slides were then averaged. The analysis was performed on digitized images that were stitched together using Adobe Photoshop (Adobe, San Jose, CA) and the areas measured using ImageJ software (NIH; http://rsbweb.nih.gov/ij/). For each section, the total callus on the medial side was recorded, which included all tissue inside the periosteal pocket (i.e., the proliferated periosteum away from the scaffold,

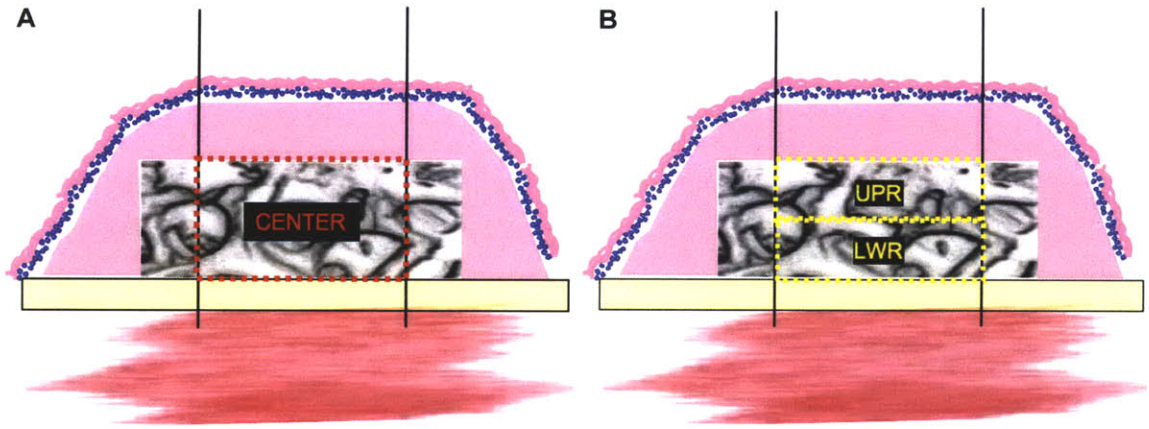

Figure 4-5 – Outline of the locations where the tissue was analyzed in Study 2 Groups S2.C,D. (A) Outline of scaffold center; an area, equal in width to half the scaffold thickness, was removed from the scaffold edge to eliminate edge effects. (B) The scaffold was separated into upper- (UPR) and lower- (LWR) half sections to help differentiate between osseous and osteoprogenitor tissue formed by the overlying periosteum (upper portion of scaffold) and by cells left on the cortical bone surface (lower portion of scaffold).

callus tissue above the scaffold, and the scaffold itself, even if no tissue had formed in the scaffold). Cell morphology and extracellular matrix appearance were used to identify tissues on H&E[2] , with periosteal callus away from the scaffold serving as an internal control for tissue appearance during histogenesis. Tissue reported as "osteoprogenitor" tissue includes any areas that were already committed to forming, or that had formed, bone (see footnote[2]); the remaining tissue was classified as

[2]During periosteal endochondral ossification, the cells first form a cartilage matrix that was morphologically similar to hyaline cartilage. Chondrocytes reside in elliptical lacunae and have a round or oval nucleus. The matrix is homogenous, basophilic, and has a glassy appearance (Bloom and Fawcett, 1968; Ham, 1969). In the next phase the chondrocytes become hypertrophic - these cells are characterized by their much larger volume, which is highly vacuolated (Bloom and Fawcett, 1968; Ham, 1969). At the expense of the hypertrophying cells, the matrix surrounding them becomes thin and fenestrated (Bloom and Fawcett, 1968; Ham, 1969). In concert with vascular invasion, the chondrocytes are replaced with osteoblasts, which deposit bone matrix on the remaining cartilage matrix (Bloom and Fawcett, 1968; Ham, 1969). As this calcifies, and the osteoblasts produce more matrix, trabeculae are formed. The matrix is visibly denser, and contains osteocytes, which are distinguishable from chondrocytes as their nucleus fills the majority of the cell and they are not as ovular (Bloom and Fawcett, 1968; Ham, 1969). The trabeculae are also characterizable by the layer of oseoblasts, which are square in shape, that line the surface. In rabbit models where the periosteal osteogensis occurs due to the periosteum being elevated from the bone, these trabeculae continue to grow until the combine with neighboring trabeculae to form a lamellar bone layer, which is continuous with the underlying cortex (see, for example, Cohen and Lacroix (1955); Stevens et al. (2005)).

non-osteoprogenitor. The osteoprogenitor tissue was further subdivided into osseous tissue (immature and maturing bone) and chondrocytic tissue (hyaline cartilage and hypertrophic chondrocytes). These tissues were readily distinguishable from each other – and from non-osteoprogenitor tissue – on H&E (see figure 4-6).

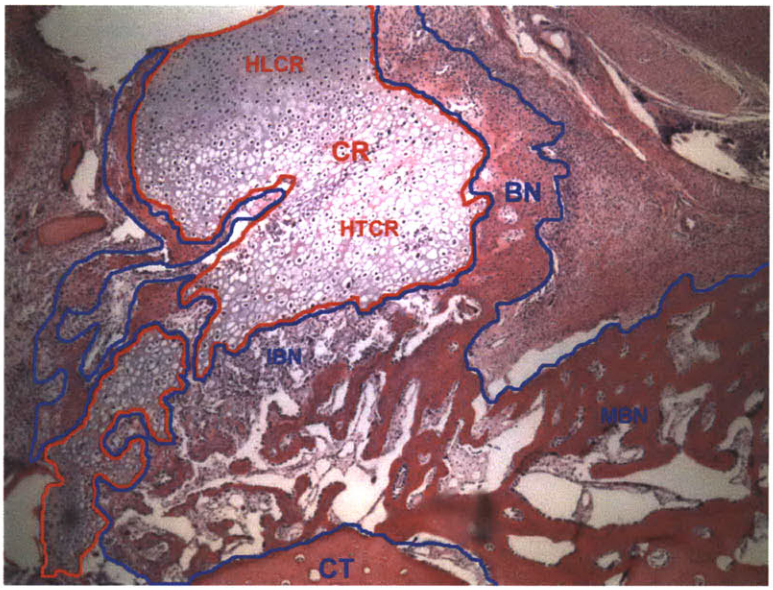

Figure 4-6 – Regions to the side of the scaffold demonstrated various phases of endochondral ossification, which were used as an internal control of histogenesis. The chondrocytic (CR) tissue is outlined in red. In the upper portion, the cartilage resembles hyaline cartilage (HLCR); as this tissue matures down the endochondral pathway, these cells become more hypertrophic (HTCR). Outlined in blue is the osseous tissue (BN), which ranged from freshly formed bone (IBN) to more maturing trabeculae (MBN). Both the chondrocytic and osseous tissue are summed together as osteoprogenitor tissue.

To identify tissue formation within the scaffold, a central portion of the scaffold was defined to eliminate edge effects. This was done by removing from the analysis region an area with a width 50% of the scaffold implant thickness (1.6mm) on both sides (see figure 4-5A). The porous area of the scaffold was calculated, and the tissue areas were recorded. The scaffold center was subdivided into the upper and lower half (see figure 4-5B). The upper half was used to analyze the response to the elevated periosteum alone; the lower half was used to evaluate the response of cells left on the cortical bone surface after periosteal elevation. Although the cortical bone surface was surgically scraped in an attempt to remove any cells from the surface, the tortuosity

of the surface protects some cells from being removed. The areas of osseous and osteoprogenitor tissue were also recorded above the scaffold and reported both as total areas and area normalized per unit length of scaffold.

4.2.3 Statistical analysis

All data is reported as the mean ± SEM of all the animals for each group. One-tailed Student t-test was used to compare ESW groups with control groups. ANOVA was used to calculate the power of the tests (note that the ANOVA p-values are two-tailed and twice the value of the one tailed values). For all tests, p-values of <0.05 and power of >0.8 were considered significant.

4.3 Results

4.3.1 Study 1: Pilot shock wave stimulated periosteum + subperiosteal scaffold study

MicroCT

The pilot study group was analyzed using microCT, which allowed for rapid visualization of the study results immediately post-sacrifice. In two of the pilot animals, there was dramatic bone formation above the scaffold and within the scaffold (see figure 4-7). In one of these animals, bone was grown to a maximum height of 2.5mm above the scaffold, and in the second animal, to 1.9mm above the scaffold. This bone appeared to be infiltrating and filling the scaffold. An additional two animals of the pilot group demonstrated bone formation below the scaffold, with the scaffold elevated off the cortical bone surface; this bone appeared to be infiltrating the scaffold from below. However, for these two animals, there was no evidence of bone formation above the scaffold. The final two animals did not demonstrate significant bone formation above or within the scaffold.

MicroCT imaging revealed that the 4 samples that did not have dramatic bone

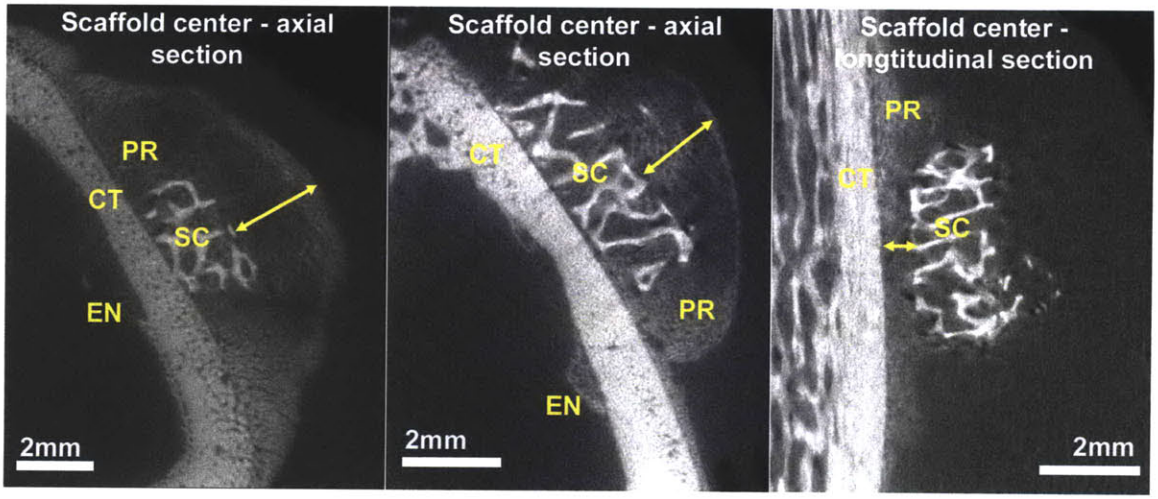

Figure 4-7 – Three sample microCT images from S1.A rabbits (pilot study: ESW + subperiosteal scaffold implant) showing cross-sections of the scaffold center. In (A) and (B) dramatic bone formation was seen above the scaffold, which appears to be infiltrating the scaffold. In (C) the scaffold was separated from the cortical bone surface by a new layer of bone that was forming on the underside. CT = cortical bone; EN = endosteum; PR = periosteum; SC = scaffold. Arrows show the periosteum derived newly formed bone.

formation above the scaffold had cortical microfractures on the postero-lateral corner (the side opposite the ESW application). These microfractures were healing with endosteal and periosteal calluses present (Note that the callus associated with the fractures in these 4 samples was much larger than was seen in the S2.D). The other two samples in the group did not demonstrate microfractures; however, there was evidence of periosteal and endosteal osteogenesis at the postero-lateral site with smaller callus size (compared to the samples with microfractures).

This indicated that the z-position (penetration depth) of the shock wave focal zone was not carefully controlled and in some animals more energy was being delivered at the postero-lateral corner than the medial side[3]. This was corrected for in Groups S3.B, D. Furthermore, in the two animals that demonstrated bone formation below

[3]For the OssaTron, the z-position was controlled by adjusting the pressure in the treatment head, which inflates/deflates the membrane; a calibration device can be attached to the head which marks the center of the treatment focus and allows the treatment depth to be calibrated. For the pilot study group (S1.A) the z-position was calibrated once prior to the beginning of the experiments. In S2 the z-position of the ESW applicator was adjusted before each treatment to ensure the treatment focus was centered on the membrane surface.

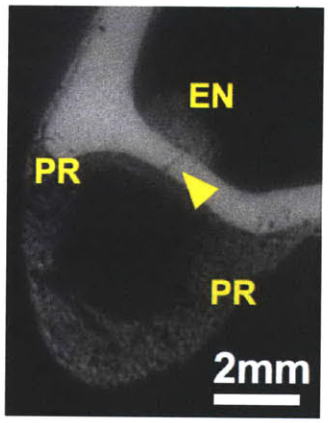

Figure 4-8 – Example of healing microfracture (arrowhead) found in postero-lateral corner of ESW-treated rabbits from Group S1.A (pilot study: ESW + subperiosteal scaffold implant) at 2wks post-scaffold implant, which did not show dramatic bone formation at the implant site. The two animals that did show bone formation at the implant did not have microfractures; however, they each had a small periosteal callus. The variation in results was attributed to improper z-alignment of the ESW focal zone. PR = periosteum; EN = endosteum.

the scaffold, it appears that the surgical technique was not fully refined in S1.A. In Groups S3.C, D, more care was taken to elevate the periosteum and remove any cells/tissue left below the elevated flap.

4.3.2 Study 2: Histomorphometrically analyzed ESW vs. control periosteum groups with and without subperiosteal scaffold.

Groups S2.A vs. S2.B: ESW-periosteum vs. control periosteum (no scaffold implanted)

In five of the six shock wave treated limbs there was a marked thickening of the periosteum as illustrated in figure 4-9. There was a 4-fold increase in the thickness of the ESW treated periosteum, when compared with the contralateral, non-stimulated controls (ESW vs. Control; 100± 24.7μm vs. 25 ±2.3μ; n = 6; mean ± SEM). This was statistically significant (t-test, p = 0.007; ANOVA, p = 0.013, power = 0.79). There was also a statistically significant, 2.7 fold, increase in periosteal cell

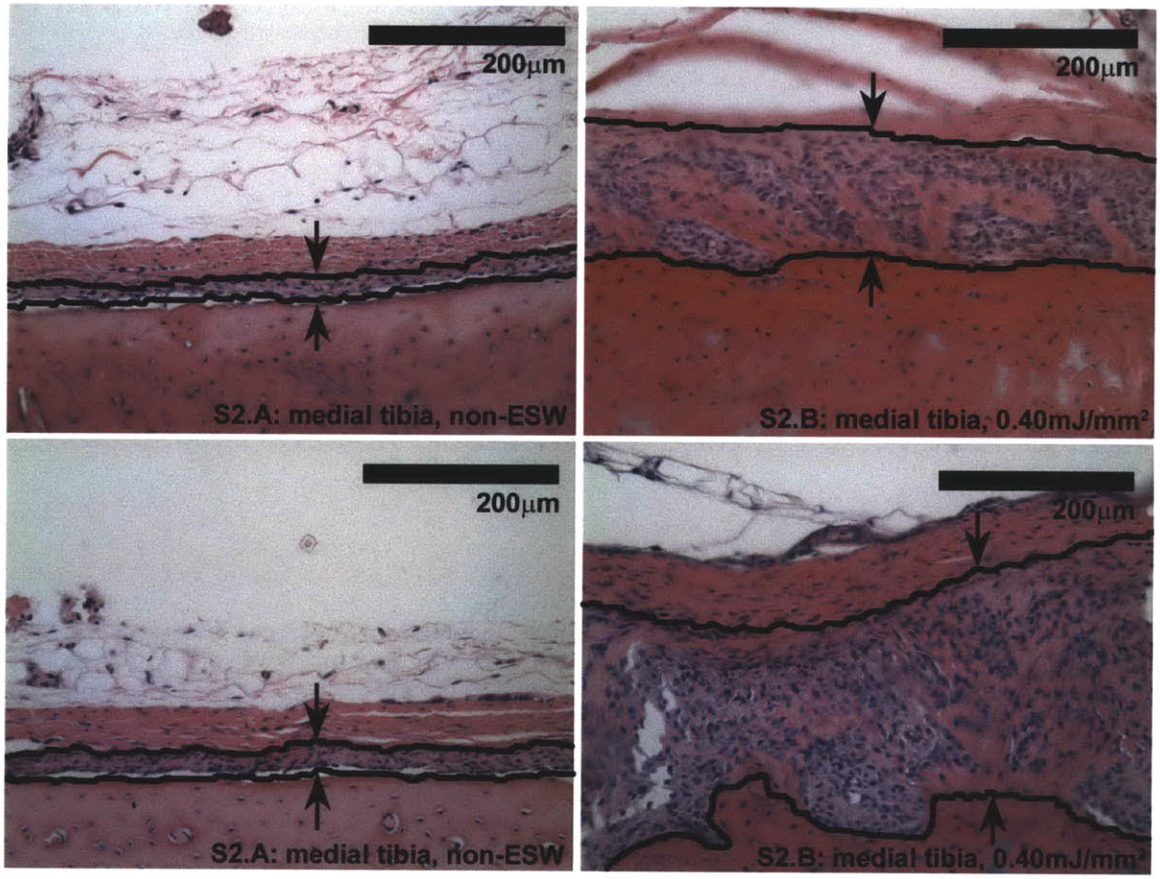

Figure 4-9 – Sample H&E images of control and ESW treated periosteum for Groups S2.A (control periosteum) and S2.B (ESW treated periosteum (no scaffold implant)) at 4 days post-ESW. Black lines and arrows outline the cambium layer of periosteal cells. The ESW-stimulated cambium cell proliferation and immature periosteal bone formation was clearly seen at 4 days.

number when compared with controls (ESW vs. Control; 38 ± 7 vs. 14 ± 1 ; $n = 6$; mean $\pm$ SEM; *t*-test, $p = 0.004$; power $= 0.842$). The microCT imaging (performed on 4 samples only) of these samples did not demonstrate any overt changes on the medial side; however, 3 of 4 samples demonstrated small, healing, microfractures on the postero-lateral corner (the side opposite ESW application), which was not seen on controls.

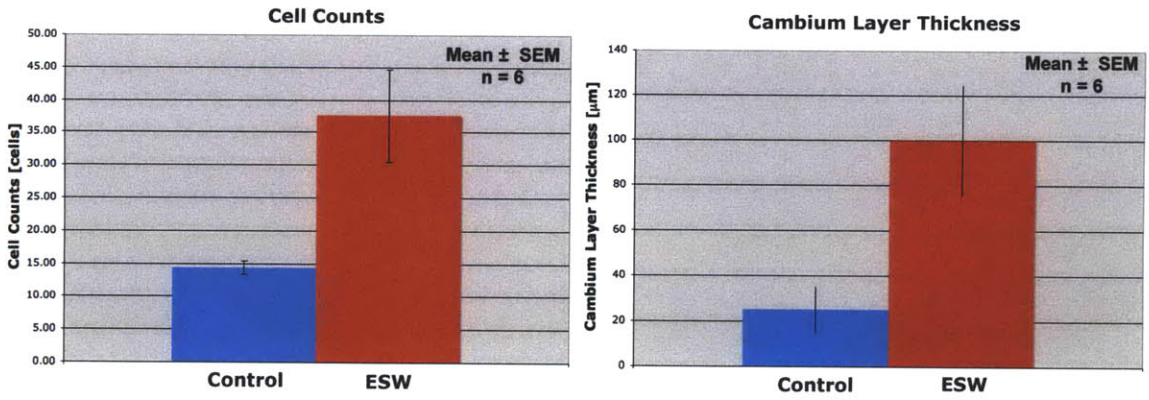

Figure 4-10 – Graphs of mean cell counts and cambium layer thickness for the Control (blue) and ESW-treated (red) animals. The bar charts demonstrate the 2.7-fold increase in cell counts and the 4-fold increase in cambium layer thickness following ESW. n = 6 for both groups; error bars show SEM.

Groups S2.C vs. S2.D: Control perisoteum + subperiosteal scaffold vs. ESW-periosteum + subperiosteal scaffold

MicroCT

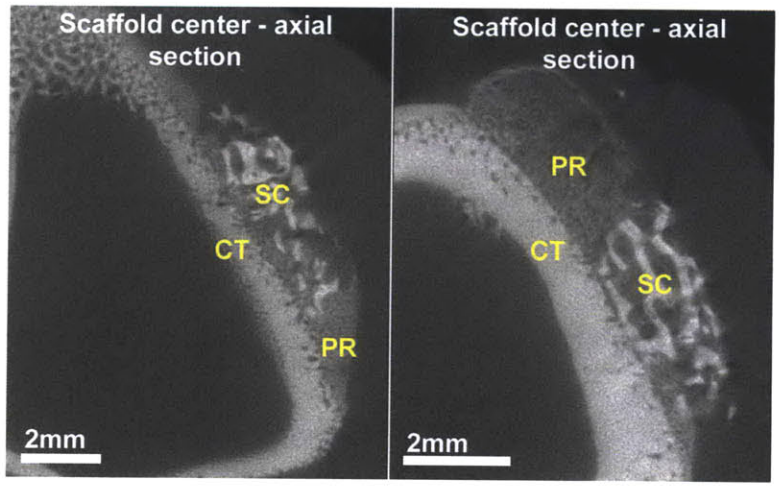

Figure 4-11 – Two sample microCT images from Group S2.C showing cross-sections of the scaffold center for control periosteum with a subperiosteally implanted calcium phosphate scaffold. In five of six control samples, there was no evidence of periosteal derived bone above the scaffold or in the upper pores. Local periosteum away from the scaffold responds to the surgical trauma by proliferation, filling an area up to the height of the scaffold top. CT = cortical bone; PR = periosteum; SC = scaffold.

Outside the scaffold boundary of the control group (S2.C), the normal periosteum

demonstrated callus formation in response to the surgical elevation. This has been demonstrated by several previous authors (Cohen and Lacroix, 1955; Hutmacher and Sittinger, 2003; Simon et al., 2003; Stevens et al., 2005). This callus was found on both sides of the scaffold, filling a region up to the edge of the scaffold surface, and some of this tissue infiltrated the scaffold at the edges. With the exception of some edge effects where the periosteal flap starts, there was no evidence of bone formation above the scaffold in 5 of 6 samples in the control group. There was some evidence of bone coming from the underside of the scaffold, which results from cells that were left behind on the cortical bone surface following scraping. The remaining one sample did demonstrate bone formation in a very thin layer above the scaffold, and this scaffold appeared to have more bone filling than the other 5 scaffolds.

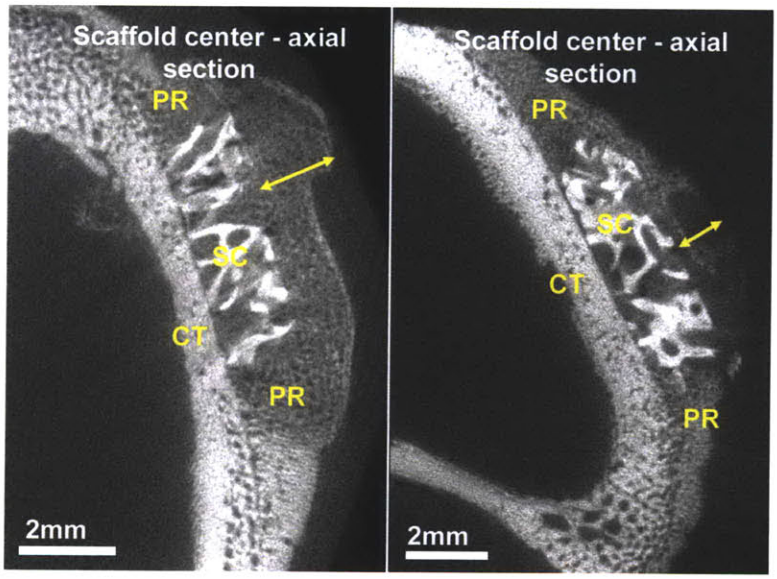

Figure 4-12 – Sample microCT images from Group S2.D showing cross-sections of the scaffold center in ESW-treated periosteum with a subperiosteally implanted calcium phosphate scaffold: In (A) and (B) dramatic bone formation was seen above the scaffold, which appears to be infiltrating the scaffold. CT = cortical bone; EN = endosteum; PR = periosteum. Arrows show the periosteum derived newly formed bone.

During one of the surgeries on S3.D samples, the periosteum tore. Although an effort was made to repair the periosteum by suturing, it contracted too much and the surgery took a long duration. A much smaller scaffold (<50% of the normal implanted diameter) was used for this surgery and the periosteum still had difficulty

covering the implant. Due to the dramatic difference in the surgery of this sample, it was excluded from analysis and the results of the remaining 5 samples only are described below.

In the ESW-group (S3.D), to the sides of the scaffold, there was osteogenesis consistent with previous reports of periosteal osteogenesis following surgical trauma. In contrast to the controls, this osteogenic tissue rose to a height above the edge of the scaffold and was continuous with the callus tissue that was forming above the scaffold. In all five samples, there was evidence of osteogenesis above and within the scaffold. In four of these five samples, the periosteum had contracted longitudinally and the most proximal (sutured) end of periosteum did not fully cover the scaffold; however, coverage was typically >75%.

Three of five ESW-treated samples had evidence of healing microfractures on microCT on the postero-lateral side (side opposite ESW treatment); the other two samples demonstrated periosteal callus formation at this site but no microfractures were seen on microCT. The thickness of these calluses was smaller than the large calluses reported in the pilot group (S1.A).

Histology

The histological results were consistent with those seen on microCT; however, they also allowed identification of regions of the tissue that were non-calcified but still contributing to the periosteal osteoprogenitor tissue.

For all control periosteum with subperiosteal scaffold samples (S3.C) , there was a periosteal callus on either side of the scaffold that had undergone osteogenesis (see fig. 4-13). This callus reached up to the height of the top of the side of the scaffold for the majority of samples. In two samples there was evidence of tissue above the scaffold: one of these samples had a cartilage nodule above the scaffold on one side; the second had a thin layer of bone across the top of the scaffold (as identified on microCT). All pores of the scaffold were filled with combinations of osteoprogenitor or non-osteoprogenitor tissue.

For the two H&E central sections, the periosteal callus was infiltrating the scaffold

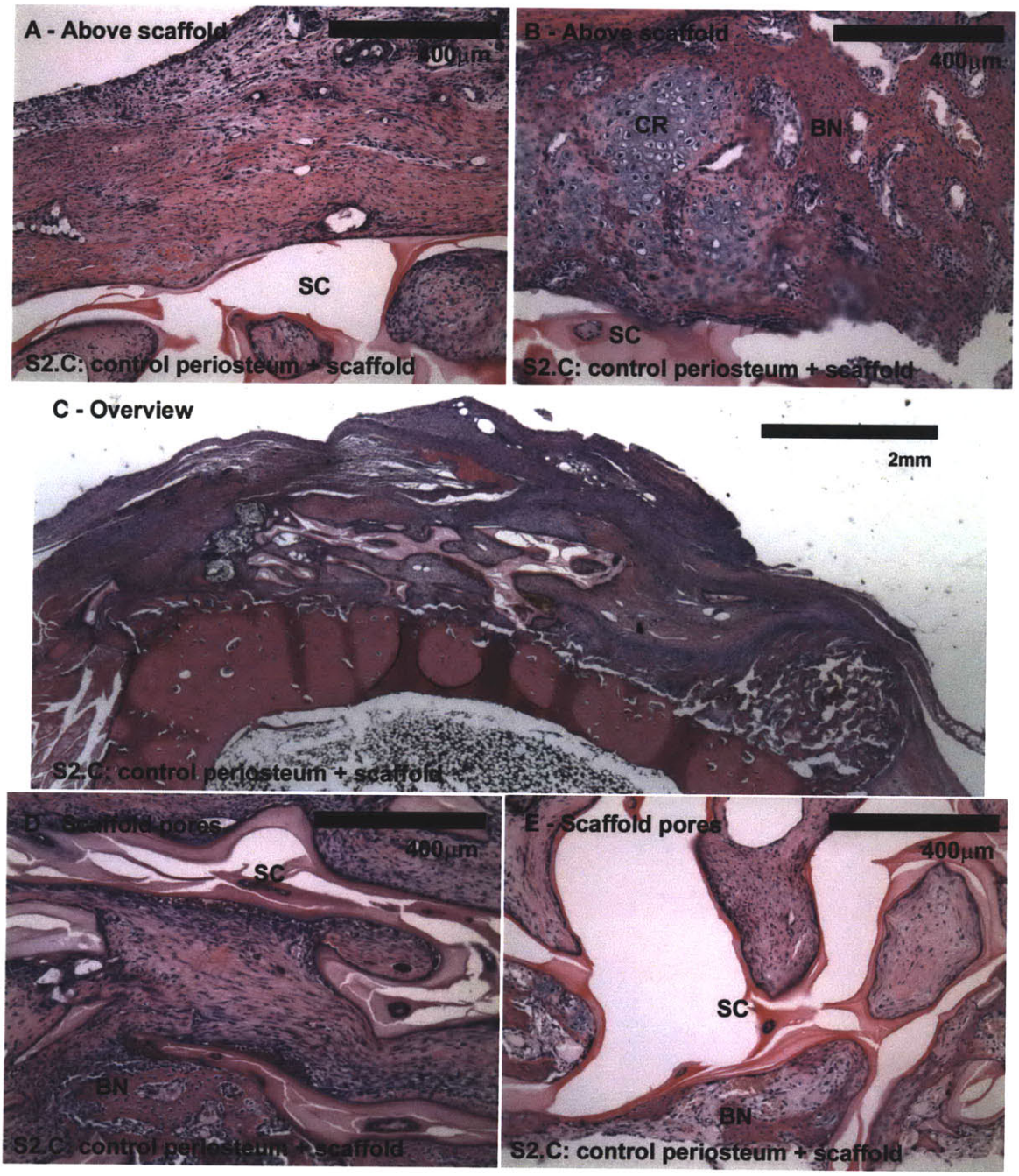

Figure 4-13 – Sample histology for Group S2.C (control periosteum + subperiosteal scaffold implant): (A) Typically the elevated periosteum demonstrated little osteoprogenitor tissue above the scaffold or in the upper pores. (B) There was one control sample that demonstrated some bone formation above the scaffold. (C) Low power overview of the tissue responses. (D, E): Bone formation occurred in the lower half of the scaffold, which appeared to be arising from cells left on the cortical surface after scraping. BN = osseous tissue; CR = chondrocytic tissue; SC = scaffold.

sides but there was minimal evidence of tissue in the upper half of the scaffold, with the exception of the sample that showed a thin bone layer above the scaffold (see fig.4-13 A, B). In the lower half of the scaffold, there was some bone formation that appeared to be growing up from the cortical bone surface (see fig.4-13 D, E). This bone formation is attributed to periosteal cells left behind on the cortical surface following scraping. The upper half of the scaffold was typically filled with non-osteoprogenitor tissue that was typically fibrous (see fig.4-13 D, E). In the sample that had bone above the height of the scaffold, there was some ongoing endochondral ossification within the scaffold pores.

For the most proximal and most distal H&E cross-sections, the tissue demonstrated different behavior. Noting that the most distal section was the section in contact with the attached flap edge, there was more bone seen in these sections than in the central sections. This is attributed to an edge effect, similar to what is seen on the scaffold sides. For sections near the sutured end of the periosteum, the scaffolds in all samples were filled with fibrous tissue almost entirely.

For the S3.D samples (ESW-periosteum + subperiosteal scaffold), there was periosteal callus on both sides of the scaffold that was undergoing osteogenesis. This callus was continuous with the callus tissue overlying the scaffold, and typically reached up higher than the scaffold edge (see fig. 4-14C). For the central H&E slides of all five samples, there was osteoprogenitor tissue above the scaffold. This tissue ranged in maturity from hyaline cartilage to trabecular bone. In the majority of samples, the tissue was a combination of chondrocytic and osseous tissue, which is consistent with periosteal tissue undergoing endochondral ossification. When chondrocytic tissue was observed, the large majority of the tissue consisted of hypertrophic chondrocytes.

The edges of the scaffold were infiltrated with bone, which was coming from the periosteal callus on each side (see fig. 4-14C). In contrast to controls, the upper half of the scaffold had osteoprogenitor tissue infiltrating the scaffold from the callus above (see fig. 4-14A, B). The tissue in the upper pores was continuous with tissue forming in the lower pores; however, as with the control samples, there was also bone formed by progenitor cells left over after scraping the surface (see fig. 4-14D, E).

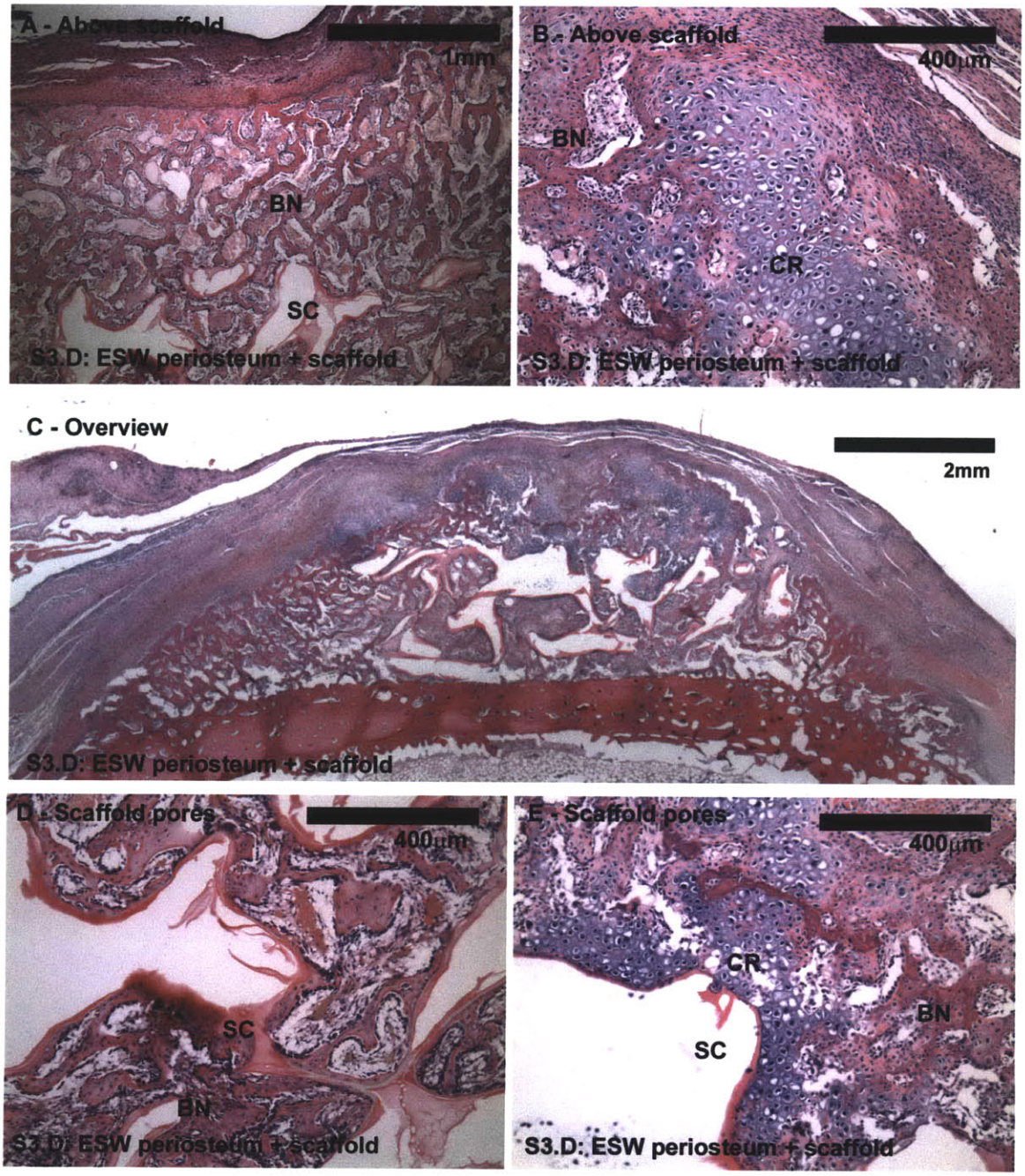

Figure 4-14 – Sample histology of S2.D (ESW-stimulated periosteum + subperiosteal scaffold implant): (A, B) ESW-treated periosteum demonstrated osseous and/or chondrocytic tissue above the scaffold tissue for all animals. (C) Low power overview of the tissue response. (D, E): Most of the scaffold center pores were filled with osseous or chondrocytic tissue. BN = osseous tissue; CR = chondrocytic tissue; SC = scaffold

The sections from each end of the scaffold (longitudinally) showed different tissue formation. For the sections that were close to the attached end of the graft, the

samples were largely filled with bone and demonstrated primarily osseous – and not chondrocytic – callus above the scaffold. As was described in the microCT results, there was contraction of the periosteum at the sutured end. For sections close to the sutured end, there was decreased filling of the scaffold and a smaller area of reparative tissue above the scaffold. Qualitatively, these samples appeared more filled with osteoprogenitor tissue than the equivalent control samples.

Histomorphometric analysis

Two central sections, spaced 1mm apart, were analyzed for all groups in S2. The data from each of these sections was averaged for each animal and the results reported below as mean ± SEM.

Osseous and osteoprogenitor tissue in scaffold pores

The osseous tissue within the scaffold center was increased 1.7-fold, but this was marginally statistical insignificant (ESW vs. Control; 50.5 ± 13% vs. 30.0 ± 5%; n = 6 controls, 5 ESW; mean ± SEM; *t*-test, p = 0.07; ANOVA, p = 0.14, power = 0.29). The mean total areas for these tissue are presented in figure 4-15A. When the chondrocytic tissue was also considered, there was an approximately 2-fold increase in ESW treated samples compared to controls (see fig. 4-15B; ESW vs. Control; 61 ± 10% vs. 34 ± 5%; n = 6 controls, 5 ESW; mean ± SEM). This difference was statistically significant (*t*-test, p = 0.02; ANOVA, p = 0.04 power = 0.57). The amount of osseous and chondrocytic tissue were both increased when compared with controls.

As described in the histology results section, there was a different behavior observed for the upper and lower half of the scaffold. The scaffold was divided into the upper and lower sections to quantitatively evaluate the observed difference. The upper half of the scaffold had an almost 4-fold increase in the percent of osseous tissue filling the scaffold pores, which was statistically significant (see fig. 4-15C; ESW vs. Control; 58 ± 13% vs. 15 ± 5%; n = 6 controls, 5 ESW; mean ± SEM; *t*-test, p = 0.004; ANOVA, p = 0.008, power = 0.866). When the chondrocytic tissue was also

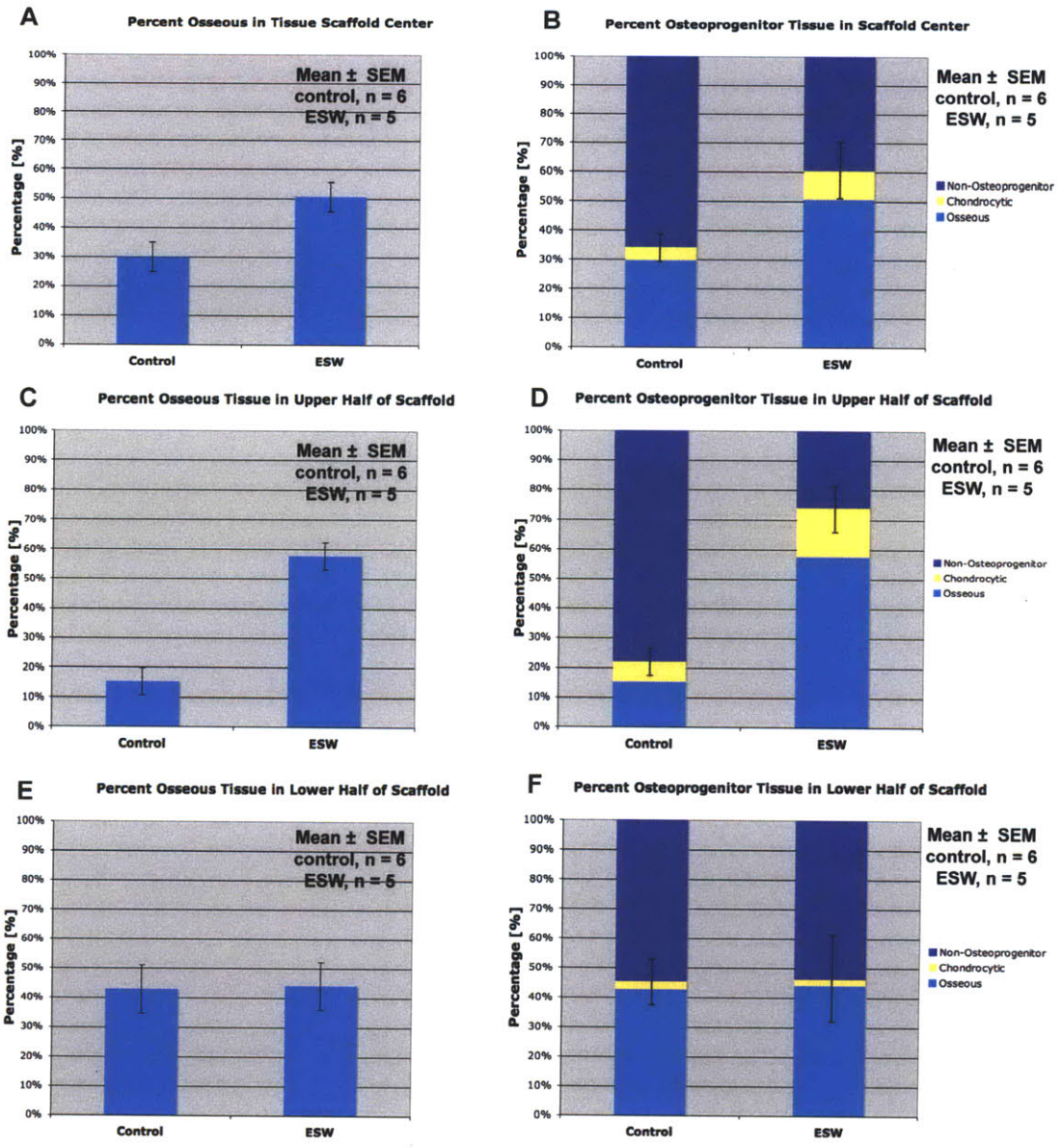

Figure 4-15 – Graphs of mean (A, C, E) osseous and (B, D, F) osteoprogenitor (osseous + chondrocytic) tissue percentages within the scaffold pores for Groups S2.C (control periosteum; n = 6) and S2.D (ESW-periosteum; n =5). (A) and (B) scaffold center; (C) and (D) upper half of the scaffold; and (E) and (F) lower half of the scaffold. The graphs demonstrate the increase filling in the scaffold upper pores following ESW (4-fold increase in osseous tissue; 3.3-fold increase in osteoprogenitor tissue), but no change between the groups for the scaffold lower pores. Error bars show SEM.

considered (see fig. 4-15D), there was a 3.3-fold increase in osteoprogenitor tissue when compared with controls, with almost three-quarters of the scaffold in the ESW treated samples filled with osteoprogenitor tissue (ESW vs. Control; 74 ± 8% vs. 22

± 5%; n = 6 controls, 5 ESW; mean ± SEM; *t*-test, p = 0002; ANOVA, p = .0003, power = 1).

In contrast to the upper half of the scaffold, there was no difference between the ESW and control tissue for the scaffold lower half for either osseous tissue (ESW vs. Control; 44 ± 15% vs. 43 ± 8%; n = 6 controls, 5 ESW; mean ± SEM; *t*-test, p = 0.47; ANOVA, p = 0.94, power = 0.05) or osteoprogenitor tissue (ESW vs. Control; 46 ± 15% vs. 45 ± 8%; n = 6 controls, 5 ESW; mean ± SEM; *t*-test, p = 0.47; ANOVA, p = 0.94, power = 0.05). This is consistent with the histological observations that showed bone infiltrating the scaffold from the cortical bone surface for both control (S2.C) and ESW samples (S2.D).

Callus total area

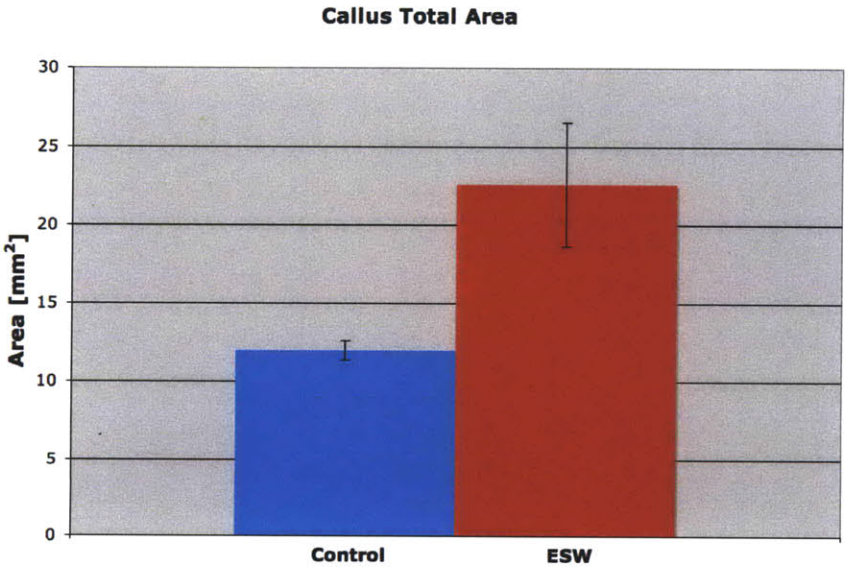

Figure 4-16 – Graphs of callus total area for the S2.C (control periosteum; blue; n = 6) and S2.D (ESW-periosteum; red; n =5) following subperiosteal scaffold implant. The callus includes all tissue under the perioseal flap (i.e., includes the scaffold and periosteal tissue to the scaffold sides). There was a 2-fold increase in callus total size following ESW. Error bars show SEM.

The callus total area was measured along the entire medial side of the tibia in axial cross-section and included all tissue under the periosteal flap (i.e. the tissue

undergoing periosteal osteogenesis on either side of the scaffold, as well as the scaffold itself and any periosteal osteoprogenitor tissue above the scaffold). The ESW treated sample demonstrated a two-fold increase in the callus total area, when compared to controls (ESW vs. Control; 23± 4mm^2 vs. 12 ± 0.3mm^2; n = 6 controls, 5 ESW; Mean ± SEM). This increase in callus area was a combination of the slightly higher periosteal callus on either side of the implant, as well as the larger amount of periosteal osteoprogenitor tissue above the scaffold. Using the *t*-test, this difference was found to be statistically significant (p = 0.01; ANOVA, p = 0.02, power = 0.72).

Osseous and osteoprogenitor tissue above scaffold

Since the elevated periosteum was overlaid on the scaffold, it was anticipated that this tissue not only infiltrates the scaffold but also forms tissue above the scaffold. The osseous and osteoprogenitor tissue above the scaffold was recorded as both total areas and was also normalized per unit length of scaffold for each animal (to compensate for variations in the scaffold dimensions). The mean total areas and normalized areas are graphed in figure 4-17. There was a ten-fold increase in osseous tissue for the total area (ESW vs. Control; 2.6 ± 0.6mm^2 vs. 0.24 ± 0.2mm^2; n = 6 controls, 5 ESW; mean ± SEM; *t*-test, p = 0.001; ANOVA, p = 0.003, power = 0.959) and a 12-fold increase when the data was normalized per unit scaffold length (ESW vs. Control; 0.578 ± 0.15 mm^2/mm scaffold vs. 0.047 ± 0.04 mm^2/mm scaffold; n = 6 controls, 5 ESW; mean ± SEM; *t*-test, p = 0.002; ANOVA, p = 0.005, power = 0.92). With chondrocytic tissue also considered, the total area osteoprogenitor tissue was increased by 7.5-fold for ESW compared to controls (ESW vs. Control; 4.7 ± 1.6 mm^2 vs. 0.63 ± 0.25 mm^2; n = 6 controls, 5 ESW; mean ± SEM; *t*-test, p = 0.01; ANOVA, p = 0.02, power = 0.72), and by 8-fold when normalized per unit scaffold length (ESW vs. Control; 1.06 ± 0.35 mm^2/mm scaffold vs. 0.13 ± 0.05 mm^2/mm scaffold; n = 6 controls, 5 ESW; mean ± SEM; *t*-test, p = 0.009; ANOVA, p = 0.017, power = 0.745). The dramatically increased osseous and osteoprogenitor tissue above the scaffold for the ESW-treated samples was continuous with the tissue in the scaffold upper pores. Thus the ESW treated periosteal cells (that were elevated off the bone)

were responsible for the increased callus, the increased callus tissue above the scaffold, and the filling of the scaffold upper half.

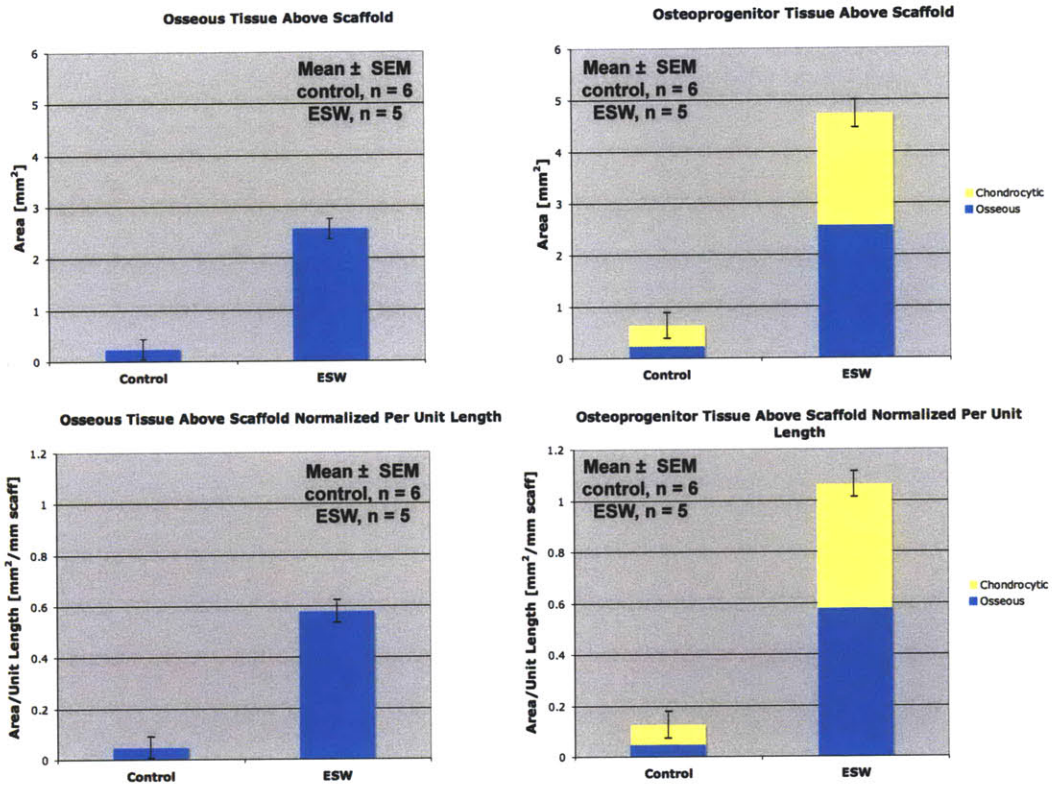

Figure 4-17 – Graphs of mean (A, C) osseous and (B, D) osteoprogenitor (osseous + chondrocytic) tissue percentages within the scaffold pores for Groups S2.C (control periosteum + subperiosteal scaffold implant; n = 6) and S2.D (ESW-periosteum + subperiosteal scaffold implant; n =5). (A, B) The total area of osseous tissue increases 8-fold and the osteoprogenitor tissue increase 7.5-fold following ESW. When normalized per unit scaffold length for each sample – (C, D) – the osseous tissue increased 12-fold and the osteoprogenitor tissue increased 8-fold for the ESW group compared to controls. Error bars show SEM.

4.3.3 Study 3: Free periosteal graft studies

Groups S3.A vs. S2.B: Control vs. ESW free periosteal autograft transplanted onto scaffold in contralateral tibia

MicroCT

On microCT, both shock wave and control samples demonstrated bone formation in the scaffold pores within the marrow cavity, which is attributed to marrow stem cells and endosteal cells (see fig. 4-18). There was also an in situ periosteal osteogenic response away from the scaffold, which is attributed to surgical stimulation of the periosteum.

It was anticipated that the observed response from the periosteal transplant would be a layer of bone above the scaffold, which would be infiltrating the upper portion of the scaffold (as was seen for the in situ study). For the S3.A samples, zero of two samples showed evidence of transplanted periosteum bone formation (see fig.4-18 A, B). In S3.B, there was a radio-opaque line above the scaffold in three of four treated samples, indicative of bone formation at the transplant site (see fig.4-18 C-F). It was difficult to determine whether bone forming in the upper scaffold pores resulted from transplanted periosteal cells infiltrating the scaffold. However, there did not appear to be continuity between the transplanted periosteum bone formation and bone formed in the scaffold pores in two of these three samples (4-18 C and F).

Histology

H&E stained slides confirmed the microCT findings (see fig.4-19). Inside the marrow cavity, marrow stem cells and endosteal cells were infiltrating the scaffold and forming new bone on its surface (see fig.4-19 A, B). The line of periosteal bone observed in the three ESW samples – which was not seen on controls – was observed under light microscopy (see fig. 4-19 C, D). At higher magnification (4-19 E, F), however, this bone did not typically look fully vital. In two of the samples, there was a layer of fibrous tissue blocking the transplanted periosteum from the scaffold (4-19C, E); however, on one sample there was continuity between the transplanted periosteum and

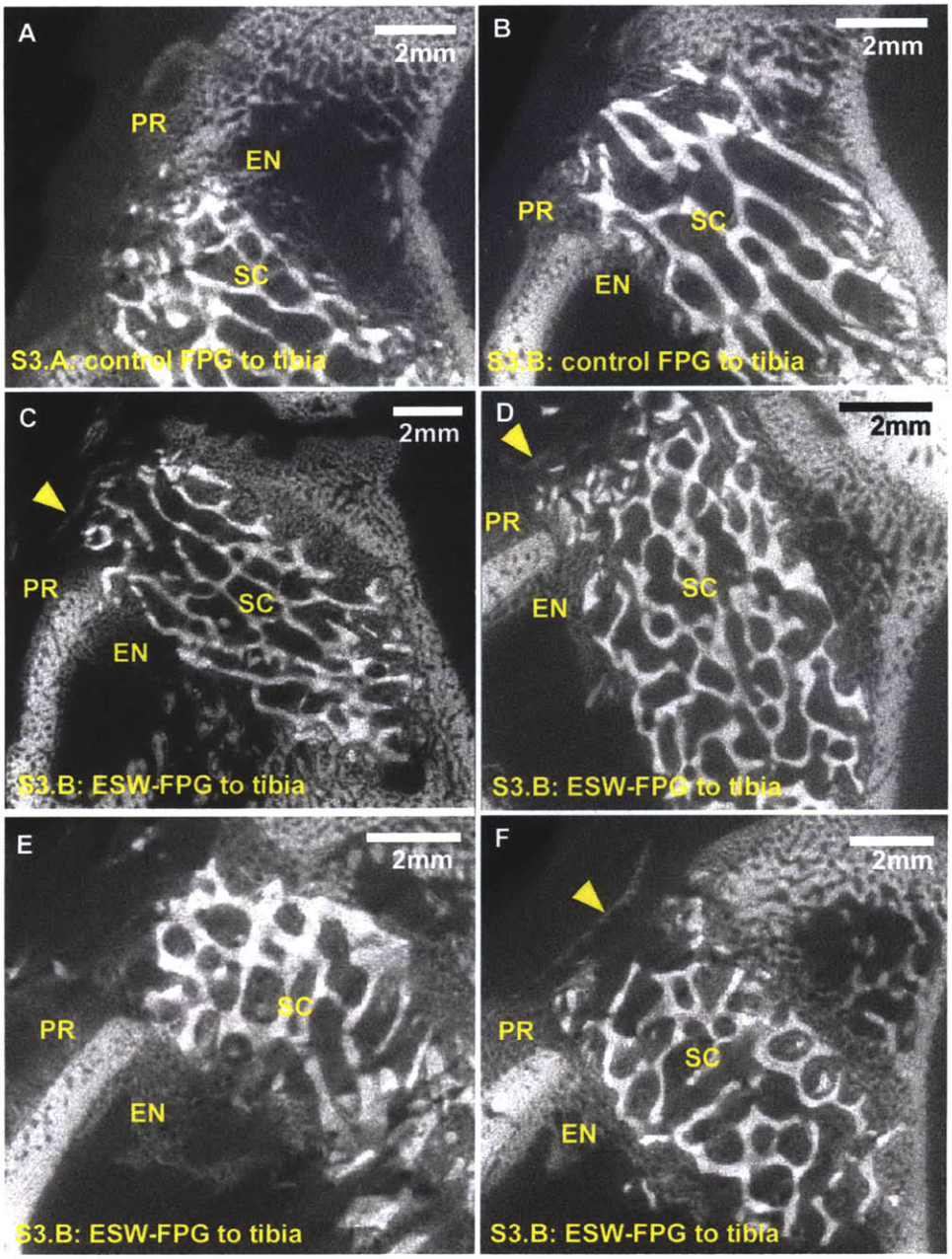

Figure 4-18 – MicroCT images from the center sections of (A, B) control (S3.A) and (C, D, E, F) ESW-treated free periosteal grafts (FPG) (S3.B) transplanted to scaffolds in the proximal tibia. All samples demonstrate bone formation in the marrow cavity. The control samples do not demonstrate any bone formation above the scaffold where the periosteal graft was placed. Three (C, D, F) of the four ESW treated grafts demonstrate bone formation (arrowheads). EN = endosteum; PR = periosteum; SC = scaffold.

new bone (4-19). It is postulated that the transplanted bone was highly metabolically active prior to transplantation to the defect site (recall the dramatic proliferation at

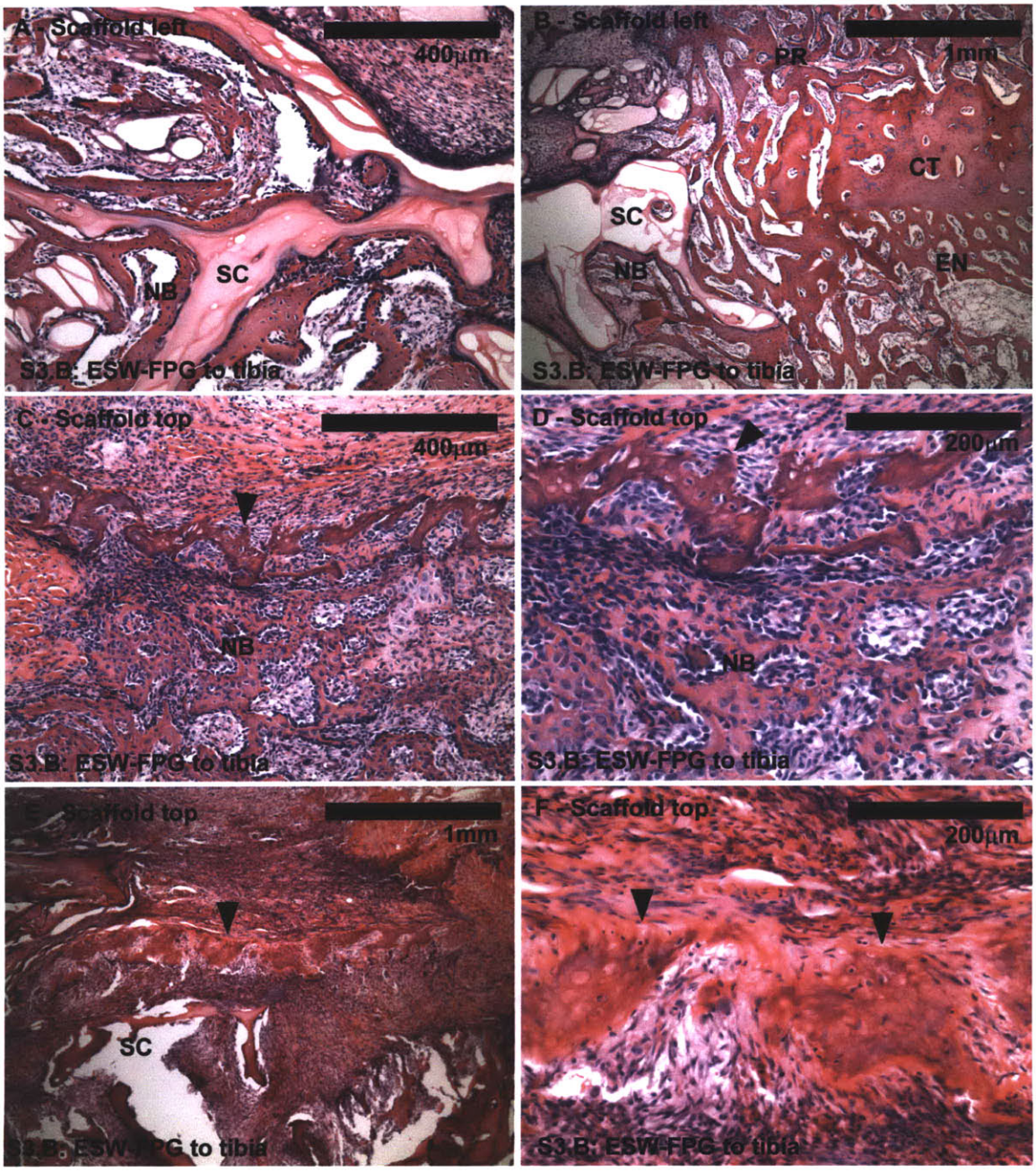

Figure 4-19 – Sample micrographs of S3.B samples: ESW-treated free periosteal autograft (FPG) transplanted to contralateral tibia at 2wks. (A, B): Endosteal and marrow progenitor cells infiltrate the scaffold inside the marrow cavity lining the scaffold struts with new bone. Samples of transplanted periosteum (arrowheads) on the top of the scaffold at lower (C, E) and higher (D, F) magnification. Although new bone was evident in the periosteum at the transplant site, the bone does not appear fully vital (empty osteocyte lanaue, lack of osteoblasts lining bone). In (C, D) the new bone from the marrow cavity was continuous with the free periosteal graft; whereas in (E, F), there was a layer of fibrous tissue that was blocking the periosteal graft from communicating with bone forming cells in the marrow cavity. CT = cortical bone; EN = endosteum; NB = new bone; PR = periosteum; SC = scaffold

4 days post-ESW and the active bone formation). At its new location, the transplant was devoid of a blood supply until neovascularization was completed. During this time the bone formation and cambium cell activity was halted and cells in the graft may have undergone apoptosis.

Group S3.C: Free ESW-stimulated periosteal autograft transplanted onto scaffold in ipsilateral femur

MicroCT

For shock wave treated periosteum transplanted to the top of the scaffold in the femur defect, there was no evidence of periosteal osteogenesis in the transplant on microCT (see fig. 4-20). There was some evidence of a periosteal osteogenic response in the local periosteum that had been retracted surgically from the implant site. There was also bone formation in the scaffold that was within the marrow cavity.

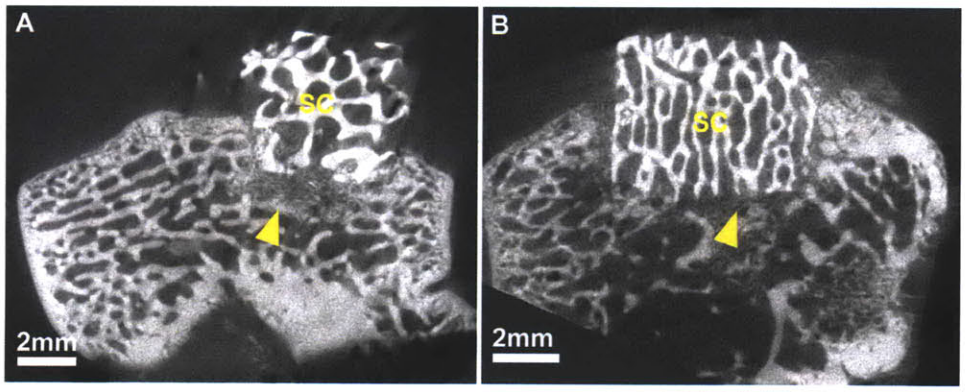

Figure 4-20 – Sample microCT images from the center of ESW treated free periosteal grafts transplanted to scaffolds in the distal femur (Group S3.C): Bone was found in the marrow cavity (arrowheads) but there was no evidence of bone formation on top of the scafold (SC) where the periosteum was attached.

Histology

Prior to beginning this study, it was postulated that soft tissue overlying the periosteum would revascularize the transplanted periosteum and that further nutrients would reach the periosteum by diffusion from the marrow cavity. On H&E, the trans-

planted periosteum appeared necrotic and the overlying soft tissue was separated from the periosteal graft (see fig. 4-21). Essentially the periosteal graft was isolated on top of the scaffold and there was insufficient neovascularization, or it was not rapid enough, to vitalize the graft and form bone at the treatment site.

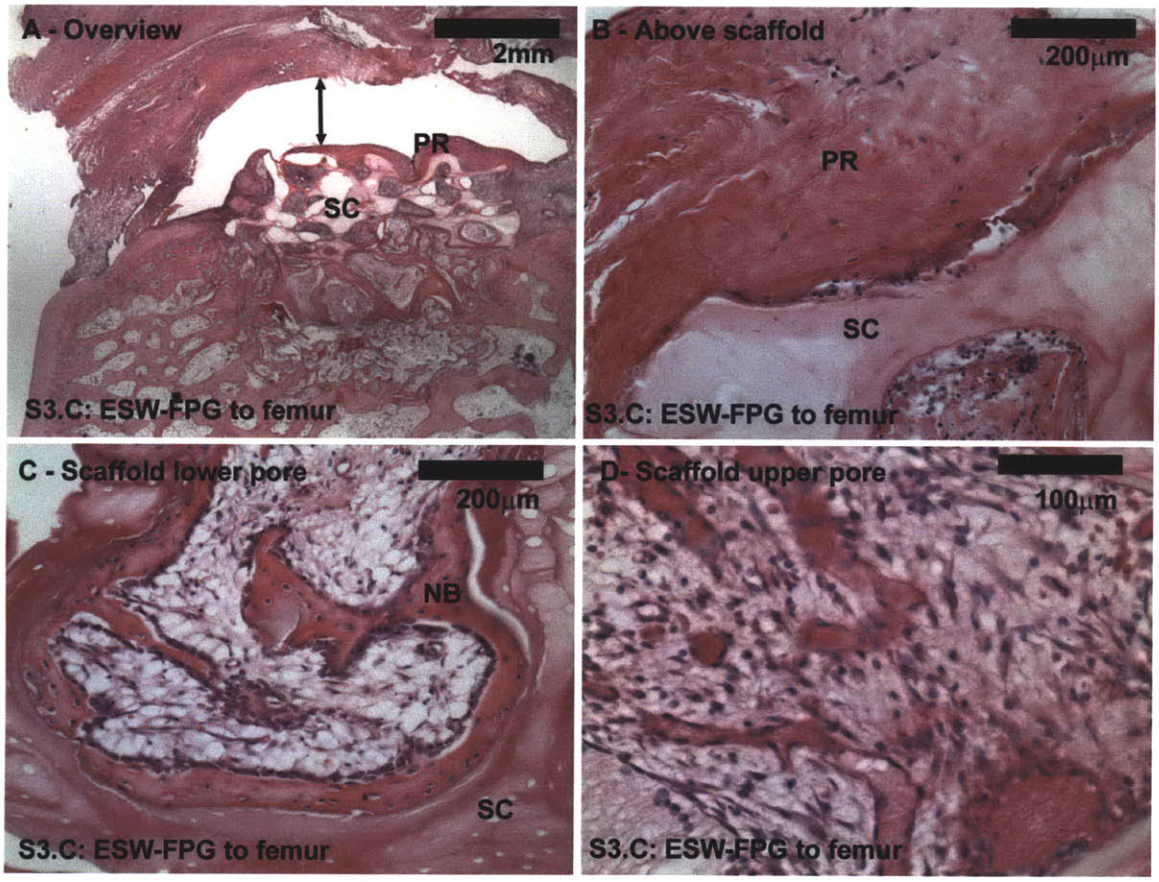

Figure 4-21 – Sample micrographs of ESW treated free periosteal grafts transplanted to scaffolds in the distal femur (Group S3.C): (A) Overview of the tissue responses-the arrow marks the gap observed between the periosteal graft and overlying soft tissue. (B) Periosteal tissue overlying the scaffold appeared necrotic and devoid of cells. (C) Pores deep in the marrow demonstrated osteoblast rich bone depositions on the scaffold struts. However, the upper pores were filled with tissue that was more necrotic looking (D).

4.4 Discussion

The primary objective of this study was to demonstrate the enhanced efficacy of ESW treated periosteal cells over non-treated controls as an overlay on a porous cal-

cium phosphate scaffold for orthotopic bone generation. In the pilot study, S1.A, ESW-stimulated periosteum was elevated at day 4 and a calcium phosphate scaffold – which had previously been implanted subperiosteally and demonstrated bone formation (Simion et al., 2006) – was implanted below the periosteum. Two of the six samples demonstrated robust subperiosteal bone formation above the scaffold (which was infiltrating the scaffold); two of the samples demonstrated bone formation below the scaffold, with the scaffold elevated off the bone surface; and the final two samples did not demonstrate bone formation subperiosteally. Interestingly, the 4 samples that did not demonstrate periosteal bone formation above and within the scaffold had large calluses on the contralateral limb that were associated with healing microfractures. The variation in results was attributed to improper z-alignment of the shock wave focal zone (penetration depth) and this was corrected in the Study 2 groups.

Study 2 groups were used to evaluate and quantify the difference between ESW and control (non-ESW) samples. In the first two groups, animals were sacrificed at the proposed periosteal harvest/elevation timepoint (4 days post-ESW) and the ESW stimulated periosteum (S2.B) was compared with contralateral controls (S2.A). The harvest timepoint was chosen based on the results from the rat study presented in Chapter 2, as well as the previously published reports of periosteal response to ESW (Takahashi et al., 2004; Tischer et al., 2008). There was a significant (2.7-fold) increase in the cambium cell number and a significant 4-fold increase in cambium layer thickness. There was also immature bone formation visible within the proliferated periosteum at 4 days. It was noted in the free graft harvest (Study 3) that the ESW-stimulated periosteal sheet was stiffer than the control periosteum and contracted less, which is attributed to the stiffer osteoid matrix. The advantage of the proliferated cell layer is twofold. First, it is proposed that the increased progenitor cell number will result in increased callus formation and increased osteogenesis within the scaffold. Second, the thickened layer (100μm) facilitates harvest when compared with normal periosteum, which is a 25μm thick layer consisting of only 3 - 5 cells.

When a calcium phosphate (anorganic bovine bone) scaffold was implanted below the periosteum, there was a significant (4-fold) increase in osseous tissue in the upper

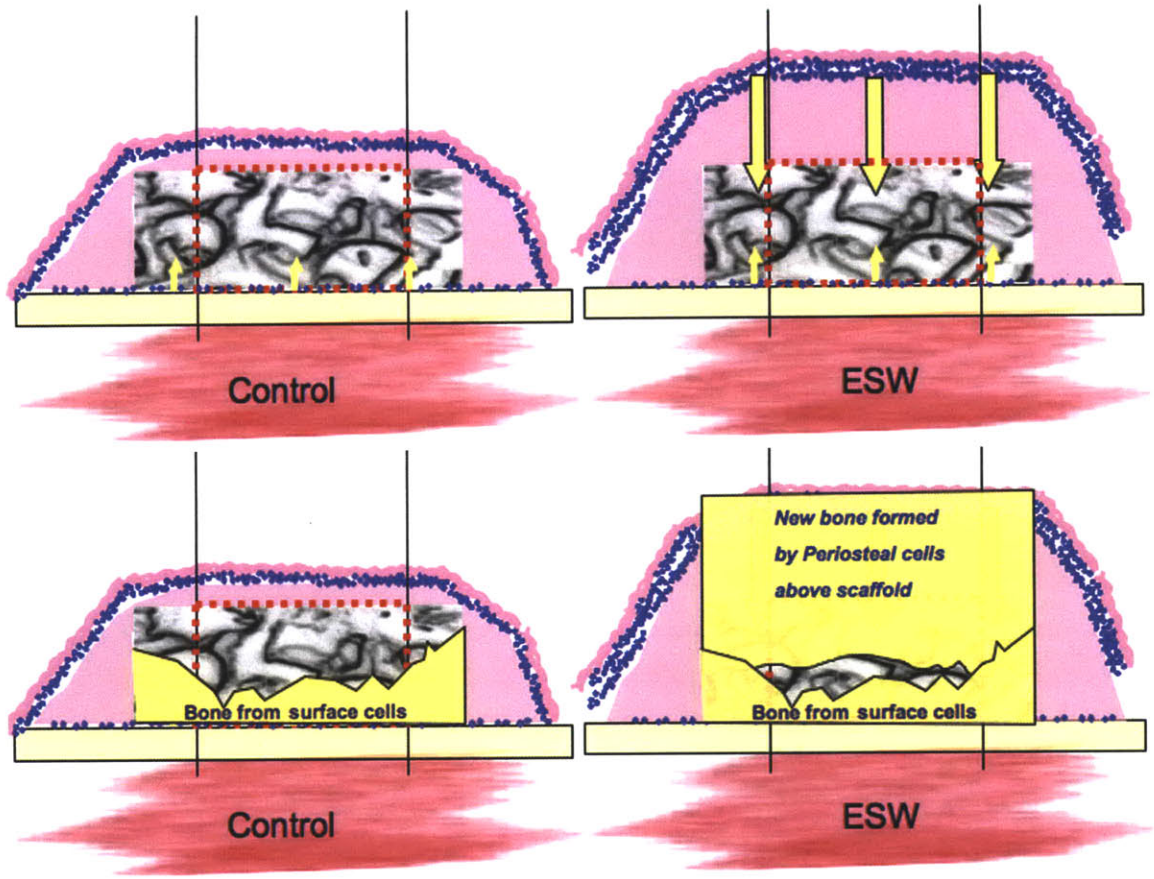

Figure 4-22 – Schematic of observed responses to control (A, C) and ESW stimulated (B, D) periosteum overlaid on a porous calcium phosphate scaffold in situ. In the control tissue little bone is formed above or within the upper half of the scaffold; bone formed in the scaffold lower half comes from cells left on the cortical bone surface. In the ESW treated samples, there was osseous/osteoprogenitor tissue above the scaffold where the ESW-treated periosteal cells were placed. These cells were infiltrating the scaffold and filling the upper half with osseous/osteoprogenitor tissue. An equivalent response to controls is seen in the scaffold lower half.

half of the scaffold, and a significant (3.3-fold) increase in osteoprogenitor (osseous plus chondrocytic) tissue filling the scaffold pores. The increased filling in the scaffold upper pores was attributed to increased periosteal cell number following ESW stimulation. These cells produced a significant 10-fold increase (12-fold when normalized per unit scaffold length) in osseous tissue above the scaffold and a 7.5-fold increase in osteoprogenitor tissue (8-fold when normalized per unit scaffold length) compared to the controls. For the majority of control samples, there was very little osteoprogenitor tissue above the scaffold (0.13 ± 0.05 mm^2/mm scaffold). This is attributed to

the very low periosteal cell number and the difficulty in successfully harvesting these cells. By extension, there was little filling of the upper pores of the scaffold ($22 \pm 5\%$). By contrast the ESW treated scaffolds had 1.06 mm^2/mm scaffold osteoprogenitor tissue, which infiltrated the scaffold upper pores and filled the scaffold area with 74% osteoprogenitor tissue. These results demonstrate the ability of the ESW-stimulated periosteal cells to migrate into the calcium phosphate scaffold and to form osseous and chondrocytic tissue.

Following ESW-stimulation, the periosteal cells respond by proliferating and undergoing ossification. At the time of a surgery, there is a second stimulus for periosteal osteogenesis. The cells proliferate further (there is a much thicker layer of subperiosteal tissue in S2.D (ESW+subperiosteal scaffold) when compared with S2.C (ESW only)) and form both bone and cartilage. Previous authors have demonstrated that normal periosteum responds to surgical elevation (or damage) by proliferating and undergoing endochondral ossification (Cohen and Lacroix, 1955; Simon et al., 2003). Following ESW-stimulation, the cells respond by intramembranous ossification. During surgical manipulation of the periosteum, vessels are damaged and this causes bleeding. The disruption of the vascular system, coupled with the further proliferation of the cambium cells, likely leads to a hypoxic environment. This favors cartilage formation and may lead to endochondral – as opposed to intramembranous – ossification.

The tissue formed in the lower half of the scaffold is attributed to periosteal cambium cells that are left on the cortical bone surface after ESW stimulation. On histology (particularly evident in the control samples, which have little tissue in the upper pores from the elevated periosteal cells) there was osseous tissue infiltrating the scaffold from below, which was continuous with the cortical bone. The lower half of the scaffold was filled approximately equally for both groups (ESW vs. control) with osseous ($\sim$44%) and osteoprogenitor tissue ($\sim$46%). This demonstrates that the periosteal response to the ESW stimulus is a one time event and that the cells are not permanently altered to a more proliferative state. From the viewpoint of safety, this is important since once the response is characterized fully, it can be controlled

and predicted.

For the free graft model, two different models were utilized. In both models, the scaffold that was within the marrow cavity demonstrated osteoblast lined bone on the scaffold struts. Progenitor cells from the endosteum and marrow stem cells appeared to be responsible for filling the scaffold inside the marrow cavity. This scaffold filling verified the suitability of the scaffold for bone tissue engineering. The marrow forming bone did not appear to fill the scaffold past the cortical bone layer.

In the tibial free graft studies (S3.A,B), the scaffold was flush with the cortical bone outer surface and the transplanted periosteum was sutured to the surrounding periosteum to encourage vascular invasion. In contrast to the controls, which demonstrated no bone formation at the periosteal transplant site, 3 of 4 ESW-treated transplants demonstrated osseous tissue. However, under microscopy this bone tissue did not appear to be fully vital, with osteocyte lacunae appearing empty or vacuolated and with a lack of osteoblasts lining the bone surface. In two of the samples, there was a layer of fibrous tissue blocking the periosteal layer from communicating with the bone forming inside the marrow cavity. In the other sample there was continuity between the grafted periosteum and the transplanted tissue, and it is possible that the transplanted cells were contributing to the new bone formation.

In the femur free transplant model (S3.C), the scaffold extended 1.5mm above the cortical surface, and the periosteum was more separated from the marrow cavity. The ESW treated periosteum was not attached to the local periosteum, which was surgically removed in the vicinity of the implant. The periosteum appeared necrotic and there was no evidence of bone formation. It was anticipated that nutrients would be supplied to the scaffold by diffusion from the marrow and that blood vessels from the soft tissue overlying the scaffold would infiltrate the scaffold and vascularize the graft. Histologically, there was a clear space between the transplanted periosteum and the overlying fibrous tissue.

For both free graft models, there appeared to be insufficient, or at least insufficiently rapid, vascularization of the graft. From the results of the ESW-only study at day 4 (Grps. S2.A and S2.B), it is clear that the periosteal cells were highly metabol-

ically active, proliferating, differentiating, and excreting osseous matrix. Further, recalling the high percentage of cells expressing von Willebrand Factor (endothelial cell marker) discussed in chapter 3, we know that the periosteal tissue is heavily vascularized at 4 days post-ESW. Upon transplantation as a free graft, the blood supplying the nutrients to facilitate this metabolic activity is cut-off; at the new treatment site the cells receive some nutrients by diffusion but are not attached to a vascular network until vascular invasion occurs. It appears that this takes too long in the current models and vascular agents may be needed to facilitate this for successful use of the grafts. It is believed that S3.B demonstrated improved results over S3.C, as there was a higher level of vascularization because (in S3.B) the transplanted periosteum was sutured to local periosteum.

Study limitations

This study successfully demonstrated the ability of ESW treated periosteum to generate bone orthotopically. A single set of ESW conditions, based on the outcome of the rat study presented in Chapter 2, was used to stimulate the periosteum. Although this treatment regimen proved successful in the current model, a more detailed investigation of the response in the rabbit model may reveal an improved set of ESW treatment conditions. In the rat model there was no evidence of microfractures; however, the rabbit model did demonstrate cortical microfractures near the posterolateral corner, opposite where ESW treatment head was applied on the medial side. Previous authors have reported no evidence of microfractures in rats (Tischer et al., 2008) and horses McClure et al. (2004), but microfractures have been reported in rabbit bone (Delius et al., 1995; Tischer et al., 2008). As previously stated, the treatment levels are consistent with clinical treatments, and it is possible based on previous reports that there is something specific about the lengthscales or physiology of the rabbit that results in them being more susceptible to ESW-induced microfractures. However, before clinical adoption of the technique, these microfractures should be investigated in larger animal models that more closely mimic human anatomy.

Although the elevated periosteum was approximated to the local periosteum fol-

lowing implantation of the scaffold in the in situ study, there was typically retraction of the periosteum at 2 weeks and the osteoprogenitor tissue did not cover the scaffold longitudinally in all samples. Coverage was typically >75%. The model could be improved by implanting the scaffold deeper into the pocket or by using an anatomic site that is concave and has more periosteal tissue available to cover the scaffold.

Finally, a single timepoint was used to evaluate the rabbit response to bone formation. The two week time-point was chosen based on numerous studies that demonstrated complete osteogenesis at this timepoint following ESW in rabbits (Delius et al., 1995; Tischer et al., 2008), and following periosteal elevation in rabbits (Cohen and Lacroix, 1955; Stevens et al., 2005) and goats (Simon et al., 2003). Further, since our model is at a site that is minimally load bearing, stress induced remodeling would complicate the observed bone formation. At longer timepoints, the periosteally formed bone is found to undergo maturation (Delius et al., 1995; Cohen and Lacroix, 1955; Stevens et al., 2005). In our results the osteoprogenitor tissue was at various phases of endochondral ossification and will undergo further osteogenesis; studies at a later timepoint should be used to confirm this.

4.5 Summary

For the in situ surgeries, the ESW treated samples outperformed the control group in all key outcome variables (e.g., osteoprogenitor tissue in the upper half of the scaffold, osteoprogenitor tissue above scaffold, callus size). The increased cambium cell number in the ESW treated periosteum generated more osteoprogenitor and osseous tissue above the scaffold and these cells were infiltrating the scaffold upper pores and filling them with osteoprogenitor and osseous tissue. In the lower half of the scaffold, cells left on the cortical bone surface responded equivalently in both groups, which demonstrates the singular, one-time, response to ESW. In the tibia free graft model, there was demonstration of periosteal bone formation; however, this tissue did not appear fully vital at 2 wks post-op. Further studies are needed to optimize the ESW treatment and the timing of the procedure.

Chapter 5

Pressure-time profiles of an electrohydraulic, and unfocused pneumatic, shock wave device in a free field, in tissue, and ex vivo

5.1 Introduction

In order to understand the biological effects of extracorporeal shock waves on specific tissues – and to help interpret the different effects observed with different ESW equimpent – it is necessary to have a recording of the pressure waveforms in the tissue. In an attempt to standardize SW measurements, the *International Society of Musculoskeletal Shock Waves* has collated data from the various musculoskeletal shock wave sources on the market. The quoted data from the OssaTron and dolorclast is included in table 5.1. This data is consistent with data provided to us during private communications with the individual companies (i.e., SANUWAVE Health Inc., EMS).

Parameter	OssaTron[12]	Dolorclast[13]
Peak Positive Pressure [MPa]	71.9	11.9
-6dB[4] focal area, $f_x = f_y$ [mm]	8.7	8
-6dB focal area, f_z [mm]	67.6	8
5MPa focal area, $f_x = f_y$ [mm]	32.0	
Positive energy flux density [mJ/mm^2]	0.34	
Total energy flux density [mJ/mm^2]	0.4	0.18
Positive energy in -6dB focus [mJ]	26.7	
Total energy in -6dB focus [mJ]	28.0	5.4
Positive energy in 5MPa focus [mJ]	96.5	
Total energy in 5MPa focus [mJ]	110.2	
Positive energy in 5mm focal area [mJ]	10.0	
Total energy in 5mm focal area [mJ]	71.9	11.9
Peak negative pressure [MPa]		-5.86
Rise time [μs]		3
Compressive pulse width [μs]		2.5

Table 5.1 – Standardized data reported on OssaTron and dolorclast devices

The amount of published data in peer-reviewed journals concerning pressure-wave measurements for individual ESW sources is limited. For the OssaTron, measurements taken at the secondary focus demonstrated a peak pressure of 37.7MPa, rise time on the order of 40ns, and a postive pulse pressure of 1.2μs (see fig. 5-1a and table 5.2) (Chitnis and Cleveland, 2006). For the dolorclast, to our knowledge, only one group reports the pressure wave profiles (Cleveland et al., 2007; Chitnis and Cleveland, 2006). Typical measurements, taken at 10mm distance from the tip of the 15mm unfocused dolorclast applicator are illustrated in figure 5-1b (note that the pressure trace in fig. 5-1b is for data taken at 3bar; however, the operating pressure and data in table 5.1 is reported at 4bar). For the fig. 5-1b waveform, the total energy flux density was calculated as 0.234mJ/mm^2. Based on the physical definition of a

[1]Data from ISMST: www.ismst.com/start/htm

[2]OssaTron data reported for maximum energy setting (28kV) equivalent to the 0.40mJ/mm^2 setting used in our studies; measurements are taken at the center of the treatment focal zone.

[3]Dolorclast measurements are taken at the maximum setting 4bar, as was used in our measurements and at 1mm from the applicator tip

[4]-6dB focal area is bound by the isobar around the focal zone where the pressure is 50% of the peak pressure.

shock wave and the biomedical definition given by McClure et al. (2004) and Weiss (2006), the wave emitted from the dolorclast is not strictly a shock wave (Cleveland et al., 2007). However, the FDA has approved this as an "Orthopaedic Extracorporeal Shock Wave Therapy Device," and the manufacturers state that its definition as a shock wave device is valid since it is still unclear which wave form characteristic causes the observed effects (Maier and Schmitz, 2008)[5].

Of note during our investigation of extracorporeal shock waves on normal rat and rabbit tissue was that the most overt response was in the periosteum. Besides the inflammation reported for certain areas of muscle (Chapter 2), the muscle, skin, nerve, and vascular tissue did not undergo changes. This prompted the hypothesis that the periosteal cells experience a unique waveform during ESW treatment (compared to the surrounding soft tissue), and that this was one of the factors contributing to their unique response. The periosteal (and endosteal) cells are the only cells in the hindlimb that have a soft matrix on one side and a hard, calcified matrix on the opposite side. The contrast in acoustic impedances at this interface affects the waveform causing reflections as well as creeping waves, which may result in a specific type of waveform that the periosteal cells respond to.

The pressure wave forms for the OssaTron and dolorclast device were recorded and are reported below, with the specific goal of interrogating the waveform that the periosteum is exposed to during treatment. Note that in the animal models reported in the earlier chapters the focused OssaTron (and EvoTron) sources were used; the unfocused dolorclast source is included here for comparison purposes. Three sets of measurements were taken: (1) free field (water bath); (2) in tissue immediately post-sacrifice (intramuscularly and at tibial bone corner); and (3) at the bone surface ex vivo. Measurements were taken using the Onda HNS-0500 needle hydrophone (ONH; Onda Corporation, Sunnyvale, CA) and a polyvinylidene difluoride (PVDF) bilaminar shielded membrane hydrophone (UW Membrane, University of Washington

[5]Cleveland et. al responded by stating that the nanosecond rise time gives a shock front spatial dimension that is on the order of a cell width and can cause intracellular stresses that would not be caused by the shock fronts of waveforms with longer rise times (Maier and Schmitz, 2008). However, they note that it is still unclear which waveform parameter is responsible for the effects seen following ESW treatment.

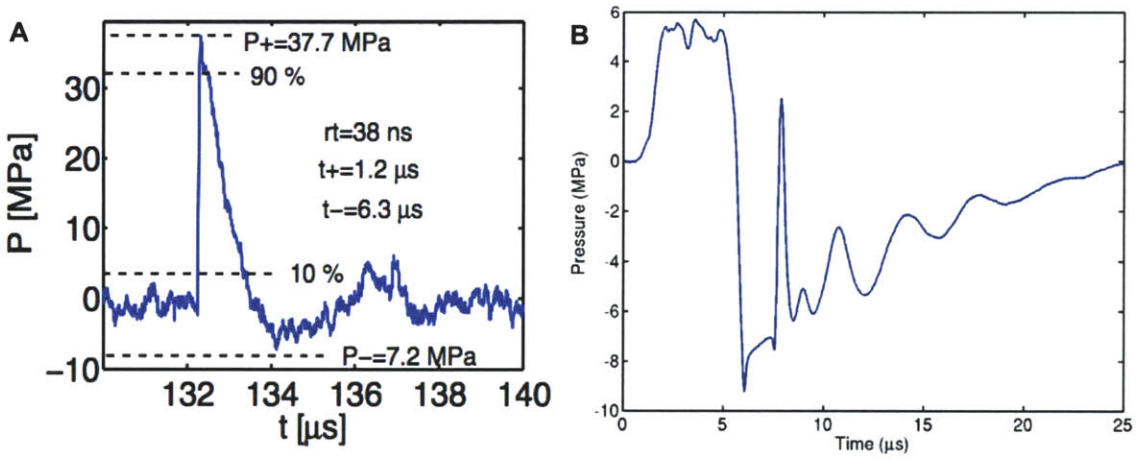

Figure 5-1 – Published data on (A) OssaTron (Chitnis and Cleveland, 2006) and (B) dolorclast waveforms (Cleveland et al., 2007).

OssaTron measurements by Chitnis and Cleveland (2006) at 28kV				
P_+ [MPa]	t_r [μs]	t_+ [μs]	P_- [MPa]	t_- [μs]
37.7	0.038	1.2	-7.2	6.3
Dolorclast measurements by Chitnis and Cleveland (2006) at 4bar				
P_+ [MPa]	t_r [μs]	t_+ [μs]	P_- [MPa]	t_- [μs]
5.6	0.8	3.8	-9.2	15
Dolorclast measurements by Cleveland et al. (2007) at 3bar				
P_+ [MPa]	t_r [μs]	t_+ [μs]	P_- [MPa]	t_- [μs]
6.0	0.6	4.2	-9.1	

Table 5.2 – OssaTron and dolorclast (operating at 4bar) measurements by Chitnis and Cleveland (2006) and dolorclast measurements (operating at 3bar) by Cleveland et al. (2007)

Maxwell et al. (2006)). A Gorillapod (Joby, San Francisco, CA) was adapted to attach the needle hydrophone on one leg to allow multidimensional positioning of the needle hydrophone. Six measurements were taken for each set-up, and measurements are reported as mean ± standard error of the mean.

5.2 Materials and methods

5.2.1 Experimental design

The majority of the measurements were taken with the ONH. The Onda needle hydrophone has a flat response from 1 - 10 MHz. Previous reports demonstrate that the frequency response of the dolorclast device has components down to the 10kHz range (Cleveland et al. (2007); see figure 5-2). However, the characteristic frequency of the waveform is 1MHz (wavelength of 10μs), which would be captured by the ONH. To ensure we were capturing the primary components of the signal,

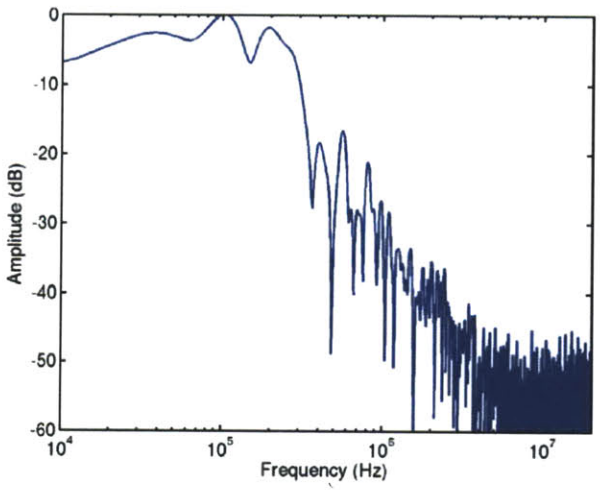

Figure 5-2 – Frequency spectrum reported by Cleveland et al. (2007) for dolorclast handpiece. The graph demonstrates that there are frequency components in the dolorclast signal as low as the 10kHz range. This highlights the need to capture the response with a needle hydrophone with a wide enough frequency spectrum.

experiments were repeated with a second needle hydrophone (Dapco), which has a lower bandwidth spectrum, under identical conditions for the free field data. For free

field measurements of the OssaTron, the pressure in the treatment head was adjusted so that the membrane extended to the center of the secondary focus and the needle hydrophone was 5mm from the tip; for the dolorclast, the needle hydrophone was positioned orthogonal to the shock wave front at 5mm from the applicator tip. The water bath was 35 x 30 cm in cross-section and was filled with distilled water to 12 cm. The water used for experiments was not degassed, as there was likely air introduced during the experiments in tissue, so this setup better matched the experiments in tissue. It is noted, however, that when water is not degassed it increases the likelihood of cavitation bubble formation (especially at the tip surface), which can collapse and cause artificially high measurements.

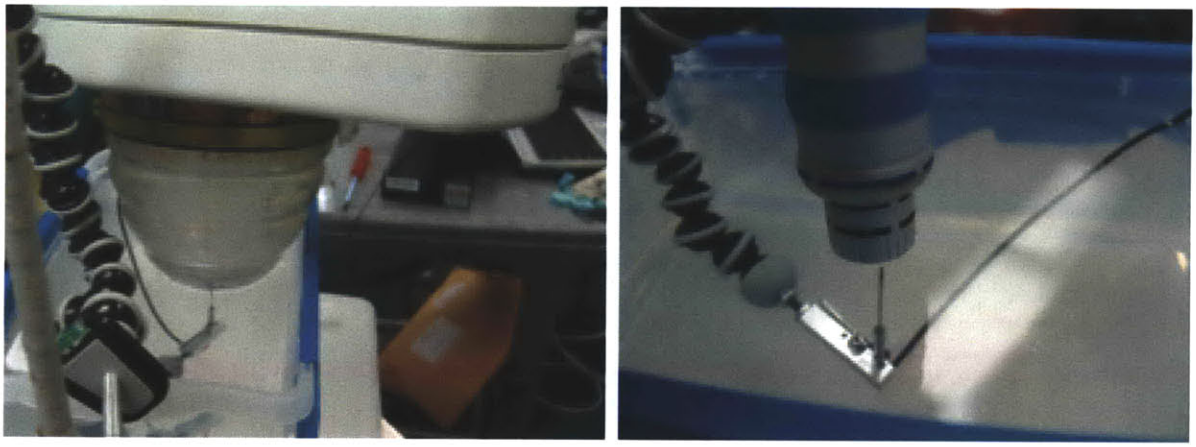

Figure 5-3 – Free field setup for the OssaTron and dolorclast devices: The needle hydrophone is seen in the water bath, connected to the adapted gorillapod that allowed for flexible positioning.

Two experiments were taken in the hindlimb of a freshly sacrificed rabbit (New Zealand White; 4kg). The ONH tip dimensions are 1.1mm ⌀ x 40mm. To position the ONH, a large bore needle was used to create a guide hole. For the intramuscular measurement, the hydrophone was inserted from the lateral side and positioned 5mm from the medial skin surface (see fig. 5-4). The SW applicator was positioned on the shaved skin surface, parallel to the hydrophone and coupled to the shaved skin using ultrasonic gel to minimize wave transmission loss. The hydrophone was then removed and a second guide hole, leading the to the bone corner, was created for the

hydrophone. The applicator was aligned to strike the bone slightly posterior, so that some of the wave would be propagated into the muscle and towards the hydrophone (see fig. 5-4).

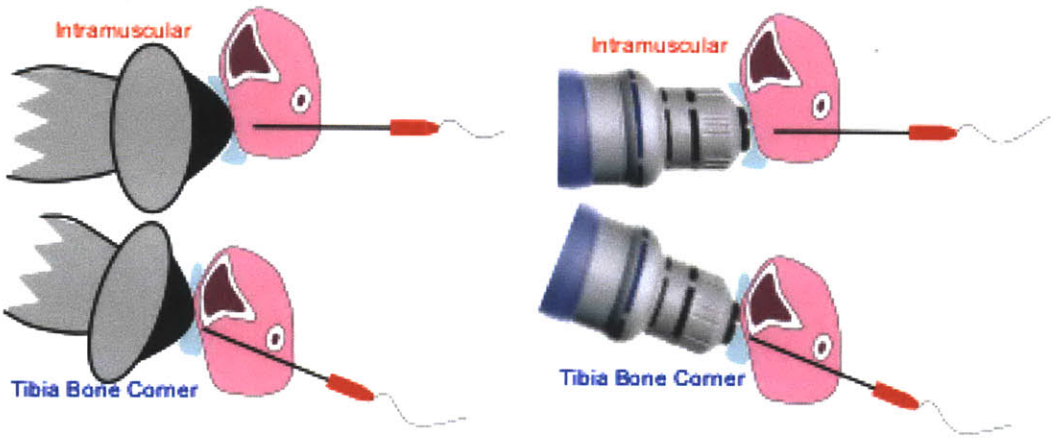

Figure 5-4 – Positioning of needle hydrophone and shock wave devices for experiments in tissue: In the first experiment, the needle hydrophone is placed intramuscularly and the ESW applied from the medial side, with the wave front perpendicular to the needle. In the second setup, the needle is positioned at the tibial bone corner and the ESW device angled so that the wave strikes both the bone and the needle.

Medium	Acoustic Speed [m/s]	Impedance [x10^3 Ns/m^3]
Air	343	0.429
Fat	1,450	1,380
Water	1,483	1,480
Steel	5,790	45,700
Lung	650 - 1,160	260 -460
Kidney	1,570	1,630
Muscle	1,545 - 1,630	1,650 - 1,740
Bone	2,700 - 4,100	3,200 - 7,400
Kidney Stone	4,000 - 6,000	5,600 - 14,400[6]

Table 5.3 – Acoustic speed and impedances of various media (Gerdesmeyer and Lowell, 2007). Note that the acoustic impedance of bone is approximately twice that of water and soft tissue.

[6]Note that these values are approximately 5 times higher than those presented in the graph in figure 5-18 (Cleveland and McAteer, 2006)

To evaluate the pressure profile on the periosteal surface more accurately, the rabbit bone was extracted. The rabbit bone was stored in ethanol between experiments, thus, there may have been minor changes to mechanical properties due to tissue fixation, although this should not affect the primary contributor to the acoustic changes – the calcified tissue, which has the largest acoustic impedance mismatch when compared with water and soft tissue (see table 5.3; Gerdesmeyer and Lowell (2007)). The bone was rehydrated in DI water for 24hrs prior to testing. The bone was then positioned in the water bath, with the needle hydrophone lying at 45° to the surface in close proximity to the periosteum. The shock wave source was aligned to direct waves at 45° to the surface (90° to the hydrophone), in an attempt to pick up both the incident and reflected waves. For controls, the shock wave source and hydrophone were left in place, with only the bone being removed, and the experiments were repeated.

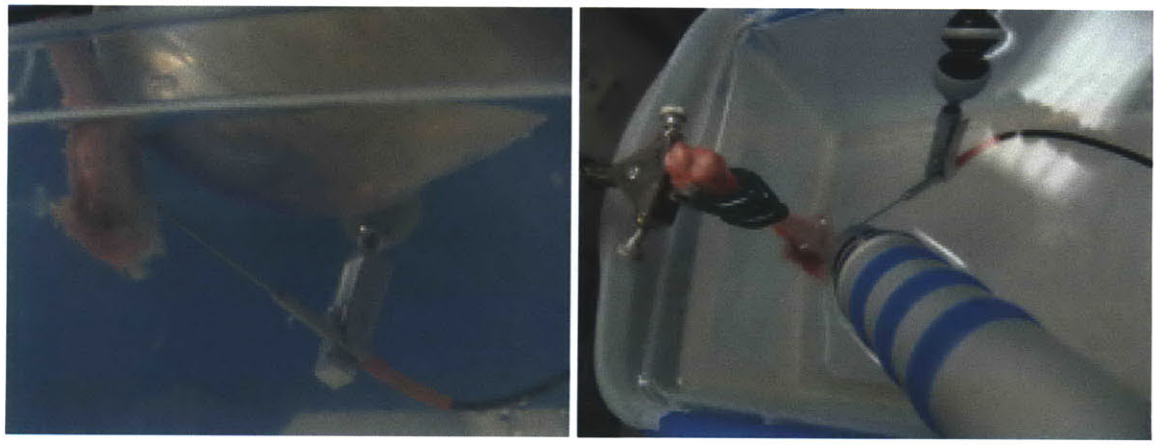

Figure 5-5 – Experimental setup for measurements of the waveform around bone ex vivo: (A) OssaTron and (B) dolorclast. The shock wave sources are pointed at the medial tibia bone surface in a water bath and the needle hydophone positioned to capture the reflected wave.

Given the positioning constraint of the needle hydrophone and its inability to truly measure the periosteal bone surface response, the membrane hydrophone was employed to make the surface measurements. The medial tibia was approximated to the membrane surface and fixed in place using duct tape (see fig. 5-6). The shock

wave sources were placed at 5mm from the membrane surface in the water bath for the measurements.

The shock wave sources employed were the OssaTron (SANUWAVE Health, Inc., Alpharetta, GA) and the EMS Dolorclast (EMS, Switzerland) with the 15mm unfocused convex applicator tip. The OssaTron was operated at 28kV, which is quoted as having an energy flux density of $0.40 mJ/mm^2$. The dolorclast was operated at 4bar, which is quoted as being an energy flux density of $0.18 mJ/mm^2$.

Figure 5-6 – For measurements at the medial tibia bone surface, the tibia was sectioned and approximated and attached to the membrane surface. The ESW devices were positioned on the opposite side of the membrane in a water bath.

5.2.2 Hydrophones

Measurements were taken using the Onda HNS-0500 needle hydrophone (ONH; Onda Corporation, Sunnyvale, CA) and a polyvinylidene difluoride (PVDF) bilaminar shielded membrane hydrophone (HGL 0200, ONDA, Sunnyvale, CA) with a 500 μm sensitive element, bandwidth of 40 MHz, and 20 dB inline amplifier. A Gorillapod (Joby, San Franciscio, CA) was adapted to attach the needle hydrophone on one leg to allow multidimensional positioning of the needle hydrophone.

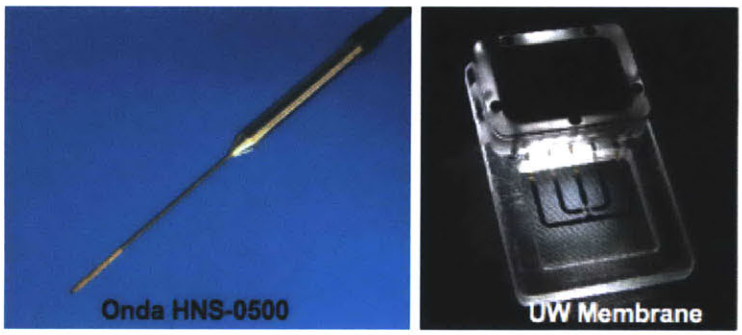

Figure 5-7 – Hydrophones (needle and membrane) used during this study for measuring pressure wave forms.

5.2.3 Data analysis

Digitized data was analyzed using Matlab. The peak positive pressure (P_+) and peak negative pressure (P_-) were recorded by finding the maximum/minimum value within a user defined time range. The rise time was calculated by calculating the time lapse between 10% and 90% of this value. Pulse widths were taken at 50% of the maximum/minimum pressures. All data are reported as mean $\pm$ standard error of the mean.

5.3 Results

5.3.1 Measurements for OssaTron - unfocused electrohydraulic shock wave source

Free field measurements

Figure 5-8 shows the individual and averaged waveforms for the focused (OssaTron) shock wave source, with key characteristics of the wave presented in table 5.4 (for previously published values, see table 5.2).

The waveform consists of a rapid rise time (80ns) up to a peak compressive pressure of 37 MPa. The duration of the compressive wave (evaluated as the amount of time with p $>p_+/2$) was 320ns. The tensile wave was less steep and had a lower absolute

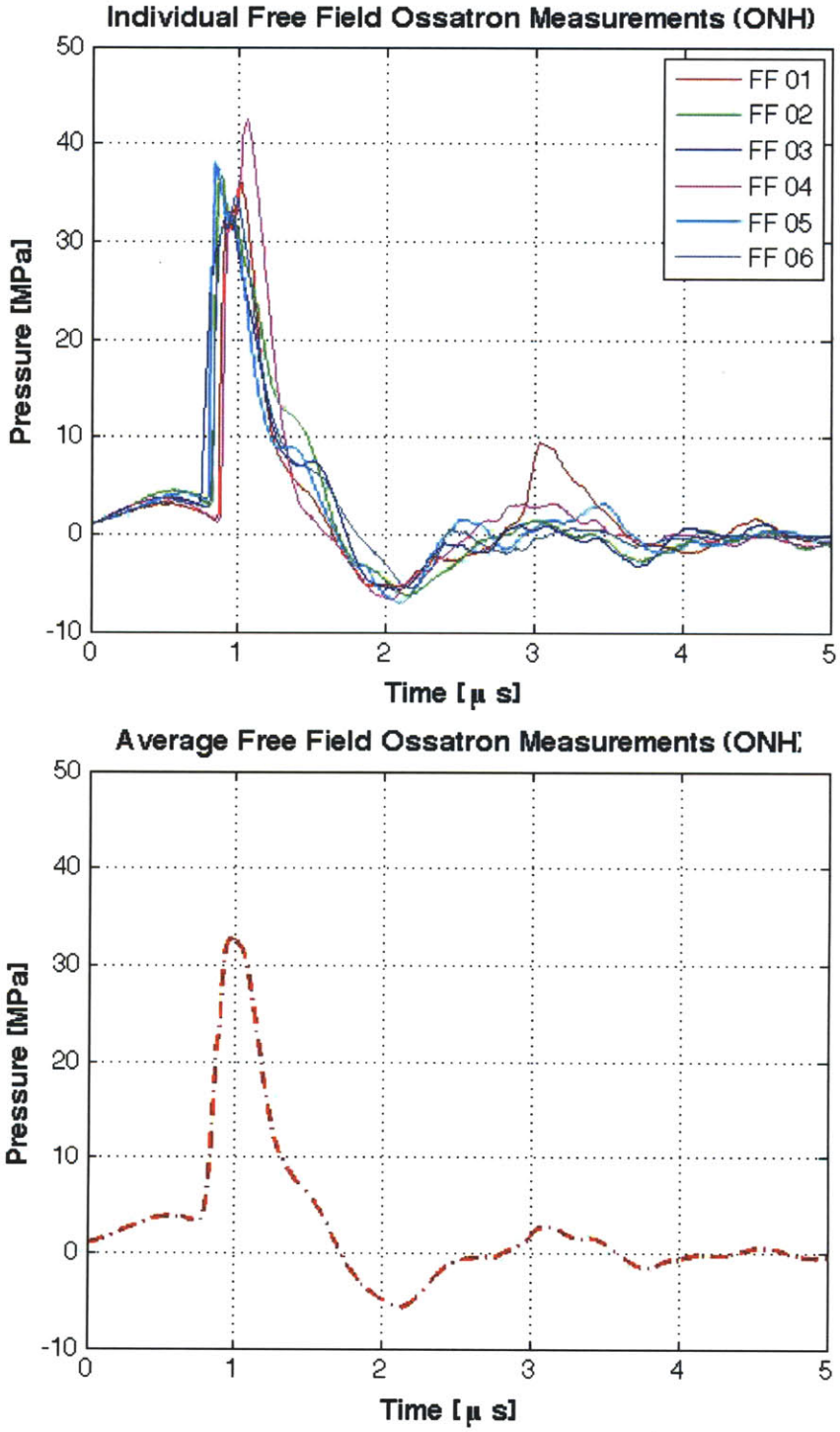

Figure 5-8 – Individual and average measurements for OssaTron in a free field at 5mm from the application tip. The waveforms demonstrate the high peak pressure, rapid rise time, and short pulse duration of the compressive shock wave, which is followed by a lower pressure and smoother tensile wave.

pressure peak (P- = -5.8MPa; t_{tens} = 480ns). The pressures closely matched the previously reported data (see table 5.2 (Chitnis and Cleveland, 2006)); however, the duration of the negative wave was shorter.

OssaTron measurements in free field at 5mm (ONH)				
P_+ [MPa]	t_r [μs]	t_+ [μs]	P_- [MPa]	t_- [μs]
37.07 $\pm$ 1.34	0.08 $\pm$ 0.02	0.32 $\pm$ 0.02	-5.8 $\pm$ 0.27	0.48 $\pm$ 0.04

Table 5.4 – OssaTron measurements in free field at 5mm using ONH. Mean $\pm$ SEM.

Pressure measurements were repeated using the Dapco needle hydrophone. The waveforms were characteristically similar, but the pressures and pulse widths recorded by the Dapco hydrophone were higher (see fig. 5-9 and table 5.5).

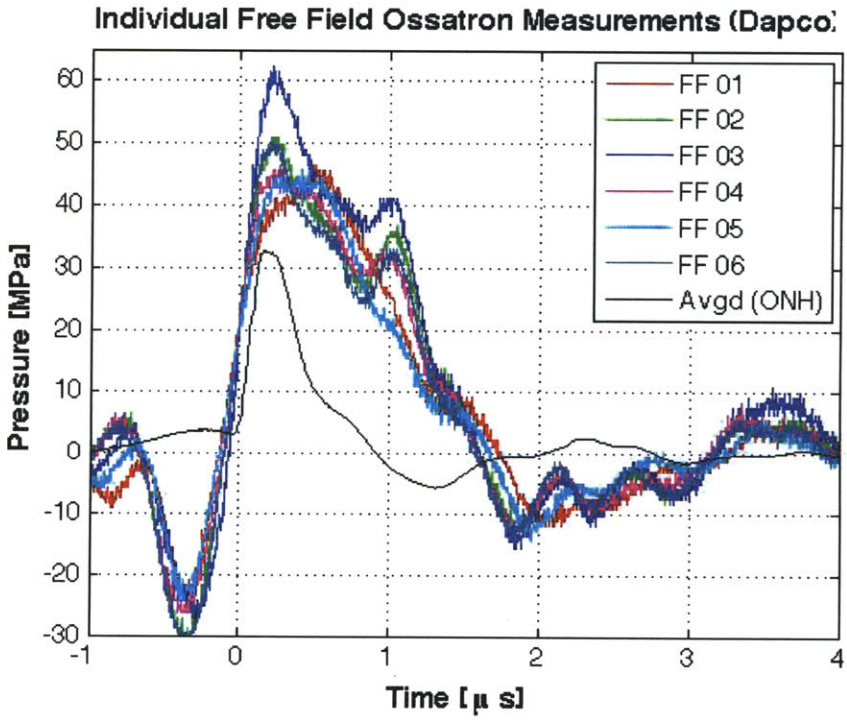

Figure 5-9 – Overlay of (individual) OssaTron measurements acquired with a second needle hydrophone(Dapco) to verify the calibration used. The average ONH measurement is lower in pressure and has a shorter pulse width than the Dapco needle hydrophone.

OssaTron measurements in free field at 5mm (Dapco)				
P_+ [MPa]	t_r [μs]	t_+ [μs]	P_- [MPa]	t_- [μs]
50.41 ± 2.5	0.25 ± 0.04	1.07 ± 0.04	-13.82 ± 0.58	0.72 ± 0.03

Table 5.5 – OssaTron measurements in free field at 5mm measured with Dapco hydrophone. Mean ± SEM.

Measurements in tissue

Figure 5-10 shows the individual and average waveforms for the OssaTron in muscle (5mm depth) and at the tibial bone corner. Table 5.6 records the measurements of 5 key characteristics of the wave. The rise time increases from the free field measurements for the intramuscular measurement (IM vs. FF; 470ns vs 80ns) and the peak pressure is reduced by 57% (IM vs. FF; 15.37 vs. 37.07). The pulse width increases slightly (IM vs. FF; 440ns vs. 320ns). The tensile wave is more comparable to the free field measurements.

The measurements at the tibial bone corner are dramatically reduced. However, it is difficult to fully interpret the waveforms at this location since the OssaTron wave and the needle hydrophone were likely poorly aligned.

OssaTron measurements in tissue: intramuscular (ONH)				
P_+ [MPa]	t_r [μs]	t_+ [μs]	P_- [MPa]	t_- [μs]
15.37 ± 2.03	0.47 ± 0.07	0.44 ± 0.05	-5.57 ± 0.34	0.76 ± 0.13
OssaTron measurements in tissue: tibia bone corner (ONH)				
P_+ [MPa]	t_r [μs]	t_+ [μs]	P_- [MPa]	t_- [μs]
6.9 ± 1.43	1.38 ± 0.09	1.31 ± 0.14	-4.03 ± 0.14	1.16 ± 0.05

Table 5.6 – OssaTron measurements in tissue using ONH. Mean ± SEM.

Ex vivo measurements

Two sets of ex vivo measurements were taken: the needle hydrophone was used to record the reflected waveforms, which are plotted fig.5-11 . The membrane hy-

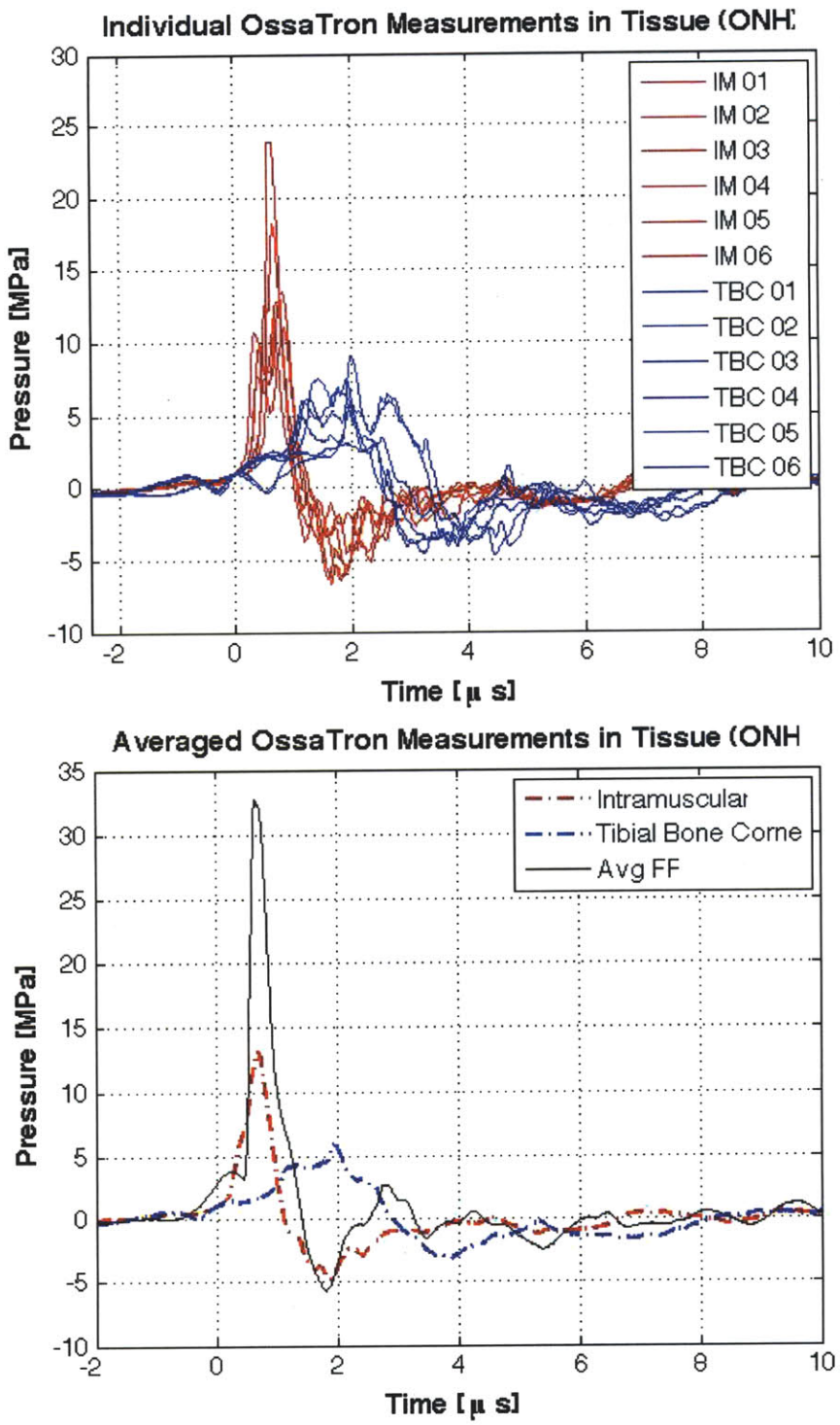

Figure 5-10 – Individual and average measurements of the OssaTron in tissue (muscle, tibia bone corner). measured as shown in table 5.6. The compressive waveform is less steep and has a lower peak pressure when compared with free field measurements; the tensile wave measured intramuscularly is more consistent with free field measurements. The waveform is drastically reduced for the tibia bone corner measurements, however, alignment issues preclude accurate measurement at this site.

drophone was used to record the transmitted and reflected waveform. Note that the speed of sound in water is 1.5mm/μs. The needle hydrophone was placed approximately 3mm (2μs) from the bone surface; the membrane hydrophone was placed 1mm (<1μs) from the bone surface. For both hydrophones the experiments were repeated with an identical setup and only the bone removed.

OssaTron measurements at bone surface ex vivo: bone reflection (ONH)				
P_+ [MPa]	t_r [μs]	t_+ [μs]	P_- [MPa]	t_- [μs]
5.67 ± 0.37	1.93 ± 0.21	1.95 ± 0.12	-4.51 ± 0.16	0.93 ± 0.08
OssaTron measurements at bone surface ex vivo: no bone (ONH)				
P_+ [MPa]	t_r [μs]	t_+ [μs]	P_- [MPa]	t_- [μs]
5.08 ± 0.35	1.77 ± 0.05	2.14 ± 0.16	-3.76 ± 0.15	2.09 ± 0.15

Table 5.7 – OssaTron measurements ex vivo using ONH. Mean ± SEM.

For the needle hydrophone experiments we note that the absolute pressures are lower than those reported for the free field measurements (see fig. 5-11 and table 5.7). This stems from the fact that the hydrophone is oriented at approximately 90° to the wavefront. Nonetheless, both waveforms appear similar at first observation. When the individual waveforms for the bone reflection samples are examined more closely, there are secondary peaks that likely result from reflected waves or by creeping waves that are released from the surface. The membrane hydrophone also picked up a double wave peak; however, the pressures were substantially reduced from those recorded for the normal incident waveform with no bone present (see fig. 5-12).

5.3.2 Measurements for dolorclast - unfocused radial shock wave source

Water Bath Measurements

The free field measurements for the dolorclast are included in figure 5-13. The waveform consisted of a primary compressive wave followed by a tensile wave that had

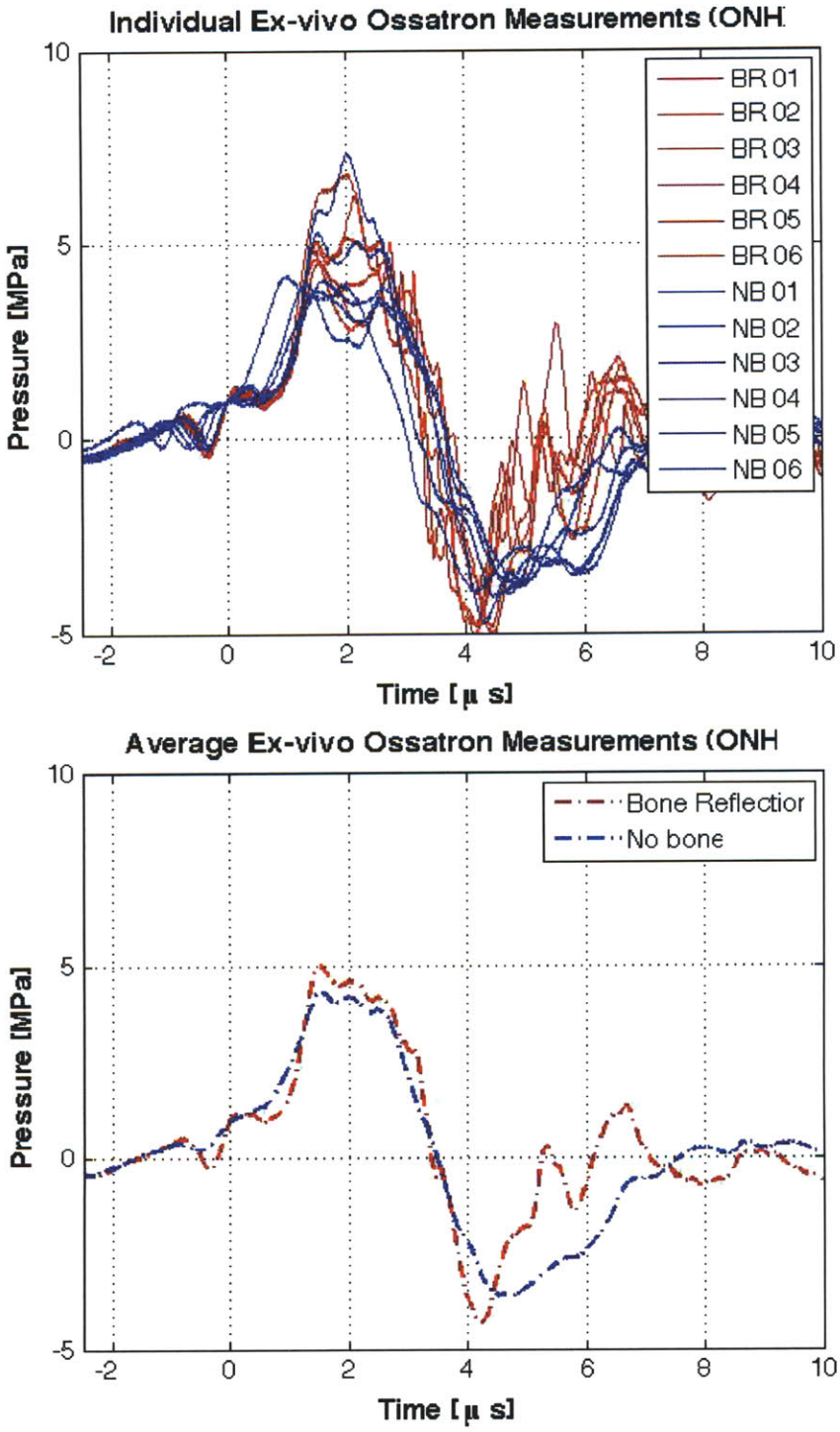

Figure 5-11 – Individual and average measurements for OssaTron bone reflection using the ONH. On close inspection, the individual waveforms for the bone reflected measurements have a characteristic second peak, which is attributed to reflected waves or creeping waves released from the bone.

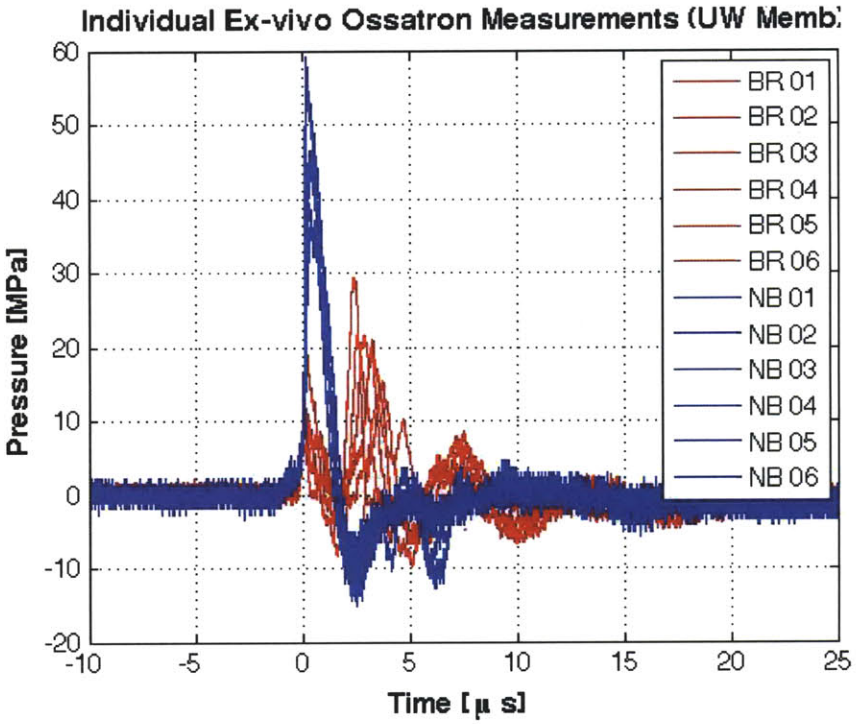

Figure 5-12 – Individual and average measurements for OssaTron bone using membrane hydrophone. With this hydrophone, the secondary compressive peaks are more clearly seen.

slightly less magnitude and a shorter pulse duration. There were a series of smaller waveforms that followed the initial pulse.

Dolorclast measurements in water bath at 5mm (ONH)				
P_+ [MPa]	t_r [μs]	t_+ [μs]	P_- [MPa]	t_- [μs]
3.93 ± 0.59	2.09 ± 0.13	5.17 ± 0.38	-2.37 ± 0.30	1.16 ± 0.03

Table 5.8 – Dolorclast free field measurements at 5mm from applicator tip using ONH. Mean ± SEM.

The data matches previously published data for the waveform reasonably accurately with the exception of the rise time, which was recorded here as 2.09μs (see table 5.8; it was previously reported as 0.6μs, see table 5.2).

Dolorclast measurements in water bath at 5mm using Dapco hydrophone)				
P_+ [MPa]	t_r [μs]	t_+ [μs]	P_- [MPa]	t_- [μs]
3.79 ± 0.11	2.60 ± 0.19	3.50 ± 0.13	-1.98 ± 0.03	1.18 ± 0.06

Table 5.9 – Dolorclast measurements in water bath at 5mm using Dapco hydrophone. Mean ± SEM.)

The Dapco measurements for the dolorclast device closely matched the recordings of the ONH (see fig. 5-14 and tables 5.8 and 5.9).

Measurements in tissue

Figure 5-15 shows individual and average waveforms, and data is tabulated in table 5.10.

Although proper alignment is difficult for these measurements – the hydophone is placed somewhat blindly – the waveform for the intramuscular measurements was quite similar to the idealized medium (water bath; see table 5.10). There was a slightly longer rise time (IM vs. FF; 2.65μs vs. 2.09μs); however, the maximum tension was slightly higher (IM vs. FF; 4.32MPa vs. 3.93MPa), which demonstrates the excellent coupling and transmission of the wave into the body. Measurements were

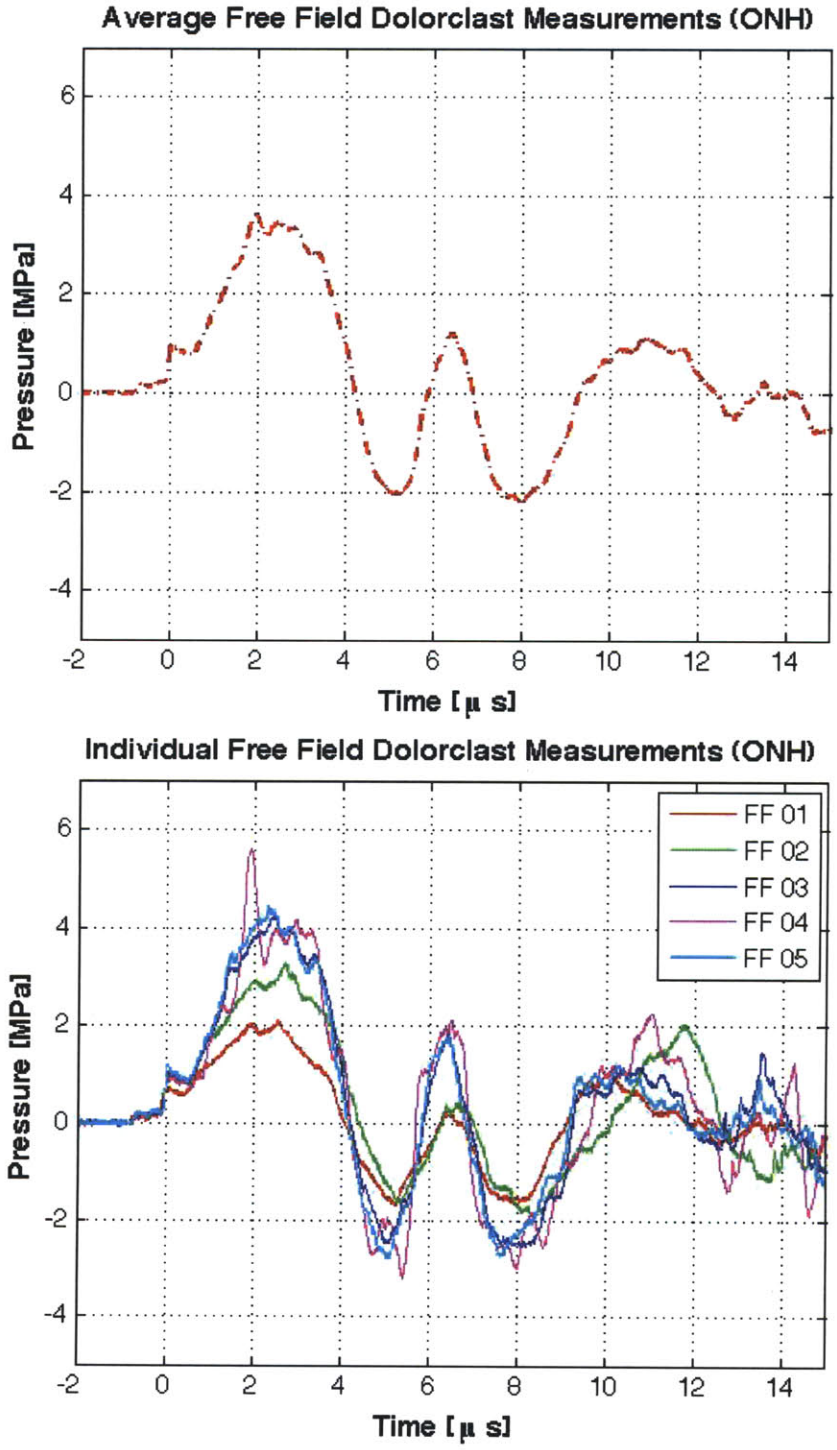

Figure 5-13 – Individual and average measurements of dolorclast pressure waveforms in a free field measured at 5mm from the application tip with the ONH. The waveform is smooth than that seen for the focused device and has a longer rise time and lower peak pressure. The tensile wave is also seen immediately following the compressive wave.

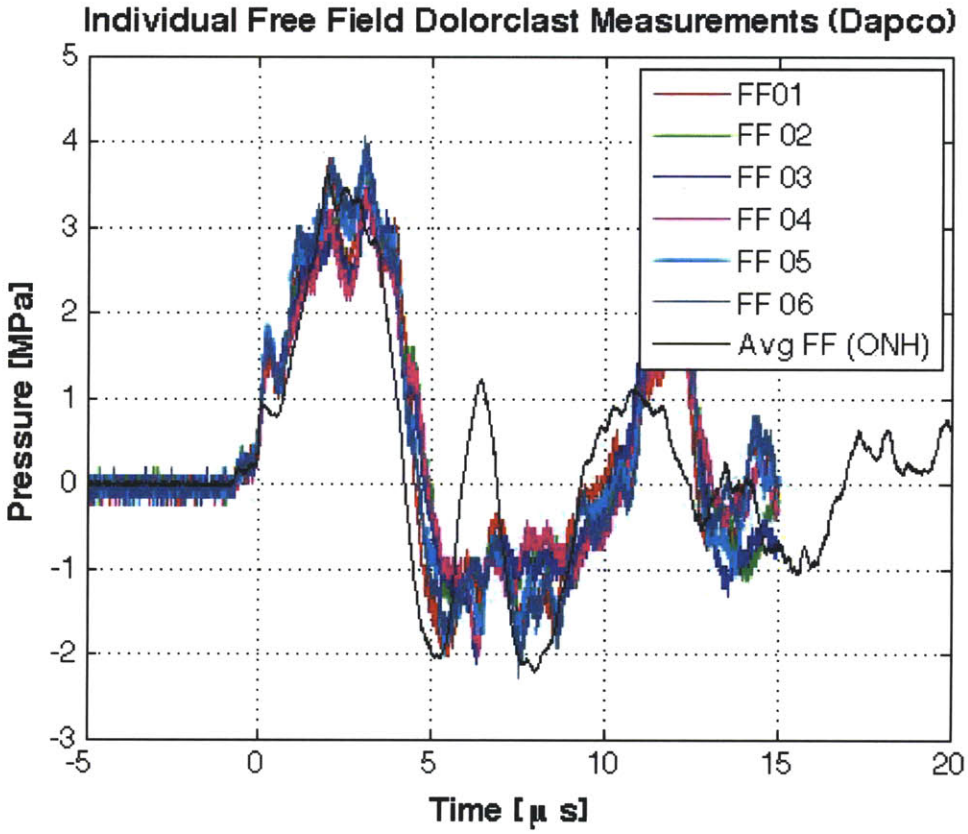

Figure 5-14 – Overlay of (individual) dolorclast measurements acquired with a second needle hydrophone (Dapco) to verify the calibration used. Previous data demonstrated a frequency response down to the 10kHz range (see fig 5-2). However, identical waveforms were captured with both hydrophones, which demonstrated the validity of the ONH hydrophone measurements.

taken at the tibia bone corner to begin to interrogate any significant effects in vivo around the bone surface, but alignment restrictions made it difficult to get an exact measurement of either the wave incident to, or reflected from, the surface. In these waveforms, there is a slight reduction in peak amplitude relative to the intramuscular measurements and a longer pulse width. Further, the secondary waves appear to be damped out.

Dolorclast measurements in tissue: intramuscular (ONH)				
P_+ [MPa]	t_r [μs]	t_+ [μs]	P_- [MPa]	t_- [μs]
4.32 ± 0.33	2.65 ± 0.33	2.78 ± 0.19	-1.98 ± 0.42	0.98 ± 0.11
Dolorclast measurements in tissue: tibia bone corner (ONH)				
P_+ [MPa]	t_r [μs]	t_+ [μs]	P_- [MPa]	t_- [μs]
3.65 ± 0.54	2.36 ± 0.35	3.17 ± 0.47	-1.60 ± 0.54	0.44 ± 0.08

Table 5.10 – Dolorclast measurements in tissue using ONH. Mean ± SEM.

Ex vivo measurements

Figure 5-16 includes the individual and average waveforms and the key parameters are tabulated in 5.11. Although the primary waveforms and data share similar characteristics for the needle hydrophone measurements with and without the bone in place, when the individual waveforms are considered, there is a characteristic second peak for all of the reflected waveforms, which is not seen on any of the control waveforms (fishers test, $p = 0.001$). Further, the secondary waves for the reflected measurements are more damped than when the bone is removed.

For the membrane measurements, there is a double peak for the measurements taken with the bone in place. However, the peak pressures are dramatically less than those recorded without the bone in place. The two peaks are slightly greater than 1μs apart, which is consistent with the bone being approximately 1mm from the bone surface (i.e. suggestive that it is a reflected wave. Also of note is that the peak pressures for the membrane hydrophone measurements were higher than those recorded with the needle hydrophone.

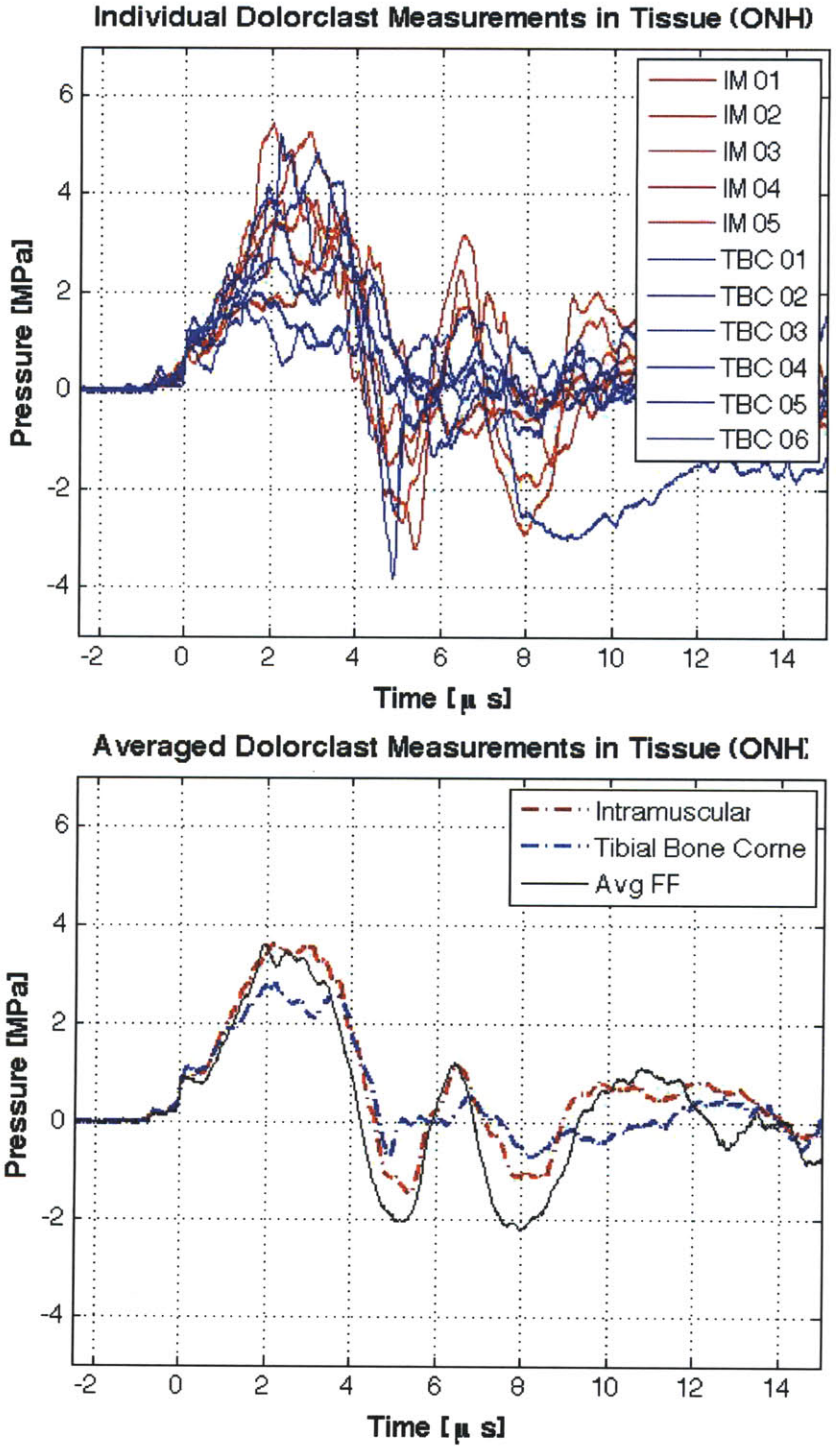

Figure 5-15 – Individual and average measurements for dolorclast measurements in tissue (muscle, tibia bone corner) measured as shown in 5-10. For the dolorclast device, the wave appears to more smoothly transition into tissue when compared with the the OssaTron device. This likely results from the fact that higher frequencies (which the OssaTron has a lot more of) are attenuated more by tissue than lower frequencies.

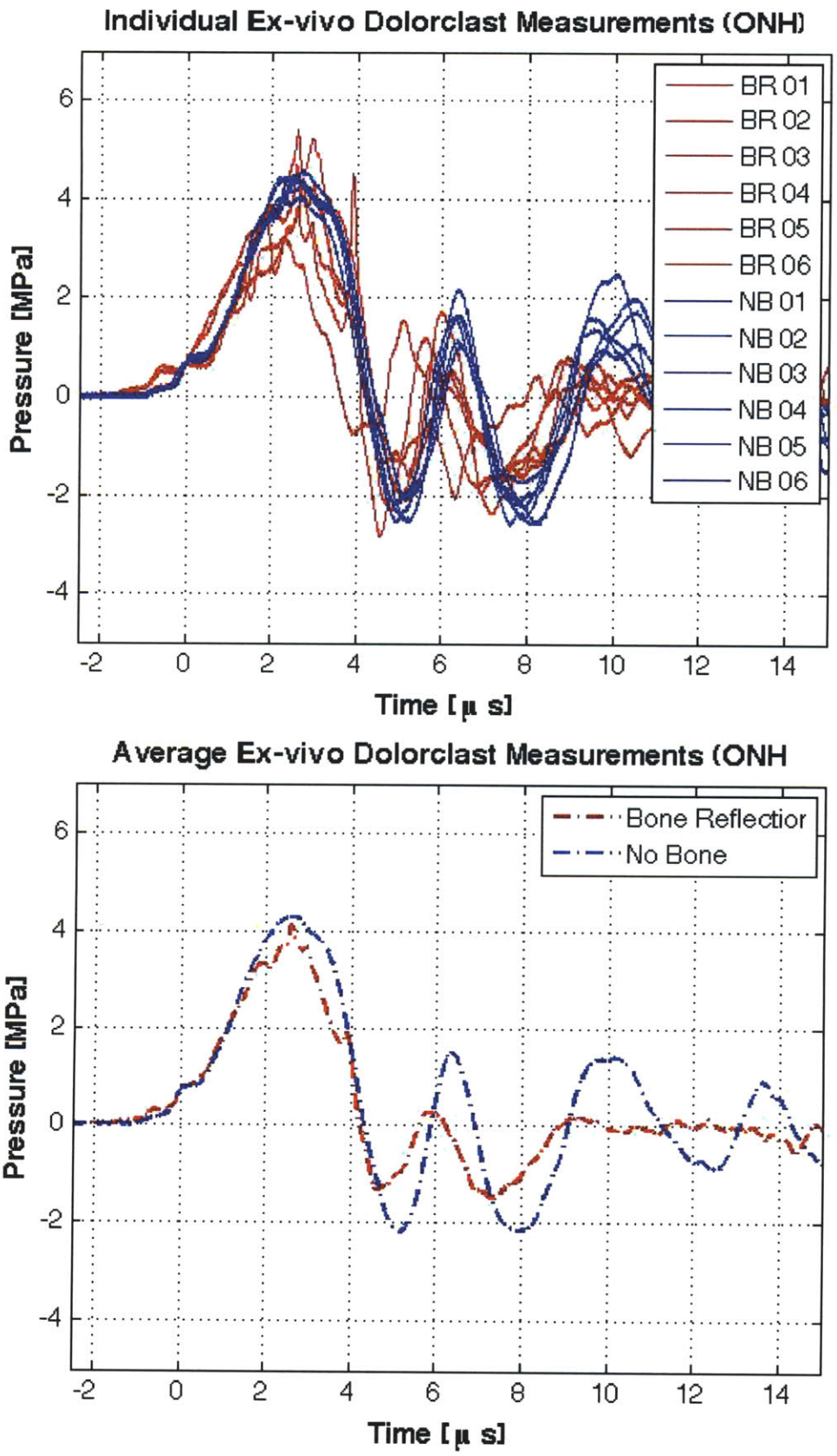

Figure 5-16 – Individual and average measurements for dolorclast bone reflection using the ONH. The individual waveforms with the bone present demonstrate a characteristic second peak in the compressive wave, which is attributed to secondary reflected or creeping waves from the bone.

Dolorclast measurements at bone surface ex vivo: bone reflection (ONH)				
P_+ [MPa]	t_r [μs]	t_+ [μs]	P_- [MPa]	t_- [μs]
4.37 ± 0.31	2.71 ± 0.10	2.34 ± 0.09	-1.82 ± 0.30	0.93 ± 0.05
Dolorclast measurements at bone surface ex vivo: no bone (ONH)				
P_+ [MPa]	t_r [μs]	t_+ [μs]	P_- [MPa]	t_- [μs]
4.37 ± 0.07	2.37 ± 0.06	2.65 ± 0.04	-2.29 ± 0.10	1.04 ± 0.03

Table 5.11 – Dolorclast measurements ex vivo using ONH. Mean ± SEM.

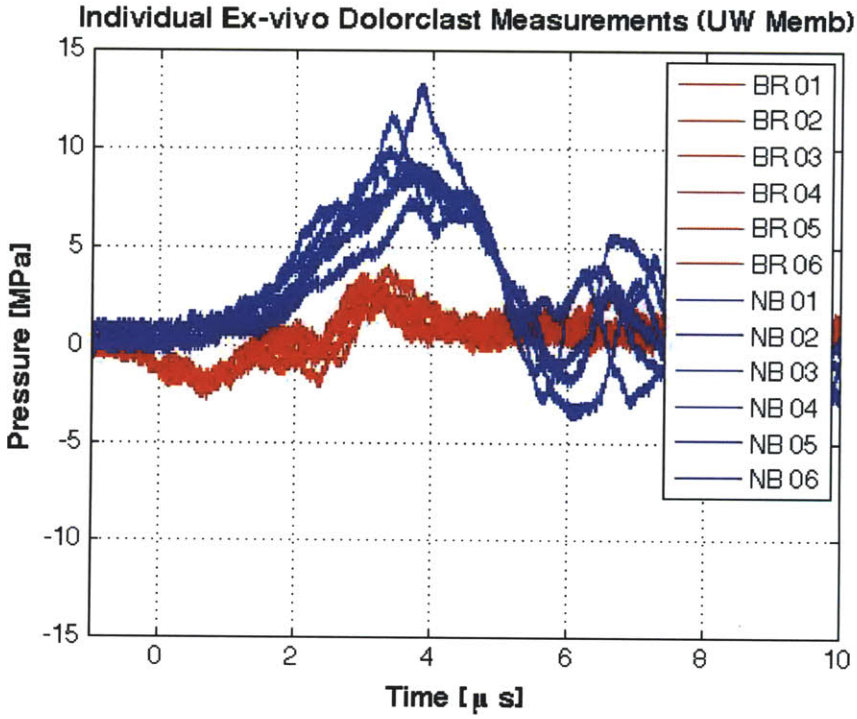

Figure 5-17 – Individual and average measurements for dolorclast bone using membrane. The secondary peaks are still seen by the membrane, however, the amplitudes are dramatically reduced. This is attributed to local changes in water bath conductivity in the vicinity of the bone.

5.4 Discussion

The free field measurements were characteristically similar to previously reported data for both devices in the literature and by the device manufacturers. For both devices, we found a slightly longer rise time than the previously reported data (Chitnis and Cleveland, 2006). It is possible that our ESW-devices had slightly different characteristics than those measured previously. In particular, the stochaistic nature of the electrohydraulic generators has been reported previously. It is well established that the needle hydrophone can record higher pressures as the tip is a blunt object in the way of the traveling wave; however, the values measured for the peak pressures were consistent with those previously recorded by a fibre optic hydrophone (OssaTron; Chitnis and Cleveland (2006)) and the flatter HGL-0200 (Onda Corp, Sunnyvale, CA) hydrophone (dolorclast; Cleveland et al. (2007)).

There was some concern regarding the validity of the measurements for the dolorclast using the Onda hydrophone, which has a bandwidth in the range of 1MHz to 10MHz. Previously reported data for the dolorclast demonstrated energy in frequencies down to 10kHz (see figure 5-2; Cleveland et al. (2007)). In order to evaluate the effectiveness of the Onda needle hydrophone in picking up the dolorclast response, data was collected with a Dapco needle hydrophone, which has a lower bandwidth. For the dolorclast data, the waveform closely matched that of the Onda hydrophone (see figure 5-14). For the OssaTron the waveforms were characteristically similar, yet the Dapco hydrophone measured a higher peak compression pressure (see figure 5-9) and a doubling in pulse width. This may have resulted from the previously mentioned pressure increase for needle hydrophones.

The Onda hydrophone successfully captured wave form data in tissue. For the OssaTron, the peak pressure was reduced and the rise time increased. This is characteristically consistent with previous measurements of electrohydraullicly generated shock waves propagating into tissue. Cleveland et al. (1998), demonstrated that the pressure wave peak pressure was reduced as it passed through tissue and that the rise time was extended. This is attributed to the fact that tissue attenuates higher

frequencies more than lower frequencies, and thus the waveform is smoothed out. By contrast the dolorclast device transmits waves more seamlessly into tissue, with the measured wave characteristics consistent with the free field measurements. This is attributed to the fact that it does not consist of higher frequencies.

One aim of the study was to evaluate whether the periosteal cells experience a unique wave form. Physically, the periosteal cells are uniquely positioned within the limb as the only cells that have soft tissue on one side and hard tissue behind. Based on the acoustic equations for energy (intensity) reflection and transmission (5.1 and 5.2), we would anticipate that the majority of the wave energy reaching the bone would be transmitted but that some would also be reflected (see figure 5-18):

$$R_I = \frac{(Z_2 - Z_1)^2}{(Z_1 + Z_2)^2} \tag{5.1}$$

$$T_I = \frac{4Z_1Z_2}{(Z_1 + Z_2)^2} \tag{5.2}$$

, where R_I = reflected intensity; T_I = transmitted intensity; $Z_{1,2}$ = are the acoustic impedances of medium 1 and 2.

Figure 5-18 demonstrates that although >50% of the energy is transmitted, there is a reflected component of the wave. The reflected (R_P), and transmitted (T_P), pressures can be calculated from:

$$R_P = \frac{(Z_2 - Z_1)}{(Z_1 + Z_2)} \tag{5.3}$$

$$T_P = \frac{2Z_2}{(Z_1 + Z_2)} \tag{5.4}$$

To try capture the surface wave, two experiments were performed. The needle hydrophone was positioned to measure the reflected wave, and second measurement was performed with a PVDF membrane hydrophone that the bone was placed flat against. Both devices picked up secondary wave peaks, which were attributed to reflected waves or creeping waves in the bone that were released. This verifies that the periosteal cells experience a specific waveform, which may contribute to the prolifera-

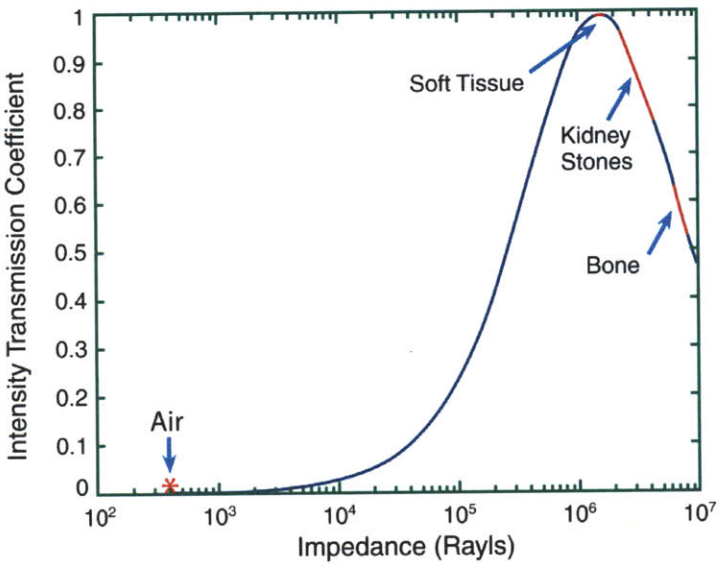

Figure 5-18 – The intensity transmission coefficient (T_I) from water (Z = 1.5 x 10^6 Rayls) to various biologically relevant media. Greater than 50% of the energy is transmitted to bone; but there is also energy reflected into the soft tissue (from Cleveland and McAteer (2006))

tive response. The membrane hydrophone had reduced peak wave measurements for both devices with the bone in place relative to the measurements without the bone. The membrane hydrophone is sensitive to the conductivity of the medium in which the measurements are taken; the piezoelectric crystal is exposed to the medium and will discharge to the surrounding medium if the conductivity is too high. Although the conductivity of the bath was monitored throughout the experiments, it is possible that the local conductivity was higher than the global measurements. Interestingly, the measurement without the bone in place, which should have matched the free field measurement were higher with the membrane hydrophone for both devices. It is possible that this was a calibration error.

5.5 Summary

Waveforms for an electrohydraulic and unfocused pneumatic shock wave source were recorded in a free field, in tissue, and ex vivo and the wave characteristics reported. For the free field devices, the waveforms were consistent with previously published

data. Measurements taken in muscle demonstrated a decreased peak pressure and an increased rise time for the electrohydraulic source; the pneumatic source did not differ in any measured parameters between the free field and tissue measurements. It is known that soft tissue attenuates higher frequencies more than lower frequencies; thus, an electrohydraulically generated wave, with its higher frequency components, is attenuated more than pneumatically generated waves. Chapters 2-4 describe the dramatic proliferation of periosteal cells, which we do not see in cells in the surrounding soft tissue. It is possible that unique characteristics of the waveform contribute to this response. Here, we begin to interrogate these waveforms in tissue and ex vivo and demonstrate a characteristic second peak at the periosteal surface. These secondary peaks are attributed to reflected waves or creeping waves that – combined with the incident wave – treat the periosteal cells with a unique waveform.

Chapter 6

Summary and Future Work

6.1 Summary of findings

The overall goal of this work is to demonstrate the efficacy of an extracorporeal shock wave (ESW)-thickened periosteum as an overlay on a porous calcium phosphate scaffold for the orthotopic growth of bone. The inspiration for the work stemmed from the demonstration of periosteal osteogenesis (Takahashi et al., 2004; Tischer et al., 2008) and the demonstrated effectiveness of ESW for fracture non-unions, as well as many other osseous defects (Birnbaum et al., 2002; Cacchio et al., 2009; Haupt, 1997; Johannes et al., 1994; Ludwig et al., 2001; Ogden et al., 2001; Rompe et al., 2001; Schaden et al., 2001; Jagt et al., 2009; Wang et al., 2001, 2008, 2005).

Extracorporeal shock waves have been used clinically since the 1980's to break up kidney stones. Recently, they have shown clinical efficacy in the treatment of several musculoskeletal disorders, and multiple devices now have FDA approval for the treatment of calcific tendonitis and plantar fasciitis (Chung and Wiley, 2002; Cosentino et al., 2004; Gerdesmeyer and Lowell, 2007; Haupt, 1997; Ogden et al., 2001, 2004; Rompe et al., 2001; Speed et al., 2003; Strash and Perez, 2002; Takayama and Saito, 2004; Theodore et al., 2004; Thiel, 2001; Tombolini et al., 2000). For medical applications, the peak ESW pressures lie in the range of 5-120MPa; the rise time is on the order of 10-100ns depending on the equipment used; and the pulse width is on the order of 1μs (Gerdesmeyer and Lowell, 2007; Chung and Wiley, 2002).

The first step taken in validating the therapeutic approach was to evaluate the effects of ESW dose and anatomic site on the periosteal cell proliferation in a rat model (Chapter 2). For anatomical site the femur was compared to the tibia; and high vs. low energy flux density ($0.40 mJ/mm^2$ vs. $0.15 mJ/mm^2$) were also compared at the same anatomic site. In all ESW-treated groups, there was a statistically significant increase in periosteal cambium layer cell counts and cambium layer thickness when compared to controls. For the anatomical location study, the tibial periosteum displayed a statistically significant increase in cambium cell proliferation in response to ESWs when compared with the femur. This is useful since the tibial periosteum is more accessible surgically (only a thin layer of skin and fascia overlies the medial tibia) than femoral periosteum. The reduced proliferation of the femoral periosteum likely results from the lower energy of shock wave that actually reaches the bone surface – there is more soft muscle mass surrounding the femur, which attenuates the wave.

Previous reports described a dose dependent response of periosteal osteogenesis to ESWs (e.g., Tischer et al. (2008)). In this study, the higher dose of ESWs also resulted in a thicker periosteum compared to the lower dose. Herein, a lower threshold of energy flux density required for periosteal cell proliferation ($0.15 mJ/mm^2$) was established; a previous study reported that a minimum energy density of $0.5 mJ/mm^2$ was required for periosteal osteogenesis (Tischer et al., 2008). The lower energy density can help reduce inflammation and anaesthesia/analgesia.

The second set of experiments aimed to identify the phenotype of the proliferating cells using immunohistochemistry (Chapter 3). Four immunohistochemical markers were used to investigate the phenotype of the ESW-stimulated periosteal cells: von Willebrand Factor (vWF) for endothelial cells; α-smooth muscle actin (SMA) for pericytes, smooth muscle cells, and migrating endothelial cells (Madri and Marx, 1992); collagen type II (collII) for chondrocytes; and osteocalcin (OCalc) for osteoblasts. All groups had evidence of osteogenesis (small islands of intraperiosteal bone) on H&E and Masson's trichrome. Osteocalcin staining was found within these immature bone trabeculae, as well as in cells distributed throughout the ESW-proliferated periosteal

cambium layer. By contrast, there was no collagen II staining, and no cells with chondrocytic morphology. This suggests that, in this model, the ESW-stimulated cells underwent intramembranous ossification but not endochondral ossification. A previous study in rats showed cells with collagen II expression, but not collagen X expression, and concluded that periosteal osteogenesis following ESWs is by intramembranous ossification (Takahashi et al., 2004).

The immunohistochemical results also demonstrated a population of smooth muscle actin positive cells, which may be activated osteoblasts, migrating endothelial cells, or other types of connective tissue cells. Most striking, however, was the relatively high percentage of cells that were vWF positive. Endothelial cells previously have been described as potential osteoprogenitor (chondroprogenitor, and adipoprogenitor) cells (Brighton et al., 1992; Diaz-Flores et al., 1992), and it is possible that the stimulation of neovascularization associated with ESW is a central contributor to ESW-stimulated periosteal osteogenesis. That previous work has reported the vascular stimulus of ESWs in bone and soft tissue supports this hypothesis (Gerdesmeyer and Lowell, 2007; Shrivastava and Kailash, 2005; Takayama and Saito, 2004).

Previous reports attribute periosteal osteogenesis following ESW to: periosteal separation with subperiosteal hemorrhage; microfractures (although this has been disputed, e.g., Tischer et al. (2008); Takahashi et al. (2004); McClure et al. (2004)); release of growth factors (e.g. VEGF, BMP and TGF-β); and direct stimulation of cambium cells. In our study we saw subperiosteal hemorrhage in only a few samples and no evidence of microfractures. Periosteum that is separated from the bone typically responds by endochondral ossification (e.g., Cohen and Lacroix (1955); Simon et al. (2003)); however, our results suggest cambium cells responded to ESW by intramembranous ossification. It is likely that the cambium cells are stimulated by growth factors released following ESW-treatment or by direct cell stimulation.

The final step in validating our therapeutic approach was to evaluate the bone formation induced by ESW-stimulated periosteum in a porous calcium phosphate block implanted orthotopically in a rabbit model (Chapter 4). Study 2 from this chapter was quantified and investigated the response of periosteum to ESW alone, and to sub-

periosteal porous calcium phosphate scaffold[1] implantation with and without ESW stimulation. For ESW treatment the same treatment conditions as the most proliferative group from Chapter 2 (i.e., 3000 shocks @ 0.40mJ/mm^2 applied to the proximal tibia) were used. The cambium cells of the rabbit medial tibia increased in number by 2.7-fold, and the thickness of the layer increased 4-fold, at 4 days post-ESW. These cells were then elevated in situ and overlaid on a porous calcium phosphate scaffold for orthotopic bone formation. The ESW treated samples outperformed the control group in all key outcome variables at the analyzed 2 week timepoint: osseous tissue in the upper half of the scaffold (4-fold increase); osseous tissue above scaffold (10-fold increase); and callus size (2-fold increase). The study confirmed the ability of the ESW-stimulated cells to migrate into the scaffold and to initiate osteogenesis. In the lower half of the scaffold, cells left on the cortical bone surface responded equivalently in both groups. This demonstrates that periosteal cells respond immediately, and just once, to ESWs: this is important from a safety standpoint; the cambium cells are not altered to a permanently proliferative state following ESWs.

There was also chondrocytic tissue found above and within the scaffold. In contrast to the ESW-stimulated group alone, which appeared to undergo intramembranous ossification, there was clear evidence of endochondral ossification following surgery. The increased tissue above the scaffold following surgery (when compared with ESW alone) demonstrates the retained ability of the ESW-stimulated periosteal cells to respond to a second stimulus – surgery in this case. It is known from previous investigations that surgically stimulated periosteum responds by endochondral ossification (e.g., Cohen and Lacroix (1955); Simon et al. (2003)). It is likely that in ESW-stimulated periosteum the vascular supply is maintained (recall the dense vWF expression in ESW-treated periosteum in Chapter 2); following surgical damage to the periosteum, the vascular supply is disrupted and may lead to a hypoxic environment and drive chondrocytic tissue formation. The maintained ability of ESW-stimulated cells to respond to a second stimulus suggests that a second dose of ESW would

[1]The calcium phosphate scaffolds used were anorganic bovine bone scaffolds, which have previously demonstrated periosteal bone formation when implanted subperiosteally (Simion et al., 2006).

further stimulate periosteal proliferation and osteogenesis.

A pilot study (study 1) was performed prior to the study 2 groups in Chapter 4. This study revealed a variation in results that was attributed to improper z-alignment of the shock wave focal zone (i.e., penetration depth was misaligned). In each group that did not demonstrate robust periosteal osteogenesis within and above the subperiosteal scaffold, there was a healing microcrack observed on microCT on the side opposite ESW treatment. These microcracks were also observed in some of the ESW-treated animals in study 2 groups (however, the callus was smaller, indicative of correct z-alignment of the ESW focal zone). Microfractures have been observed previously in ESW studies of rabbit bone (e.g., Tischer et al. (2008)), but not in rats (e.g., the Ch. 2 results herein and Takahashi et al. (2004)) or horses (McClure et al., 2004). It is possible that there is something unique about the lengthscale of the rabbit bones or about their physiology that makes them more susceptible to microfracture. Although all treatment doses used in this study are consistent with those used in the clinic, it is necessary to verify that ESWs are not inducing harmful fractures prior to clinical adoption of the technique.

The ability of ESW-treated periosteum to form bone in a subperiosteal scaffold, prompted the investigation of the ESW-treated periosteum as a free graft. Two models were tested. In the first model, the periosteum was transplanted to the contralateral tibia. At this site the porous calcium phosphate scaffold was push-fit into a surgically created defect in the medial tibia and made flush with the outer cortical bone surface. The periosteum was overlaid on the scaffold surface and sutured to local periosteum. Successful bone generation in the scaffold pores within the marrow cavity was attributed to endosteal and marrow progenitor cells. In the transplanted periosteal graft, there was a bone formed in 3 of the 4 samples. In 1 of these samples, there was continuity between the bone from the periosteal transplant and the new bone arising from the marrow; in the other two samples, there was a fibrous layer blocking the periosteum from communicating with the marrow. On closer histological inspection, however, the bone formed in the periosteal transplant bone did not appear fully vitalized.

In the second model, the free periosteal graft was transplanted to the ipsilateral femur. Here, the scaffold was implanted into the distal femur marrow cavity but extended 1.5mm above the height of the native cortical bone; the local periosteum was removed in the vicinity of the defect. In this model, the periosteum was overlaid on and tied down onto the scaffold. At 2 weeks, the tissue appeared necrotic histologically and there was no evidence of bone formation.

The results of both free graft studies suggest that there is insufficient, or insufficiently rapid, neovascularization at the transplant site. Prior to transplantation, the cells are highly metabolically active (e.g., proliferating, differentiating, and forming osseous matrix). Further, the vWF immunohistochemistry in Chapter 3 reveals the dense vascular network in the proliferating layer. Upon transplantation, the cells are isolated from this vascular network and have insufficient resources and nourishment to maintain their activity. This appears to cause the cells to undergo apoptosis or become more quiescent.

In our studies, the most dramatic tissue response observed was on the periosteal surface. Periosteal cells are uniquely positioned as they have soft matrix on one side and a hard, calcified, bone matrix on the other. It was our supposition that the periosteal cells experienced a unique waveform, which contributed to this response. In the final set of experiments (Chapter 5), the focus is switched to the ESW technology and the pressure waveforms experienced during ESW treatment. Experiments were performed in a free field (water bath); in tissue (rabbit muscle and tibial bone corner); and ex vivo (around an explanted bone) for an electrohydraulic (OssaTron) and an unfocused pneumatic (dolorclast) ESW device. The measurements taken in a free field were consistent with previously described data and demonstrated the abrupt, rapid rise time for the electrohydraulic device and the slower rise time for the pneumatic device. In tissue, the pressure peak for the electrohydraulic device was attenuated by 57% in muscle, and the rise time lengthened, whereas the pneumatic device did not show any changes in the time or pressure profiles. It is known that tissue attenuates higher frequencies more than lower frequencies, which would cause the 'rounding-out' of the spiked pressure profile of the electrohydraulic applicator.

For the measurements in tissue and the ex-vivo measurements, secondary peaks were observed at the periosteal surface. These peaks are attributed to either reflected or creeping waves from the bone. This wave – in combination with the incident wave – should be considered when interpreting the periosteal cell response to ESWs.

Overall this work successfully demonstrated the potential of the proposed therapeutic strategy. The results support our hypothesis that ESW treatment can stimulate osteogenic cells in periosteum for formation of bone in orthotopic implants. This has the potential of serving as a new rapid and cheap therapeutic approach for the treatment of an array of oral-maxillofacial and orthopaedic problems.

6.2 Future work

The ultimate goal of the research is to implement this therapeutic approach in the clinic. With this in mind, ESW treatment doses were based on clinically used treatments. Moreover, anorganic bovine bone calcium phosphate scaffolds, such as the one used herein, are routinely used in the clinic. Given the successful demonstration of the technique, there may be sufficient data for a preliminary clinical study. In particular, the dental application (alveolar ridge augmentation) lends itself to the application of ESW since, as shown by Simion et al. (2009, 2006), periosteal cells can be used in situ to generate bone for vertical ridge augmentation procedures. Based on the observations in the models herein, increasing the periosteal cell population by ESW treatment should enhance the outcome of these strategies.

The most probable next step, however, is a larger animal model (e.g., goat, sheep). This would more closely mimic the human bone sizes, and allow for more careful examination of the response. In this model, it would be necessary to explore more fully the dose response of the periosteal cells to ESW treatment and more fully optimize the treatment. In performing this analysis, it is important to verify that unwanted microfractures are not created as a result of the ESW-treatment for the larger species. Additionally, repeat ESW doses could be given at various stages of the bone formation process, which may improve results. Secondly, a model of a specific clinical

application should be tested. For example, a suitable dental study would be alveolar ridge augmentation; a suitable orthopaedic model would be the filling of a surgically created defect that simulated an osteolytic defect. These would allow for a more comprehensive evaluation of the surgical model and strengthen the evidence for a clinical trial. It is also noted that all these studies were performed on normal healthy rabbits and that the response of diseased or aged periosteum to ESW would have to be investigated if the technique was proposed clinically for these situations.

The long term outcome of the ESW-stimulated periosteum with subperiosteal scaffold implantation also needs to be investigated. It is likely that some of the generated bone will resorb, however, the previous demonstration of periosteum's ability to fix and maintain bone in an anorganic bovine bone scaffold long term is a promising indication that the bone formed by the technique herein will perform similarly (Simion et al., 2006).

The work has laid the basis for further exploration of other variables in the strategy. This project focused on just one component of the tissue engineering triad – the cell source. In this model, the cell source was used as a flap and the results suggest that the vascularization of the tissue is central to the success of the procedure. However, these cells could also be harvested, the ECM digested, and the increased cell population seeded on scaffolds for tissue engineering.

Based on its previous successful demonstration of bone formation in multiple models and species, anorganic bovine bone scaffolds were used as the scaffold for these tests. There are many scaffolds that offer many (situationally dependent) advantages, and there are more in development. There is certainly space for exploring more optimal scaffolds for combination with the ESW-stimulated periosteum.

Likewise, no growth factors were explored in this study. The results presented demonstrate the ability of the periosteal cells to migrate into the scaffold and generate bone and it is possible that growth factors may not be required when the ESW-stimulated periosteum is used. However, for larger defects, growth factors may prove beneficial in improving infiltration of the cells into the scaffold. Suitable candidates include platelet derived growth factor (e.g., PDGF-BB) and the bone morphogenetic

proteins (BMPs).

The pilot studies of rabbit free graft transplants to the medial tibia indicated bone formation in 3 of 4 ESW-transplants but no bone formation in 2 of 2 controls. The bone in the ESW-transplants did not look fully vital on histology after 2 wks, which was attributed to a lack of vascularization. This demonstrates the potential of the free graft model, which would offer an additional degree of flexibility to the proposed technique. With either a surgical technique that could allow for vascularization, or with vascular growth factors, these transplants should get the additional nourishment needed to perform as well as in situ grafts. This would open the door to more clinical applications.

In the rat study (ESW alone) it was noted that there was no collagen II positive cells, nor cells with chondrocytic morphology, and that intramembranous ossification was the mode of osteogenesis. In the rabbit study, however, there was evidence of chondrocytic cells in the ESW-treated samples following elevation from the bone. This demonstrates that the ESW-treated cambium cells maintain their ability to undergo chondrocytic differentiation when stimulated by surgical elevation. That periosteum has been proposed for cartilage generation previously (Emans et al., 2005) indicates the potential for using ESW-stimulated periosteum for cartilage repair. There have been attempts by other authors to stimulate periosteal cell proliferation for use in cartilage tissue engineering (e.g., Reinholz et al. (2009)); ESW-stimulated periosteum may offer a rapid and cheap method for achieving the required proliferation.

There is still a dearth of basic science elucidating the mechanisms of ESWs on tissues and cells. In this thesis, the cell populations and waveforms were explored but the detailed molecular mechanisms resulting in periosteal cell proliferation were not investigated. As ESW therapy continues to undergo R&D, it is imperative that the underlying mechanisms are established. This would lead to improved device design and better control of the treatment/response. Further, if the underlying mechanisms are elucidated, other modalities for achieving the beneficial results of ESWs could be explored.

Although the acoustic properties of ESWs are well documented in an idealized

medium, during our investigation of the pressure-time response of ESWs, we found surprisingly little data concerning the waveforms in tissue. Our investigations demonstrated a dramatic drop in the peak pressure for the electrohydraulic device, as well as an increased rise time. In understanding the mechanistic response of cells and tissue to shock waves, it is imperative that we first understand the wave forms they are experiencing. This would allow for more careful in vitro investigation and study design, with appropriate waveforms being applied to the cells. However, the primary limitation is equipment design. As advances are made in hydrophone technology and devices that are robust – yet small enough to be implantable and not alter waverform – are developed more precise data should be recorded. This can then be incorporated to future iterations of both the ESW technology and the experiments.

Overall, in the models tested herein, ESW-stimulated periosteal cells have shown efficacy for bone tissue engineering. There are several factors and variables to be confirmed or improved upon before introduction to the clinic. However, the foundation for the proposed clinical application has been demonstrated and the technique shows much promise.

Appendices

Appendix A

Extracorporeal shock wave induced lubricin upregulation in tendons and septa

A.1 Introduction

Lubricin is a mucinous glycoprotein found in synovial fluid following its production by synovial cells; it is the principal lubricating molecule in diarthroidal joints (Rhee et al., 2005; Swann et al., 1985). Zhao et al. (2010) showed that lubricin can enhance tendon gliding in vitro and Kohrs et al. (2010) demonstrated this in vivo. Homologues to lubricn include superficial zone protein (SZP; produced by superficial zone chondrocytes (Jay et al., 2001; Schumacher et al., 1994)) and megakaryocyte stimulating factor (MSF, (Flannery et al., 1999)). Lubricin, which has anti-adhesive and lubricating properties (Englert et al., 2005), has been found in: bovine ligaments (Lee et al., 2008), in canine tendons (Sun et al., 2006), and within fascicles and fascicular sheaths in caprine and human tendons (Funakoshi and Spector, 2010; Funakoshi et al., 2008), where they likely play a role in interfascicular tribology.

Certain mechanical (Sun et al., 2006), as well as biochemical stimuli (Jones and Flannery, 2007; Lee et al., 2008), have been shown to regulate lubricin expression

in vivo. That ESWs provide not only a mechanical stimulus, but also upregulate select cytokines (e.g., TGF-β1 (Chen et al., 2004), which are known to stimulate the expression of lubricin (Jones and Flannery, 2007; Lee et al., 2008)) and are clinically used to heal tendinitis (Chung and Wiley, 2002; Cosentino et al., 2004; Gerdesmeyer and Lowell, 2007; Rompe et al., 2001; Takayama and Saito, 2004), prompted the supposition that ESWs may induce lubricin expression in tendons.

The objective of this study is to examine the expression of ESW in tendons and septa following ESW-treatment. The rat hindlimb model was chosen in order to evaluate lubricin in several different types of tendons in the same sample. The septa within the same hindlimbs were also evaluated as comparative controls, because they also comprise bands of fibrous tissue. Two different doses of ESW were used to examine a dose dependent response of lubricin, which was seen for periosteal proliferation.

A.2 Materials and methods

The methods and samples used in this study were identical to those described in chapter 2 and are not repeated here. To stain for lubricin, the primary antibody used was an anti-lubricin monoclonal antibody (S6.79, provided by the Rush University Medical Center, Chicago, IL; 15 minutes). The corresponding negative control was negative mouse immunoglobulin-2b (IgG2b; 15 minutes) control (X0944; Dako). The S6.79 anti-lubricin antibody is an IgG2b immunoglobulin developed in the mouse against human lubricin, found to react with a variety of mammalian lubricin molecules, including human, dog, bovine, guinea pig, and rabbit (Su et al., 2001).

Digital micrographs were acquired from the slides. Tendons and septa were identified based on histological morphology and anatomic location (see fig. A-1). Lubricin expression in tendons and septa was evaluated separately in the extracellular matrix (ECM) and intracellularly (IC). The samples were graded semi-quantitatively on a scale from 0-5 for lubricin chromogen expression, where 0 = no staining; 1 = <5% of cells or ECM; 2 = 5% to 25%; 3 = 25% to 50%; 4 = 50% to 75%; 5 = 75% to 100%. All measurements were recorded by one collaborator (Dafang Zhang).

The following tendons and septa were evaluated (see fig. A-1):

Tendons: gracilis (g); semitendinosis (st); flexor digitorum longus (fdl); tibialis cranialis (tcn); tibialis caudalis (tcd); extensor digitorum longus (edl); peroneus longus (pl); biceps femoris (bf); soleus (s). The side of the pl tendon closer to the anterior intermuscular septum (pl-s) was evaluated separately from the side closer to the fibula (pl-f).

Septa: interosseous membrane (iom); anterior intermuscular septum (ais); transverse intermuscular septum (tis). The tibial side of the iom (iom-t) was evaluates separately from the fibular (iom-f).

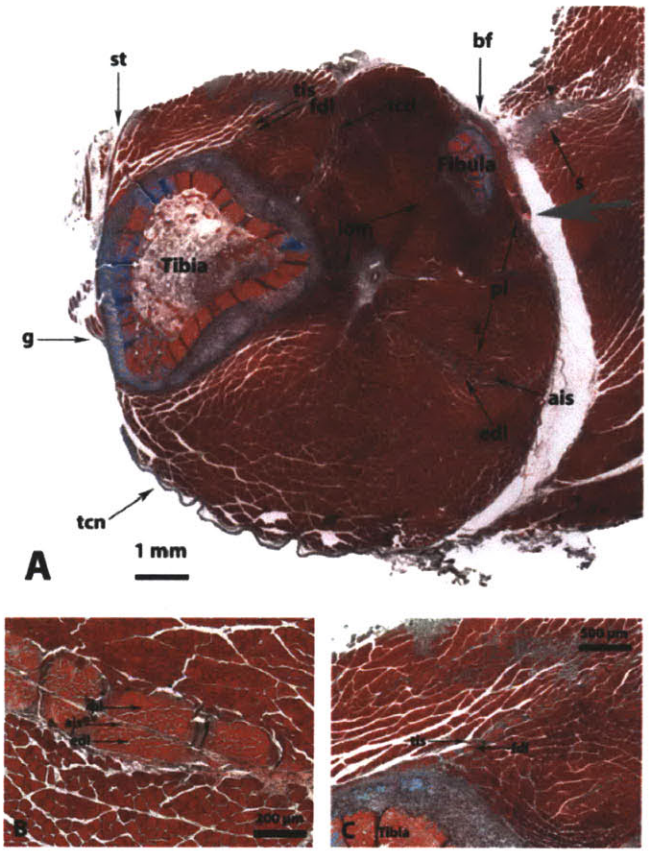

Figure A-1 – (A) The low-magnification micrograph of the rat hindlimb shows notable anatomic structures. The gray arrow indicates the direction of applied ESWs. (B, C) The high-magnification micrograph of tendons (fascicles and bundels of fibers) and septum (narrower, no fascicles) highlights histological differences (Masson's trichome stain).

The Wilcoxon signed-rank test was employed for the paired data comparing the

ESW dose and control in the same animals. Kruskal-Wallis testing of the unpaired non-parametric ECM and IC lubricin scores was employed to determine the significance of the effect of ESW dose (0, 0.15 and 0.40 mJ/mm^2) on ECM and IC lubricin expression for all of the tendon, or septa, samples combined. Mann-Whitney testing was employed for the comparison of the unpaired data comparing the low- and high-dose ESW-treatment. P-values <0.05 were considered statistically significant.

A.3 Results

In support of our hypothesis, positive immunostaining for lubricin was observed in all of the tendons and septa of the low-dose (fig. A-2 B) and high-dose (fig. A-2C) ESW-treated hindlimbs, compared to the majority of the non-ESW-treated control tendon and septa samples which stained negative for lubricin. If there was staining in the control tissue, it was typically trace staining (see fig. A-2A). Rat articular cartilage stained with the same protocol served as positive controls, and there was a red chromogen (i.e., lubricin rich) layer on the top surface in all positive control samples; all negative controls demonstrated no staining. It is noted that fresh cut surfaces of the tissues, produced during handling, did not stain for lubricin (i.e., surface staining is not a result of edge-artifacts). Intracellular lubricin staining was seen in the cytoplasm of elongated cells resembling fibroblasts typically seen in tendons and septa (Figure 3). In all samples, the intensity of red chromogen was highest at the bony interface, and the intensity of staining decreased as distance from the bone-tendon or bone-septum interface increased.

Table A.1 shows the marked increase in intracellular and extracellular lubricin expression following ESW-treatment for all tedons and septa. There is also increased expression when the high-dose is compared with the low-dose ESW-treatment. Note that these data are mean values and non-parametric; thus, they are employed for summary assessment only. To complete statistical analysis, Wilcoxon signed-rank testing was used on the paired data to compare the effect of ESWs (high and low dose combined) with control. This revealed a significant effect of ESWs on lubricin

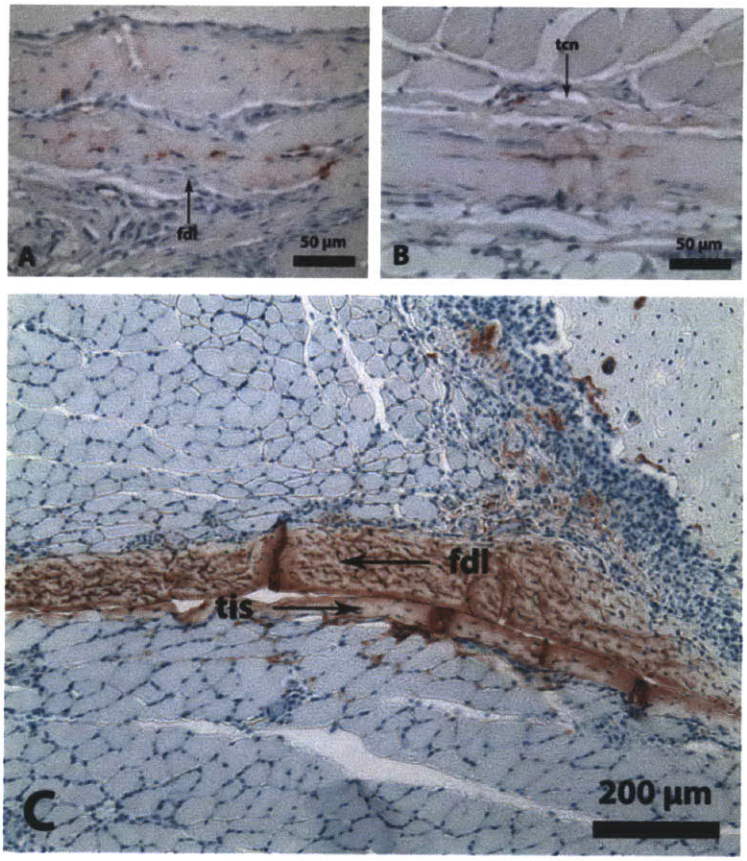

Figure A-2 – The micrographs show immunostaining for lubricin (red chromogen) in (A) control tissues, (B) low-dose, and (C) high-dose ESW-treated tendons and septa, showing both ECM and IC staining.

expression in the ECM and IC in tendons (both p-values <0.0001) and septa (ECM: p = 0.001, IC: p = 0.003). The Kruskal-Wallis testing of the non-paired, non-parametric semi-quantitative lubricin scores for all of the tendons (or septa) combined revealed that ESW dose (comparing 0, 0.15, and 0.4 mJ/mm^2) had a significant effect on the ECM and IC lubricin score in tendons (both p-values <0.0001) and septa (ECM: p <0.0001, IC: p = 0.0002). Finally, the Mann-Whitney test was used to compare the unpaired non-parametric high vs. low dose data for all the tendons or septa combined. Mann-Whitney unpaired testing revealed that high-dose samples exhibited significantly different lubricin expression compared with low-dose samples in tendons IC (p-value = 0.0006) and in the ECM (p ¡ 0.0001), but not in the septa, neither IC (p-value = 0.2) nor in the ECM (p-value = 0.8).

	Control	Low dose	High dose
Extracellular matrix			
Tendons	0.28 0.08	1.35 ± 0.20	2.82 ± 0.23
Septa	0.10 ± 0.05	1.15 ± 0.25	1.68 ± 0.46
Intracellular			
Tendons	0.19 ± 0.06	1.25 ± 0.19	2.19 ± 0.18
Septa	0.03 ± 0.03	0.85 ± 0.28	1.58 ± 0.43

Table A.1 – Mean scores ± SEM for the extracellular matrix and intracellular staining of lubricin in tendons and septa. The samples were graded semi-quantitatively on a scale from 0-5 for lubricin chromogen expression, where 0 = no staining; 1 = <5% of cells or ECM; 2 = 5% to 25%; 3 = 25% to 50%; 4 = 50% to 75%; 5 = 75% to 100%.

A.4 Discussion

The principal finding of this study was that ESWT increased the amount of lubricin detected in tendons of the rat hindlimb. The lubricin expression was found both intracellularly (expressed by tenocytes) and extracellularly. Interestingly, the septa also demonstrated increased lubricin expression, which suggests that both these tissue respond to the same ESW driven stimulus by upregulating lubricin expression. Consistent with the observed does response in periosteum, lubricin expression increased with increasing ESW dose. However, this was only found to be significant in tendon and not in septa.

Although the exact mechanism is unclear, and was not studied herein, it was demonstrated that ESW induces excessive expression of lubricin in vivo. This result provides a basis for the hypothesis that increased lubricin deposition in tendons and septa following ESW-treatment contributes to the beneficial effects of ESW-treatment by facilitating movement macroscopically between gross structures as well as microscopically between collagen fascicles. Future studies will be required to determine the mechanism by which ESW achieves this effect.

Appendix B

Micro computed tomography and scanning electron microscope imaging of a novel scaffold for bone ingrowth

B.1 Introduction

A novel scaffold, which is currently in the R&D phase at Bio2 Technologies (Woburn, MA), was implanted in the rabbit distal femur and analyzed for bone ingrowth using microCT and scanning electron microscopy (SEM). It is manufactured from a resorbable bioactive glass using a proprietary cross-linked microstructure process. The scaffold is designed to combine high porosity with mechanical properties that mimic natural bone.

Scaffolds were implanted in rabbit distal femurs for a period of 2wks or 8wks. At sacrifice, the scaffold and surrounding bone were excised and the block imaged using microCT. The block was then embedded in LR White, sectioned using a diamond saw, and ground and polished for backscatter electron imaging in a scanning electron microscope.

Exp. Grp.	Scaffold	n	Sacrifice Time [wks]
1	Bio2	2	2
2	Bio2	2	8

Table B.1 – Experimental groups for Bio2 implant studies.

During the examination of samples in a scanning electron microscope, high energy electrons are elastically reflected by the surface. The intensity of these backscattered electrons is strongly related to the atomic number and elemental density of the specimen. The image contrast of backscattered electron imaging (BEI) is a function of elemental composition of the features being examined. BEI of implants in bone can distinguish the biomaterial and bone by the relative intensity of the features. In addition, the appearance of osteocyte lacunae can assist in the identification of osseous structures. In examining mineral samples, including bone, the intensity is related to the degree of mineralization.

In EDX, the high energy electron beam, penetrating the first several microns of the samples surface, displaces electrons from their unexcited states in electron shells around the nuclei. An electron from a higher energy state fills the hole left by this electron and the difference in energy between the two states is typically released as an x-ray. These x-rays are collected by an energy dispersive spectrometer and the pulses recorded and analyzed. Since the x-ray's energy is a function of the energy change between the two states and the element's atomic structure, the elemental composition of the material can be interrogated.

B.2 Materials and methods

B.2.1 Experimental design and animal model

All procedures were approved by the VA Boston Healthcare System Institute Animal Care and Use Committee. Four new zealand white rabbits (4 - 4.5kg) were used in the study, divided into 2 groups as listed in table B.1. For all groups, the scaffold was implanted in the distal femur.

In preparation for surgery, the rabbit was anaesthetized using Ketamine (10mg/kg) and ace promazine (0.5mg/kg) for induction and given isoflurane (1-2%; endotracheal intubation) and O_2 throughout the procedure. A 1.5cm skin incision was made on the medial side of the distal femur, the muscle and overlying soft tissue incised and retracted, and the femoral distal condyle exposed. An orthopaedic drill bit, which matched the scaffold diameter, was used to create the surgical defect. Guide holes were used to ensure proper alignment and to reduce the potential for fracture during the procedure. The Bio2 scaffold (4mm ⌀x 8mm length) was push-fit into the defect. The muscle, soft tissue, and skin were replaced and each layer sutured closed. Ketofen (2mg/kg) and cefazolin (20mg/kg) were given subcutaneously for 48 hrs post-op and animals were sacrificed at the end of 2wks or 8wks by pentobarbitol overdose.

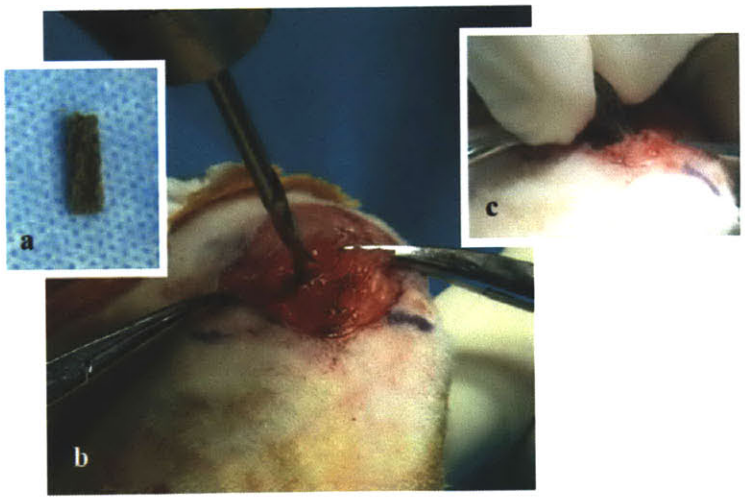

Figure B-1 – Sample surgery pictures. (A) The Bio2 implant. (B) The drill used to prepare the implant site in the medial aspect of the distal femur of the rabbit. (C) The implant was inserted into the hole by hand with a press fit.

B.2.2 Analysis procedures

Following sacrifice, the implants and surrounding bone were excised and imaged using microCT (GE Healthcare eXplore Locus; 27μm 88min Short Scan; GE Healthcare, Piscataway, NJ). The undecalcified samples were then fixed in formalin and embedded using LR White embedding medium (Ted Pella Inc., Redding, CA). A diamond

saw (Buehler Isomet Precision Saw, Buehler, Lake Bluff, IL) operating at 250RPM, with distilled water for lubrication, was used to section the embedded blocks and expose the midplane of the scaffold and surrounding tissue. The surfaces were then ground using silicon carbide papers (Struers Inc., Cleveland, OH) and polished using a 1μm diamond suspension (Struers Inc., Cleveland, OH), followed by a colloidal silica suspension (Struers Inc., Cleveland, OH). The sections were fixed to a 25mm $\varnothing$aluminum stub, using carbon tape, and coated with $\sim$10nm of gold-palladium. The samples were then imaged using a JEOL JSM 6700F scanning electron microscope (SEM) in backscatter mode (BEI). The machine was operated at an accelerating voltage of 15kV and a working distance of 8mm. A second variable pressure SEM, Leo VP438 (Zeiss, Oberkochen, Germany; operating at 20kV and 10-15mm working distance), was used to collect SEI images as well as to perform energy dispersive x-ray analysis (EDX).

B.3 Results

B.3.1 Group 1: Bio2 2 week study

MicroCT

MicroCT images of the non-implanted samples (fig. B-2) demonstrated the highly porous nature of the samples with large (several hundred micrometers in diameter) interconnecting pores.

The radiodensity of the Bio2 material (x arrows in fig. B-3 A and B) was slightly lower than that of the surrounding mature trabecular bone. Because the radiodensity of the Bio2 was similar to that of the newly formed (immature) trabecular bone, it was often not possible to definitively distinguish the new bone growing into the pores from the Bio2 material. There were, however, pores in which the newly formed bone could be distinguished from the Bio2 material by its microstructure.

MicroCT showed that after only 2 weeks of implantation, trabecular bone formed in the gaps between the implant surface and surrounding bone and in surface pores

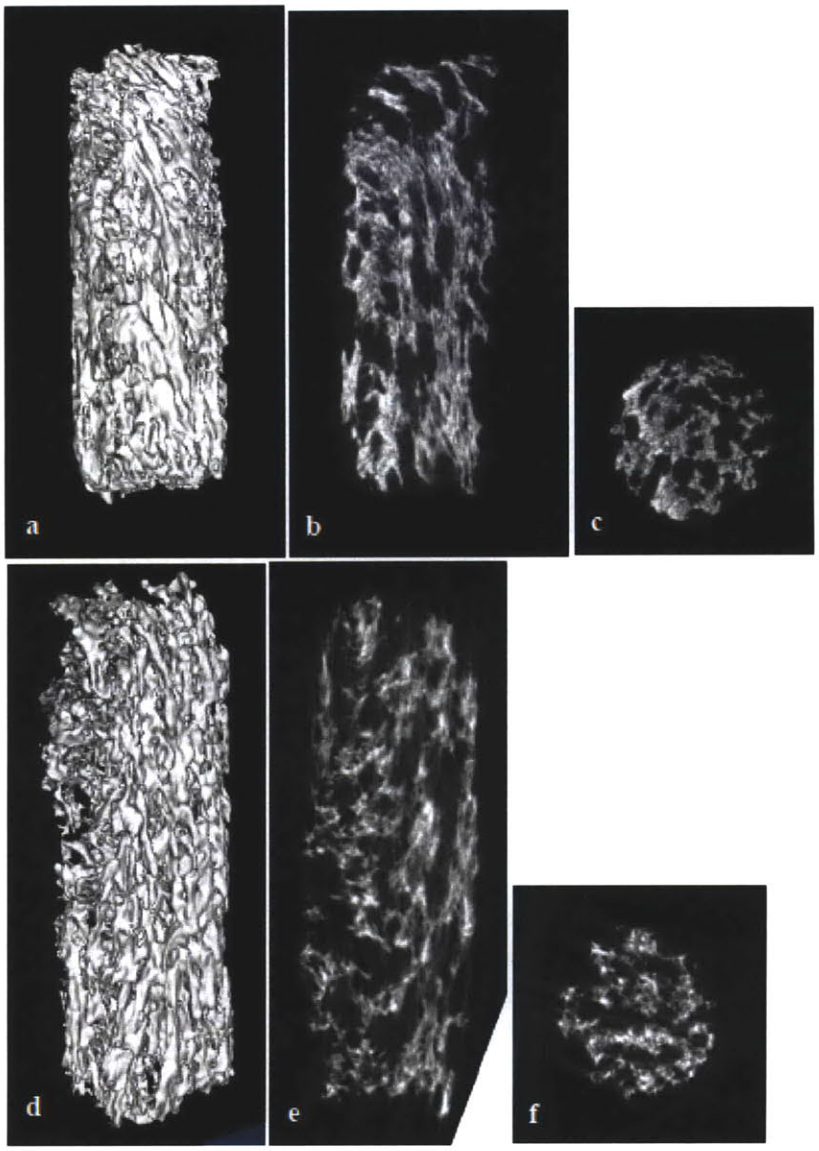

Figure B-2 – MicroCT images of two unimplanted samples, which were approximately 4 mm in diameter. (A and D) Reconstructed images of the surface. (B and E) Y-slice images through the middle of the samples. (C and F) Z-slice images through the samples.

(y arrows in fig. B-4 a and b). This new bone appeared to be growing up to the Bio2 surface (i.e., osseointegration). Also of note was the clear indication in the microCT images of bone ingrowth into interior pores of the implants (z arrows in fig.B-3).

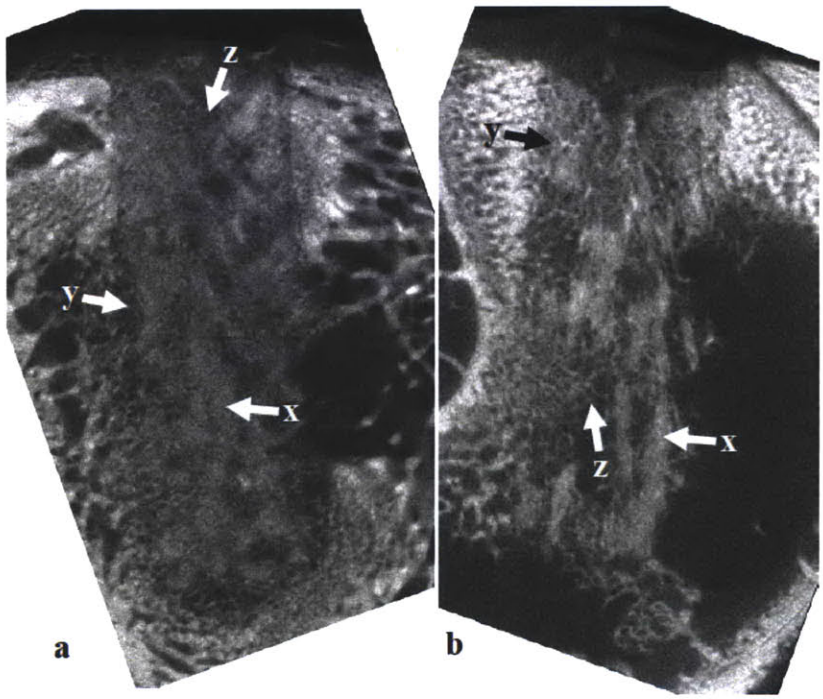

Figure B-3 – MicroCT images of the Bio2 implants 2 weeks after implantation in two different rabbits (A) and (B). The Bio2 implant material is shown by the arrows labeled x. Examples of newly formed bone are shown: y, in the gaps between the implant perimeter and surrounding cancellous bone and in surface pores; and z, in interior pores of the implant. All such features are not labeled with arrows.

Scanning Electron Microscopy

Figure B-4 E, F shows representative micrographs of a non-implanted scaffold. In contrast to the implanted samples, the struts appear homogenous on BEI. The circular features within the Bio2 are unknown to us.

Figure B-4 A-D demonstrates that by 2 weeks of implantation new bone has formed around, and in the pores of, the Bio2 sample. Of importance is that each of the images shows bone directly formed on the surface of the Bio2. That there is a continuity of mineral from the bone to the Bio2 samples is reflective of direct bone bonding to Bio2 (i.e., chemical bonding of bone to Bio2). The images of the Bio2 material itself demonstrate that there is a variation of mineral within the struts of the Bio2. The circular features, observed in the control scaffolds, are also present in the struts of the non-implanted scaffold.

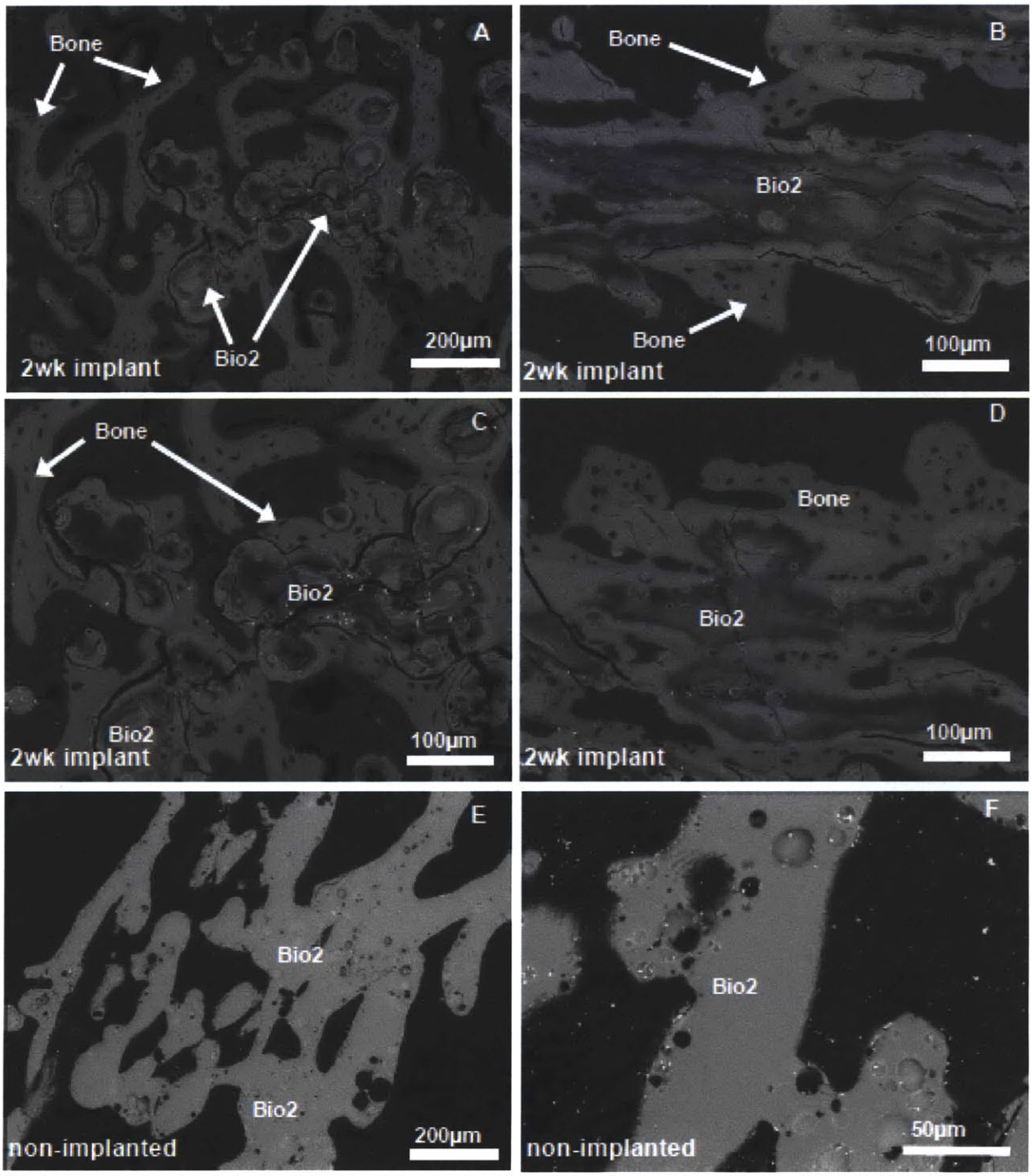

Figure B-4 – Sample BEI images of (A-D) explanted Bio2 implants at 2wks and (E,F) non-implanted Bio2 scaffolds.

EDX was used to interrogate the makeup of the non-implanted scaffold and the implanted scaffolds. It was also employed to investigate the apparent inhomogeneity

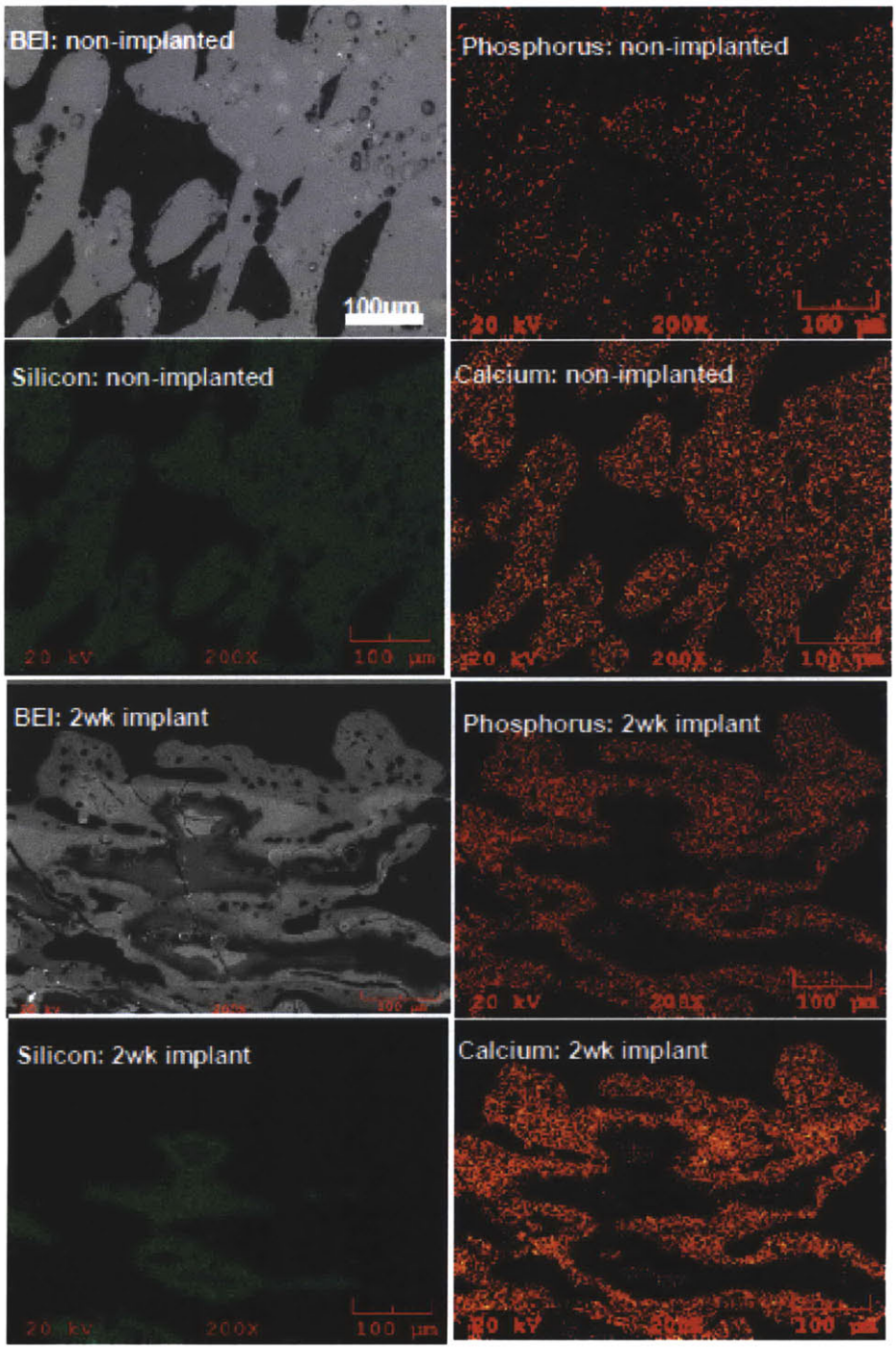

Figure B-5 – Maps of calcium, phosphorus, and silicon and corresponding BEI images for non-implanted and 2wk implanted Bio2 specimens

of the implanted Bio2 scaffolds and the elemental components of the scaffold.

B-5 shows maps of where 3 elements (calcium, silicon, and phosphorus) are found

within a region (the corresponding BEI image illustrates this region) of the unimplanted sample and from a sample implanted in the rabbit femur and explanted at 2wks. These three minerals are chosen as there is calcium and phosphorus in bone mineral as well as in the Bio2, which also has silicon.

In the control sample we see that the minerals are distributed throughout the scaffold. For the implanted sample, we see calcium and phosphate in the newly formed bone. Interestingly, there is little calcium and phosphate left in the core of the scaffold struts, whereas silicon remains. The outer surface of the scaffold is now calcium and phosphate rich, although it appears to have less silicon. These results suggest that the calcium and phosphate in the scaffold are dissolving out and either attaching to the surface, or new calcium phosphate from the surrounding tissue is being deposited on the surface. The silicon appears to maintain the central region of the scaffold but is found in much less quantity at the surface 2wks after implantation.

B.3.2 Group 2: Bio2 8 week study

MicroCT

The microCT findings for the 8wk samples are consistent with results from the 2 week study. As previously described, the radiodensity of the Bio2 material was slightly lower than that of the surrounding mature trabecular bone, which makes it difficult to definitively distinguish the new bone growing into the pores from the Bio2 material. There is, however, some evidence of new bone formation in the pores, where bone can be distinguished from the Bio2 material by its microstructure. Further, the macroporous structure of the Bio2 material is no longer apparent on the implanted microCT images at 8 weeks, which is believed to be due to the filling of the pores. It is difficult to fully interpret whether the Bio2 material remains at week 8 from the microCT images alone; however, the top of the scaffold was seen at the cortical bone surface on explant, suggesting that some of the scaffold remains (see fig. B-6).

MicroCT demonstrates that trabecular bone formed up to the Bio2 scaffold surface by week 8 of implantation; however, there are some gaps between the implant surface

Figure B-6 – Photograph of rabbit distal femur following explant at week 8 post-implantation. The top of the Bio2 scaffold is seen on the cortical bone surface.

and surrounding cancellous bone due to the irregular sample perimeter (fig. B-7, X-arrows). The new bone appears to have osseointegrated the implant, fixing it in place in the bone. Also of note was the clear indication in the microCT images of bone ingrowth into interior pores of the implants (Y-arrows in fig. B-7). From the microCT images, Bio2 #1771 appears to demonstrate more mature trabecular bone that that seen in Bio2 #1679, which may result from a variation from animal to animal, or a variation in the scaffold architecture/structure.

Scanning electron microscopy

Figure B-8 demonstrates that at 8wks new bone had been formed around and within the pores of the Bio2 samples. For both samples, there is clear evidence of bone formation on the surface of the Bio2 samples, as well as continuity of mineral between the Bio2 samples and newly forming bone.

As was suggested by the microCT images of the 8wk samples, the bone response to sample #1771 appeared to be more mature than that of #1679. Qualitatively, sample #1679 demonstrated responses similar to that seen for the 2 wk results: the scaffold struts are clearly delineated and there is a gradient of mineral content within the struts (see fig. B-8 a-c). The response to sample #1771 appeared to be more advanced. In this sample, it was difficult to identify the boundary between scaffold and bone as they're so closely integrated (see fig. B-8 d-f). The images suggest that the scaffold is being dissolved or resorbed, and replaced by bone.

Notably, there appeared to be more of an interfacial gap between the Bio2 sample

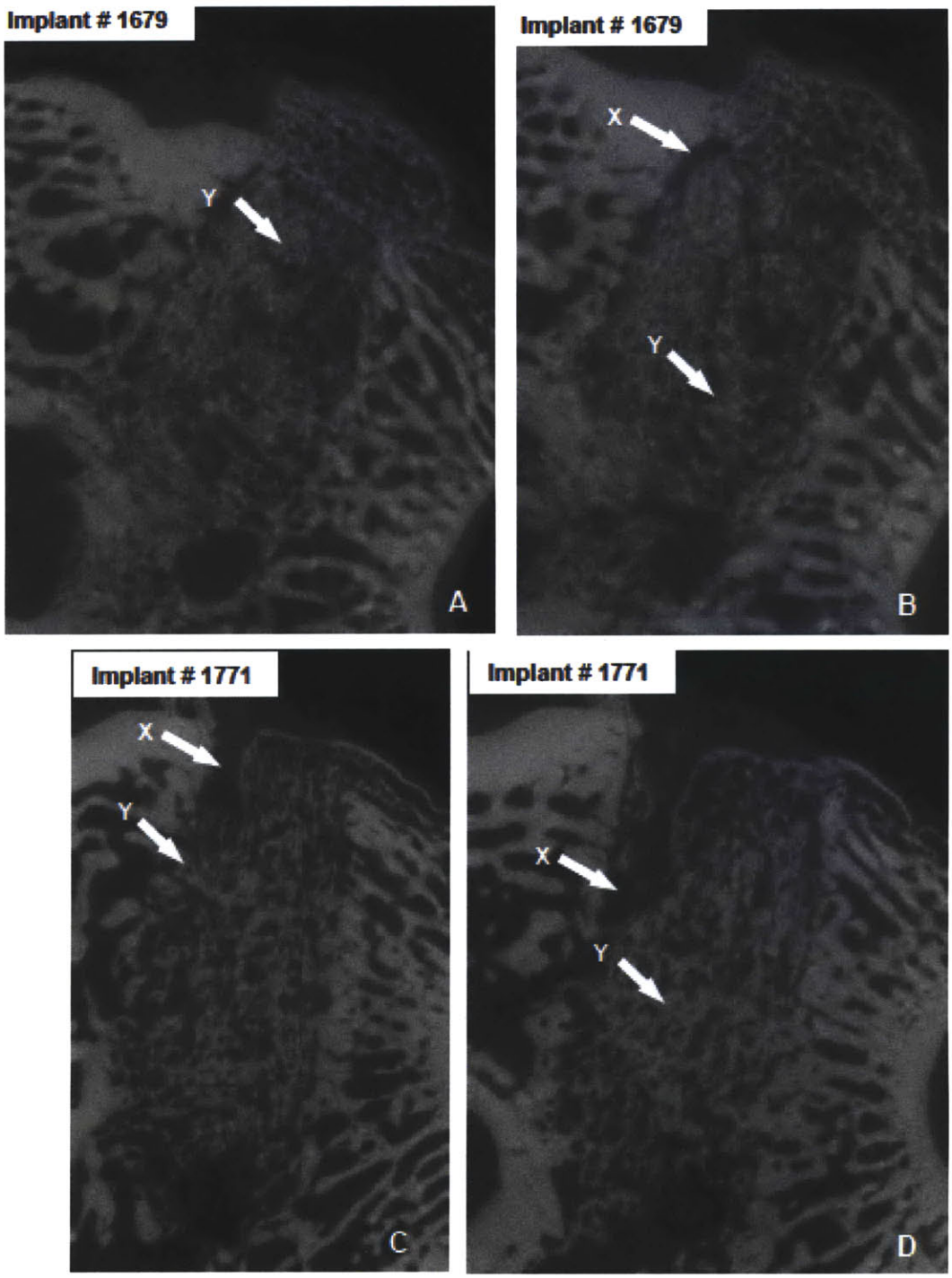

Figure B-7 – Representative cross-section images of Bio2 implants in rabbit distal femur at 8weeks using microCT. X-arrows point to gaps between Bio2 material and surrounding bone (due to surface irregularities); Y-arrows point to regions demonstrative of new bone formation within the scaffold.

and surrounding trabecular bone for #1679 when compared with #1771. It is difficult to interpret post-testing whether this gap was due to sample shape/surgical technique or if it results from the tissue response. However, it likely played a role in the bone formation response.

For sample #1679, we see that the outer surfaces are now calcium and phosphorus rich, with the center of the struts demonstrating little CaP. It is possible that these elements are dissolving out and partaking in the bone forming/deposition processes. For sample #1771, it is very difficult to separate the scaffold and new bone. The images in figure B-9 are consistent with this; there is no clear distribution of the silicon relative to scaffold struts. There is, however, continuous calcium and phosphorus in the non-marrow regions.

B.4 Discussion

The implanted scaffolds demonstrated bone formation onto the scaffold surface. At very high magnification in BEI, there was no separation visible between the bone surface and the scaffold. This indicates that the scaffold is osteoconductive and suitable for select applications in bone.

The Bio2 samples at 2wks showed bone forming within the pores, a clear indication of osseointegration. The scaffold has an open porous structure, which enabled the new bone to infiltrate the inside of the scaffold. This new bone would be expected to solidly fix the implant to bone. In fact, it is likely that enough new bone had formed by 7-10 days after implantation to adequately stabilize the Bio2 rods.

By week 8, there was maturation of the bone within the scaffold, which appeared to be accompanied by a dissolution or resorption of the scaffold material. This was particularly evident in the sample with more advanced bone formation when viewed under BEI (#1771); the scaffold appears to be getting replaced by the new bone as it forms and less scaffold is evident in the cross-section.

For the Bio2 samples, there is evidence of scaffold dissolution or material inhomogeneities by week 2. On BEI imaging, the scaffold appears homogenous prior to

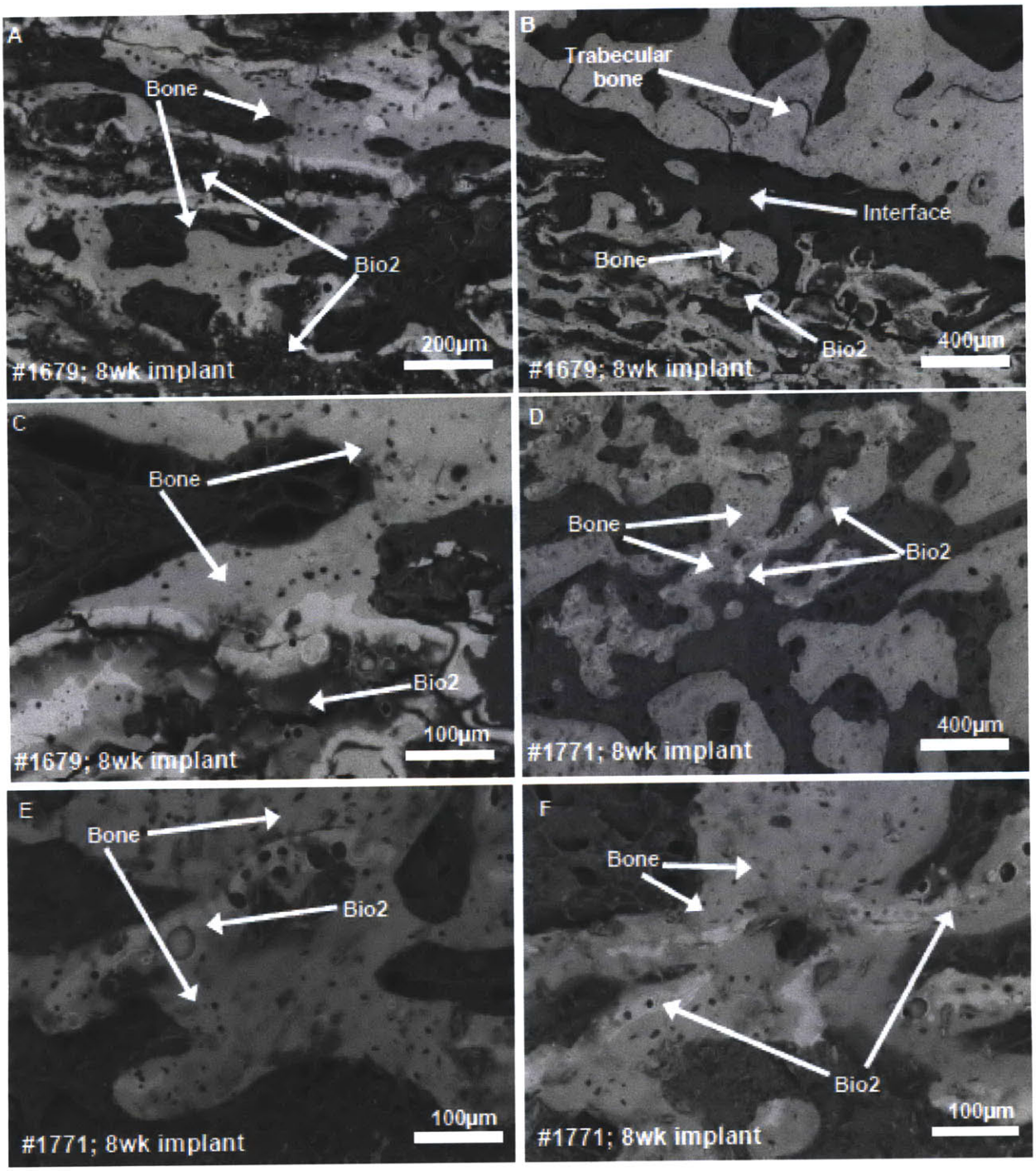

Figure B-8 – BEI micrographs of Bio2 samples following 8 weeks of implantation

implantation. At two weeks implantation, there is a gradient in the electron density of the material on BEI, with the outer parts of the scaffold becoming more electron dense and the inner parts appearing less dense. It appears that some of the scaffold

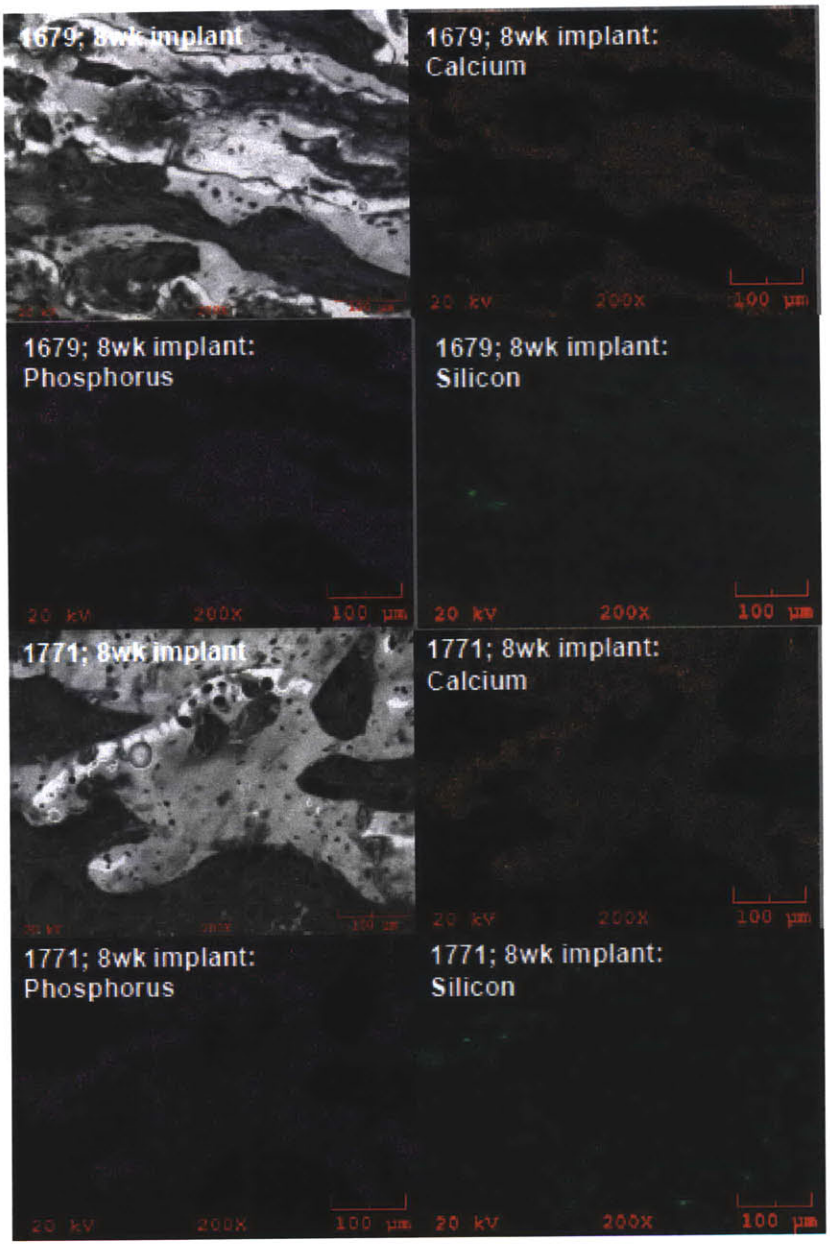

Figure B-9 – EDX generated images of mineral distributions for Bio2 samples implanted for 8wks

materials are dissolving out and depositing on the surface where the new bone is being deposited. This was confirmed on EDX, which showed that the inside of the scaffold was more silicon rich, with the outer borders of the scaffold showing more calcium and phosphorus ions. Calcium and phosphorus are the components of hydroxyapatite, the principal mineral components of bone, and may be dissolving from

the scaffold and partaking in the bone formation process.

Appendix C

Protocols

C.1 EvoTron operation

1. Attach all leads and the foot pedal to the machine and switch on

2. When prompted, insert EvoTrode

3. Depress/release foot pedal when instructed by machine

4. In main screen, use up down arrows to select energy flux density

5. Press top button to scroll through other options (e.g., number of shocks, frequency). Press button between arrows to return to main options and begin treatment (note: holding this button pressed will reset the shock count to zero).

6. Apply coupling gel to shaved limb and depress foot pedal once accurate alignment has been achieved.

7. At end of treatment, remove EvoTrode from device before switching off machine (otherwise it will lock in). Also, remove leads and foot pedal for storage.

Note: the EvoTrode has to be replaced every 6 months or 50,000 shocks, whichever comes sooner.

C.2 OssaTron operation

1. Prior to initiating the machine, check the water conductivity. If it is not between 300-400 Siemens/m, replace with DI water and add saline (starting with 5ml) until the desired conductivity is reached.

2. Switch on the machine using the key switch.

3. Conduct collision test by lifting the rim above the applicator head until a click is heard, and then release.

4. Allow machine to degas.

5. Repeat steps 2 - 4.

6. When degassing is finished, remove bolts from arm and extend arm out. Replace bolts. Rotate head around until it is face up.

7. Open head, remove safety electrode and place OssaTron electrode inside (*Note: lifespan of OssaTron electrodes 2000 - 3000 shocks*). Close head.

8. Adjust pressure and rotate head to"change position" (head automatically locks). Push on the head to remove air during the first 30 seconds of filling. If there is excess air, deflate head and repeat step.

9. When filling is complete, rotate device around until arm is at vertical. Place bow on head and adjust the pressure until secondary focus (marked by bow tips) is at desired treatment point.

10. Set treatment kV and frequency with arrows on control pad.

11. Using coupling gel to acoustically couple the device to the shaved treatment site, apply desired treatment.

12. Clean head, deflate membrane, rotate head to electrode change position, and remove electrode.

13. Place safety electrode in head for storage. Rotate arm back and return arm to storage postion.

Note: the two most common reasons the machine is not working correctly is (1) conductivity is incorrect, and (2) the brakes are not on.

C.3 Scaffold preparation

In situ surgery scaffolds

The raw material is provided as a block 1cm x 1cm x 2cm. Using a buehler diamond saw (Buehler Isomet, Lake Bluff, IL) operating at 325RPM, the block is sliced into 1.6mm thick sections. The blade is moved in increments of 2.25mm (blade thickness ~0.5mm) to produce this thickness. Water is used for lubrication. The scaffold is then laid on a hard surface and covered in DI water. A burr operating at slow speed is used to remove the edges and trim the scaffold down to 5.5mm ⌀. The scaffold is then air dried and sterilized using Sterrad (Brigham and Women's Hospital).

In situ surgery scaffolds

Starting with the raw material block, the scaffold is wetted with DI water. The handle of skin biopsy punches (Integra Miltex Inc., York, PA; one per scaffold) are removed using a saw. The biopsy punch is clamped into a vertical drill press, so that it can be used as a trephine (NB: clamp as tight as possible to eliminate wobble in the drill press). The drill press, operating at slow speed and with water lubrication is approximated to the block and smoothly pressed through the block to core out the scaffold. A small needle can be used to carefully push the scaffold out of the biopsy punch if necessary. The scaffold is then air dried and sterilized using Sterrad (Brigham and Women's Hospital).

C.4 Surgery

In situ surgery

The rabbits are induced using IV injections of ketamine (10mg/kg) and ace promazine

(0.5mg/kg) and given cefazolin (20mg/kg subcu) pre-op. The rabbit is then intubated on 1-2% isoflourane with O_2. All surgical procedures are carried out under sterile conditions. A 1.5cm skin incision, on the medial side of the ipsilateral limb that the ESW dose was applied, is made so as to expose the periosteal implant site (tibia medial condyle) and the periosteum exposed (only a thin layer of fascia underlies the skin). Using a scalpel, an arc (1.2cm long) is scored proximal to the implant harvest site. The periosteum is then elevated off the bone using a periosteal elevator to create a pocket for the implant. The underlying cortical bone surface is scraped clean with an osteotome. Using sterile saline to lubricate the region, the scaffold (wetted with saline) is implanted into the periosteal pocket. The periosteum (which retracts following elevation off the bone) is approximated back into place using 3 or 4 6-0 sutures around the arc. The fascia and skin are closed with sutures.

Free graft surgery

The rabbits are induced using IV injections of ketamine (10mg/kg) and ace promazine (0.5mg/kg) and given cefazolin (20mg/kg subcu) pre-op. The rabbit is then intubated on 1-2% isoflourane with O_2. All surgical procedures are carried out under sterile conditions. A 1.5cm skin incision, on the medial side of the ipsilateral limb that the ESW dose was applied, is made so as to expose the periosteal harvest site (tibia medial condyle; only a thin layer of fascia underlies the skin). The ESW treated periosteum is scored with a scalpel and elevated off the bone using a periosteal elevator. The periosteum is flattened onto a sterile tongue depressor with the cambium cells face up, wrapped in gauze and stored in room temperature sterile saline while the implant site is prepared.

A 1.5cm skin incision is made over the implant site and the skin and musculature is retracted laterally to expose the bone. Successively increasing diameter surgical drill bits are used to create the defect. The scaffold is then push-fit into the defect and periosteum secured in place by suturing to the surrounding periosteum or attaching to the scaffold. The muscle, fascia, and skin are replaced and sutured closed.

C.5 MicroCT

1. Switch on the control box by turning the key on the front. Wait 30 minutes for the camera to cool to its target temperature.

2. Initiate the x-ray warm up procedure by double-clicking the icon. Click on the idle button.

3. When idle is complete, click on the <3min button

4. When all warmups are complete, launch scan control.

5. Choose scan a new subject or add scan to existing subject and enter names for the specimen etc.

6. Select protocol (27μm 90 mins). Select recon after scan in the options menu.

7. Click fluoro and place scaffold on scanner bed when prompted (note: best scan results are achieved by leaving the samples in ETOH or DI Water in 50ml tubes and placing tube on scanner bed).

8. Position the stage so that the desired scan region is displayed on x-ray. Using the mouse, select the two corners of the scan region using CTRL + Left/Right mouse button. Close flouro screen to save.

9. Press start scan button and wait for scan to finish.

10. Designate a region of interest by launching ROI tab and adjusting the settings. Click on save crop when the selected region is achieved.

11. Click load crop in the reconstruction window. Select **Full Res** and deselect **Mini Volume**

12. Click **Recon**

13. Use GE Microviewer to obtain pictures and videos of scans.

C.6 Scanning electron microscope

JEOL JSM 6700F SEM *Samples should be dry, only handled using gloves, and sputter coated (gold-palladium) if not already conductive.*

1. At start, exchange chamber should be vented, gun valve closed, stage should be in exchange position, and HLDR light off (i.e. no specimen in chamber)
2. Launch the software and check the penning vacuum gauge should be below 5 x 10^{-4} (click PVG button).
3. Click the **specimen holder exchange button**, select the holder type and click exchange. This moves the stage to the exchange position.
4. Under maintenance menu, click **gun** and check that SIP-1 <3 x 10^{-8} and SIP-2 <4 x 10^{-7}.
5. Fill the cold trap with liquid nitrogen.
6. Check the physical working distance is 8mm (NB: sample height must be <8mm above top of holder). Press **VENT** button. When venting is complete, loosen clips, open chamber door and mount specimen. Press **EVAC** button to evacuate the chamber.
7. When evacuation is complete, bring rod down, gently push the sample into the chamber, and replace the rod to start position. **HLDR** should now be lit. Press and hold the **VENT** button and the check the penning vacuum gauge again.
8. Click the column button and select imaging parameters.
9. Click **Hight Tension** button and wait for the current to reach the set level. Press the **Gun Valve Close** button on the front of the microscope to open the gun valve.
10. A low mag image should appear. Adjust the brightness and contrast and move stage in plane until the specimen is visible.

11. Switch off **Low Mag** and adjust the Z distance until the sample comes into focus. Increase the magnification and perform fine focusing with the knob.

12. The **Gun Alignment**, **Stigmation**, and **Objective Lens Alignment** should now be adjusted to optimize the image.

13. To use the backscatter detector, ensure the working distance is set to 8mm and the sample is in focus. Close the gun valve and press the **RBEI** button to move the backscatter detector into the chamber. Open the gun valve again. For polished embedded bone samples, use the **COMPO** mode, which gives atomic number contrast. *The **TOPO** mode gives contrast between topological features.*

14. To remove the backscatter detector, perform the reverse (i.e. close the gun valve, remove backscatter detector).

15. To remove samples, set the stage to exchange position. Press the **HT** button to turn off the emitter and press the **Gun Valve Close** button. Press and hold **EVAC** button. Gently bring rod down and insert it into chamber. Slide sample out with rod and replace rod to start position. Press and hold **VENT** to vent sample chamber and open door and remove sample.

C.7 Hemotoxylin and eosin Staining

Formalin fixed, paraffin embedded specimens

Solutions

Hematoxylin

Gills Hematoxylin Solution, Fisher Cat# 23245656 (3x); Filter 200ml of working solution into staining dish.

Acid Alcohol

0.5 % in 80% EtOH (100ml of 80% EtOH + 0.5 ml HCl)

Eosin

Eosin Y Solution Aqueous, Sigma Cat# HT110-2-128

Cytoseal Cytoseal 60, Cat# 18006, Electron Microscopy Sciences.

1. Deparaffinize and Rehydrate
    - Xylenes 2 x 5mins
    - 100%EtOH 2 x 3mins
    - 95%EtOH 2 x 2mins
    - 80% EtOH 1min
    - Wash in running tap water 5mins
2. Hematoxylin, 3mins (Note: be sure to filter hematoxylin).
3. Wash in tap water for 5mins.
4. Decolorization: three quick dips in acid alcohol.
5. Wash in tap water for 5mins.
6. Eosin, 30-60 seconds.
7. 100% alcohol 2 x 3mins.
8. Xylene 2 x 3mins.
9. Air dry. Coverslip with Cytoseal

C.8 Masson's trichrome

Description: This method is used for the detection of collagen fibers in formalin fixed, paraffin embedded tissues such as skin and heart. The collagen fibers will be stained blue, the nuclei will be stained black, and the background is stained red.

Solutions:

Weigert's Iron Hematoxylin Solution:

Stock Solution A: Hematoxylin (1 g) + 95% Alcohol (100 ml)

Stock Solution B: 29% Ferric chloride in water (4 ml) + Distilled water (95 ml) + Hydrochloric acid, concentrated (1ml) / 25% v/v

Weigert's Iron Hematoxylin Working Solution:

Mix equal parts of stock solution A and B. This working solution is stable for 3 months

Biebrich Scarlet-Acid Fuchsin Solution:

Biebrich scarlet, 1% aqueous (90 ml) + Acid fuchsin, 1% aqueous (10 ml) + Acetic acid, glacial (1 ml)

Phosphomolybdic-Phosphotungstic Acid Solution:

5% Phosphomolybdic acid (25 ml) + 5% Phosphotungstic acid (25 ml)

Aniline Blue Solution:

Aniline blue (2.5 g) + Acetic acid, glacial (2 ml) + Distilled water (100 ml)

1% Acetic Acid Solution:

Acetic acid, glacial (1 ml) + Distilled water (99 ml)

Procedure:

1. Deparaffinize and rehydrate
    - Xylenes 2 x 5mins
    - 100%EtOH 2 x 3mins
    - 95%EtOH 2 x 2mins
    - 80% EtOH 1min
    - Wash in running tap water 5mins
2. Stain in Weigert's iron hematoxylin working solution for 10mins.
3. Rinse in running warm tap water for 10mins.
4. Wash in distilled water.
5. Stain in Biebrich scarlet-acid fuchsin solution for 15mins. Solution can be saved for future use.

6. Wash in distilled water.

7. Differentiate in phosphomolybdic-phosphotungstic acid solution for 15mins or until collagen is not red.

8. Transfer sections directly (without rinse) to aniline blue solution and stain for 5-10mins. Rinse briefly in distilled water and differentiate in 1% acetic acid solution for 2-5mins.

9. Wash in distilled water.

10. Dehydrate very quickly through 95% ethyl alcohol, absolute ethyl alcohol (these steps will wipe off Biebrich scarlet-acid fuchsin staining) and clear in xylene.

11. Mount with resinous mounting medium.

C.9 Immunohistochemistry

Solutions

Tris-Buffred Saline(TBS) Stored at RT in packets

1 package(Dako, S3001) to 1L dH2O Stored at 4°C in solution.

Wash Buffer with Tween 20 Stored at 4 °C

(Dako Cytomation, S3006, 1000ml)

500ml of x10 in 4500ml dH2O

0.1% (w/v) Protease XIV Stored at -20°C

10mg Protease (Sigma P5174)

10 ml TBS

Peroxidase Blocking Reagent Stored at 4 °C

(Dako, S2001)

Read-to-Use

Primary Antibody

Osteocalcin

Ab 13418 monoclonal mouse IgG2a osteocalcin antibody OC4-30 (1mg/mL); Stored

at -20 °C

Dilute 1:100

60mins incubation

α-Smooth Muscle Actin

Sigma A5228 monoclonal mouse IgG2a anti-SMA; Stored at -20 °C

Dilute 1:400

15mins incubation

vonWillebrand Factor

Dako A0082 polyclonal rabbit IgG anti-vWF (3.3mg/ml); Stored at 4 °C

Dilute to 25μg/mL

30mins incubation

Collagen type II

DSHB Iowa City mouse monoclonal IgG2a anti-collII (0.6mg/mL); Stored at -20 °C

Dilute 1:200

15mins incubation

Lubricin

(Provdided by Dr. T. Schmid, Rush University Medical Center) mouse monoclonal IgG2b anti-lubricin stored at 4 °C

Dilute 1:1000

15mins incubation

Negative Control

- Negative controls are matched to the monoclonal antibody at corresponding concentration and incubation times

Mouse IgG2a negative control

Dako, X0943; Negative mouse IgG2a control (100mg/l); stored at 4 °C

Mouse IgG2b negative control

Dako, X0944; Negative mouse IgG2b control (100mg/l); stored at 4 °C

Rabbit Immunoglobulin Fraction

Dako X0936; Negative control rabbit IgG fraction (Solid-phase absorbed; 15g/l); stored at 4 °C

Diluting agent for all primary antibodies and negative controls

Universal AB diluent (Dako S0809)

Biotinylated Link (Stored at 4°C)

(Dakocytomation, LSAB-2 kit for use with rat tissue only, K0609)

Ready to use.

Streptavidin Peroxidase (HRP)

Dakocytomation, LSAB-2 kit for use with rat tissue only, K0609

Ready to use

AEC Plus Substrate Chromagen Stored at 4 °C

Dakocytomation, K3461

Ready to use.

Counter stain

Mayer's Hematoxylin (Filter before use) Stored at RT

(Sigma: MHS 16-500ML)

Aqueous Mounting Media

Faramount, Dako S3025; Stored at RT

1. Launch the Dako Autostainer and program the individual steps and copy and paste to the desired number of slides

    - Rinse (TBS+Tween)
    - Add 0.1% Protease - 40mins.
    - Rinse with (TBS+Tween)
    - Enzyme Block: H2O2 - Peroxidase blocking solution - 10mins.

- Rinse (TBS+Tween)
- Pretreatment Protein Block Serum-Free - 10mins.
- NO RINSE
- Incubate with primary antibody or corresponding negative controls as listed above.
- Rinse (TBS+Tween)
- Biotinylated link - 15mins.
- Streptavidin HRP - 15mins.
- Rinse (TBS+Tween)
- Switch
- Substrate: AEC Plus - 10mins.

2. Click next and add the appropriate amount of wash buffer, DI water.
3. Deparaffinize and rehydrate via the following:
   - Xylenes 2 x 5mins
   - 100%EtOH 2 x 3mins
   - 95%EtOH 2 x 2mins
   - 80% EtOH 1min
   - rinse in large beaker of tap water
   - water rinse and load slides into autostainer
4. Load prepared solutions into autostainer and begin run
5. At end of run remove slides and place in container of TBS
6. Counter stain with Mayer's Hematoxylin for 90secs
7. Rinse in running tap water for 3mins
8. Transfer into a container of TBS and coverslip slides with aqeous mounting media

C.10 LR White plastic embedding of bone

Solution: LR White Embedding Medium (Ted Pella Product Nos. 18181, Medium Grade, 500ml)

Order from: http://www.tedpella.com/chemical_html/chem1.htm

As per package insert instructions, mix provided catalyst into main bottle with a magnetic stirrer for 30mins and let stand for at least a further 30mins at room temperature before use. Shelf life is 1yr from addition of catalyst (can be frozen for longer term storage).

1. Formalin fix tissue (I found 7-10 days to give good results for rabbit bone samples)

2. Rinse with buffer solution (such as PBS) three times, and then leave the fixed sample in buffer solution at 4C for 24h, with gentle shaking, to remove fixatives

3. Dehydrate sample through a series of ethanol: 50%, 75%, 85%, 90%, 100% (twice), 30mins for each concentration

4. Infiltrate with 1/2 (volume ratio, fresh resin/ethanol), 1/1, and pure fresh resin (twice) at 4 °C under vacuum, 24h each step; (can reduce last step to 8hrs)

5. Embed in fresh LR White resin at 60°C for 24-48h; the container should be covered to minimize oxygen; Before putting in oven, put final LR White in a vacuum for 24hrs at room temperature. At the same time, put enough LR white to fill the bottom of the 50mL falcon tubes (these are used as the molds) to create a base for your sample and cure for 24hrs at 55 °C. Place the sample, oriented as you would like to cut it, and fill with LR white to ~15mL above top of sample. Seal tubes tightly and wrap with parafilm (to minimize oxygen exchange - causes cracking). Place in oven at 24hrs at 55°C.

C.11 Polishing protocol for LR White embedded samples

1. Remove blocks from tubes and slice the plane you wish to view using a diamond saw (water lubricated, ~250RPM. Use the beuhler sharpening block every 2 cuts)

2. Using a high grit size paper, grind the block so that the faces are parallel and the correct plane is exposed.

3. Starting with the #500 grinding paper (Struers waterproof silicon carbide paper, FEPA #500, 30?m grit size) and using reasonable force with water flowing, grind for 2-3mins rotating the sample every 30secs to help eliminate directionality. If doing two samples at once (one in each hand), switch hands half way through to ensure balance. After polishing, place in distilled water and put in sonicator for 3-5mins. Wash grinding wheel after step with water and dry.

4. Repeat step 3 using #1200 paper (Struers, as above). Slightly less force than first step, 2-3mins and sonicate/clean as before

5. Repeat step 3 using #4000 paper (Stuers, as above). Same force as (4) and 2-3mins and sonicate/clean as before.

6. Using red cloth magnetic disc (for use with DiaDuo). Pour Dia Duo (1μm, Struers, PALINO, water based) onto disc and use sample to spread evenly. Do not run water. If more lubrication is needed, add DP lubricant (Struers, cat#40700025 (red in color)). Polish for 4-5mins with a lighter force than before. Sonicate in DI water for 4-5mins. Do not wash cloth before or after.

7. Swich to blue cloth magnetic disc. Wash with DI water and use cotton wool to make sure its clean. Add Op-S Colloidal Silica suspension (Struers, Code: OPSOT, Cat #40700000). Polish for 3mins with a light force. Add water if lubrication is needed. Sonicate in DI water for 4-5mins. Remove and dry under hand dryer. Clean off cloth as before use.

8. Place under vacuum, with a low heat (<40°C) overnight to dry sample and store under vacuum with dry rite before imaging in SEM.

Supplies can be found at:
http://www.struers.com/resources/elements/12/102726/Struers%20Grinding%20Products.pdf
http://www.struers.com/resources/elements/12/81202/DiaDuo%20brochure%20English.pdf

C.12 Notes

- All microtoming was performed on the Shandon Finesse Model ME+ (Thermo Fisher Scientific, Waltham, MA). Samples were cut at 7-8μm thickness, with the exception of some of the rabbit samples, which cut better at 9-10μm thickness. To improve the sections on microtoming, samples were first trimmed to remove the overlying paraffin layer. They were then soaked for a period of at least 2hrs in iced water (longer soaking times appeared to improve results). Addition of a droplet or two of ammonium hydroxide to the ice water bath also appeared beneficial. Frequently changing the blade during the cutting process further improved results.

- Decalcification with 10% formic acid (diluted with DI water) demonstrated most rapid results when combined with rocking of the samples, daily changing of formic acid. X-ray of the samples was used to determine complete decalcification (rat bone ~1wk; rabbit bone ~2wks).

Bibliography

Arnsdorf, E. J., L. M. Jones, D. R. Carter, and C. R. Jacobs (2009, Sep). The periosteum as a cellular source for functional tissue engineering. *Tissue Eng Part A 15*(9), 2637–42.

Aro, H. T., B. W. Wippermann, S. F. Hodgson, and E. Y. Chao (1990, Mar). Internal remodeling of periosteal new bone during fracture healing. *J Orthop Res 8*(2), 238–46.

Atala, A., R. Lanza, J. A. Thomas, and R. M. Nerem (2008). *Principles of Regnerative Medicine* (1st ed.). Oxford, UK: Elsevier.

Bassett, C. (1962). Current concepts of bone formation. *The Journal of Bone and Joint Surgery 44*(6), 1217.

Birnbaum, K., D. C. Wirtz, C. H. Siebert, and K. D. Heller (2002, Jul). Use of extracorporeal shock-wave therapy (eswt) in the treatment of non-unions. a review of the literature. *Arch Orthop Trauma Surg 122*(6), 324–30.

Blaisdell, F. E. (1925). The osteogenic function of periosteum. *Arch Surg 11*, 933.

Bloom, W. and D. W. Fawcett (1968). *A textbook of hisotology* (9th ed. ed.). Philadelphia, PA: Saunders.

Boden, S. (1999, Jan). Bioactive factors for bone tissue engineering. *Clinical Orthopaedics and Related Research* (367), S84–S94.

Brighton, C., D. Lorich, R. Kupcha, T. Reilly, A. Jones, and R. Woodbury (1992). The pericyte as a possible osteoblast progenitor cell. *Clinical orthopaedics and related research 275*, 287.

Brittberg, M., A. Lindahl, A. Nilsson, C. Ohlsson, O. Isaksson, and L. Peterson (1994, Jan). Treatment of deep cartilage defects in the knee with autologous chondrocyte transplantation. *New Engl J Med 331*(14), 889–895.

Bruder, S. and B. Fox (1999, Jan). Tissue engineering of bone - cell based strategies. *Clin Orthop Relat R* (367), S68–S83.

Burg, K. J., S. Porter, and J. F. Kellam (2000, Dec). Biomaterial developments for bone tissue engineering. *Biomaterials 21*(23), 2347–59.

Cacchio, A., L. Giordano, O. Colafarina, J. D. Rompe, E. Tavernese, F. Ioppolo, S. Flamini, G. Spacca, and V. Santilli (2009, Nov). Extracorporeal shock-wave therapy compared with surgery for hypertrophic long-bone nonunions. *The Journal of Bone and Joint Surgery 91*(11), 2589–2597.

Chen, D., M. Zhao, and G. Mundy (2004, Jan). Bone morphogenetic proteins. *Growth Factors 22*(4), 233–241.

Chen, Y., C. Wang, K. Yang, Y. Kuo, H. Huang, Y. Huang, Y. Sun, and F. Wang (2004, Jan). Extracorporeal shock waves promote healing of collagenase-induced achilles tendinitis and increase tgf-beta 1 and igf-1 expression. *J Orthopaed Res 22*(4), 854–861.

Chen, Y.-J., Y.-R. Kuo, K. D. Yang, C.-J. Wang, H.-C. Huang, and F.-S. Wang (2003, Dec). Shock wave application enhances pertussis toxin protein-sensitive bone formation of segmental femoral defect in rats. *J Bone Miner Res 18*(12), 2169–79.

Chen, Y.-J., T. Wurtz, C.-J. Wang, Y.-R. Kuo, K. D. Yang, H.-C. Huang, and F.-S. Wang (2004, May). Recruitment of mesenchymal stem cells and expression of

tgf-beta 1 and vegf in the early stage of shock wave-promoted bone regeneration of segmental defect in rats. *J Orthop Res 22*(3), 526–34.

Chiapasco, M., E. Romeo, P. Casentini, and L. Rimondini (2004, Feb). Alveolar distraction osteogenesis vs. vertical guided bone regeneration for the correction of vertically deficient edentulous ridges: a 1-3-year prospective study on humans. *Clin Oral Implants Res 15*(1), 82–95.

Chitnis, P. V. and R. O. Cleveland (2006, Jan). Acoustic and cavitation fields of shock wave therapy devices. *Therapeutic Ultrasound: 5th International Symposium on Therapeutic Ultrsound*, 1–5.

Choi, Y.-S., S.-E. Noh, S.-M. Lim, C.-W. Lee, C.-S. Kim, M.-W. Im, M.-H. Lee, and D.-I. Kim (2008, Apr). Multipotency and growth characteristic of periosteum-derived progenitor cells for chondrogenic, osteogenic, and adipogenic differentiation. *Biotechnol Lett 30*(4), 593–601.

Chow, G. K. and S. B. Streem (2000, May). Extracorporeal lithotripsy. update on technology. *Urol Clin North Am 27*(2), 315–22.

Chung, B. and J. P. Wiley (2002, Jan). Extracorporeal shockwave therapy: a review. *Sports Med 32*(13), 851–65.

Cleveland, R., D. Lifshitz, B. Connors, A. Evan, L. Willis, and L. Crum (1998, Jan). In vivo pressure measurements of lithotripsy shock waves in pigs. *Ultrasound Med Biol 24*(2), 293–306.

Cleveland, R. O., P. V. Chitnis, and S. R. McClure (2007, Jan). Acoustic field of a ballistic shock wave therapy device. *Ultrasound Med Biol 33*(8), 1327–1335.

Cleveland, R. O. and J. A. McAteer (2006). *Smith's textbook of endourology - Ch. 38* (2nd ed.). BC Decker.

Cohen, J. and P. Lacroix (1955). Bone and cartilage formation by periosteum: Assay of experimental autogenous grafts. *The Journal of Bone and Joint Surgery 37*(4), 717.

Cosentino, R., E. Selvi, R. D. Stefano, E. Frati, S. Manca, M. Hammoud, and R. Marcolongo (2004, Jan). Extracorporeal shock wave therapy for chronic calcific tendinitis of the shoulder. *Clin Rheumatol 23*(5), 475–477.

Dattani, R. (2007, Jan). Femoral osteolysis following total hip replacement. *Postgrad Med J 83*(979), 312–316.

Delius, M., K. Draenert, Y. A. Diek, and Y. Draenert (1995, Jan). Biological effects of shock waves: in vivo effect of high energy pulses on rabbit bone. *Ultrasound in Medicine & Biology 21*(9), 1219–25.

Diaz-Flores, L., R. Gutierrez, A. Lopez-Alonso, R. Gonzalez, and H. Varela (1992). Pericytes as a supplementary source of osteoblasts in periosteal osteogenesis. *Clinical orthopaedics and related research 275*, 280.

Ducy, P., T. Schinke, and G. Karsenty (2000, Jan). The osteoblast: A sophisticated fibroblast under central surveillance. *Science 289*(5484), 1501–1504.

Duhamel, H. L. (1742). Sur le development et la crue des os des animaux. *Hist. Acad. Inscr. Paris 2*, 481.

Emans, P., D. Surtel, E. Frings, S. Bulstra, and R. Kuijer (2005). In vivo generation of cartilage from periosteum. *Tissue engineering 11*(3-4), 369–377.

Englert, C., K. B. McGowan, T. J. Klein, A. Giurea, B. L. Schumacher, and R. L. Sah (2005, Apr). Inhibition of integrative cartilage repair by proteoglycan 4 in synovial fluid. *Arthritis Rheum 52*(4), 1091–9.

Fell, H. B. (1932). The osteogenic capacity in vivo of periosteum and endosteum isolated from the limb skeleton of fowl embryos and young chicks. *Journal of Anatomy 66*, 157.

Flannery, C. R., C. E. Hughes, B. L. Schumacher, D. Tudor, M. B. Aydelotte, K. E. Kuettner, and B. Caterson (1999, Jan). Articular cartilage superficial zone protein

(szp) is homologous to megakaryocyte stimulating factor precursor and is a multifunctional proteoglycan with potential growth-promoting, cytoprotective, and lubricating properties in cartilage metabolism. *Biochemical and Biophysical Research Communications 254*(3), 535–41.

Funakoshi, T., T. Schmid, H.-P. Hsu, and M. Spector (2008, Jan). Lubricin distribution in the goat infraspinatus tendon: A basis for interfascicular lubrication. *J Bone Joint Surg Am 90A*(4), 803–814.

Funakoshi, T. and M. Spector (2010, Jan). Chondrogenic differentiation and lubricin expression of caprine lnfraspinatus tendon cells. *J Orthopaed Res 28*(6), 716–725.

Gerdesmeyer, L. and S. W. Lowell (2007). *Extracorporeal shockwave therapy.* Towson: Data Trace.

Ham, A. (1969). *Histology* (6th ed. ed.). Philadelphia, PA: Lippincott Company.

Haupt, G. (1997). Use of extracorporeal shock waves in the treatment of pseudarthrosis, tendinopathy and other orthopedic diseases. *The Journal of Urology 158*(1), 4–11.

Herzog, E., L. Chai, and D. Krause (2003, Jan). Plasticity of marrow-derived stem cells. *Blood 102*(10), 3483–3493.

Hofmann, A., U. Ritz, M. H. Hessmann, M. Alini, P. M. Rommens, and J.-D. Rompe (2008, Dec). Extracorporeal shock wave-mediated changes in proliferation, differentiation, and gene expression of human osteoblasts. *J Trauma 65*(6), 1402–10.

Hutmacher, D. (2000). Scaffolds in tissue engineering bone and cartilage. *Biomaterials 21*(24), 2529–2543.

Hutmacher, D. and M. Sittinger (2003). Periosteal cells in bone tissue engineering. *Tissue Engineering 9*(4, Supplement 1), 45–64.

Ikeda, K., K. Tomita, and K. Takayama (1999). Application of extracorporeal shock wave on bone: Preliminary report. *The Journal of Trauma: Injury, Infection, and Critical Care 47*(5), 946.

Isogai, N., W. Landis, R. Mori, Y. Gotoh, L. Gerstenfeld, J. Upton, and J. Vacanti (2000). Experimental use of fibrin glue to induce site-directed osteogenesis from cultured periosteal cells. *Plastic and Reconstructive Surgery 105*(3), 953.

Jagt, O. P. V. D., J. C. V. D. Linden, W. Schaden, H. T. V. Schie, T. M. Piscaer, J. A. N. Verhaar, H. Weinans, and J. H. Waarsing (2009, Nov). Unfocused extracorporeal shock wave therapy as potential treatment for osteoporosis. *J Orthop Res 27*(11), 1528–33.

Jaquiéry, C., S. Schaeren, J. Farhadi, P. Mainil-Varlet, C. Kunz, H.-F. Zeilhofer, M. Heberer, and I. Martin (2005, Dec). In vitro osteogenic differentiation and in vivo bone-forming capacity of human isogenic jaw periosteal cells and bone marrow stromal cells. *Ann Surg 242*(6), 859–68.

Jay, G. D., U. Tantravahi, D. E. Britt, H. J. Barrach, and C. J. Cha (2001, Jul). Homology of lubricin and superficial zone protein (szp): products of megakaryocyte stimulating factor (msf) gene expression by human synovial fibroblasts and articular chondrocytes localized to chromosome 1q25. *J Orthop Res 19*(4), 677–87.

Johannes, E., D. K. Sukul, and E. Matura (1994). High-energy shock waves for the treatment of nonunions: an experiment on dogs. *The Journal of surgical research 57*(2), 246–252.

Jones, A. R. C. and C. R. Flannery (2007, Jan). Bioregulation of lubricin expression by growth factors and cytokines. *Eur Cell Mater 13*, 40–5; discussion 45.

Joyce, M., A. Roberts, M. Sporn, and M. Bolander (1990, Jan). Transforming growth-factor-beta and the initiation of chondrogenesis and osteogenesis in the rat femur. *J Cell Biol 110*(6), 2195–2207.

King, K. and A. Melbourne (1976). Periosteal pedicle grafting in dogs. *Journal of Bone & Joint Surgery, British Volume 58*(1), 117.

Kinner, B., L. Gerstenfeld, T. Einhorn, and M. Spector (2002). Expression of smooth muscle actin in connective tissue cells participating in fracture healing in a murine model. *Bone 30*(5), 738–745.

Kohrs, R. T., C. Zhao, Y.-L. Sun, G. D. Jay, L. Zhang, M. L. Warman, K.-N. An, and P. C. Amadio (2010, Sep). Tendon fascicle gliding in wild type, heterozygous, and lubricin knockout mice. *J Orthop Res*, 384–389.

Langer, R. and J. Vacanti (1993, Jan). Tissue engineering. *Science 260*(5110), 920–926.

Laurencin, C. T., A. M. Ambrosio, M. D. Borden, and J. A. Cooper (1999, Jan). Tissue engineering: orthopedic applications. *Annu Rev Biomed Eng 1*, 19–46.

Lavender, G. (1938). A study of bone generation. *Surg Gyecol Obstet 61*, 705.

Lee, S. Y., T. Nakagawa, and A. H. Reddi (2008, Nov). Induction of chondrogenesis and expression of superficial zone protein (szp)/lubricin by mesenchymal progenitors in the infrapatellar fat pad of the knee joint treated with tgf-beta1 and bmp-7. *Biochemical and Biophysical Research Communications 376*(1), 148–53.

Lee, S. Y., T. Niikura, and A. H. Reddi (2008, Nov). Superficial zone protein (lubricin) in the different tissue compartments of the knee joint: modulation by transforming growth factor beta 1 and interleukin-1 beta. *Tissue Eng Part A 14*(11), 1799–808.

Lieberman, J. R., A. Daluiski, and T. A. Einhorn (2002, Jun). The role of growth factors in the repair of bone. biology and clinical applications. *J Bone Joint Surg Am 84-A*(6), 1032–44.

Ludwig, J., S. Lauber, H. J. Lauber, U. Dreisilker, R. Raedel, and H. Hotzinger (2001, Jun). High-energy shock wave treatment of femoral head necrosis in adults. *Clinical orthopaedics and related research* (387), 119–26.

Madri, J. and M. Marx (1992). Matrix composition, organization and soluble factors: modulators of microvascular cell differentiation in vitro. *Kidney Int 41*(3), 560–565.

Maier, M., B. Averbeck, S. Milz, H. J. Refior, and C. Schmitz (2003, Jan). Substance p and prostaglandin e2 release after shock wave application to the rabbit femur. *Clinical Orthopaedics and Related Research* (406), 237–45.

Maier, M. and C. Schmitz (2008, Nov). Shock wave therapy: what really matters. *Ultrasound in Medicine & Biology 34*(11), 1868–70.

Malizos, K. N. and L. K. Papatheodorou (2005, Nov). The healing potential of the periosteum molecular aspects. *Injury 36 Suppl 3*, S13–9.

Mardones, R. M., G. G. Reinholz, J. S. Fitzsimmons, M. E. Zobitz, K.-N. An, D. G. Lewallen, M. J. Yaszemski, and S. W. O'Driscoll (2005, Jan). Development of a biologic prosthetic composite for cartilage repair. *Tissue engineering 11*(9-10), 1368–78.

Maxwell, A., O. Sapozhnikov, and M. Bailey (2006). P2c-2 a new pvdf membrane hydrophone for measurement of medical shock waves. *IEEE Ultrasonics Symposium, 2006*, 1608–1611.

McClure, S. R., D. V. Sickle, and M. R. White (2004, Jan). Effects of extracorporeal shock wave therapy on bone. *Vet Surg 33*(1), 40–8.

Medici, D., E. M. Shore, V. Y. Lounev, F. S. Kaplan, R. Kalluri, and B. R. Olsen (2010, Dec). Conversion of vascular endothelial cells into multipotent stem-like cells. *Nature Medicine 16*(12), 1400–6.

Melcher, A. and G. Accursi (1971). Osteogenic capacity of periosteal and osteoperiosteal flaps elevated from the parietal bone of the rat. *Archives of oral biology 16*(6), 573.

Mizuno, H., K. Hata, K. Kojima, L. Bonassar, C. Vacanti, and M. Ueda (2006). A novel approach to regenerating periodontal tissue by grafting autologous cultured periosteum. *Tissue engineering 12*(5), 1227–1335.

Muschler, G., C. Nakamoto, and L. Griffith (2004). Engineering principles of clinical cell-based tissue engineering. *The Journal of Bone and Joint Surgery 86*(7), 1541–1558.

NIHCDP (1995, Jun). Nih consensus conference: Total hip replacement. nih consensus development panel on total hip replacement. *JAMA 273*(24), 1950–6.

O'Driscoll, S. (2001, Jan). Technical considerations in periosteal grafting for osteochondral injuries. *Clin Sport Med 20*(2), 379.

O'Driscoll, S. and J. Fitzsimmons (2001, Jan). The role of periosteum in cartilage repair. *Clinical orthopaedics and related research* (391), S190–S207.

O'Driscoll, S. W., A. D. Recklies, and A. R. Poole (1994, Jul). Chondrogenesis in periosteal explants. an organ culture model for in vitro study. *J Bone Joint Surg Am 76*(7), 1042–51.

Ogden, J. A., R. G. Alvarez, R. Levitt, and M. Marlow (2001, Jun). Shock wave therapy (orthotripsy) in musculoskeletal disorders. *Clinical orthopaedics and related research* (387), 22–40.

Ogden, J. A., R. G. Alvarez, R. L. Levitt, J. E. Johnson, and M. E. Marlow (2004, Oct). Electrohydraulic high-energy shock-wave treatment for chronic plantar fasciitis. *J Bone Joint Surg Am 86-A*(10), 2216–28.

Ollier, L. (1860). Recherches experimentales sur les graffes osseuses. *J Physiol Homme et Animaux 3*, 88.

Poussa, M. (1980). Vascularization of free periosteal and 100 micron thick osteoperiosteal grafts in muscle tissue environment. *Acta Orthopaedica 51*(1-6), 197–204.

Poussa, M. and V. Ritsilä (1979). The osteogenic capacity of free periosteal and osteoperiosteal grafts: A comparative study in growing rabbits. *Acta Orthopaedica 50*(5), 491–499.

Press, E. (1924). Experimentelle studien uber der knochewbildende kraft des periosten. *Arch J Klin Chir 129*, 750.

Ranta, R., P. Ylipaavalniemi, and M. Altonen (1981, Jan). Transplantation of free tibial periosteal graft on alveolar bone defect in adult rabbit. *International journal of Oral Surgery*.

Reinholz, G. G., J. S. Fitzsimmons, M. Casper, H.-W. Chung, T. Reusink, J. Schagemann, and S. W. O'Driscoll (2008). Rejuvenation of periosteum for tissue engineering using local growth factor injection. *54th Ann. Meet. ORS*.

Reinholz, G. G., J. S. Fitzsimmons, M. E. Casper, T. J. Ruesink, H. W. Chung, J. C. Schagemann, and S. W. O'Driscoll (2009, Jan). Rejuvenation of periosteal chondrogenesis using local growth factor injection. *Osteoarthr Cartilage 17*(6), 723–734.

Rhee, D., J. Marcelino, M. Baker, Y. Gong, P. Smits, V. Lefebvre, G. Jay, M. Stewart, H. Wang, M. Warman, and J. Carpten (2005, Jan). The secreted glycoprotein lubricin protects cartilage surfaces and inhibits synovial cell overgrowth. *J Clin Invest 115*(3), 622–631.

Rompe, J., J. Zoellner, and B. Nafe (2001, Jan). Shock wave therapy versus conventional surgery in the treatment of calcifying tendinitis of the shoulder. *Clinical orthopaedics and related research* (387), 72–82.

Rubak, J., M. Poussa, and V. RITSILA (1982, Jan). Chondrogenesis in repair of articular-cartilage defects by free periosteal grafts in rabbits. *Acta Orthop Scand 53*(2), 181–186.

Saris, D., A. Sanyal, K. An, J. Fitzsimmons, and S. O'Driscoll (1999). Periosteum responds to dynamic fluid pressure by proliferating in vitro. *Journal of Orthopaedic Research 17*(5), 668–677.

Schaden, W., A. Fischer, and A. Sailler (2001). Extracorporeal shock wave therapy of

nonunion or delayed osseous union. *Clinical Orthopaedics & Related Research 387*, 90–94.

Schumacher, B. L., J. A. Block, T. M. Schmid, M. B. Aydelotte, and K. E. Kuettner (1994, May). A novel proteoglycan synthesized and secreted by chondrocytes of the superficial zone of articular cartilage. *Arch Biochem Biophys 311*(1), 144–52.

Shrivastava, S. K. and Kailash (2005, Mar). Shock wave treatment in medicine. *J Biosci 30*(2), 269–75.

Simion, M., S. Jovanovic, C. Tinti, and S. Benfenati (2001). Long-term evaluation of osseointegrated implants inserted at the time or after vertical ridge augmentation: A retrospective study on 123 implants with 1-5 year follow-up. *Clinical Oral Implants Research 12*(1), 35.

Simion, M., S. Jovanovic, P. Trisi, A. Scarano, and A. Piattelli (1998). Vertical ridge augmentation around dental implants using a membrane technique and autogenous bone or allografts in humans. *The International journal of periodontics & restorative dentistry 18*(1), 8.

Simion, M., M. Nevins, I. Rocchietta, and F. Fontana (2009, Jan). Vertical ridge augmentation using an equine block infused with recombinant human platelet-derived growth factor-bb: a histologic study in a canine model. *The International journal of periodontics & restorative dentistry*.

Simion, M., I. Rocchietta, D. Kim, M. Nevins, and J. Fiorellini (2006, Oct). Vertical ridge augmentation by means of deproteinized bovine bone block and recombinant human platelet-derived growth factor-bb: a histologic study in a dog model. *The International journal of periodontics & restorative dentistry 26*(5), 415–23.

Simon, T., D. V. Sickle, D. Kunishima, and D. Jackson (2003, Jan). Cambium cell stimulation from surgical release of the periosteum. *J Orthopaed Res 21*(3), 470–480.

Speed, C., D. Nichols, J. Wies, H. Humphreys, C. Richards, S. Burnet, and B. Hazleman (2003, Jan). Extracorporeal shock wave therapy for plantar fasciitis. a double blind randomised controlled trial. *J Orthopaed Res 21*(5), 937–940.

Stevens, M., R. Marini, D. Schaefer, J. Aronson, R. Langer, and V. Shastri (2005). In vivo engineering of organs: the bone bioreactor. *Proceedings of the National Academy of Sciences 102*(32), 11450.

Strash, W. W. and R. R. Perez (2002, Oct). Extracorporeal shockwave therapy for chronic proximal plantar fasciitis. *Clin Podiatr Med Surg 19*(4), 467–76.

Su, J. L., B. L. Schumacher, K. M. Lindley, V. Soloveychik, W. Burkhart, J. A. Triantafillou, K. Kuettner, and T. Schmid (2001, Jun). Detection of superficial zone protein in human and animal body fluids by cross-species monoclonal antibodies specific to superficial zone protein. *Hybridoma 20*(3), 149–57.

Sukul, D. M. K., E. J. Johannes, E. G. Pierik, G. J. van Eijck, and M. J. Kristelijn (1993, Jan). The effect of high energy shock waves focused on cortical bone: an in vitro study. *The Journal of surgical research 54*(1), 46–51.

Sun, Y., E. J. Berger, C. Zhao, G. D. Jay, K.-N. An, and P. C. Amadio (2006, Sep). Expression and mapping of lubricin in canine flexor tendon. *J Orthop Res 24*(9), 1861–8.

Swann, D., F. Silver, H. Slayter, W. Stafford, and E. Shore (1985, Jan). The molecular-structure and lubricating activity of lubricin isolated from bovine and human synovial-fluids. *Biochem J 225*(1), 195–201.

Takahashi, K., M. Yamazaki, T. Saisu, A. Nakajima, S. Shimizu, S. Mitsuhashi, and H. Moriya (2004). Gene expression for extracellular matrix proteins in shockwave-induced osteogenesis in rats. *Calcified tissue international 74*(2), 187–193.

Takato, T., K. Harii, T. Nakatsuka, and K. Ueda (1986, Jan). Vascularized periosteal grafts: An experimental study using two different forms of tibial periosteum in rabbits. *Plastic and Reconstructive Surgery*.

Takayama, K. and T. Saito (2004). Shock wave/geophysical and medical applications. *Annu. Rev. Fluid Mech. 36*, 347–79.

Tamma, R., S. DellEndice, A. Notarnicola, L. Moretti, S. Patella, V. Patella, A. Zallone, and B. Moretti (2009, Dec). Extracorporeal shock waves stimulate osteoblast activities. *Ultrasound in Medicine & Biology 35*(12), 2093–2100.

Theodore, G., M. Buch, A. Amendola, C. Bachmann, L. Fleming, and C. Zingas (2004, Jan). Extracorporeal shock wave therapy for the treatment of plantar fasciitis. *Foot Ankle Int 25*(5), 290–297.

Thiel, M. (2001, Jan). Application of shock waves in medicine. *Clinical orthopaedics and related research* (387), 18–21.

Thomson, R., A. Mikos, E. Beahm, J. Lemon, W. Satterfield, T. Aufdemorte, and M. Miller (1999). Guided tissue fabrication from periosteum using preformed biodegradable polymer scaffolds. *Biomaterials 20*(21), 2007–2018.

Tinti, C. and S. Parma-Benfenati (1998). Vertical ridge augmentation: surgical protocol and retrospective evaluation of 48 consecutively inserted implants. *The International journal of periodontics & restorative dentistry 18*(5), 434.

Tischer, T., S. Milz, C. Weiler, C. Pautke, J. Hausdorf, C. Schmitz, M. Maier, and O. Surgery (2008). Dose-dependent new bone formation by extracorporeal shock wave application on the intact femur of rabbits. *Eur Surg Res 41*(1), 44–53.

Tombolini, P., M. Ruoppolo, C. Bellorofonte, C. Zaatar, and M. Follini (2000, Jan). Lithotripsy in the treatment of urinary lithiasis. *J Nephrol 13 Suppl 3*, S71–82.

Trueta, J. (1963, Jan). The rolle of the vessels in osteogenesis. *J Bone Joint Surg Br 45*(2), 402–418.

Ueno, T., T. Kagawa, M. Kanou, N. Shirasu, M. Sawaki, H. Imura, A. Hirata, E. Yamachika, N. Mizukawa, and T. Sugahara (2007). Evaluation of osteogenic potential

of cultured periosteum derived cells-preliminary animal study. *Journal of Hard Tissue Biology 16*(2), 50–53.

Vermeeren, J., D. Wismeijer, and M. Waas (1996). One-step reconstruction of the severely resorbed mandible with onlay bone grafts and endosteal implants a 5-year follow-up. *International Journal of Oral & Maxillofacial Surgery 25*(2), 112–115.

Wagner, D. (1990). Cell biology of von willebrand factor. *Annual Review of Cell Biology 6*(1), 217–242.

Wang, C., H. Chen, C. Chen, and K. Yang (2001). Treatment of nonunions of long bone fractures with shock waves. *Clinical orthopaedics and related research 387*, 95–101.

Wang, C.-J., F.-S. Wang, C.-C. Huang, K. D. Yang, L.-H. Weng, and H.-Y. Huang (2005, Nov). Treatment for osteonecrosis of the femoral head: comparison of extracorporeal shock waves with core decompression and bone-grafting. *J Bone Joint Surg Am 87*(11), 2380–7.

Wang, C.-J., F.-S. Wang, J.-Y. Ko, H.-Y. Huang, C.-J. Chen, Y.-C. Sun, and Y.-J. Yang (2008, Apr). Extracorporeal shockwave therapy shows regeneration in hip necrosis. *Rheumatology (Oxford) 47*(4), 542–6.

Wang, C.-J., F.-S. Wang, K. D. Yang, L.-H. Weng, and J.-Y. Ko (2006, Apr). Long-term results of extracorporeal shockwave treatment for plantar fasciitis. *Am J Sports Med 34*(4), 592–6.

Wang, F., C. Wang, H. Huang, H. Chung, R. Chen, and K. Yang (2001). Physical shock wave mediates membrane hyperpolarization and ras activation for osteogenesis in human bone marrow stromal cells. *Biochemical and Biophysical Research Communications 287*(3), 648–655.

Wang, F. S., K. D. Yang, R. F. Chen, C. J. Wang, and S. M. Sheen-Chen (2002, Apr). Extracorporeal shock wave promotes growth and differentiation of bone-marrow

stromal cells towards osteoprogenitors associated with induction of tgf-beta 1. *J Bone Joint Surg Br 84*(3), 457–61.

Wang, F.-S., K. D. Yang, Y.-R. Kuo, C.-J. Wang, S.-M. Sheen-Chen, H.-C. Huang, and Y.-J. Chen (2003, Apr). Temporal and spatial expression of bone morphogenetic proteins in extracorporeal shock wave-promoted healing of segmental defect. *Bone 32*(4), 387–96.

Weiss, O. (2006). Physics and technology of shock wave therapy. *International Society for Musculoskeletal Shockwave Therapy 2*(1), 2–12.

Wozney, J. (2002, Jan). Overview of bone morphogenetic proteins. *Spine 27*(16), S2–S8.

Zhao, C., Y.-L. Sun, R. L. Kirk, A. R. Thoreson, G. D. Jay, S. L. Moran, K.-N. An, and P. C. Amadio (2010, Jan). Effects of a lubricin-containing compound on the results of flexor tendon repair in a canine model in vivo. *J Bone Joint Surg Am 92A*(6), 1453–1461.